

University of Alberta

Phase Behavior Studies of Edible Lipids and their Industrial Applications

by

Kerry Lyn Humphrey



A thesis submitted to the Faculty of Graduate Studies and Research
in partial fulfillment of the requirements for the degree of

Doctor of Philosophy

in

Food Science and Technology

Department of Agricultural, Food and Nutritional Science

Edmonton, Alberta

Fall 2007



Library and
Archives Canada

Bibliothèque et
Archives Canada

Published Heritage
Branch

Direction du
Patrimoine de l'édition

395 Wellington Street
Ottawa ON K1A 0N4
Canada

395, rue Wellington
Ottawa ON K1A 0N4
Canada

Your file *Votre référence*
ISBN: 978-0-494-32980-1
Our file *Notre référence*
ISBN: 978-0-494-32980-1

NOTICE:

The author has granted a non-exclusive license allowing Library and Archives Canada to reproduce, publish, archive, preserve, conserve, communicate to the public by telecommunication or on the Internet, loan, distribute and sell theses worldwide, for commercial or non-commercial purposes, in microform, paper, electronic and/or any other formats.

The author retains copyright ownership and moral rights in this thesis. Neither the thesis nor substantial extracts from it may be printed or otherwise reproduced without the author's permission.

AVIS:

L'auteur a accordé une licence non exclusive permettant à la Bibliothèque et Archives Canada de reproduire, publier, archiver, sauvegarder, conserver, transmettre au public par télécommunication ou par l'Internet, prêter, distribuer et vendre des thèses partout dans le monde, à des fins commerciales ou autres, sur support microforme, papier, électronique et/ou autres formats.

L'auteur conserve la propriété du droit d'auteur et des droits moraux qui protègent cette thèse. Ni la thèse ni des extraits substantiels de celle-ci ne doivent être imprimés ou autrement reproduits sans son autorisation.

In compliance with the Canadian Privacy Act some supporting forms may have been removed from this thesis.

Conformément à la loi canadienne sur la protection de la vie privée, quelques formulaires secondaires ont été enlevés de cette thèse.

While these forms may be included in the document page count, their removal does not represent any loss of content from the thesis.

Bien que ces formulaires aient inclus dans la pagination, il n'y aura aucun contenu manquant.


Canada

Abstract

Due to the adverse affect of consuming *trans* fats, the presence of *trans* fats in edible oil products such as a shortening is under fire. However the removal of *trans* fats without increasing the level of saturated fats is not trivial as *trans* and saturated fats tend to have high melting points and contribute to the formation of a solid crystal network. Therefore a series of comprehensive and extensive phase behavior studies of canola and other vegetable oil based shortenings were developed to design a zero *trans*, lowered saturates shortening with hardness commensurate that of a commercial product which utilizes the structure enhancing properties of specific TAGs.

Binary shortening systems containing fully hydrogenated canola, cottonseed, lard, palm, soybean or tallow in soybean oil were investigated in an attempt to drastically alter the molecular composition of the shortening samples utilizing commercial raw materials. The composition affected the growth mode of the crystal network as well as SFC, polymorphism, hardness and the enthalpies of crystallization and melt. SFC was found to be unpredictable of final hardness, while polymorphism could be explained by changes in the molecular ensemble. The final physical properties of the shortenings seemed to be significantly influenced by amounts of the TAGs PSS, PSP, or PPS, and not just SSS.

Given this observation, the canola shortening system initially investigated was enriched with pure PSS as well as PSS as a component of fully hydrogenated canola and cottonseed oil and the effect of PSS was observed. It was found that by careful blending

of fully hydrogenated canola and cottonseed oils one could increase hardness whilst limiting total added saturated fat. The increase in hardness as seen on the lab scale was also observed for shortenings produced at the pilot plant scale.

In an effort to further enhance the crystal network formed, the processing conditions and tempering were varied. The increase in hardness due to the careful blending of raw materials could be further enhanced given optimal processing and tempering parameters. Finally, the PSS enriched shortenings were made into cream icings and demonstrated greater suitability for icings than shortenings without enrichment.

I dedicate this thesis to
all of my Grandparents, both biological and adopted.

Acknowledgments

I would like to thank my supervisor Dr. Suresh Narine for his ongoing guidance and support, without which I would have floundered aimlessly. I am indebted to Dr. Narine for suggesting I apply for a transfer to the PhD program, for providing me with a multitude of opportunities to present my work at conferences, interact with those in industry, for only insisting that I pull that one all nighter, and for never again repeating his Mustang Sally anecdote. I am also grateful to the members of my supervisory committee, Dr. Phillip Choi and Dr. Lech Ozimek for their guidance.

I am thankful for the assistance of Marc Boodhoo as without his extensive knowledge of the literature, observations, and assistance in making my writing eloquent, this thesis would not be completed for some time. I would also like to acknowledge the technical assistance of Ereddad Kharraz, Kevin Pocklington, Baljit Ghotra, Sarah McCalla, Bruce Liao, Maria Irizar, Marsha Khelawan, and everyone else at in the ALUP. Thanks are also due to the staff at Bunge Foods for their assistance with the pilot plant scale study as well as icing formulation and testing.

Gratitude is also due to my first year physics professor (Dr. Alan Slavin, Trent University) for assigning me a failing grade on that assignment, for helping me to recover from receiving my first 'F', and telling me that graduate school was an option for me. I had never even considered graduate school as an option until that day in February 1999. Your suggestion raised the bar for my success, and for that I thank you.

To my parents for constantly reminding me to do my best when I thought my best was not good enough, having a job that paid the bills so that I could join clubs, be a part of so many extracurricular activities, travel all over creation, go away to university and have a place to call home. I owe thanks to my entire family and to my “families” in Bright and Edmonton for their support. I am grateful to everyone who ever wrote me a letter of support for scholarship and university applications. I hope that I didn’t make a liar out of anyone.

To Andrew, who has seen the best and the worst of me throughout my studies, who knows that I really did mean to say “get lost” in a nicer tone, for screening my calls and knowing exactly which ones to pass on to me while I was studying, for keeping me in tea, for pretending to listen as I endlessly rehearsed presentations, for always having a useful comment when I wanted you to listen, for sharing your knowledge of chemistry and your textbook supply, and most of all for your unwavering love and support. Thank you for always believing in me.

Finally, I would like to thank Archer Daniel Midland, Bunge Oils, Alberta Agricultural Research Institute, Alberta Canola Producers Commission, Alberta Crop Industry Development Fund, Alberta Agriculture Food and Rural Development, and NSERC for their generous financial support for the research.

Table of Contents

1.	INTRODUCTION AND BACKGROUND INFORMATION	
1.1	Introduction.....	1
1.2	Fats and Oils Background.....	3
1.2.1	Chemistry of Lipids.....	3
1.2.2	Function of Lipids.....	8
1.2.3	Sources of Edible Oils.....	9
1.3	Lipid Modification.....	11
1.4	Crystallization of Lipid Mixtures.....	16
1.4.1	Nucleation.....	18
1.4.2	Crystallization.....	26
1.4.3	Monitoring Lipid Crystallization	28
1.5	Lipid Phase Behavior.....	31
1.5.1	Types of Phase Behavior.....	34
1.5.2	Ideal Solubility Behavior.....	40
1.5.3	Lipid Phase Behavior Determination.....	43
1.5.3.a	Solid Content.....	43
1.5.3.b	Melting Point.....	45
1.5.3.c	Polymorphic Type.....	47
1.5.3.d	Volume Expansion.....	47
1.5.4	Studies in the Literature.....	48
1.5.5	Constructing Lipid Phase Diagrams.....	49
1.5.6	Interpretation of Phase Diagrams.....	51
1.6	Low <i>Trans</i> Shortening Solutions.....	61
1.7	The Challenge.....	64
1.8	References.....	65
2.	A COMPARISON OF LIPID SHORTENING FUNCTIONALITY AS A FUNCTION OF MOLECULAR ENSEMBLE AND SHEAR: CRYSTALLIZATION AND MELTING	

2.1	Introduction.....	83
2.2	Experimental Procedures.....	85
	2.2.1 Fatty Acid Content of the Fully Hydrogenated Fats.....	85
	2.2.2 Sample Preparation.....	86
	2.2.3 DSC Measurements, Thermal Behavior.....	87
2.3	Results and Discussion.....	88
2.4	References.....	128
3.	A COMPARISON OF LIPID SHORTENING FUNCTIONALITY AS A FUNCTION OF MOLECULAR ENSEMBLE AND SHEAR: MICROSTRUCTURE, POLYMORPHISM, SOLID FAT CONTENT AND TEXTURE	
3.1	Introduction.....	130
3.2	Experimental Procedures.....	132
	3.2.1 Sample Preparation.....	132
	3.2.2 NMR Measurements, SFC Determination.....	133
	3.2.3 Relative Hardness Measurements.....	134
	3.2.4 Microstructure Determination.....	134
	3.2.5 XRD Measurements, Polymorphism.....	135
3.3	Results and Discussion.....	135
3.4	References.....	155
4.	USING 1 – PALMITOYL, 2,3 – DISTEAROYL – SN - GLYCEROL (PSS) AS A STRUCTURAL ENHANCER SO AS TO DECREASE THE LEVEL OF SATURATES IN ZERO-TRANS SHORTENINGS	
4.1	Introduction.....	157
4.2	Experimental Procedures.....	159
	4.2.1 Sample Preparation.....	160
	4.2.2 Relative Hardness Measurements.....	160
	4.2.3 DSC Measurements, Thermal Behavior.....	162
	4.2.4 XRD Measurements, Polymorphism.....	163
	4.2.5 NMR Measurements, SFC Determination.....	163

4.2.6	Microstructure Determination.....	165
4.3	Results and Discussion.....	166
4.3.1	Relative Hardness.....	166
4.3.2	Polymorphism.....	168
4.3.3	Solid Fat Content.....	175
4.3.4	Melting Enthalpy.....	188
4.3.5	Crystallization Enthalpy.....	195
4.3.6	Microstructure.....	200
4.4	Conclusions.....	207
4.5	References.....	208
5.	USING 1 – PALMITOYL, 2,3 – DISTEAROYL – SN - GLYCEROL (PSS) AS A STRUCTURAL ENHANCER SO AS TO DECREASE THE LEVEL OF SATURATES IN ZERO-TRANS SHORTENINGS: PILOT SCALE STUDIES	
5.1	Introduction.....	211
5.2	Experimental Procedures.....	212
5.2.1	PSS Enrichment as the Pilot Plant Scale and the Effect of Processing Conditions and Tempering.....	212
5.2.1.a	Sample Preparation.....	212
5.2.1.b	Relative Hardness Measurements.....	215
5.2.1.c	NMR Measurements, SFC Determination.....	217
5.2.2	Applications Testing of PSS Enriched Samples.....	217
5.2.2.a	Sample Preparation.....	218
5.2.2.b	Trench Score.....	218
5.2.2.c	Specific Gravity.....	218
5.2.2.d	Buskometer Slump Tests.....	219
5.2.2.e	One Week Observations.....	219
5.3	Results and Discussion.....	221
5.3.1	PSS Enrichment as the Pilot Plant Scale and the Effect of Processing Conditions and Tempering.....	221
5.3.2	Applications Testing of PSS Enriched Samples.....	234

5.4	Conclusions.....	245
5.5	References.....	246
6.	CONCLUSIONS	
6.1	General Discussion.....	248
6.2	Future Prospects.....	249
6.3	General Discussion and Conclusions.....	253
6.4	References.....	256
A1.	PHASE BEHAVIOR OF A BINARY LIPID SHORTENING SYSTEM	
A1.1	Introduction.....	257
A1.1	Experimental Procedures.....	258
	A1.1.1 Sample Preparation.....	258
	A1.1.2 NMR Measurements.....	259
	A1.1.2.a SFC Determination.....	259
	A1.1.2.b SFC Analysis.....	260
	A1.1.2.c Crystallization Onset Measurement.....	260
	A1.1.3 DSC Measurements, Thermal Behavior.....	261
	A1.1.3.a Tempering DSC Samples.....	261
	A1.1.4 Relative Hardness Measurements.....	261
	A1.1.4.a Analysis of Instron Samples.....	262
	A1.1.5 XRD Measurements, Polymorphism.....	262
	A1.1.6 Microstructure Determination.....	262
A1.2	Results and Discussion.....	263
A1.3	References.....	283

A2.	DIMINISHING MARGINAL UTILITY OF COOLING RATE INCREASE ON THE CRYSTALLIZATION BEHAVIOR AND PHYSICAL PROPERTIES OF A LIPID SAMPLE	
A2.1	Introduction.....	286
A2.2	Experimental Procedures.....	288
	A2.2.1 Sample Preparation.....	289
	A2.2.2 Relative Hardness Measurements.....	289
	A2.2.3 DSC Measurements, Thermal Behavior.....	290
	A2.2.4 XRD Measurements, Polymorphism.....	291
	A2.2.5 NMR Measurements, SFC Determination.....	292
A2.3	Results and Discussion.....	293
A2.4	References.....	312
A3.	CREAM ICING TEST (METHOD 17-73)	
A3.1	Use for Shortenings.....	317
A3.2	Purpose.....	317
A3.3	Apparatus.....	317
A3.4	Formula.....	317
A3.5	Procedure.....	318
A4.	BUSKOMETER SLUMP TEST (METHOD 1-88)	
A4.1	Purpose.....	319
A4.2	Apparatus.....	319
A4.3	Procedure.....	319
A4.4	Report.....	320

List of Tables

Table 1.1:	Typical fatty acids in edible oils, names, melting points and sources.....	6
Table 1.2:	Typical vegetable, marine and animal oils.....	10
Table 2.1:	Ingredients of the five market shortenings used, as listed on the shortenings' packaging.....	95
Table 4.1:	Compositions of the 20 samples used in this study.....	161
Table 4.2:	TAG composition of the samples at all levels of total added saturated fat as a percentage of both the total sample and the total added saturated fat	180
Table 5.1:	Sample compositions of all 5 sample mixtures used in this study.....	213
Table 5.2:	Processing conditions for pilot scale samples in this study.....	216
Table 5.3:	Cream icing trench scores.....	235
Table 5.4:	Specific gravities, slide, and slump values for the control icings.....	236
Table 5.5:	Visual observations of the icings after one week.....	243
Table 6.1:	TAG profiles of fully hydrogenated vegetable oils (% w/w).....	250
Table A1.1:	Relative percentages of the TAGs in soybean oil and fully hydrogenated canola oil.....	266
Table A1.2:	Classification of XRD curves by shape.....	278
Table A1.3:	Average d value for each class of XRD curves.....	278

List of Figures

Figure 1.1:	Schematic diagram of the structure of a) MAG, b) DAG, and c) TAG molecules.....	5
Figure 1.2:	Chemical structures of a) stearic, b) oleic, c) linoleic, and d) linolenic fatty acids.....	7
Figure 1.3:	General equation for random interesterification.....	12
Figure 1.4:	Possible outcomes for the hydrogenation of oleic acid a) stearic and b) elaidic acid.....	14
Figure 1.5:	Crystallization procedure for shortenings and margarines.....	15
Figure 1.6:	Lipid crystallization flow chart.....	17
Figure 1.7:	Viscosity of a cocoa butter alternative as a function of temperature.....	19
Figure 1.8:	Effect of rate of cooling on the supercooling of a sample.....	25
Figure 1.9:	Ideal phase behavior of the benzene/toluene system.....	33
Figure 1.10a:	Phase behavior of a theoretical monotectic system.....	36
Figure 1.10b:	Phase behavior of a theoretical monotectic system with solid solution changing.....	37
Figure 1.11:	Phase behavior of a theoretical eutectic system.....	39
Figure 1.12:	Phase behavior of a theoretical peritectic system.....	41
Figure 1.13:	Enthalpy of melt curve and 1 st derivative curve from DSC. The onset of melt and peak maximum is indicated by the arrows.....	46
Figure 1.14:	SFC versus temperature for varying fractions of milk fat. (■ represents LMF, Δ represents another LMF, ▲ represents MMF, ● represents HMF).....	52
Figure 1.15a:	Experimental binary monotectic of fully hydrogenated canola in soybean oil via SFC.....	54
Figure 1.15b:	Experimental ternary monotectic of HMF (5S), LMF (-28L), and MMF (-28S) at 30 °C via iso-solid lines.....	55

Figure 1.15c: Experimental binary monotectic of MMF and HMF via iso-solid lines. The bottommost line represents 90% SFC, and subsequent lines decrease in increments of 5% to a minimum of 5% SFC as the uppermost line.....	56
Figure 1.16a: Experimental ternary eutectic of HMF (5S), LMF (-28L), and MMF (-28S) at 0 °C via iso-solid lines.....	58
Figure 1.16b: Experimental binary eutectic of cocoa butter – HMF via iso-solid lines. The bottommost line represents 90% SFC, and subsequent lines decrease in increments of 5% to a minimum of 5% SFC.....	59
Figure 1.16c: Experimental binary eutectic of cocoa butter – MMF via iso-solid lines, an exaggerated case. The bottommost line represents 75% SFC, and subsequent lines decrease in increments of 5% to a minimum of 10% SFC.....	60
Figure 2.1: Fatty acid composition of the fully hydrogenated fats and soybean oil...	90
Figure 2.2: TAG composition of the fully hydrogenated fats.....	91
Figure 2.3: TAG composition of soybean oil.....	93
Figure 2.4: Crystallization peak maximum versus concentration for unsheared mixtures.....	97
Figure 2.5a: Crystallization onset temperatures versus concentration for unsheared mixtures.....	99
Figure 2.5b: Slope of line of best fit for all hard fat crystallization onset temperature curves.....	101
Figure 2.6: Crystallization onset temperatures versus concentration for unsheared mixtures arranged by fully hydrogenated fat.....	104
Figure 2.7: Crystallization onset temperatures versus fully hydrogenated fat for unsheared mixtures arranged by concentration.....	105
Figure 2.8: Crystallization curves for unsheared systems arranged by increasing concentration of hard fat (a) canola, (b) cottonseed, (c) lard, (d) palm, (e) soybean, (f) tallow.....	108
Figure 2.9: Crystallization curves for unsheared systems arranged by concentration (a) 10%, (b) 15%, (c) 20%, (d) 25%.....	110
Figure 2.10: Market shortening crystallization curves.....	112

Figure 2.11:	Enthalpy of melt peak maximum versus concentration for sheared samples.....	115
Figure 2.12:	Enthalpy of melt peak maximum versus concentration for unsheared samples.....	117
Figure 2.13:	Melting onset temperatures versus concentration for sheared and unsheared mixtures at 0 and 48 hours with inset market shortenings onset of melt graph.....	119
Figure 2.14:	Enthalpy of melt curves for sheared samples arranged by increasing concentration of hard fat (a) canola, (b) cottonseed, (c) lard, (d) palm, (e) soybean, (f) tallow.....	122
Figure 2.15:	Enthalpy of melt curves for unsheared samples arranged by increasing concentration of hard fat (a) canola, (b) cottonseed, (c) lard, (d) palm, (e) soybean, (f) tallow.....	123
Figure 2.16:	Enthalpy of melt curves for sheared samples arranged by concentration (a) 10%, (b) 15%, (c) 20%, (d) 25%.....	124
Figure 2.17:	Enthalpy of melt curves for unsheared samples arranged by concentration (a) 10%, (b) 15%, (c) 20%, (d) 25%.....	125
Figure 2.18:	Enthalpy of melt curves for the market shortenings.....	126
Figure 3.1:	SFC versus concentration for sheared systems 48 hours after tempering.....	136
Figure 3.2:	SFC versus concentration for unsheared systems 48 hours after tempering.....	138
Figure 3.3:	Composite diagram of smoothed X-ray diffractometry curves for 25% fully hydrogenated fats both unsheared (lower) and sheared (upper), and market shortenings with distance versus sample graph (right).....	140
Figure 3.4:	Composite diagram of the microstructure of sheared samples at 25% concentration after 48 hours. The samples vary with respect to fully hydrogenated fat: (a) canola (b) cottonseed (c) lard (d) palm (e) soybean (f) tallow (bar = 500 μm).....	144
Figure 3.5:	Composite diagram of the microstructure of unsheared samples at 25% concentration after 48 hours. The samples vary with respect to fully hydrogenated fat: (a) canola (b) cottonseed (c) lard (d) palm (e) soybean	

	(f) tallow (bar = 500 μm).....	145
Figure 3.6:	Composite diagram of microstructure of market shortenings. The samples a-e were taken of the shortenings as purchased in the store, and the samples in f-j were melted and cooled at a rate of 10 $^{\circ}\text{C}/\text{min}$. (a) All Vegetable Shortening (b) Blue Crisco (c) Golden Crisco (d) Pure Lard (e) Tenderflake (f) All Vegetable Shortening (g) Blue Crisco (h) Golden Crisco (i) Pure Lard (j) Tenderflake (bar = 500 μm).....	148
Figure 3.7:	Variation in the hardness of sheared systems for the 15-25% (w/w) concentrations of the local fats and the market shortenings.....	150
Figure 3.8:	Variation in the hardness of unsheared systems for the 15-25% (w/w) concentrations of the local fats.....	152
Figure 4.1a:	Relative hardness of the shortening samples after 13 days as a function of sample types at with total added saturated fat of i) 15.0%, ii) 17.1-17.5%, iii) 19.6-20.0%, iv) 22.1-22.5%, and v) 24.6-25.0%.....	167
Figure 4.1b:	Relative hardness versus time of shortening samples of all types with 17.1% (PSS/SSS Match) to 17.5% (No Added PSS, 5% PSS, and 5% Cottonseed) total added saturates.....	169
Figure 4.2a:	Polymorphism of the shortening samples after 2 days for the No Added PSS sample compared with the 5% PSS sample.....	171
Figure 4.2b:	Polymorphism of the shortening samples after 2 days for the No Added PSS sample compared with the 5% Cottonseed sample.....	172
Figure 4.2c:	Polymorphism of the shortening samples after 2 days for the No Added PSS sample compared with the PSS/SSS Match sample.....	173
Figure 4.2d:	The effect that storage has on polymorphism for the PSS/SSS Match sample after 1 hour, 2 days, and 13 days.....	174
Figure 4.3:	SFC of the shortening samples as a function of total added saturated fat after a) 1 hour, b) 2 days and c) 13 days.....	176
Figure 4.4a:	Avrami Constant obtained by fitting continuous NMR growth curves with the Avrami equation as a function of the total added saturated fat.....	178
Figure 4.4b:	Avrami Exponent obtained by fitting continuous NMR growth curves with the Avrami equation as a function of the total added saturated fat.....	181
Figure 4.5a:	Schematic of the double length TAG packing at an angle θ	183

Figure 4.5b:	Schematic of the TAG packing of the SSS-SSS system.....	184
Figure 4.5c:	Schematic of the TAG packing of the PSS-PSS system.....	185
Figure 4.5d:	Schematic of the TAG packing of the PSS-SSS system.....	187
Figure 4.6a:	Peak maximum of melting by DSC as a function of the total added saturated fat.....	189
Figure 4.6b:	FWHM of DSC melting peak as a function of the total added saturated fat.....	191
Figure 4.6c:	Melting onset after 2 days as a function of the total added saturated fat.....	194
Figure 4.7a:	Start of enthalpy of crystallization curves versus total added saturates...	196
Figure 4.7b:	Onset of enthalpy of crystallization curves versus total added saturates.....	197
Figure 4.7c:	Crystallization peak maximum versus total added saturates.....	199
Figure 4.7d:	Crystallization enthalpy versus total added saturates.....	201
Figure 4.8a:	Microstructure of the No Added PSS samples 1 hour after processing. (White bar = 100 μm).....	202
Figure 4.8b:	Microstructure of the 5% PSS samples 1 hour after processing. (White bar = 100 μm).....	204
Figure 4.8c:	Microstructure of the 5% Cottonseed samples 1 hour after processing. (White bar = 100 μm).....	205
Figure 4.8d:	Microstructure of the PSS/SSS Match samples 1 hour after processing. (White bar = 100 μm).....	206
Figure 5.1:	Schematic diagram of a pilot plant shortenings crystallizer with Pin RPM, Pump Speed, and Fill Temperature indicated on corresponding units...	214
Figure 5.2:	Dimensions of the apparatus used to measure the plasticity of the icings and resistance to flow (Slump-Slide Box Dimensions).....	220
Figure 5.3:	Effect of pump speed and fill temperature on the rate of cooling and effective undercooling within a shortening crystallizer.....	222

- Figure 5.4a:** Relative hardness of the shortening samples after 7 days as a function of the processing condition. Hardness for samples tempered at (i) 70 °F and (ii) 85 °F is shown. The vertical bars represent the hardness of the shortening samples with No Added PSS, the white triangles represent that of the 5% Cottonseed samples and the black circles represent that of the PSS/SSS Match samples.....225
- Figure 5.4b:** Relative hardness of the shortening samples after 14 days as a function of the processing condition. Hardness for samples tempered at (i) 70 °F and (ii) 85 °F is shown. The vertical bars represent the hardness of the shortening samples with No Added PSS, the white triangles represent that of the 5% Cottonseed samples and the black circles represent that of the PSS/SSS Match samples.....226
- Figure 5.5a:** SFC of the shortening samples after 7 days. The SFC for samples tempered at (i) 70 °F and (ii) 85 °F is shown. The vertical bars represent the SFC of the shortening samples with No Added PSS, the white triangles represent that of the 5% Cottonseed samples and the black circles represent that of the PSS/SSS Match samples.....228
- Figure 5.5b:** SFC of the shortening samples after 14 days. The SFC for samples tempered at (i) 70 °F and (ii) 85 °F is shown. The vertical bars represent the SFC of the shortening samples with No Added PSS, the white triangles represent that of the 5% Cottonseed samples and the black circles represent that of the PSS/SSS Match samples.....230
- Figure 5.6a:** Peak maximum of DSC melting curves after 7 days tempered at 70 °F (i) and 85 °F (ii). The vertical bars represent the melting peak maxima of the shortening samples with No Added PSS, the white triangles represent that of the 5% Cottonseed samples and the black circles represent that of the PSS/SSS Match samples.....231
- Figure 5.6b:** Peak maximum of DSC melting curves after 14 days tempered at 70 °F (i) and 85 °F (ii). The vertical bars represent the melting peak maxima of the shortening samples with No Added PSS, the white triangles represent that of the 5% Cottonseed samples and the black circles represent that of the PSS/SSS Match samples.....232
- Figure 5.7:** Specific gravities of each of the test icings processed with the conditions (a) HMM, (b) LMH, (c) HLH, and (d) LLH. The vertical bars represent the specific gravities of the icings made from the No Added PSS shortenings, the white triangles represent that of the 5% Cottonseed samples and the black circles represent that of the PSS/SSS Match samples.....237

Figure 5.8a:	Amount of horizontal slump of each of the test icings made from the shortenings tempered at 70 °F as a function of processing conditions...	239
Figure 5.8b:	Amount of horizontal slump of each of the test icings made from the shortenings tempered at 85 °F as a function of processing conditions...	240
Figure 6.1:	Hardness of samples enriched with pure PSS, PSP, and PPS as a function of total added saturates.....	251
Figure 6.2:	Hardness of samples enriched with PSS, and PSP as components of cottonseed and palm oil respectively.....	252
Figure A1.1:	Crystallization heat flow versus temperature with inset enthalpy of crystallization versus composition curve. Each curve represents the heat flow during the cooling process for a sample. The 0% canola sample is the bottommost curve on the graph and the percent canola composition of the samples increases by 5% for each subsequent curve to the 100% canola sample at the top of the graph.....	267
Figure A1.2:	Crystallization onset time.....	269
Figure A1.3:	Melting heat flow versus temperature curves after 48 hours with inset enthalpy of melting versus composition curve. Each curve represents the heat flow during the melting process for a sample. The 0% canola sample is the bottommost curve on the graph and the percent canola composition of the samples increases by 5% for each subsequent curve to the 100% canola sample at the top of the graph.....	270
Figure A1.4:	Variation of hardness with composition.....	272
Figure A1.5:	Iso-solid lines created using the interpolation method. Each curve connects points with a common SFC value. The leftmost curve is the 5% SFC line with the percent SFC increasing in 5% increments as one moves right on the graph.....	275
Figure A1.6:	X-ray diffraction curves versus d. Each curve is a diffraction spectrum for a specific sample composition. The bottommost curve is the 15% canola blend, and the percent canola increases by 5% for each curve above. The uppermost curve is the spectrum obtained for the 100% canola sample.....	276
Figure A1.7:	Composite diagram of the microstructure of selected samples after 48 hours. The given samples vary with respect to percent canola: (a) 40%, (b) 45%, (c) 50%, (d) 55%, (e) 80%, (f) 85%, (g) 90%, and (h) 95%. (bar = 500 μm).....	281

Figure A2.1: Effect of rate of cooling on the supercooling of a sample.....	287
Figure A2.2: Hardness by cone penetrometry versus cooling rate.....	294
Figure A2.3: Stacked crystallization curves for samples processed at all cooling rates from 0.1 °C/min (bottom line) to 20 °C/min (uppermost line).....	295
Figure A2.4a: Onset of crystallization and start of crystallization event versus cooling rate.....	297
Figure A2.4b: Location of peak maximum and shoulder peak of the crystallization event versus cooling rate.....	298
Figure A2.5: Viscosity of Temcote as a function of temperature.....	300
Figure A2.6: Stacked melting curves for samples processed at all cooling rates from 0.1 °C/min (uppermost line) to 20 °C/min (bottom line).....	302
Figure A2.7: FWHM of the main melting peak versus cooling rate as a function of temperature.....	304
Figure A2.8a: SFC versus time. From left to right curves obtained with: 15.9 °C/min, 1.6 °C/min, and 0.1 °C/min cooling rate.....	307
Figure A2.8b: Induction time versus cooling rate by NMR.....	308
Figure A2.8c: Final SFC versus cooling rate by NMR.....	310

List of Abbreviations

DAG	diacylglycerol
DSC	differential scanning calorimetry
FHC	fully hydrogenated canola
FHCo	fully hydrogenated cottonseed
FWHM	full width at half maximum
GC	gas chromatography
GC-FID	gas chromatography with a flame ionization detector
HMF	high melting fraction of milk fat
L	linoleic acid
LLL	trilinolein
LLO	1,2 – dilauroyl, 3 – oleic – <i>sn</i> - glycerol
LMF	low melting fraction of milk fat
MAG	monoacylglycerol
MMF	mid-melting fraction of milk fat
NMR	nuclear magnetic resonance
P	palmitic acid
POS	1 palmitoyl – 2 oleic – 3 stearoyl – <i>sn</i> - glycerol
PPP	tripalmitin
PPS	1,2 – dipalmitoyl, 3 – stearoyl – <i>sn</i> - glycerol
PSP	1,3 – dipalmitoyl, 2 – stearoyl – <i>sn</i> - glycerol
PSS	1 – palmitoyl, 2,3 – distearoyl – <i>sn</i> - glycerol
RPM	revolutions per minute

S	stearic acid
SFC	solid fat content
SFI	solid fat index
<i>sn</i> -1	first position on the glycerol backbone
<i>sn</i> -2	second position on the glycerol backbone
<i>sn</i> -3	third position on the glycerol backbone
SOS	1,3 – distearoyl, 2 – oleic – <i>sn</i> - glycerol
SPS	1,3 – distearoyl, 2 – palmitoyl – <i>sn</i> - glycerol
SSO	1,2 – distearoyl, 3 – oleic – <i>sn</i> - glycerol
SSS	tristearin
TAG	triacylglycerol
w/w	with respect to weight
XRD	x-ray diffraction

1. Introduction and Background Information

1.1 Introduction

Phase behavior studies have been shown to be an effective tool to aid in the study of crystallizing lipid systems [1-6]. Additionally, *trans* fats have been found to be harmful to human health and thus the inclusion of *trans* fats in a shortenings product is not acceptable [7-11]. However, *trans* fats contribute a great deal to the structure of a shortenings product, and thus the removal of these fats from a product, without increasing the saturated fat content (also harmful to health and a functional component [10, 12]), is not a trivial task. Therefore, this work was targeted at the development of a novel shortening system with zero *trans* fats and lowered levels of saturated fat, with hardness values commiserate with that of traditional shortening systems.

To that end, this work begins with a review of lipid crystallization, phase behavior studies of lipids, and low *trans* shortening formulations. A comprehensive and complete phase behavior study, designed to aid in the understanding and formulation of a typical all purpose shortening was performed. The study is provided in Appendix 1, and is an investigation of shortening type samples of fully hydrogenated canola (FHC) oil in soybean oil at varying dilutions of the fully hydrogenated fat.

*A version of section 1.5 of this chapter has been published.
Humphrey, K.L. and S.S. Narine, Lipid Phase Behavior. In: Fat Crystal Networks,
ed. A.G. Marangoni. 2004, New York: Marcel Dekker. 83-114.*

An extensive phase behavior study of blends of refined soybean oil with a fully hydrogenated saturated fat originating from canola, cottonseed, lard, palm, soybean and tallow in varying mass ratios has been performed and summarized in Chapters 2 and 3. Potential structure forming compounds within typical shortening systems were identified based on the melting and crystallization behavior of each fat blend in Chapter 2. The identified structure enhancer was suggested to be tristearin (SSS) in combination with 1-palmitoyl, 2-3 distearoyl *sn*-glycerol (PSS). The effect of composition and shear on the solid fat content, hardness, microstructure and polymorphism of the shortenings in Chapter 2 is summarized in Chapter 3 of this thesis.

Utilizing pure PSS and a binary shortening system of FHC in soybean oil, the shortening system was enriched with a small amount of PSS (Chapter 4). Upon observing an increase in hardness of the shortening system (compared with that of the binary system at equivalent levels of saturated fat), the binary shortening was also enriched with PSS as a component of added fully hydrogenated cottonseed oil (FHCo). It was found that the relative amounts of PSS and SSS in the shortening sample, and not merely the addition of random amounts of either PSS or FHCo, was linked to enhanced physical properties of the shortening. This allowed us to define the parameters of a novel shortening product with enhanced hardness as a result of the incorporation of PSS, either pure or in other carriers such as FHCo into a typical all purpose shortening. Furthermore, the work suggested that since the inclusion of PSS at preferred ratios with SSS enhanced hardness, that such structural enhancement could be exploited to reduce total saturates in a shortening product, whilst still maintaining expected hardness. Additionally, since only

fully hydrogenated samples of refined oil were used, the ensuing formulations would contain zero *trans* as well as reduced saturated fats.

The utility of varying the cooling rate during the crystallization of a lipid network at the lab scale as well as at the pilot plant scale was investigated. The intensive lab scale study of the effect of cooling rate on a lipid system appears in Appendix 2, while the pilot plant scale up of a novel shortening system, utilizing fully hydrogenated cottonseed as a source for PSS, and crystallizing in a scraped surface heat exchanger, is discussed in Chapter 5. The parameters of the crystallizer were modified to further enhance the effect of the structure modifier. Finally, the enriched, zero *trans*, lowered saturates shortenings were made into cream icings to demonstrate the functionality of the novel shortening blend, also in Chapter 5.

1.2 Fats and Oils Background

1.2.1 *Chemistry of lipids*

Fats and oils make up 99% of the lipids of plant and animal origin [13]. Fats and oils are distinguished by the physical state of each at room temperature. The term fat refers to the lipid mixture which is solid at room temperature, while oil refers to that which is liquid at room temperature. All fats and oils are lipids and in this paper, the terms fats and oils are used interchangeably. Lipid molecules have a glycerol backbone with up to three fatty acids esterified to it. A glycerol molecule with three fatty acids on it is called a triacylglycerol (TAG) while those with two fatty acids are called diacylglycerides (DAG), and if only one fatty acid is present, it is a monoacylglyceride

(MAG). Figure 1.1 shows the basic structure of TAG, DAG, and MAG molecules with R_1 , R_2 , and R_3 representing fatty acid chains. MAGs and DAGs can have the fatty acids esterified to any of the positions, not necessarily the ones shown.

Fatty acids are characterized by the number of carbons and degree of saturation. Typical edible oils, as listed in Table 1.1, have fatty acids of carbon length ranging from 4 to 20 [14-17]. Fatty acids can be further separated into two categories – saturated and unsaturated. Saturated fatty acids are those which contain no double bonds as each carbon atom is surrounded by other carbon atoms and hydrogen atoms. These fatty acid molecules are joined in a zig-zag chain as there is free rotation about the carbon atoms due to the absence of double bonds. Fat molecules with saturated fatty acids align easily to create a closely packed structure. Figure 1.2 illustrates the typical structure of the 18 carbon chain fatty acids with one (mono-unsaturated), two, and three (polyunsaturated) double bonds as well as that of stearic acid, the corresponding saturated fatty acid. There are also two possible configurations for a double bond. Double bonds for which the hydrogen atoms are on the same side of the chain are “*cis*” double bonds and those where hydrogen atoms are at opposite sides of the bond are called “*trans*”. *Cis* and *trans* fatty acids will be discussed further below.

Unsaturated fatty acids contain carbon to carbon double bonds. These fatty acids can have one (mono-unsaturated), or more (poly- and super- unsaturated) double bonds. Due to the presence of one or more double bonds in unsaturated fatty acids creating kinks

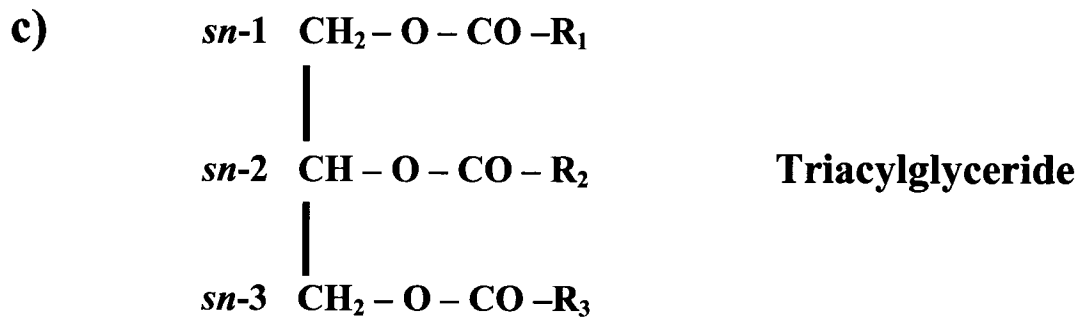
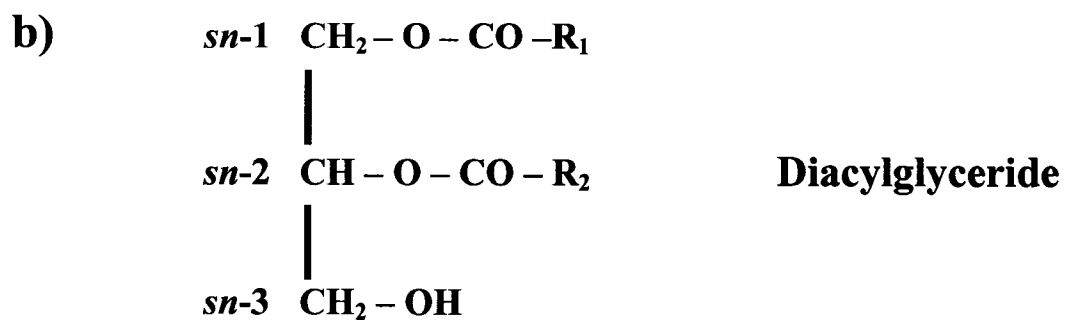
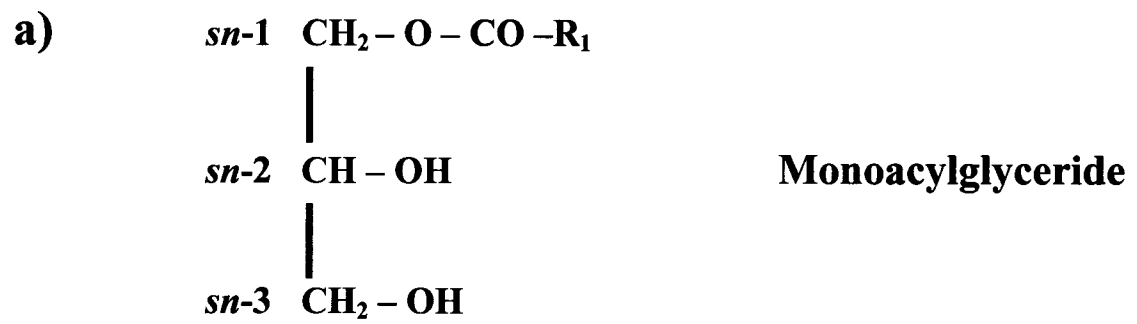


Figure 1.1: Schematic diagram of the structure of a) MAG, b) DAG, and c) TAG molecules

Table 1.1: Typical fatty acids in edible oils, names, melting points and sources ^a[16],
^b[17], [14]

Systematic Name	Trivial Name	C#	Melting Point (°C)	Source
butanoic	butyric (B)	4:0	-8 ^a	milk fat
hexanoic	caproic (Co)	6:0	-4 ^a	milk fat, coconut oil
octanoic	caprylic (Cy)	8:0	16.7 ^a	milk fat, coconut, and palm kernel oil
decanoic	capric (C)	10:0	31.3 ^a	milk fat, coconut oil
dodecanoic	lauric (L)	12:0	43.5 ^a	coconut, and palm kernel oil
tetradecanoic	myristic (M)	14:0	54.4 ^a	milk fat, coconut, palm kernel, herring, and nutmeg oil
hexadecanoic	palmitic (P)	16:0	62.9 ^a	milk fat, coconut, palm, soybean, cottonseed, lard, tallow, and herring oil
9-hexadecenoic	palmitoleic	16:1	0.5 ^a	milk fat, fish, and whale oil
octadecanoic	stearic (S)	18:0	70 ^b	milk fat, lard, and tallow
9-octadecenoic	oleic (O)	18:1	13 ^b (+44 trans)	milk fat, peanut, sesame, soybean, olive, canola, corn, canola, and olive oil
9,12-octadecadienoic	linoleic (Li)	18:2	-5 ^b (+28 trans)	safflower, sunflower, soybean, canola and poppy seed oils
9,12,15-octadecatrienoic	linolenic (Ln)	18:3	-12 ^b (+29 trans)	herring and linseed oil
eicosanoic	arachidic (A)	20:0	75.4 ^a	milk fat and peanut oil

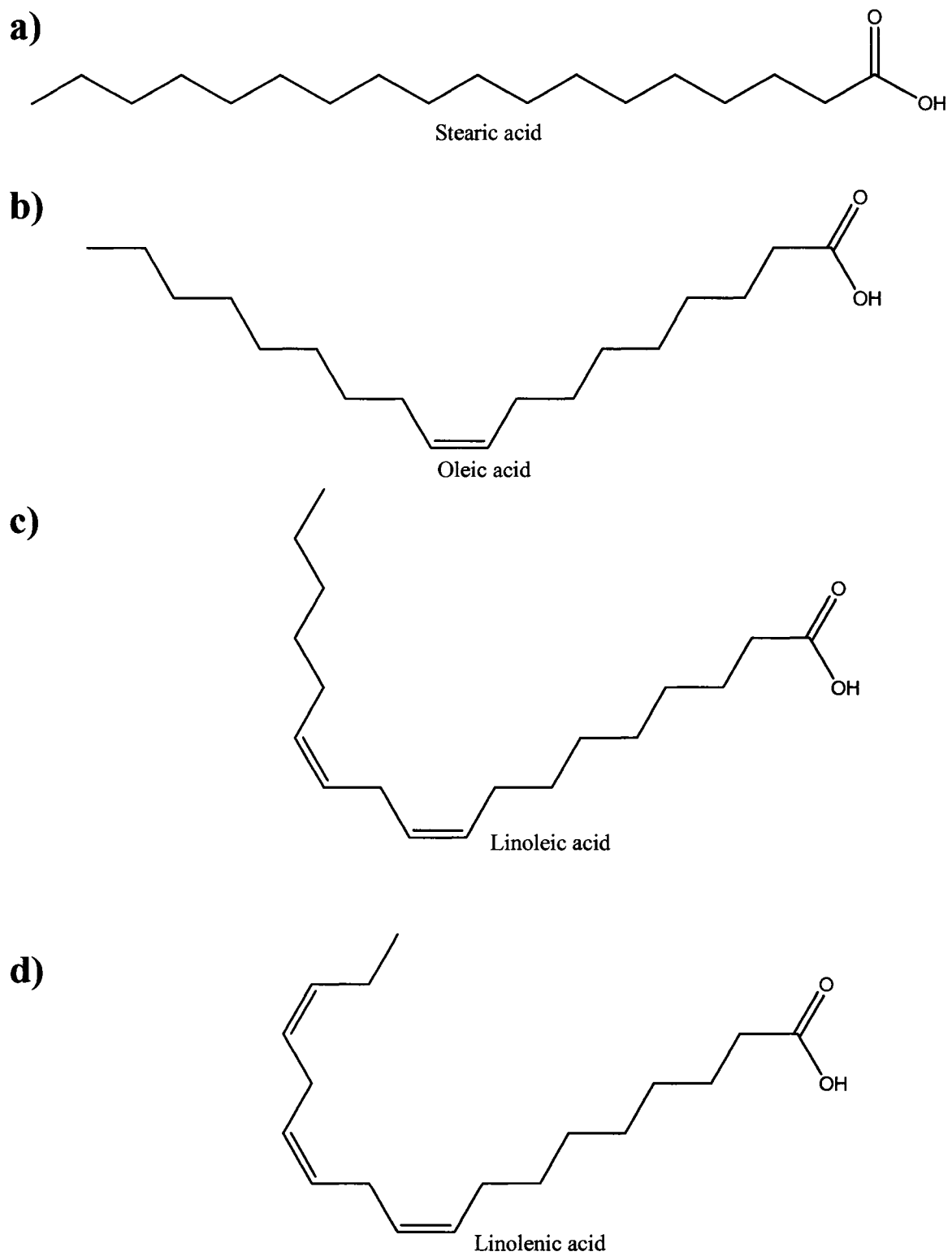


Figure 1.2: Chemical structures of a) stearic, b) oleic, c) linoleic, and d) linolenic fatty acids

in the fatty acid carbon chain (as shown in Figure 1.2 for the 18 carbon chain length fatty acids), the TAGs containing unsaturated fatty acids do not align easily to form tightly packed structures.

The melting points of fatty acids depend on the chain length of the fatty acid as well as the degree of unsaturation of the molecule (Table 1.1). For saturated fatty acids, the melting point increases as the chain length increases. The melting point of unsaturated *trans* fatty acids is greater than that of *cis* fatty acids of the same chain length, with this difference being as large as 20 °C for corresponding structures. The melting characteristics of TAGs depends on the composite fatty acids and their positions on the glycerol backbone.

1.2.2 *Function of Lipids*

Fats are an important component of many food products as they contribute to the mouth feel (texture and lubricity) and volatility of the flavor compounds of the food product [13]. Shortening formulations are used to shorten a baked good's gluten network to maintain tenderness and/or flakiness, structural integrity, aid in the incorporation of air, and to extend shelf life [18]. In chocolates and other confectionary applications, cocoa butter and other fats contributes to the “snap”. Vanaspati (or vegetable ghee) is a common product consumed in Iran, India, Pakistan, Egypt, Saudia Arabia, and Iraq and is used for cooking as well as the preparation of confections [19, 20]. Fats are also used for frying foods. MAGs are among the molecules often used as emulsifiers in food products.

This contribution will mainly discuss the structure and function of all purpose shortenings.

Fats and oils are also nutritionally important. The human body requires fats and oils as an energy supply, a source of essential fatty acids and to ensure the uptake of vital fat-soluble nutrients [16, 21]. Essential fatty acids are vital for growth, building cell walls and aid in the construction of phospholipids [16, 21]. Essential fatty acids also aid in lowering excessive cholesterol levels in the body, thereby decreasing the occurrence of cardiac disease. Stores of fat within the human body are important as they provide quick access to energy while fasting, act as insulation from hypothermia, and that surrounding the organs provides an internal layer of protective padding [16, 21].

The ingestion of fats however, must be done with moderation. It has been found that saturated fats lead to an increase in LDL cholesterol, the so-called “bad” cholesterol, which leads to coronary heart disease [8, 11]. *Trans* fats, introduced during partial hydrogenation (discussed below), causes an increase in LDL cholesterol while concurrently decreasing HDL cholesterol.

1.2.3 Sources of Edible Oils

There are three main sources of edible oils: plant, marine, and animal. Some common sources of edible oils are listed in Table 1.2. The composition of milk fat, a common animal fat, changes drastically throughout the year due to changes in animal

Table 1.2: Typical vegetable, marine and animal oils [16, 22]

Plant	Animal	Marine
Canola	Butterfat	Anchovy
Cocoa	Lard	Herring
Coconut	Tallow	Sardine
Corn		and other Fish
Cottonseed		
Olive		
Palm		
Peanut		
Rapeseed		
Safflower		
Sesame		
Soybean		
Sunflower		

feed and environmental conditions with each TAG varying up to 5% between summer and winter [16].

1.3 Lipid Modification

Edible oils are modified to change their TAG composition and thus their physical properties through the use of interesterification or hydrogenation. Blending an oil and a hard fat does not create a homogeneous mixture as fat is only partly soluble in oil [16]. Interesterification allows one to create a more homogeneous mixture of TAGs as the fatty acids of the hard fat are partly substituted with that of the oil and vice versa [16, 23]. Figure 1.3 shows a simplified diagram of random interesterification with the oil TAG having the fatty acids “A” and the hard fat having the fatty acids “B”. Given 50% AAA and 50% BBB in the starting mixture random interesterification, at equilibrium, will yield 12.5% of AAA, BBB, ABA and BAB [24]. The asymmetrical TAGs, AAB and BBA will be produced at percentages of 25% each [24]. In directed interesterification, the mixture is held above the melting point of the desired TAG as a crystallized TAG will not participate in the interesterification process, and the process will continue until there is a lack of components to produce the high melting TAG in the melt [16]. In addition to chemical catalysts, enzymes can also be used to cleave fatty acids from the glycerol backbone. There are two types of enzymes used for TAG modification; unspecific, and 1,3 specific (which does not cleave the fatty acid in the *sn*-2 position).

The oxidative and thermal stability of unsaturated oils can be improved through hydrogenation, which converts unsaturated fatty acids into saturated fatty acids.

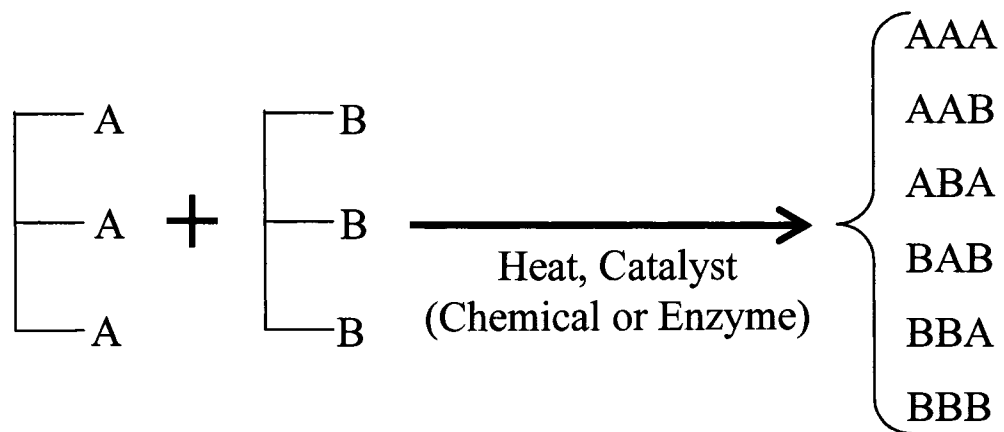


Figure 1.3: General equation for random interesterification

Hydrogenation is also used to increase the hardness of the fat and therefore is also referred to as “hardening” [16]. During hydrogenation, double bonds of the unsaturated fatty acids are converted to single bonds by the addition of hydrogen to the unsaturated bond of the fatty acid chain. The hydrogenation process requires both hydrogen and a catalyst, such as nickel, iron, platinum, and copper. A complex is formed with the catalyst at the double bond site and thus a hydrogen atom is able to form a complex with the double bond. A second hydrogen atom can then saturate the site of the former double bond, although it is also possible for the complex with the single hydrogen and the double bond to revert back to the double bond. There are many possible outcomes of hydrogenation:

- 1) Saturation of the double bond
- 2) Conversion of the double bond from *cis* to *trans*
- 3) Changing the position of the double bond on the fatty acid chain
- 4) No change, the double bond remains

Figure 1.4 illustrates outcomes 1 and 2 of the hydrogenation of Oleic acid (18:1).

Fats and oils which have been refined and purified are made into a variety of products, such as margarines, confectionary and coating fats, and shortenings, by blending oils, fats, and partially or fully hydrogenated oils and crystallizing the raw materials. This process, shown in Figure 1.5, is typically done with the aid of a scraped surface heat exchanger. The raw materials are melted and mixed prior to being cooled and sheared within the “A-unit”. Within the heat exchanger, the rate of shear, time spent within the crystallizer, and cooling conditions can be altered to accommodate a variety of

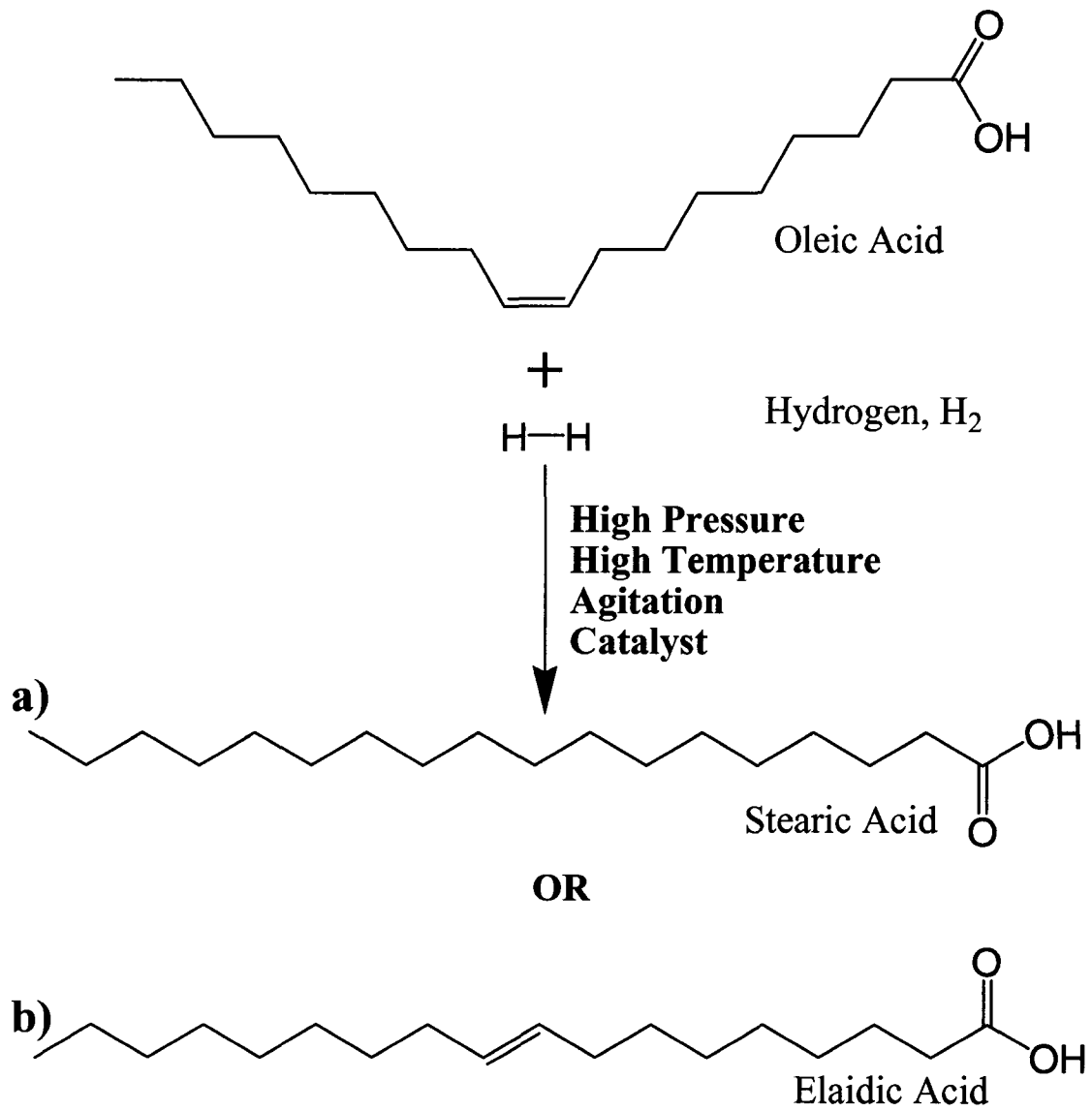


Figure 1.4: Possible outcomes for the hydrogenation of oleic acid a) stearic and b) elaidic acid

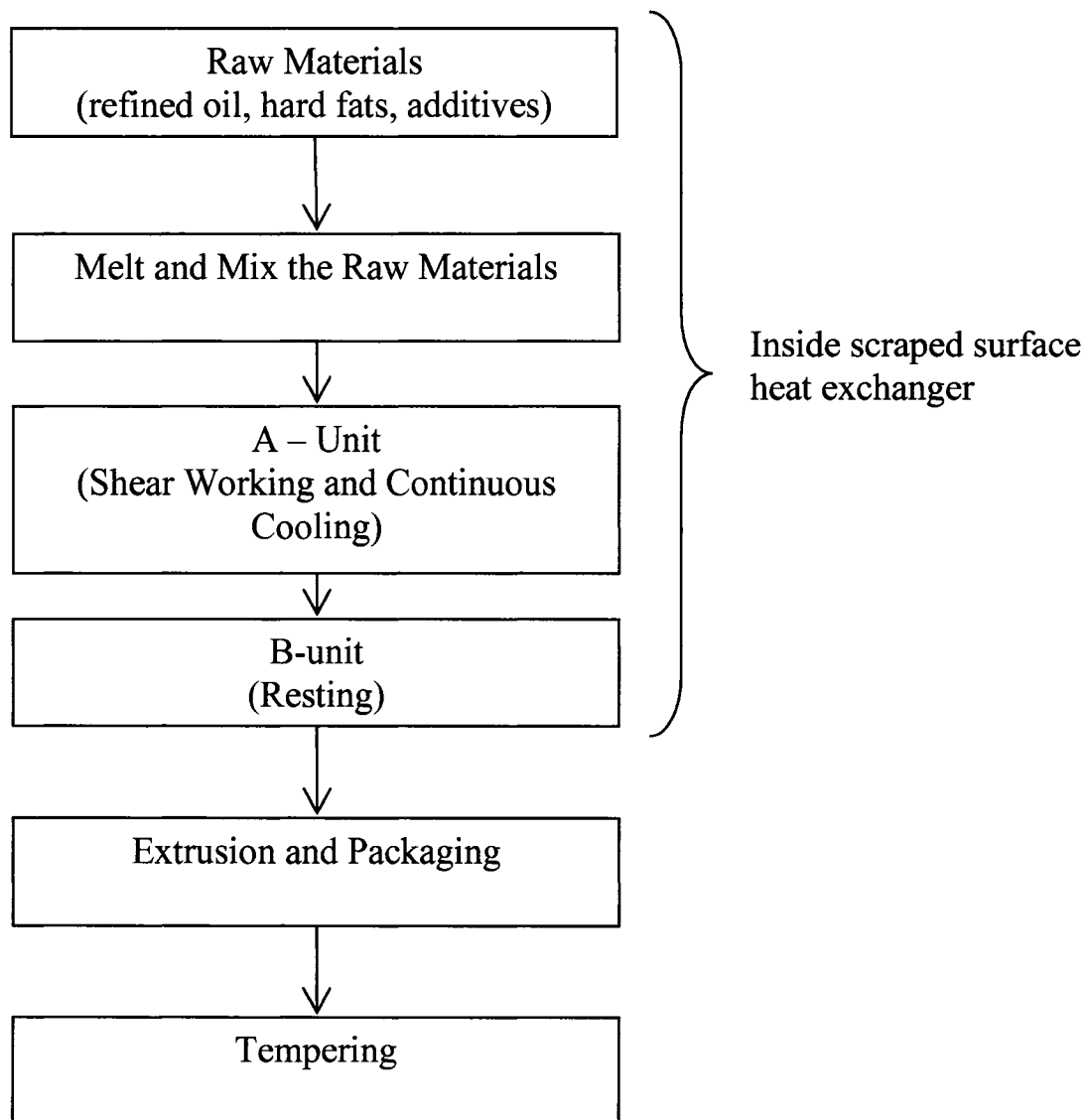


Figure 1.5: Crystallization procedure for shortenings and margarines

margarine or shortening type products. The crystallized material is then put into a “B-unit” or resting tube prior to packaging to allow for the low melting components of the shortening blend to be crystallized. After crystallization, the product is then tempered (for a number of days) to allow for the final crystal network to be developed and to allow for crystal ripening to occur.

1.4 Crystallization of Lipid Mixtures

In addition to diffracting X-rays, a crystalline material exhibits the first order transition: melting [18]. Crystallization is the transition from the melt to the solid state wherein the molecules in the melt pack to form a solid lattice [22]. TAG molecules closely pack and are held together by weak van der Waals forces when crystallized. The weak bonds in addition to the length and flexibility of the TAG molecules allows for crystallization in a variety of packing types or polymorphs to be created [22]. Clearly, given the variety of polymorphs and the wide range of TAGs in a margarine or shortening product, the crystallization of an edible oil is quite complex and many different crystals may be formed.

The lipid crystallization process can be divided into three processes which occur both consecutively and concurrently: nucleation, crystal growth, and crystal ripening. The flow chart in Figure 1.6 illustrates how these processes interact and form the final crystal network from the melt (adapted from Narine and Marangoni [25-27]).

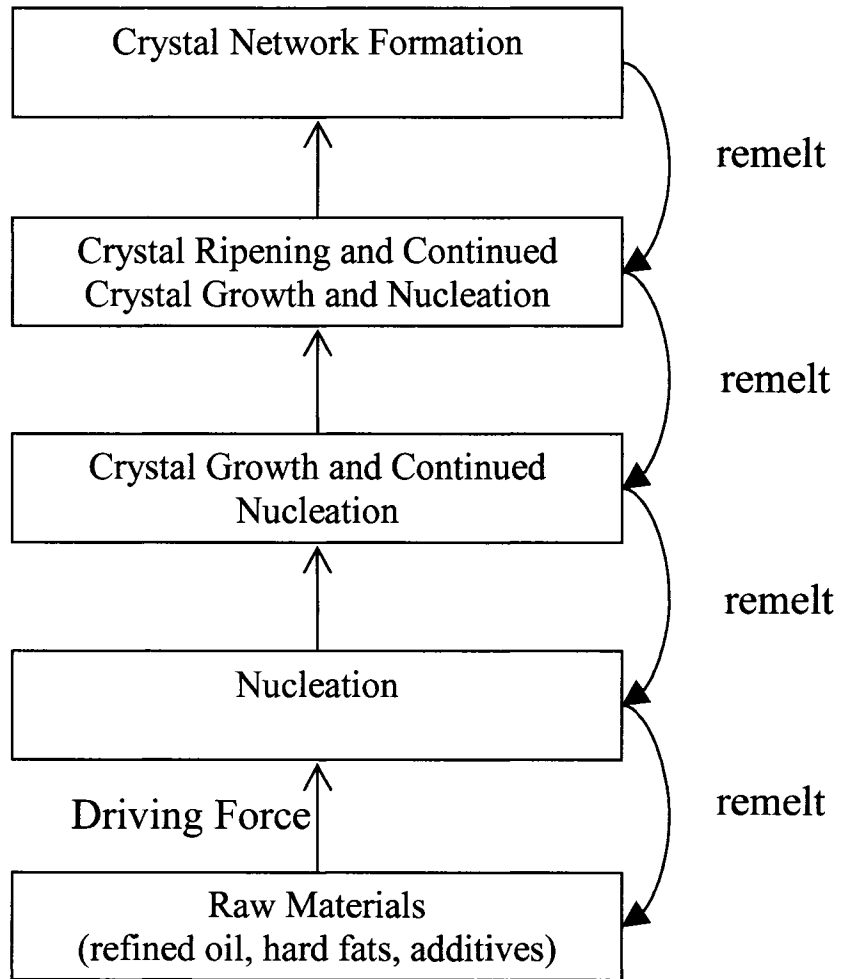


Figure 1.6: Lipid crystallization flow chart

The typical industrial crystallization process begins with a collection of molecules in liquid state. The molecules within the melt have kinetic energy and thus move throughout the melt, their movement hindered by viscosity and other mass transport limitations. As a thermodynamic driving force is applied, it is suggested that the molecules within the melt associate to form a lamellar structure with the fatty acids lining up with the neighboring fatty acids [22]. With a continued driving force, the lamellar structure becomes larger as the thermal energy of the entities within the melt is reduced. The increase in the size of the lamellar structure can be supported by the increase in viscosity noted upon cooling the liquid fat as shown in Figure 1.7 for a cocoa butter alternative [28].

Further cooling of the melt to below the melting temperature (or the application of another driving force) of the sample will induce nucleation, the precursor to crystallization, in which the alkyl chains of the TAGs in the lamellar structure orient and become a stable, ordered, solid structural entity referred to as a crystal.

1.4.1 Nucleation

There is an energy barrier to the formation of a crystalline material [14, 22, 29]. Therefore, the first step for crystallization, primary nucleation, requires a driving force to overcome the energy barrier. There are two possible driving forces for nucleation, either supersaturation or supercooling. Supercooling is the difference ($T_M - T$), where T_M is the melting temperature (or beginning of melt for a complex sample) and T is the

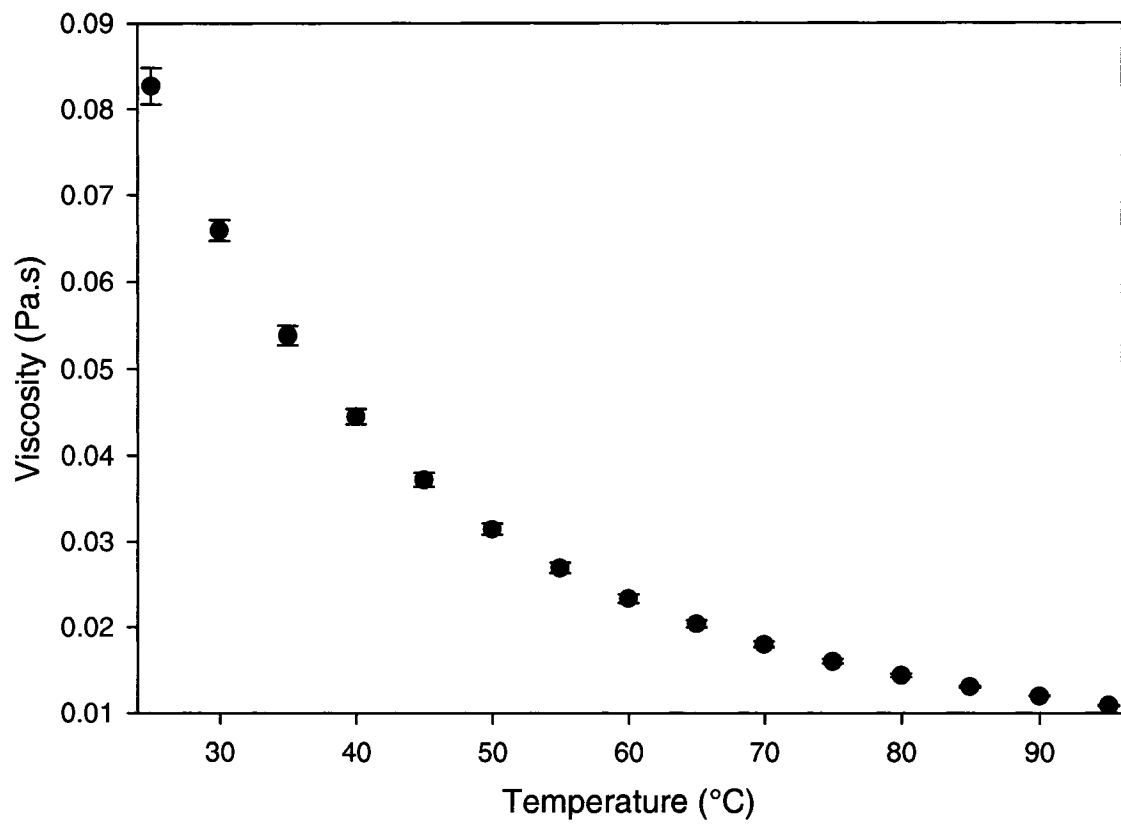


Figure 1.7: Viscosity of a cocoa butter alternative as a function of temperature

crystallization temperature. The driving force is then the difference in the energy potential ($\Delta\mu_{melt}$):

$$\Delta\mu_{melt} = \Delta H \frac{T_M - T}{T_M} \quad (1)$$

where the enthalpy of fusion is given by (ΔH).

A supersaturated solution has more of a component in it than can be theoretically dissolved in the solution at a given temperature. The supersaturation ($\ln\beta$) depends on the fraction of solute in the solution (C_s), and the amount of solute in the saturated solution (C) where:

$$\ln\beta = \ln\frac{C}{C_s} \quad (2)$$

The supersaturation driving force is the difference in chemical potential ($\Delta\mu_{sol}$) between a supersaturated and saturated solution. For ideal solutions, $\Delta\mu_{sol}$ is a product of $\ln\beta$, the universal gas constant (R_g) and the temperature (T) and is given by:

$$\Delta\mu_{sol} = R_g T \ln\beta \quad (3)$$

Nucleation occurs upon the formation of a nucleus of a certain stable critical size from the molecules in the liquid. However, as mentioned above, there is an energy barrier to nucleation as the growing crystal will mean a growing crystal surface area. The components on the surface of the growing crystal require a higher energy to offset the forces of the nearest neighbors within the crystal; this energy is called the free surface energy, or surface tension. Classical nucleation theory gives the energy barrier as the

Gibbs free energy (ΔG), the sum of the change in the surface free energy ($\Delta G_s = \sigma$) and the change in the free energy of the system per unit volume (ΔG_v) [14]:

$$\Delta G = \Delta G_s S + \Delta G_v V \quad (4)$$

where, assuming a spherical nucleus of radius r , the volume (V) and the surface area (S) of the ordered domain are given by:

$$V = \frac{4}{3} \pi r^3 \quad (5)$$

$$S = 4\pi r^2 \quad (6)$$

Combining Equations 4, 5 and 6 and $\Delta G_s = \sigma$, Equation 4 becomes:

$$\Delta G = 4\pi r^2 \sigma + \frac{4}{3} \pi r^3 \Delta G_v \quad (7)$$

For a nucleus of critical size ($r = r^*$), ΔG is at a maximum. Thus, differentiating Equation 7, one can find r^* :

$$0 = 8\pi r^* \sigma + 4\pi (r^*)^2 \Delta G_v \quad (8)$$

therefore,

$$r^* = \frac{-2\sigma}{\Delta G_v} \quad (9)$$

Substituting Equation 9 into Equation 7 the activation free energy for nucleation is:

$$\Delta G^* = \frac{16\pi\sigma^3}{3\Delta G_v^2} \quad (10)$$

The free energy change of the unit volume of the system can be expressed in terms of $\Delta\mu$, and the molar volume (V_M):

$$\Delta G_v = \frac{-\Delta\mu}{V_M} \quad (11)$$

Thus, combining Equations 1, 10 and 11:

$$\Delta G_{melt}^* = \frac{16\pi\sigma^3 (T_M V_M)^2}{3(\Delta H \Delta T)^2} \quad (12)$$

Also combining Equations 3, 10 and 11:

$$\Delta G_{sol}^* = \frac{16\pi\sigma^3 V_M^2}{3R_g^2 T^2 (\ln \beta)^2} \quad (13)$$

Clearly, an increase in either the supercooling or supersaturation of the system lowers the activation free energy for nucleation and therefore both are considered driving forces for the creation of liquid lamellae leading to the formation of nuclei of critical size.

The nucleation rate (J) gives the number of nuclei of critical size formed per unit volume per unit time. J is dependent on both the molecular collision frequency ($\frac{kT}{h}$, with h being Planck's constant and k is Boltzman's constant) and the molecular conformation and can be written as an Arrhenius-like activation energy equation:

$$J = \frac{NkT}{h} e^{\left(\frac{-\Delta G^*}{kT}\right)} \quad (14)$$

In addition to the free energy barrier to nucleation, the diffusion of molecules (diffusion) and the conformation (entropy) of molecules with respect to the growing nucleus also affect the nucleation rate. Supercooling, as well as crystallization, increases viscosity (Figure 1.7) and thus decreases molecular diffusion. The loss of entropy as TAG molecules form a nucleus is given by $\Delta H/T_M$. The probability that a fraction of the molecules (α) in the melt is in the correct conformation for participation in the surface of the nuclei is given by $e^{\left(\frac{\alpha\Delta S}{R}\right)}$. Since viscosity is a function of time and temperature, one may assume that α also takes into consideration viscosity barriers. Assuming the maximum collision frequency combined with the activation free energy for

molecular diffusion of a mole of molecules in the correct conformation to the growing surface of the nucleus (ΔG_D), leads to the Fisher-Turnbull Equation [14]:

$$J = \frac{NkT}{h} e^{\left(\frac{-\Delta G^*}{kT}\right)} e^{\left(\frac{-\Delta G_D}{kT}\right)} \quad (15)$$

where N is Avogadro's number. Fisher and Turnbull [30] proposed their model (Equation (15)) from studies on the germination of drops of a liquid in a gas [31, 32] for the homogeneous nucleation of a solid in a liquid.

Additives and impurities, such as other ingredients in the fat mixture (i.e. emulsifiers and water) and items added to alter the crystallization (i.e. seeding the nucleation of cocoa butter) alter the nucleation of the lipid. Additives can act as an ordering component to arrange molecules within an emulsion or a physical barrier between nucleating entities thereby inhibiting nucleation [33]. Additives act as a surface for heterogeneous nucleation either lowering or increasing the activation free energy for nucleation [22]. Thus the required supersaturation or supercooling for nucleation to occur is reduced or increased accordingly. ΔG^* for heterogeneous nucleation depends on the wetting angle (θ) between the nucleus, the particle (impurity), and the liquid phase. Assuming that the surface of the catalyst is flat and that the nucleus is a semi-sphere, ΔG^* for heterogeneous nucleation:

$$\Delta G^*_{het} = f(\theta)\Delta G^* \quad (16)$$

where [14]

$$f(\theta) = \frac{1}{4}(2 + \cos \theta)(1 - \cos \theta)^2 \quad (17)$$

Temperature and supersaturation, being the driving forces for nucleation, are clearly factors which influence nucleation. Other influencing factors include cooling rate, viscosity, and shear rate. Cooling rate affects the viscosity, which in turn with shear rate affects the mass transfer within the sample. It has been shown that the cooling rate (r') affects the structural order of a crystallized sample which in turn influences the final properties of the lipid network, as illustrated in Appendix 2 [28]. Faster cooling rates during non-isothermal crystallization result in a higher degree of cooling than slow cooling rates at any point in time during the cooling process, as shown (Figure 1.8). When a lipid sample is cooled quickly, the system crystallizes before the optimal spatial organization of the molecules is reached due to insufficient mass transfer rates. Conversely, during slower cooling rates, mass transfer rates are increased (due to lower viscosity and longer induction time prior to solidification) and the organization of the molecules occurs faster and to a greater extent [34-37]. The rate of cooling may cause changes in the growth mode of the network, and can lead to polymorphic, microstructural, and solid fat content changes, and therefore changes in the final physical properties of the network [38, 39].

When the final crystallization temperature is close to the melting temperature, if one compares low cooling rates to high cooling rates of the same lipid ensemble, regardless of the speed of the temperature decrease, at the point that the crystallization temperature is achieved, the effective supercooling is relatively the same. Thus, if $T_M - T$ is small, regardless of the speed at which this difference is achieved, the supercooling remains relatively unchanged. Therefore, if the crystallization temperature

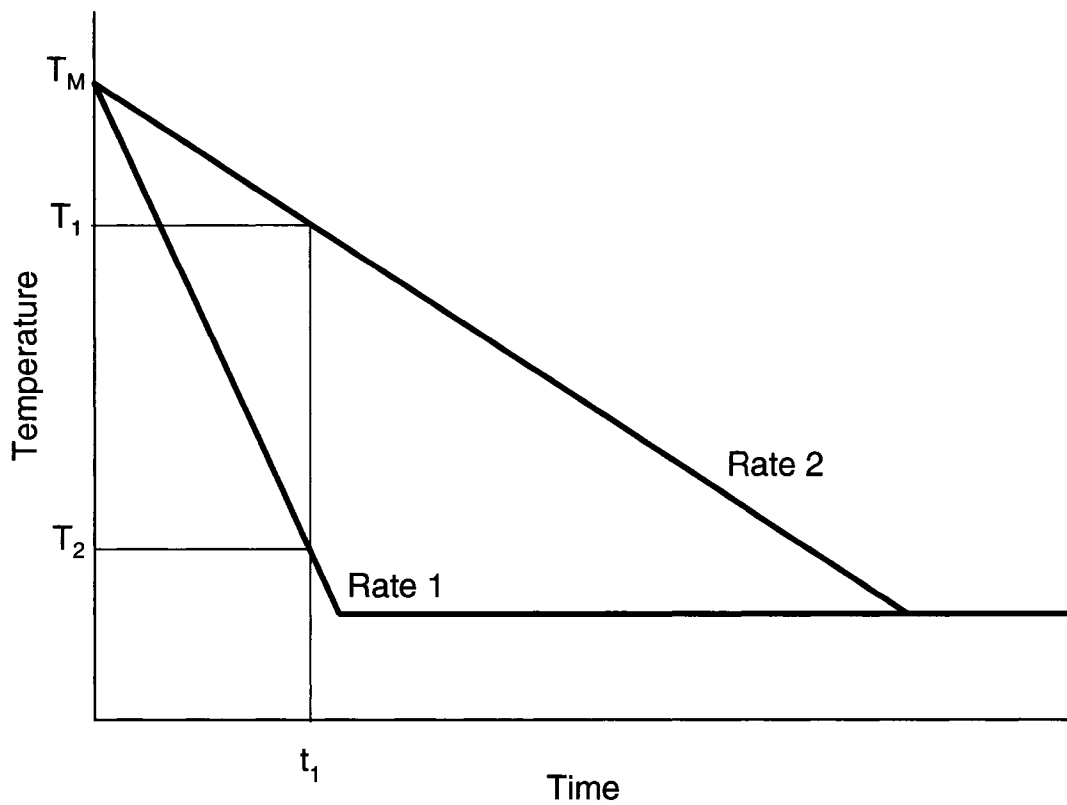


Figure 1.8: Effect of rate of cooling on the supercooling of a sample

is sufficiently high one would have increased the viscosity (and therefore decreased the mass transfer of molecules in the melt) faster due to an increased cooling rate while providing a relatively small increase in thermodynamic driving force. Under such conditions it will take longer for mass transfer to occur prior to crystallization, resulting in a depression of the onset of crystallization.

1.4.2 Crystallization

After the occurrence of primary nucleation (the first nuclei to appear in a melt), crystallization, secondary nucleation and remelt are all potential outcomes for the lipid sample. Unlike nucleation which requires a driving force, the crystallization process is spontaneous given that the temperature does not exceed T_M , and that the building blocks for a lipid crystal (the TAGs) are still available at the nucleus. In fact, the main factor for crystal growth is the efficient removal of the heat of fusion, which is quite high for lipids [18]:

$$\frac{\Delta H}{kT_M} \approx 60 \quad (18)$$

Other factors affecting continued crystal growth include mass transfer to the crystallization site (governed by viscosity, and shear), existence of additives or impurities (which might impede or improve crystallization) and growth mode.

The types of nuclei formed, and the density of the crystals within a unit volume also affect the crystallization of the sample. The nuclei formed will have a number of surface dislocations, so called “kink sites”, at which liquid TAGs incorporate during the crystallization process [40]. Slow crystallization will occur if the nuclei have very few

kink sites available for further growth. The nuclei type can be controlled through the use of seed crystals, a common method in cocoa butter crystallization. The number of growing crystallites within a unit volume also affects the rate of crystal growth as the growth centers compete for available liquid TAGs. A large number of crystals within a unit volume would also pose problems for further growth as the heat evolved during the crystallization of one crystal can potentially melt its nearest neighbors.

Thus the rate of crystal growth is affected by molecular conformation, surface defects, shear rates (macro and microscopic), molecular diversity, impurities, mass and heat transfer, and viscosity of the liquid fraction of the lipid.

During crystal growth, if the conditions for nucleation persist, nucleation will continue. Re-melt, due to the heat of crystallization or the bulk temperature of the lipid, is also a possible action within the lipid.

The crystal growth process is deemed to end when the crystal aggregates begin to touch. At this point, any additions to the solid network are referred to as crystal ripening. Often the final solid fat crystal network formed has solid bridges between the individual fat crystals as they are “sintered” together [17, 18].

Clearly, with the number of factors influencing nucleation and crystallization, one can see the advantage of utilizing a scraped surface heat exchanger to control crystallization and aid in heat and mass transfer in the crystallizing sample. In addition,

the crystal ripening process, which can take a number of days to complete, is aided by careful storage of the product at a given temperature, a process called tempering.

1.4.3 Monitoring Lipid Crystallization

There are a variety of methods used to monitor lipid crystallization in an effort to gain more knowledge of the final crystal network formed as well as the process through which it was formed. These methods include, but are not limited to: differential scanning calorimetry, nuclear magnetic resonance, x-ray diffraction, microscopy and texture evaluation.

Differential scanning calorimetry (DSC) is used in the study of lipid crystallization to monitor the heat evolved during both the crystallization, and melting processes. The enthalpy of crystallization and of melt curves provides a significant amount of information about the crystallization process. The enthalpy of the event is given by the area under the curve. The start and end of the event are determined by the deviation of the curve from the baseline. The start and end of the event are an indication of the time (or temperature) span of crystallization and melt. The onset of the event has been described in many different ways by a variety of researchers [41, 42]. However, the onset of crystallization or melt is another indicator of the start of the event, with the onset typically being recorded after the first deviation from the baseline. The full width at half maximum (FWHM) of the event is another indicator of the time (or temperature) span of the majority of the event. The peak maximum is the temperature or time at which the bulk of the entities are crystallized or melted.

The solid fat content (SFC) of the crystallized lipid is typically determined via nuclear magnetic resonance (NMR)[43-46]. The change in SFC over time during the crystallization process can be monitored as well as the SFC at any single point in time. The induction time for crystallization can be estimated by the time at which the SFC of a crystallizing lipid sample becomes greater than zero. The induction time cannot be determined fully via NMR as small crystals may be present in the sample prior to solids being detected by the NMR [47]. The shape of the SFC versus time curve is indicative of the mode of crystal growth, and the crystal growth rate [47]. The Avrami model is used to determine the growth rate and mode from a crystallization curve [48-52]:

$$\theta(t) = \frac{F(t)}{F_{\infty}} = 1 - e^{-At^m} \quad (19)$$

where $\theta(t)$ is the relative crystallinity at time t , $F(t)$ is the absolute crystallinity at time t , F_{∞} is the final absolute crystallinity, A is the crystallization rate constant containing the nucleation and growth rates, and m is the Avrami index which elucidates information about the growth mode. In the case that the crystallization curve is not a sigmoid but rather a series of sigmoids or growth segments, a modified version of the Avrami model which takes into account variances in the growth curve is applicable [51]. Within the modified form of the Avrami model, the crystallization of the system is observed as a series of different crystallization events ($i = 1, 2, \dots, p$), each with its own A_i and m_i . Therefore, Equation 19 becomes:

$$\theta(t_i) = \frac{F_i(t)}{F_{i\infty}} = 1 - e^{-A_i(t-t_i)^{m_i}} \quad (20)$$

where $F_i(t)$ is the absolute crystallinity at time t , F_{∞} is the crystallinity at some time when the growth rate or the nucleation conditions change, and t_i is the induction time for the crystallization of the sample. The entire crystallization event can then be described by:

$$F(t) = \sum_{i=1}^p F(t_i) \quad (21)$$

where the total absolute crystallinity $F(t)$ is the sum of p individual crystallization steps (*i.e.* segments in the SFC (%) vs. time plot) [51]. In this thesis the number of crystallization segments and values of incubation times have been determined empirically using $\ln[-\ln(1-F)]$ versus $\ln(t)$ plots of experimentally determined SFC versus time data. No fitting was done for the plateau region as the SFC (%) changes are small and the system is close to being at solid – liquid equilibrium for the systems studied in this thesis.

The polymorphism, indicative of the type of molecular packing occurring, is most typically determined by x-ray diffraction (XRD). A change in the peak shape or position (of a diffraction profile) is indicative of a change in the polymorphism. The XRD spectral range is divided into the short spacing ($3.0 \text{ \AA} \leq d \leq 5.0 \text{ \AA}$) and long spacing ($d \geq 5.0 \text{ \AA}$) regions. The alpha (α) polymorphic form has a d value of 0.42 nanometers, the beta-prime (β') d value is within the range of 0.42 to 0.43 nanometers and 0.37 to 0.40 nanometers, and the beta (β) form has a d value of 0.46 nanometers [18, 22, 53]. The thermodynamic stability of the polymorphic forms increase from $\alpha \rightarrow \beta' \rightarrow \beta$ with β being the most stable polymorphic form. In addition to the packing information gained from the short spacings region of the XRD spectra, the long spacing region also illuminates information about the packing. The peaks in the long spacing region are used to calculate

the angle of tilt, θ , of the lamellar repeat unit using basic trigonometry. An increasing angle of tilt suggests that the layers of molecules within a repeating unit will become thinner and more tightly packed [53]. The lamellar layers will adhere more firmly to each other as a result of this close packing. This in turn suggests that the flexibility of the polymorphs will increase as the stability of the polymorph decreases (\downarrow flexibility, and \uparrow stability: $\alpha \rightarrow \beta' \rightarrow \beta$).

Polarized light microscopy can be used to elucidate the microstructure of the crystallized fat. With light microscopy one can see the structure of the crystal networks, not that of the individual crystals [54].

Cone penetrometry or force-displacement diagrams from constant speed penetration are a useful tool for determining the texture of a lipid sample [41]. The texture, or hardness, of a lipid sample is an indicator of the strength of the lipid network.

1.5 Lipid Phase Behavior

A phase is a domain homogenous with respect to chemical composition and physical state [55, 56]. Some natural fats are examples of systems of coexisting homogeneous domains; though not necessarily in equilibrium. The phases within a fat system may be categorized in terms of liquid/solid, polymorphic forms, and volume expansion upon crystallization of the fat. Because many physical definitions of a phase exist, it is important to define very carefully what is used as a phase in any particular study of lipids. For example, within the solid phase of a fat many different polymorphs

can exist, and within each polymorphic type there is a potential for many different microstructures. Therefore, clear definitions of what constitutes a phase are important in any particular study. The relationship and occurrence of phase change in a fat system is referred to as the phase behavior of the lipid. Phase behavior, such as that obtained through the study of the solid fat content (SFC), dilatometry, melting behavior, and/or polymorphism of a lipid sample, is important in optimizing production processes and maintaining production quality. It has been used in the past to predict important attributes such as mouth-feel and hardness in fat-containing food products. Studies of phase behavior also help to provide a better understanding of the ways in which fat blends interact; an important understanding as the large scale industrial production of shortenings, and other fat-containing products often requires blending of lipids from many different sources.

Phase behavior is commonly connected with the equilibrium mixture of liquid, vapor, and solid phases of a mixture of substances, as a function of temperature pressure and composition, and is therefore well represented by phase diagrams. Liquid-vapor pressure composition diagrams, as shown in Figure 1.9 describe the liquid-vapor equilibria of a binary mixture of substances, in this case, benzene and toluene at 20 °C (after Barrow [57]). The benzene-toluene system is commonly used to illustrate phase behavior as the system approximates an ideal system due to the molecular complementarities of the component substances. One can determine the composition of the liquid that gives rise to a given vapor pressure, as well as the composition of the vapor at the given pressure and temperature. The inverse is also true in the case when

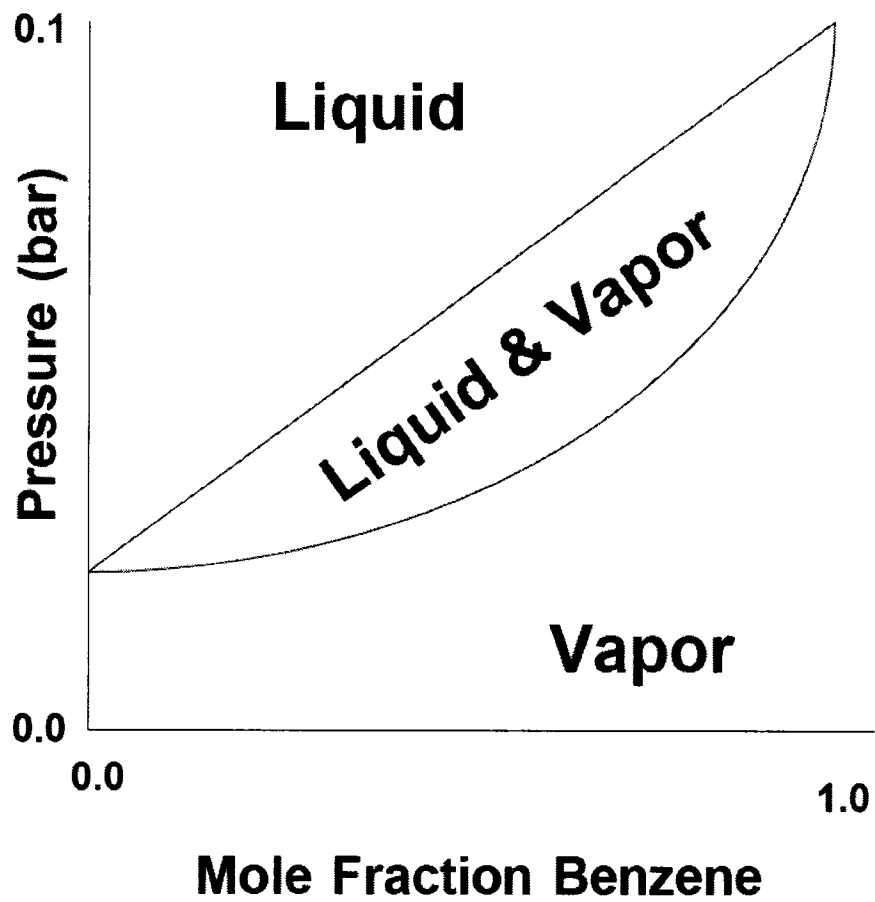


Figure 1.9: Ideal phase behavior of the benzene/toluene system

one knows the composition of the solution; one can find the vapor pressure of the solution and the composition of said vapor at a particular temperature. Thus, the phase behavior diagram imparts information as to the properties and states of the system composed of the two substances.

Also associated with the phase behavior is a phase rule which gives the relation between the number of phases (P), components (C), and degrees of freedom (Φ) [57]. The number of components is defined as “the least number of independently variable chemical species necessary to describe the composition of each and every phase of the system” [57]. The degree of freedom is described as “the least number of intensive variables that must be specified to fix the values of all the remaining intensive variables” [57]. The phase rule for a multi-component system is given as:

$$\Phi = C - P + 2 \quad (22)$$

For a one component system, the phase rule can be simplified to:

$$\Phi = 3 - P \quad (23)$$

1.5.1 Types of Phase Behavior

Many different types of phase behavior exist. The main classes are monotectics, eutectics, and peritectics [1]. Binary systems for which the melting points or boiling points of the solutions of differing compositions are not lower than the melting points or boiling points of either of the components are called monotectic systems (note that “solutions” are used here in both the solid and liquid sense). Eutectic, in Greek means “easily melted” [57] and indicates a melting point or boiling point lower for the solution

than that of the individual pure products in solution. Peritectics or “incongruent melting points” are seen in compounds which decompose upon melting into another solid instead of taking on a liquid form [58]. Given these definitions and the plurality of definitions of lipid phase behavior mentioned before, it is obvious that when one discusses a particular type (monotectic, eutectic, peritectic) of behavior for lipids, one must do so within the particular confines of the physical state being investigated. That is, solid-liquid phase behavior and polymorphic type phase behavior will mean different things in terms of a monotectic, eutectic, or peritectic.

Monotectic systems are those in which the components have similar melting points, molecular volumes, and polymorphic forms [1]. An example of a monotectic binary lipid system is 1-palmitoyl, 2-oleoyl, 3-stearoyl-*sn*-glycerol (POS) and 1,3-stearoyl, 2-oleoyl-*sn*-glycerol (SOS) [1]. Figures 1.10a and 1.10b illustrate monotectic binary systems. Figure 1.10a shows a monotectic continuous solid state phase diagram of a binary mixture of theoretical TAGs X and Y. The monotectic- partial solid solution phase diagram of the binary mixture of TAGs X and Y is shown in Figure 1.10b. Figures 1.10a and 1.10b differ in that the solid phase in Figure 1.10a is continuous and not differentiated, while in Figure 1.10b both the solid and liquid phases are differentiated, in that one can define a partial solid/liquid phase as well as differentiate the type of solid that exists at various compositions (e.g. solid XY or solid Y). A solid solution exists for all compositions of X and Y in the lowermost region of Figure 1.10a. A true solid solution does not exist in Figure 1.10b as the lower left hand side region consists of a solid component Y dispersed in liquid X, and the lower right hand side region consists of

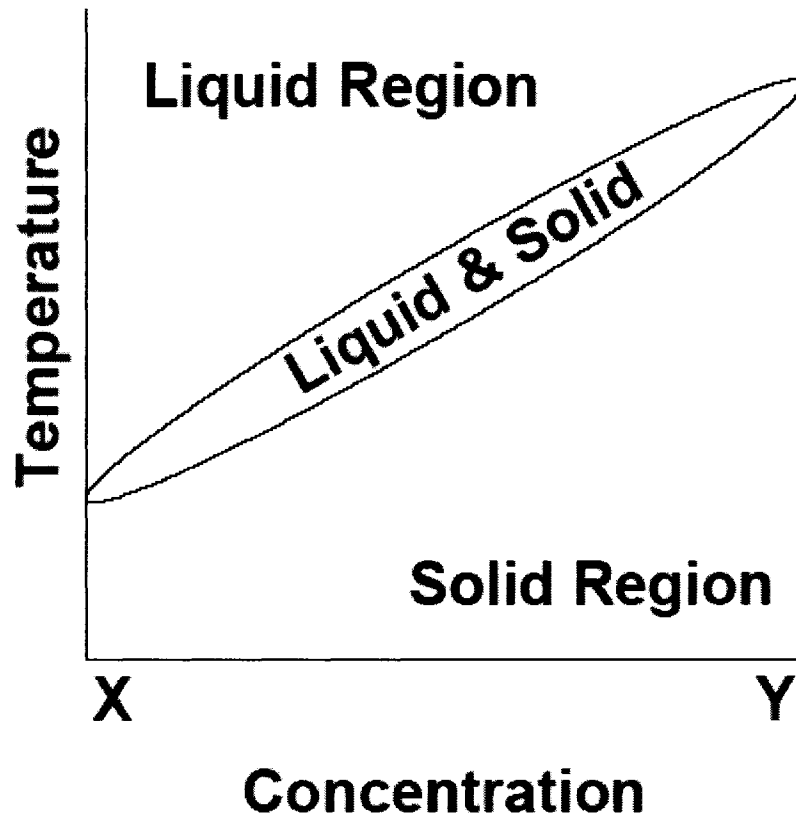


Figure 1.10a: Phase behavior of a theoretical monotectic system

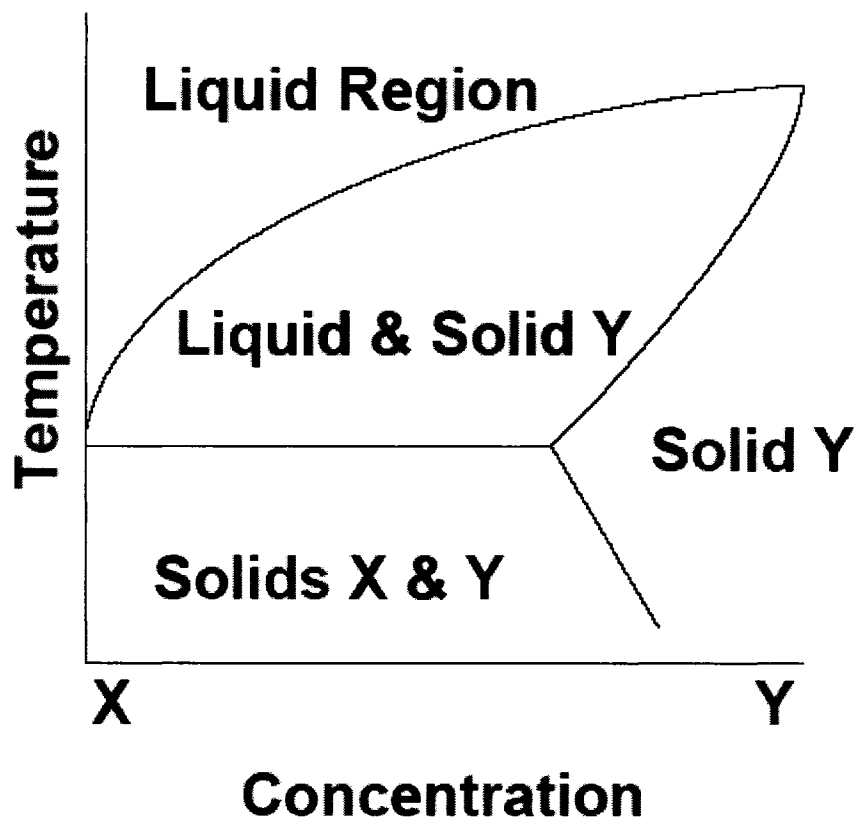


Figure 1.10b: Phase behavior of a theoretical monotectic system with solid solution changing

purely solid Y. The mid-section in Figure 1.10a defines the temperature and composition constraints wherein both components, X and Y, exist in a mixture of liquid and solid forms. A similar region exists in Figure 1.10b; however, the solid portion is composed only of component Y. In each of Figures 1.10a and 1.10b, the uppermost region illustrates a region, defined by temperature and composition, where a solution of X and Y exist in liquid form.

The most common binary mixtures of TAGs which form eutectics are those with components which differ with respect to molecular volume, shape, and polymorph, and which do not vary drastically with respect to melting point [1]. Some examples of such systems are tri-palmitoyl-*sn*-glycerol (PPP) and tri-stearoyl-*sn*-glycerol (SSS), POS and 1,3-palmitoyl, 2-olyoyl-*sn*-glycerol (POP), and SOS and 1,2-stearoyl, 3-oyloyl-*sn*-glycerol (SSO) [1]. Figure 1.11 shows an example of a binary eutectic system for a mixture of TAGs X and Y. A liquid mixture of components X and Y exists in the uppermost region of Figure 1.11. The existence of a minimum point of the lower boundary line for this region indicates that the system represented is a eutectic. In the area to the left of this minimum point, towards a greater concentration of component X, there exists solid X within a binary liquid. To the right of the minimum point, component Y exists in a solid form within a binary liquid. TAG X can be found in solid form when the temperature and concentration conditions are within the range as indicated by the lower left hand portion of Figure 1.11. For a range of temperatures, as the sample approaches 100% Y, as illustrated by the lower right region of Figure 1.11, Y is present in pure solid form. Components X and Y coexist in solid form for lower temperatures as

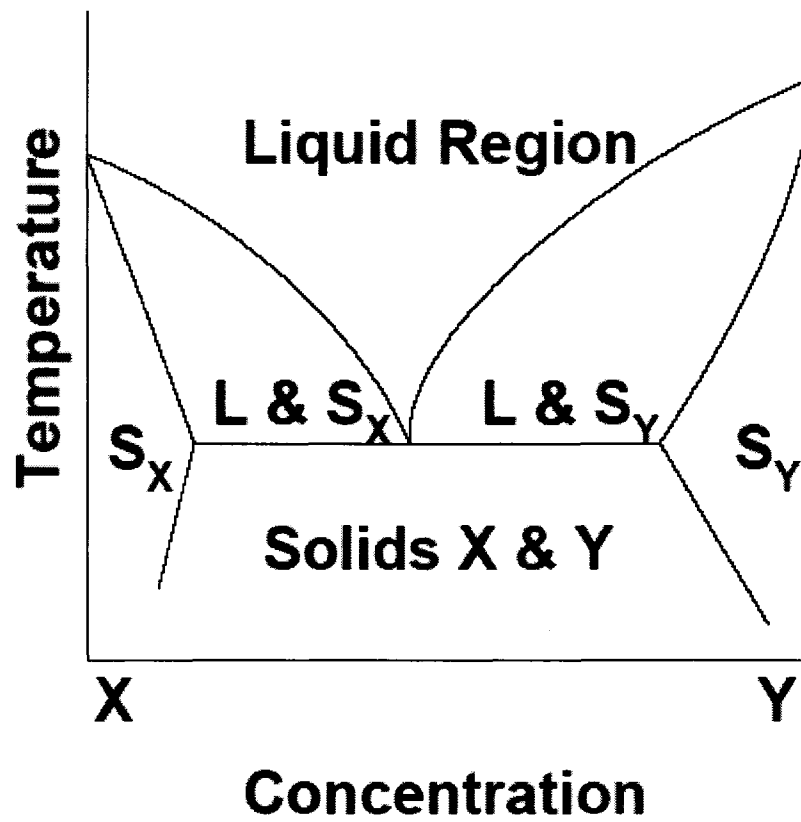


Figure 1.11: Phase behavior of a theoretical eutectic system

indicated by the bottom-most and central region of Figure 1.11. The eutectic behavior results in the liquidation of the mixture at specific compositions. This can be a catastrophic situation in lipid applications where hardness, texture, and SFC are important. However, it is also beneficial when one wants to avoid crystallization.

Peritectics normally occur in mixed saturated – unsaturated systems with at least one TAG which has two unsaturated fatty acids [1]. Figure 1.12 shows an idealized binary peritectic system of the theoretical TAGs X and Y. These TAGs, X and Y, exist in solid form in the lower left and right sides of the graph respectively. In the lower mid-region of Figure 1.12, components X and Y exist in solid form without exclusion. Component X also exists in solid form, but within the binary liquid in the region to the left of the graphs at temperatures above the region where solid X exists exclusively. For temperatures higher than those in which component X exists as a solid, X exists as a liquid, either concurrently with solid Y or with liquid Y.

1.5.2 Ideal Solubility Behavior

Since the phase behavior of any particular mixture of substances is related integrally to the degree of intersolubility of the components in the mixture, ideal solution behavior is briefly discussed here. The melting temperature of blends of solid TAGs have been found to be independent of the nature of any liquid oils present in the blend if the liquid oils do not participate in crystallization [59]. The solubility effects of a lipid mixture are important as they affect the crystallization behavior of TAGs, and hence the phase

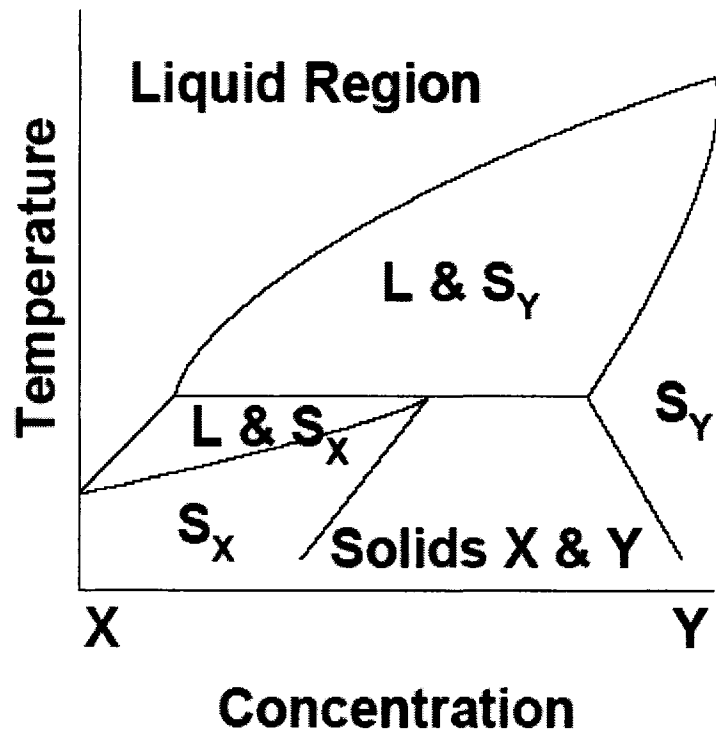


Figure 1.12: Phase behavior of a theoretical peritectic system

behavior of the TAGs in the mixture. The ideal solubility behavior of a binary lipid mixture can be predicted by the Hildebrand equation [59, 60]:

$$\log_{10} X = \frac{\Delta H_f}{R} \left(\frac{1}{T_m} - \frac{1}{T_b} \right) \quad (24)$$

where X represents the mole fraction of the higher melting component, ΔH_f the enthalpy of melt for the higher melting component (in J/mol), R is the universal gas constant (8.314 J/mol K), and T_m and T_b are the melting temperatures of the higher melting component and the blend (in K) respectively. For those binary mixtures which demonstrate ideal solubility behavior, it is clear that the solid-liquid boundary at various compositions can be established by application of the Hildebrand equation. Furthermore, it is clear that binary mixtures which demonstrate ideal solubility behavior would produce a straight line plot if $\log_{10}X$ is plotted against $1/T_b$. This therefore can become a predictive equation for phase behavior if it is known *a priori* that a binary mixture forms an ideal solution. Furthermore, for binary lipid mixtures that demonstrate a straight line plot of $\log_{10}X$ versus $1/T_b$ for only a limited range of X, over that range, the Hildebrand equation becomes predictive of the phase behavior of the sample. In practice, the higher melting component may actually be an ensemble of TAGs, rather than a single molecular species. In this case, many researchers tend to use the onset of melt of the ensemble, or the melting maximum of the ensemble as determined by Differential Scanning Calorimetry (DSC) as T_m and utilize a weighted mean molecular mass of the ensemble to determine X. ΔH_f is also an experimentally determined value usually based on DSC data. In this manner, the practicability of the Hildebrand equation can be extended to those blends which are primarily of a high melting ensemble of molecules and a low melting

ensemble of molecules, such as the blending of a hydrogenated fraction with a base oil, as is done in the manufacturing of many shortenings and margarines.

TAGs found in North American vegetable oils are typically those containing C16 and C18 fatty acids. It is claimed that these TAGs obey the Hildebrand solubility equation which is also known as the ideal solubility law [60]. However, work by Humphrey *et al.* [61] has pointed to the formation of mixed crystals with C16:0 and C18:0 mixed TAGS. Deviations from ideality can occur at high solvent to solute ratios as the change in volume increases the entropy of mixing during melting [60]. As well, solid solutions or the formation of imperfect crystals can also cause derivations from ideality as imperfect crystals have greater solubility than perfect crystals.

1.5.3 Lipid Phase Behavior Determination

The phase behavior of lipid systems has been researched by many [1, 2, 4, 59-78]. The methods used by researchers to produce phase diagrams include: SFC to produce iso-solid lines, liquid-solid phase diagrams, polymorphism phase diagrams and iso-dilatation lines.

1.5.3.a Solid Content

The SFC of a fat system is the amount of solid fat as a percentage of the total fat present. Pulsed-NMR is one popular method used to determine the SFC of a fat system at a series of temperatures after a given tempering scheme and is used often in the

creation of iso-solid phase diagrams. NMR provides an accurate measure of SFC ($\pm 0.5\%$ generally) given the time and temperature resolution of the instrument [1]. The generally-accepted procedure for SFC measurements to create iso-solid phase diagrams is to cool the fat sample at a desired rate to $0\text{ }^{\circ}\text{C}$ and hold at $0\text{ }^{\circ}\text{C}$ for 90 minutes prior to sampling the SFC [1]. The sample is then heated at a constant rate to $5\text{ }^{\circ}\text{C}$, and this temperature is held for 30 minutes prior to sampling the SFC. The temperature of the sample is continually increased in this manner by $5\text{ }^{\circ}\text{C}$ increments, holding for 30 minutes at each temperature. One problem with this series of measurements is that each change in temperature and each waiting time will affect the SFC of subsequent measurements. Thus, one must be precise in the temperature scheme used to heat the sample. Alternatively, one may choose to perform the measurements in parallel rather than in series, which eliminates the changes occurring within the fat as the temperature is stabilized at each measurement temperature. That is, samples would be cooled to $0\text{ }^{\circ}\text{C}$, held for 90 minutes and then heated to the required temperature directly. The SFC of a lipid sample can also be established via the use of DSC or dilatometry however, SFC determination via NMR is an American Oil Chemists' Society recommended practice [1, 79].

It is important to note here that SFC and solid fat index (SFI) are not interchangeable terms. The SFI of a lipid is obtained by dividing the dilatation by 25 [1]. This method assumes that all fats have the same total melt dilatation of a factor of 2500 and that the variation of dilatation with temperature is negligible. In fact, at $0\text{ }^{\circ}\text{C}$, the

total melt dilatation average factor is 2000 for a variety of fats, and the total melt dilatation depends on the particular fat sample as well as the cooling scheme [1].

1.5.3.b Melting Point

Data for liquid-solid phase diagrams can be obtained via the use of DSC, slip melting points, Mettler dropping points, and Wiley melting points. Currently, the most widely accepted and reliable method of obtaining the melting point of a fat is through the use of DSC. DSC measurements are taken by heating the fat sample at a constant rate (e.g. 5 °C per minute[28, 41, 61, 80], 2 °C per minute [70], or 0.2 °C per minute [4]), and determining the temperatures at which peaks occur. Decisions on appropriate heating rates relate to the resolution of the particular instrument as well as to the melting range of the lipid sample. Researchers have used both the onset of melt as well as the peak maximum as the melting point. Figure 1.13 shows a typical DSC melting curve, with the onset of melt and peak maximum indicated. These melting temperatures, which indicate the boundaries between phases, are then plotted against the composition of the fat sample (i.e. percent concentration in a binary lipid sample) [1, 70]. One of the disadvantages of using DSC measurements to construct phase diagrams is the assumption of a definite temperature at which the phase transition occurs [4]. In pure substances, it would be ideal if transitions occurred at one temperature rather than a temperature span but this is seldom the case. Finite sample size and instrumental effects contribute to the widening of the window within which the phase transition can occur [4]. Furthermore, and as is usually the case, the crystallized portion of the sample is composed of an ensemble of different molecules and a continuous variation of molecular compounds of differing

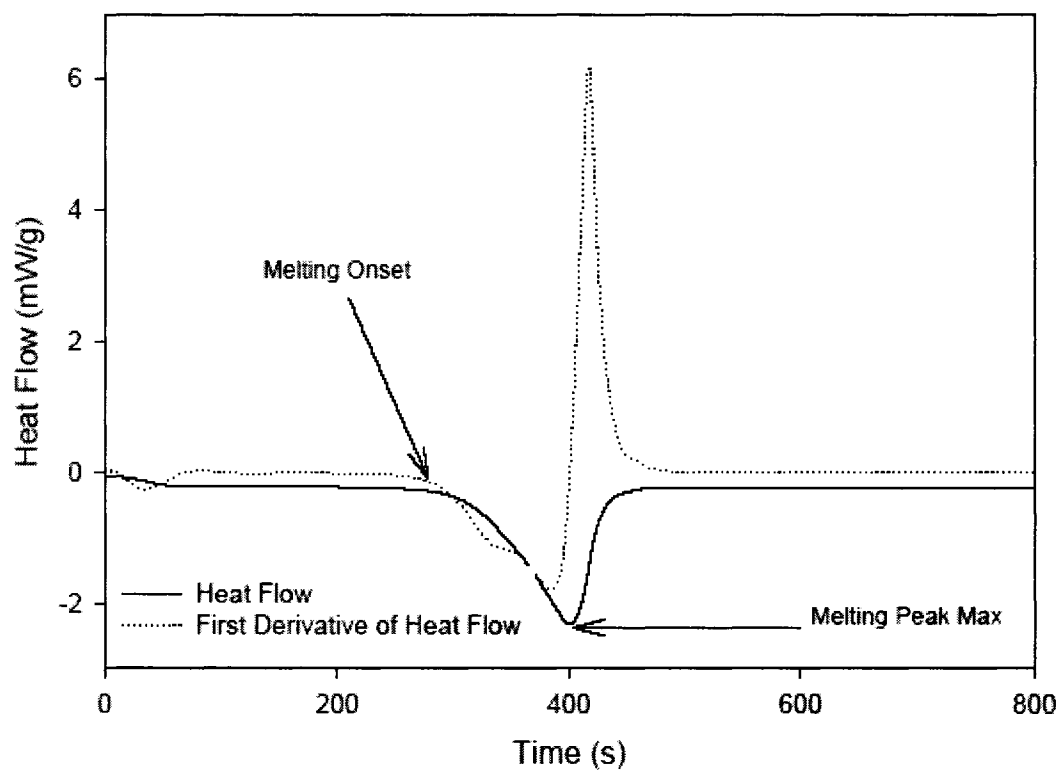


Figure 1.13: Enthalpy of melt curve and 1st derivative curve from DSC. The onset of melt and peak maximum is indicated by the arrows.

crystallization and melting temperatures, so that the “window” of crystallization temperatures in “real” systems can be widened significantly. Another complication is the possibility of formation of different polymorphs upon crystallization of the same ensemble of molecules with different polymorphs having variable crystallization and melting temperatures. Therefore the liquid-solid transition can be complicated significantly by these effects.

1.5.3.c Polymorphic Type

The phase changes caused by a change in the polymorphism of a lipid sample are usually measured with XRD, although infra-red vibrational spectroscopy [81-88], atomic force microscopy [89], and nuclear magnetic resonance spectroscopy [53, 90-96] have also been used. In order to find the polymorphic form of a sample for the purposes of creating a phase behavior diagram, where in this case, a phase is defined as the polymorphic type of crystal, the sample is tempered to 0 °C or lower, and then heated in 5 °C intervals at a constant rate [68]. The polymorphic form is determined and then plotted against the composition of the lipid blend. Polymorphism phase data are often included in liquid-solid phase diagrams along with the melting point data, such as in the case of Figure 1.10b.

1.5.3.d Volume Expansion

Dilatometry is used to determine the iso-dilatation lines of a fat sample, which imparts information on the rate of expansion versus temperature [65]. The dilatation tube

is constructed and filled as described by Jasperson and McKerrigan [65]. The tube itself is a U-shaped volumetric type tube with a 6-7 mL bulb which is sealed with a ground glass stopper with a convex bottom. The other arm of the U is a graduated (± 0.005 mL) capillary tube with a 2mm interior diameter. The bulb is filled with 1.5 mL of water which is carefully drawn up the capillary tube. When the fat is added to the bulb portion and stoppered, the lipid sample pushes the water up the tube. The filled tube is heated to above the melting point of the fat, and then allowed to cool to 4 °C overnight. To obtain the measurements for the dilatation curve, the dilatometer is immersed in temperature controlled water baths at intervals of 5 °C for 15-30 minutes beginning at 10 °C, and the height of the water in the stem of the tube is recorded at each temperature. Volume expansion of lipid samples, in addition to the error-inducing effects mentioned before, can be dependent on the rate of increase so that this rate must be kept carefully controlled to ensure that the crystal polymorphism and microstructure is grown along similar templates. For example, a faster rate of cooling may lead to a denser microstructure [97] thus resulting in a smaller volume expansion.

1.5.4 Studies in the Literature

Much investigation of the physical properties of lipids has been perfected using phase behavior studies. Many such studies on cocoa butter have been completed [1, 2, 68] (and others too numerous to list). One reason for the attention that cocoa butter receives is due to its industrial importance as a confectionery fat. Cocoa butter requires careful tempering to achieve desired results, so there are many efforts focused on finding suitable replacements for cocoa butter which do not require such careful treatment.

Loisel [68] and Minato *et al.* [70] have investigated the polymorphic phase transitions of cocoa butter and PPP-POP mixtures respectively. Knoester *et al.* [60] studied the solid-liquid phase behavior of TAGs containing palmitic and stearic acids, and Timms [77] used both solid-liquid behavior as well as iso-solid lines to study palm kernel oil, a lipid used as a cocoa butter replacement. Iso-solid diagrams were also used by Lambelet and Raemy [66] in their study of cocoa butter and milk fat fractions and by Rousseau *et al.* [98] in their study of the interesterification of butterfat. Marangoni and Lencki [69] extended the concept of iso-solid binary phase behavior to ternary phase behavior for milk fat fractions. Dilatation was used by Jasperson and McKerrigan [65] on the “natural fats”; cocoa butter, palm kernel oil, palm oil, lard, and tallow, and by Rossell [2] on the study of cocoa butter alternatives and mixtures of pure TAGs. Inoue *et al.* [4, 64] used both DSC and XRD data to create liquid-solid phase diagrams in the study of binary mixtures of palmitoleic, ascelepnic and *cis*-monounsaturated acids of varying omega chain length.

1.5.5 Constructing Lipid Phase Diagrams

In order to effectively study lipids using phase behavior techniques, one must be able to construct and correctly interpret a phase diagram. Liquid-solid phase diagrams and polymorphism phase diagrams are relatively easily constructed. The melting point and/or polymorphic form are plotted against the composition of the sample. If the DSC thermogram has more than one melting peak, the temperature of each peak maxima or onset is plotted. For each composition point, the highest melting temperature forms the liquidus line. At temperatures above the liquidus line, the entire sample is in liquid form.

The lower melting temperatures form the solidus line, below which the entire sample is solid. Between the liquidus and solidus lines, the sample is a solution of liquid and solid phases. XRD adds another dimension of information to the liquid-solid diagram. At any point on the phase diagram where a solid exists, the solid can be classified with respect to polymorphic form. Therefore, the region below the solidus line may be further subdivided, using polymorphic data from XRD, into its composite polymorphic forms if there is indeed a phase transition between forms occurring in the sample. The liquid may also exhibit some structural organization observable by XRD, and the liquid section may also be divided according to the organization that takes place at different concentrations and dilutions.

Phase diagrams containing iso-solid or iso-dilatation lines are not as easily created as the liquidus-solidus phase diagrams. There are three ways to construct iso-solid or iso-dilatation graphs. The first method consists in plotting the average of the actual results using a method for iso-dilatation lines outlined by Rossell [2]. A series of dilatation curves are drawn for measurements made at regular composition intervals. The number and size of intervals will affect the quality of the final iso-dilatation curve as too few measurements will cause the curves to be discontinuous, and potentially inaccurate. If one chooses too small an interval the measurements become very time consuming. A series of dilatation values are then chosen and the temperatures which give these dilatations are read off the dilatation curves. A plot is then made of these temperatures with respect to the composition, with each line representing a dilatation value.

A second, less time consuming and more easily reproducible method consists of using a quadratic interpolation, as previously described [75], to build iso-solid lines at specific percent SFC. The SFC is again plotted against temperature as shown in Figure 1.14 (in this case for fractions of milk fat). An equation to describe the SFC versus temperature curve is obtained using computer assisted quadratic or parabolic interpolation methods. A table of iso-solid temperatures for each sample is constructed and this data is interpolated in the same manner to find the temperature data at 1% composition intervals. The interpolated temperatures are then plotted against composition, with a line for each SFC value. Timms [99] has created a commercial program, IsoSol, that calculates the appropriate tables and interpolations seamlessly.

The third method also requires that the SFC be plotted versus temperature for each dilution, as in Figure 1.14. This graph can then be interpolated to obtain the necessary temperature to achieve given SFC using appropriate graphing software (i.e. GraphPad by Prism). A multiple line graph of temperature versus composition can be made, as in the method above with each line representing one SFC value [61].

1.5.6 Interpretation of Phase Diagrams

The phase behavior of a lipid sample can be illustrated by phase diagrams, be it liquid-solid, polymorphism, iso-dilatation, or iso-solid phase diagrams or a combination of these different forms. Phase diagrams impart a great deal of information about the lipid sample if they are correctly interpreted.

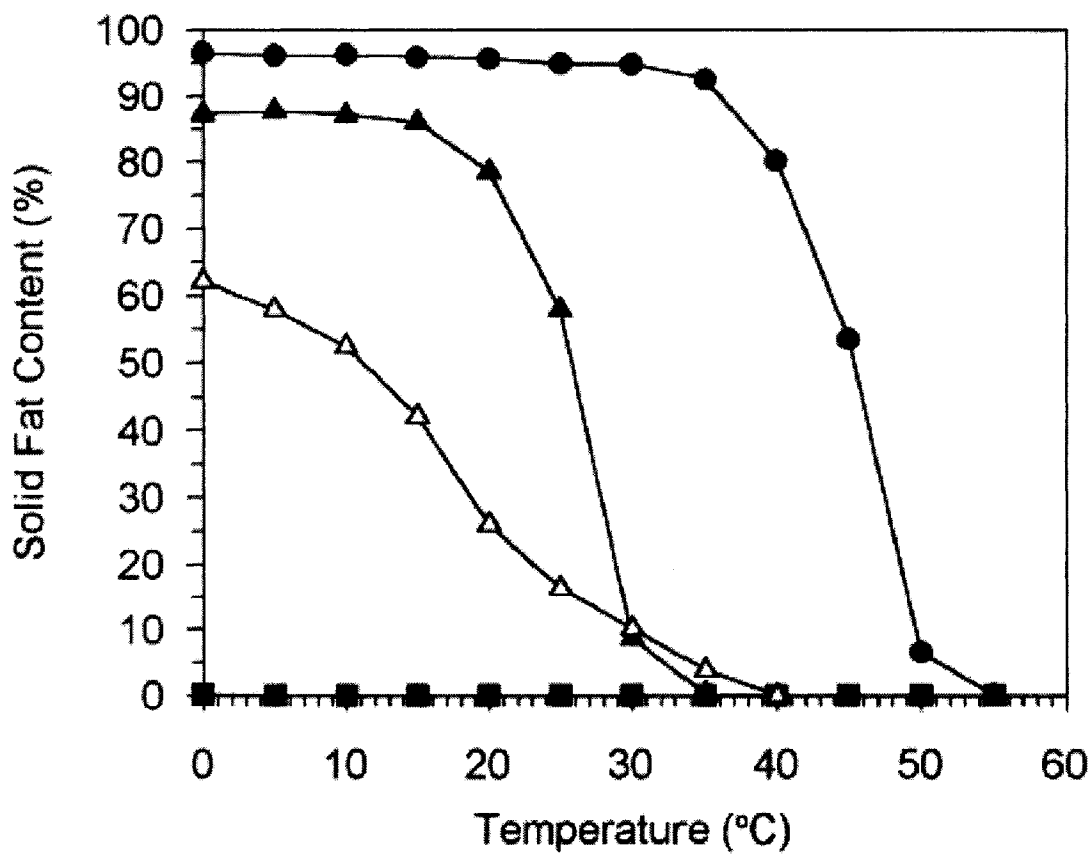


Figure 1.14: SFC versus temperature for varying fractions of milk fat. (■ represents LMF, Δ represents another LMF, ▲ represents MMF, ● represents HMF.)

Figure 1.15a shows a monotectic system of FHC in soybean oil. This monotectic is illustrated via a SFC versus composition graph. As the composition tends to 25% FHC in soybean oil, the SFC of the sample increases without any local maxima or minima. Thus, the samples exhibit ideal solubility behavior.

Solubility behavior can also be deduced from phase diagrams. The iso-solid phase diagram, Figure 1.15b, shows a ternary monotectic of high melting milk fraction (HMF) (5S), mid-melting milk fraction (MMF) (-28S), and low melting milk fraction (LMF) (-28L) at 30 °C. The nearly straight line of 10% SFC, parallel to the bottom axis, indicates ideal mixing behavior as predicted by the Hildebrand solubility equation [69]. Ternary phase diagrams are a relatively new addition to the study of lipid phase behavior as Timms stated: “No complete and reliable phase diagram for mixtures of more than two TAGs has been reported” [1]. However, ternary phase diagrams have been used extensively in the engineering sciences, and more recently in select lipid studies [100-111].

Figure 1.15c is an iso-solid diagram of HMF in MMF, with the bottom line representing 5% SFC, and the uppermost representing 90% SFC. As one moves up the graph the SFC value of the lines increases in 5% increments. There is an increasing trend as the composition of the sample tends to 100% HMF, with the minimum occurring at 0% HMF. There is no composition for which a given SFC occurs at a lower temperature than at 0% HMF, thus the system illustrated is a monotectic system.

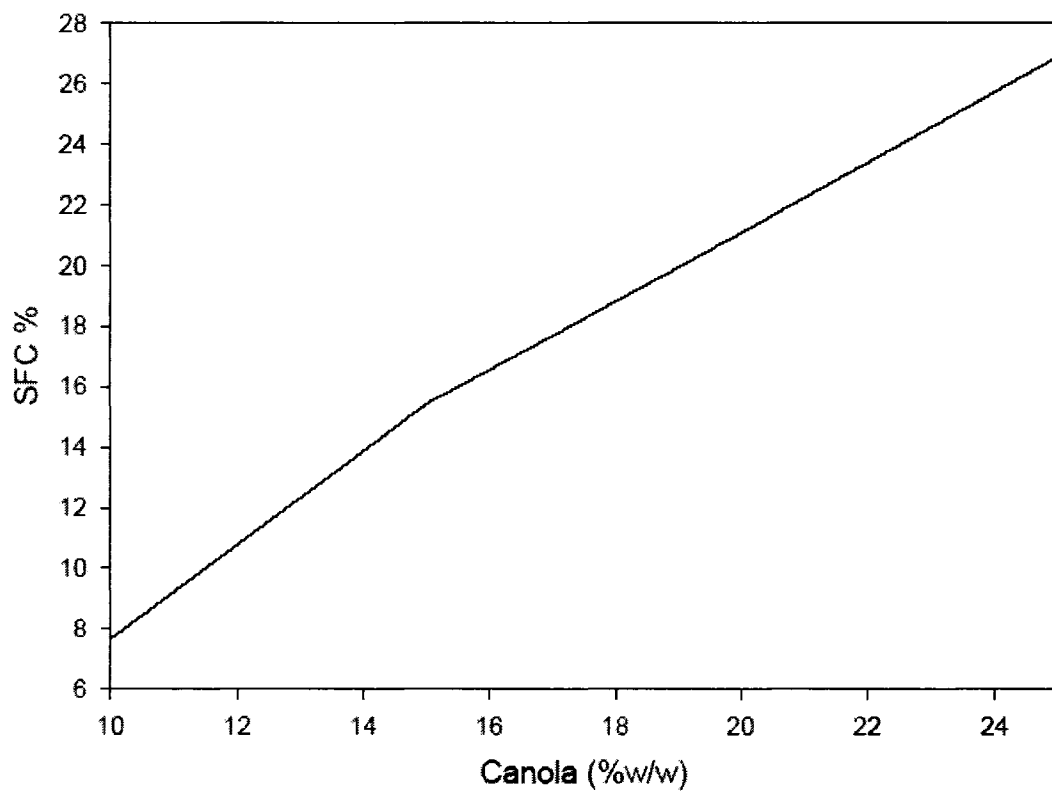


Figure 1.15a: Experimental binary monotectic of FHC in soybean oil via SFC

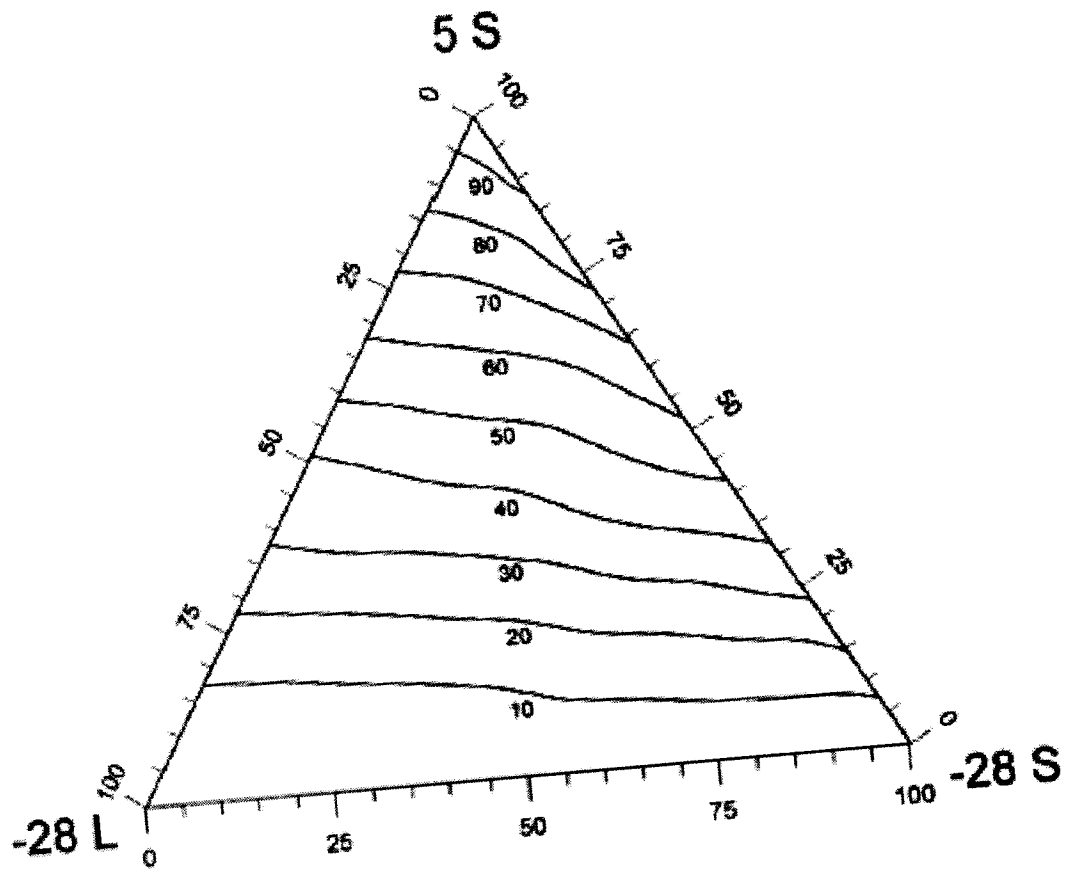


Figure 1.15b: Experimental ternary monotectic of HMF (5S), LMF (-28L), and MMF (-28S) at 30 °C via iso-solid lines [69]

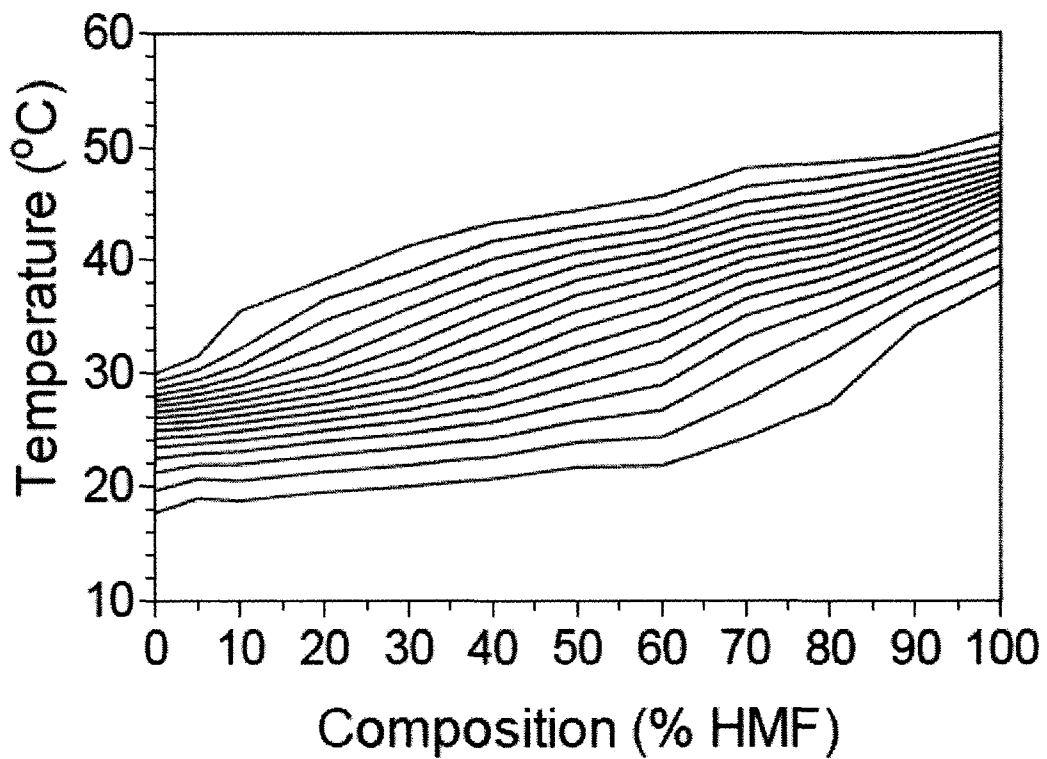


Figure 1.15c: Experimental binary monotectic of MMF and HMF via iso-solid lines.

The bottommost line represents 90% SFC, and subsequent lines decrease in increments of 5% to a minimum of 5% SFC as the uppermost line

Figure 1.16a is an iso-solid phase diagram showing the ternary phase behavior of HMF, MMF, and LMF at 0 °C. The eutectic in Figure 1.16a is distinguished by the lines which deviate from linearity (i.e. the 40% SFC line) which indicate a formation of solution intermediates between the three components [69].

Figures 1.16b and 1.16c are iso-solid diagrams. Figure 1.16b illustrates the phase behavior of the HMF in cocoa butter system. The bottom line represents 5% SFC, while the subsequent lines increase in 5% increments to 90% SFC. As the composition of the binary system approaches 100% HMF, the SFC lines increase in temperature. This trend is true for all but the six lowest iso-solid lines on the figure. These lines demonstrate no increase with %HMF until approximately 50% HMF. There is a noticeable decrease in temperature in the curves of iso-solid lines at approximately 70% HMF. This indicates that at these compositions and at an SFC range of 5 to 10% an eutectic exists. Furthermore, a second eutectic is presented at approximately 90% HMF by the lowermost five iso-solid lines in the figure. These curves indicate that the sample is slightly eutectic, more so than Figure 1.15c. Figure 1.16c illustrates the phase behavior of the MMF/cocoa butter system. The bottom line represents 10% SFC, while the subsequent lines increase to 90% SFC in 5% increments. Unlike, Figure 1.16b, Figure 1.16c has a minimum point for all SFC lines occurring between 40 and 60% MMF. This minimum point indicates a very strong eutectic. Due to the trend established in each of Figures 1.16c, 1.16b, and 1.16c, one might be tempted to conclude, as Timms did, that “no significant improvement in hardness of milk chocolate with hydrogenation and fractionation of milk fat was observed” [1]. In fact, while this statement is true in the

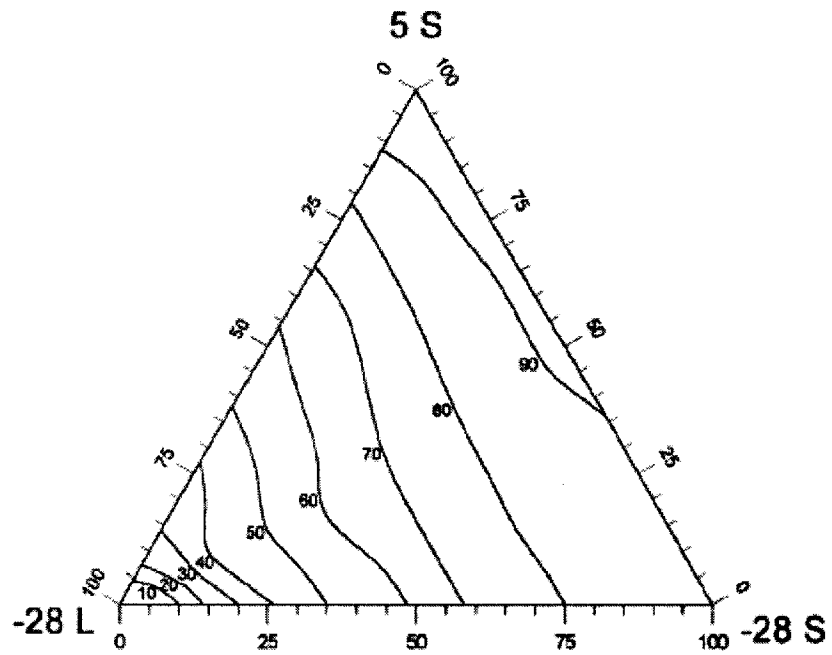


Figure 1.16a: Experimental ternary eutectic of HMF (5S), LMF (-28L), and MMF (-28S) at 0 °C via iso-solid lines [69]

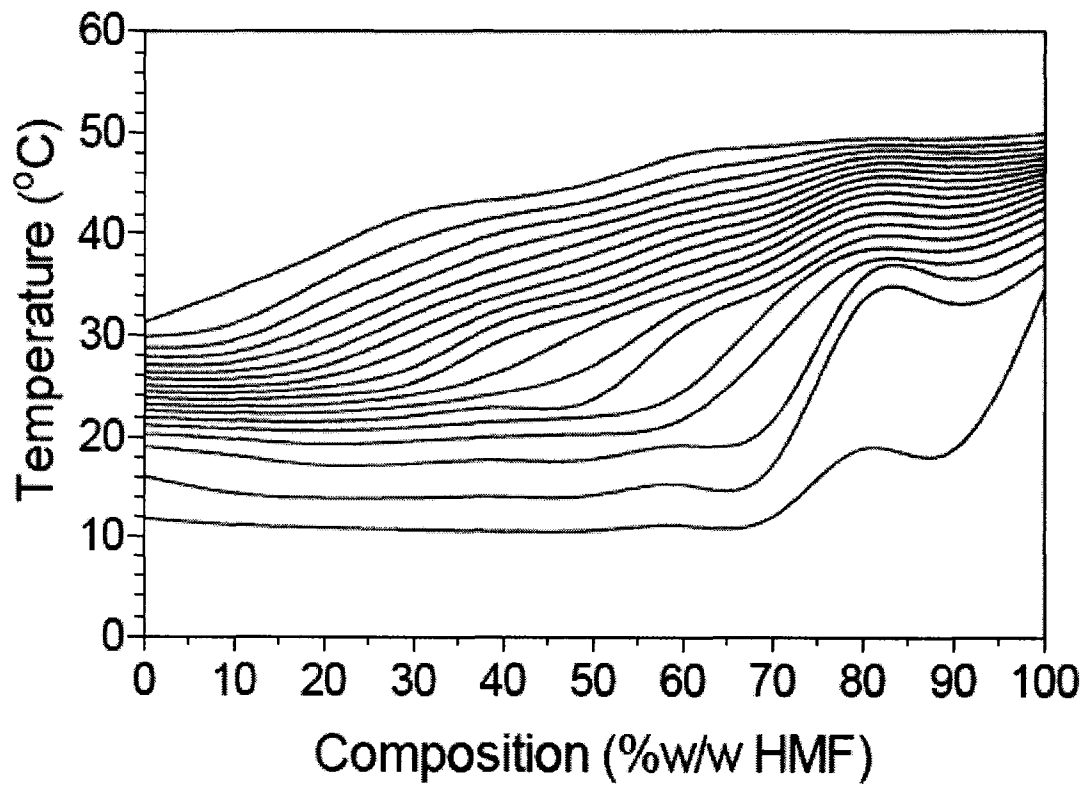


Figure 1.16b: Experimental binary eutectic of cocoa butter – HMF via iso-solid lines.

The bottommost line represents 90% SFC, and subsequent lines decrease in increments of 5% to a minimum of 5% SFC

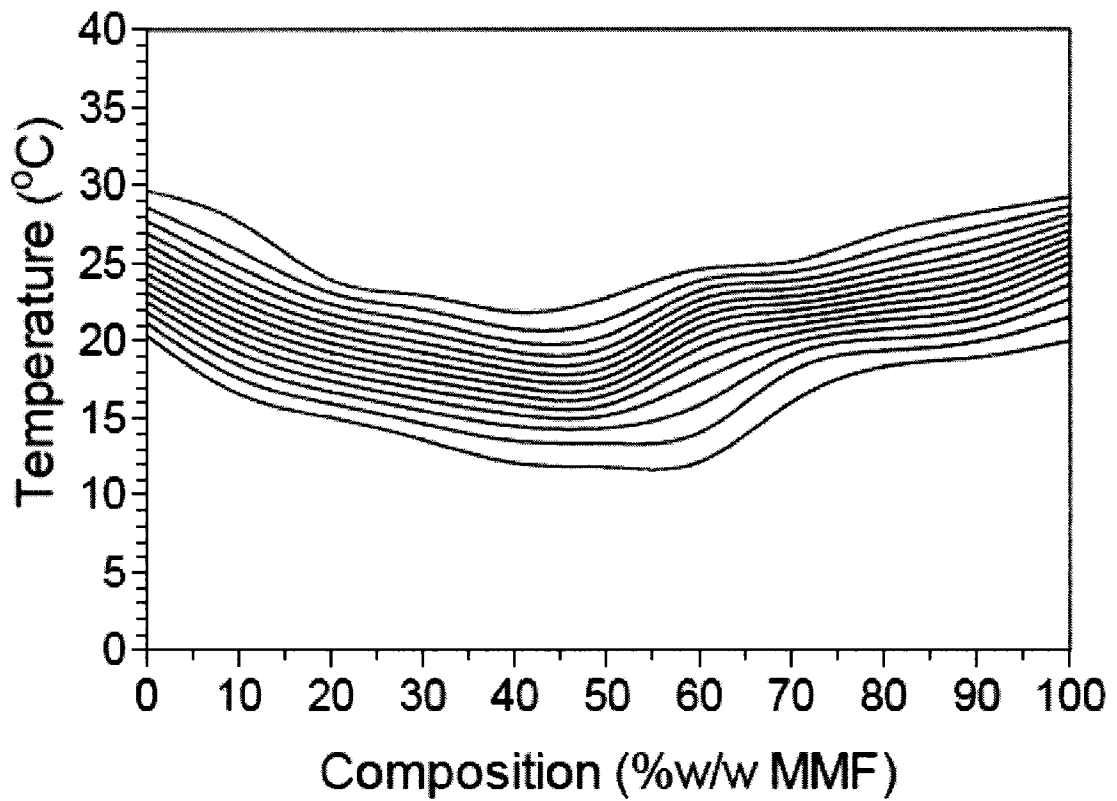


Figure 1.16c: Experimental binary eutectic of cocoa butter – MMF via iso-solid lines, an exaggerated case. The bottommost line represents 75% SFC, and subsequent lines decrease in increments of 5% to a minimum of 10% SFC

specific case that Timms refers, it is not generally true that eutectics as demonstrated by iso-solid phase diagrams impart information on hardness of the solutions at the eutectic compositions. In many instances, iso-solid line behavior may not indicate changes in polymorphism of the samples and certainly does not impart information beyond the prediction of hardness by SFC, a method that has been shown to be imperfect [25, 54, 112]. As well, the solution behavior demonstrated by iso-solid line diagrams does not always account for all observed trends in the melting behavior, as both intersolubility and polymorphic changes may occur simultaneously. Phase behavior as observed from iso-solid lines are important in elucidating some aspects of inter-solubility behavior, but is ultimately limited in scope, as are most physical techniques applied in isolation to the study of structure-composition-functionality studies. On the other hand, DSC phase measurements can reflect changes in polymorphism as well as intersolubility. However, such changes are not attributable to either polymorphic or inter-solubility effects in isolation utilizing just DSC data. Therefore, it is important to study phase behavior using a number of different techniques.

1.6 Low *trans* Shortening Solutions

Trans fats have been found to induce and stabilize the desirable β' polymorphic form within a fat [113], reduce the risk of oxidation in frying fats [114], and to increase the crystallization rate of the product [115] by raising the melting point of the fat [114]. However the presence of *trans* fats in soft margarines (8.7-12.1% [113], 10-18% [114]), stick margarines (17-36% [114]), cocoa butter substitutes (60-80% [116]), and all purpose shortenings (22% [114]) has been found to be unsuitable. Mensink and Katan

[9] discovered that *trans* fatty acids lead to an increase in LDL cholesterol just like saturated fats. However *trans* fats also simultaneously decrease the HDL cholesterol causing *trans* fats to be a much larger precursor to coronary heart disease and many other studies have reported similar results [8, 11]. Therefore, it has become increasingly important to produce products in which there is little or no *trans* fats [10]. To that end, the edible oils industry has developed a variety of solutions for delivering a quality low *trans* product to the consumer.

Saturated and/or *trans* fats within hardstock have been substituted with fatty acids esters [117] or a mixture of the fatty acids found in fully hydrogenated oil and short chain acids [118]. Mixing vegetable oil, such as palm and cottonseed, with tallow to reduce the levels of *trans* fats whilst maintaining the desirable β' have also been proposed [114], although it would not be suitable for those with dietary restrictions (i.e. vegetarians, kosher, halal dietary restrictions). A zero *trans* shortening made from palm oil has also been proposed by the Loders Croklaan company [119].

Shortenings with up to 25% (by volume) inert gas, 10 to 20% hardstock, and less than 10% *trans* fats in addition to the base oil and an emulsifier have also been proposed by Roberts *et al.* and have been found to have a combination of β and β' polymorphs [120]. Inert gas was also used (up to 25% volume) in a β' stable shortening ideal for frying where the hardstock had more than 65% PSP and PSS [121]. It is impractical to acquire specific ratios of PSP and PSS as required for the hardstock in high volume applications [12].

Interesterification has also been used as an alternative to hydrogenation, a process through which *trans* fats can be introduced [19, 20, 122-126]. Blends of palm oil, palm stearin (hardstock) and rice bran oil are chemically interesterified so that the rice oil contributes micronutrients such as tocopherols and sterols whilst making the crystallized shortening less susceptible to changes in temperature during storage [127, 128]. Palm oil, fractionated to separate the TAGs containing palmitic acid followed by random chemical interesterification with non-hydrogenated palm kernel stearin has also been used as a *trans* free hardstock for shortening blends [125]. Fractionation of palm oil followed by interesterification with base oil has also been applied in vanaspati production as shown by Khatoon *et al.* [19]. Alkaline metal catalysts such as sodium methoxide and sodium methylate are used for interesterification [126].

Enzymatic interesterification of either the individual or blend of raw materials has also been used to produce zero *trans* vanaspati using a 1,3 specific lipase [20]. Interesterification using a 1,3 specific enzyme catalyst does not affect the *sn*-2 position of the TAG, and thus oxidation is not a major problem with the resulting fat [20].

Hydrogenation at 80-130 °C with the use of a nickel catalyst has also been shown to produce fewer *trans* fatty acids [129]. Nickel catalyst which has been conditioned to reduce its activity via contact with phosphoric acid, and/or organic acid phosphate has also been used for the hydrogenation of an edible fat to achieve a hydrogenated product with less than 10% *trans* [12].

1.7 The Challenge

In 1969, 100 years after the invention of margarine, Feron wrote:

“The number of possible combinations (of oils) is unlimited..., so availability of supplies and nutritional and other requirements can be taken into account” [130].

It is hoped that this study, in addition to providing fundamental knowledge of edible oil blends, will provide a framework for solving future challenges in the edible oils industry and reigning in the unlimited number of combinations of edible oils.

1.8 References

1. Timms, R.E., *Phase Behaviour of Fats and their Mixtures*. Progress in Lipid Research, 1984. **23**: p. 1-38.
2. Rossell, J., *Interactions of triglycerides and of fats containing them*. Chemistry and Industry, 1973: p. 832-835.
3. Dewettinck, K., et al., *Phase Behavior of Cocoa Butter in a Two-Step Isothermal Crystallization*. Crystal Growth and Design, 2004. **4**(6): p. 1295-1302.
4. Inoue, T., et al., *Phase behavior of binary mixtures of cis-monounsaturated fatty acids with different omega-chain length*. Chemistry and physics of lipids, 1992. **63**: p. 243-250.
5. Kloek, W., P. Walstra, and T. van Vliet, *Crystallization Kinetics of Fully Hydrogenated Palm Oil in Sunflower Oil Mixtures*. J.Am.Oil Chem.Soc., 2000. **77**(4): p. 389-398.
6. van Malssen, K., et al., *Phase behavior and extended phase scheme of static cocoa butter investigated with real-time X-ray powder diffraction*. Journal of the American Oil Chemists Society, 1999. **76**(6): p. 669-676.
7. Hunter, J. and T. Applewhite, *Reassessment of Trans Fatty Acid Availability in the US Diet*. Am.J.Clin.Nutr., 1991. **54**: p. 363-369.

8. Mensink, R. and M. Katan, *Trans monounsaturated fatty acids in nutrition and their impact on serum lipoprotein levels in man*. *Prog.Lipid Res.*, 1993. **32**(1): p. 111-122.
9. Mensink, R.P. and M.B. Katan, *Effect of dietary trans fatty acids on high-density and low-density lipoprotein cholesterol levels in healthy subjects*. *New England Journal of Medicine*, 1990. **323**(7): p. 439-445.
10. Canada, H. *TRANSforming the Food Supply*. 2006 [cited 2007 February 7, 2007]; Available from: http://www.hc-sc.gc.ca/fn-an/nutrition/gras-trans-fats/tf-ge/tf-gt_rep-rap_e.html.
11. Willett, W.C., et al., *Intake of trans Fatty Acids and Risk of Coronary Heart Disease Among Women*. *Lancet*, 1993. **341**: p. 581-585.
12. Higgins, N.W., *Low Trans-Stereoisomer Shortening Systems*, U.S.P.a.T. Office, Editor. 2004: USA. p. 12.
13. Nawar, W.W., *Lipids*, in *Food Chemistry*, O.R. Fennema, Editor. 1996, Marcel Dekker: New York. p. 225-319.
14. Walstra, P., *Physical Chemistry of Foods*. Food Science and Technology, ed. O.R. Fennema, et al. 2003, New York: Marcel Dekker, Inc. p. 807.
15. Christie, W.W., *Lipid Analysis*. 3rd ed. Vol. 15. 2004, Brigwater, England: The Oily Press. 416.

16. Bockisch, M., *Fats and Oils Handbook*. 1998, Champaign, Illinois: AOCS Press. p. 838.
17. de Man, J., *Relationship Among Chemical, Physical, and Textural Properties of Fats*, in *Physical Properties of Fats, Oils and Emulsifiers*, N. Widlak, Editor. 1999, AOCS Press: Champaign, Illinois. p. 79-95.
18. Ghotra, B.S., S.D. Dyal, and S.S. Narine, *Lipid shortenings: a review*. Food Research International, 2002. **35**(10): p. 1015-1048.
19. Khatoon, S. and S.Y. Reddy, *Plastic Fats with Zero trans Fatty Acids by Interesterification of Mango, Mahua and Palm Oils*. European Journal of Lipid Science and Technology, 2005. **107**: p. 786-791.
20. Farmani, J., M. Safari, and M. Hamed, *Application of Palm Olein in the Production of Zero-trans Iranian Vanaspati through Enzymatic Interesterification*. European Journal of Lipid Science and Technology, 2006. **108**: p. 636-643.
21. Bockisch, M., *Importance of Fats*, in *Fats and Oils Handbook*. 1998, AOCS Press: Champaign, Illinois. p. 1-52.
22. Hartel, R.W., *Crystallization in Foods*. 2001, Gaithersburg, MD: Aspen Publishers Inc. p. 325.
23. Dziezak, J., *Fats, Oils, and Fat Substitutes*. Food Technology, 1989: p. 66-74.

24. Rozenaal, A., *Interesterification of fats and oils*. INFORM, 1992. **3**(11): p. 1232-1237.
25. Narine, S.S. and A. Marangoni, *Factors Influencing the Texture of Plastic Fats*. Inform, 1999. **10**(6): p. 565-570.
26. Narine, S.S. and A.G. Marangoni, *Fractal nature of fat crystal networks*. Physical Review E, 1999. **59**(2): p. 1908-1920.
27. Narine, S.S. and A. Marangoni, *Structure and Mechanical Properties of Fat Crystal Networks*. Advances in Food and Nutrition Research, 2002. **44**: p. 33-145.
28. Humphrey, K. and S. Narine, *Diminishing marginal utility of cooling rate increase on the crystallization behavior and physical properties of a lipid sample*. Journal of the American Oil Chemists' Society, 2007. **84**: p. 709-716.
29. Walstra, P., *Fat Crystallization*, in *Food Structure and Behavior*, J. Blanshard and P. Lillford, Editors. 1987, Academic Press: London. p. 67-85.
30. Turnbull, D. and J. Fisher, *Rate of Nucleation in Condensed Systems*. J. of Chemical Physics, 1949. **17**(1): p. 71-73.
31. Volmer, M. and A. Weber, Z. Phys. Chem., 1926. **119**: p. 227.
32. Tampe, R., et al., *Reconstitution and Electron paramagnetic resonance-spectroscopic characterization of glycoporphin containing phospholipid vesicles*. Chemistry and Physics of Lipids, 1989. **51**: p. 91-103.

33. Hartel, R.W., *Nucleation*, in *Crystallization in Foods*. 2001, Aspen Publishers, Inc: Gaithersburg, Maryland. p. 145-191.
34. Martini, S., M.L. Herrera, and R.W. Hartel, *Effect of Cooling Rate on Nucleation Behavior of Milk Fat - Sunflower Oil Blends*. *J. Agric. Food Chem.*, 2001. **49**(7): p. 3223-3229.
35. Herrera, M., *Crystallization Behavior of Hydrogenated Sunflowerseed Oil: Kinetics and Polymorphism*. *J. Am. Oil Chem. Soc.*, 1994. **71**(11): p. 1255-1260.
36. Martini, S., M. Herrera, and R. Hartel, *Effect of Cooling Rate on Crystallization Behavior of Milk Fat Fraction/Sunflower Oil Blends*. *J. Am. Oil Chem. Soc.*, 2002. **79**(11): p. 1055-1062.
37. Toro-Vazquez, J., et al., *Induction Time of Crystallization in Vegetable Oils, Comparative Measurements by Differential Scanning Calorimetry and Diffusive Light Scattering*. *Journal of Food Science*, 2002. **67**(3): p. 1057-1065.
38. Narine, S.S. and A.G. Marangoni, *Relating Structure of Fat Crystal Networks to Mechanical Properties: A Review*. *Food Res. Int.*, 1999. **32**: p. 227-248.
39. Campos, R., S.S. Narine, and al, *Effect of Cooling Rate on the Structure and Mechanical Properties of Milk Fat and Lard*. *Food Res. Int.*, 2002. **35**: p. 971-981.

40. Hartel, R.W., *Crystal Growth*, in *Crystallization in Foods*. 2001, Aspen Publishers, Inc: Gaithersburg, Maryland. p. 192-232.
41. Bouzidi, L., et al., *Use of first and second derivatives to accurately determine key parameters of DSC thermographs in lipid crystallization studies*. *Thermochimica Acta*, 2005. **439**: p. 94-102.
42. Foubert, I., P. Vanrolleghem, and K. Dewettinck, *A differential scanning calorimetry method to determine the isothermal crystallization kinetics of cocoa butter*. *Thermochimica acta*, 2003. **400**(1-2): p. 131-142.
43. *Standard Methods for the Analysis of Oils, Fats, and Derivatives*, in *International Union of Pure and Applied Sciences*. 1979.
44. *Solid Content Determination in Fats by Low Resolution Nuclear Magnetic Resonance v. 2.150*, in *International Union of Pure and Applied Sciences*. 1987.
45. *Determination of Solid Fat Content by Pulsed NMR Method*, in *International Standard, Animal and Vegetable Fats and Oils*. 1991.
46. *AOCS Method Cd 16b-93*, in *Official and tentative methods of the American Oil Chemists' Society*, W.E. Link, Editor. 1998, AOCS Press: Champaign, IL.
47. Wright, A.J., S.S. Narine, and A.G. Marangoni, *Comparison of Experimental Techniques Used in Lipid Crystallization Studies*, in *Crystallization and Solidification Properties of Lipids*, N. Widlak, R. Hartel, and S.S. Narine, Editors. 2001, AOCS Press: Champaign, Illinois. p. 120-131.

48. Avrami, M., *Kinetics of Phase Change. I. General Theory*. Journal of Chemical Physics, 1939. **7**: p. 1103-1112.
49. Avrami, M., *Kinetics of Phase Change. II. Transformation-Time Relations for Random Distribution of Nuclei*. Journal of Chemical Physics, 1940. **8**: p. 212-224.
50. Avrami, M., *Kinetics of Phase Change. III: Granulation, Phase Change, and Microstructure*. Journal of Chemical Physics, 1941. **9**: p. 177-184.
51. Narine, S., K. Humphrey, and L. Bouzidi, *Modification of the Avrami Model for Application to the Kinetics of the Melt Crystallization of Lipids*. J. Am. Oil Chem. Soc., 2006. **83**(11): p. 913-921.
52. Sharples, A., *Overall Kinetics of Crystallization*, in *Introduction to Polymer Crystallization*. 1966, Edward Arnold: London. p. 44-59.
53. Eads, T., et al., *Molecular motion and transitions in solid tripalmitin measured by deuterium nuclear magnetic resonance*. J. Am. Oil Chem. Soc., 1992. **74**: p. 1213-1220.
54. Narine, S.S., Marangoni, A.G., *Microscopic and Rheological Studies of Fat Crystal Networks*. Journal of Crystal Growth and Design, 1999. **198/199**: p. 1315-1319.
55. Atkins, P.W., *Phase Diagrams*, in *Physical Chemistry*, P.W. Atkins, Editor. 1998, Oxford University Press: Oxford. p. 191-214.

56. Moore, W., *States of Matter*, in *Basic Physical Chemistry*. 1983, Prentice-Hall Inc: Englewood Cliffs, New Jersey. p. 27.
57. Barrow, G., *Phase Equilibria*, in *Physical Chemistry*, G. Barrow, Editor. 1988, McGraw-Hill Book Company: New York. p. 381-431.
58. Noggle, J.H., *Equilibrium in Pure Substances*, in *Physical Chemistry*, J.H. Noggle, Editor. 1989, Scott, Foresman and Company: Glenview, Illinois. p. 171-209.
59. Wright, A.J., et al., *Solvent effects on the crystallization behavior of milk fat fractions*. *Journal of Agricultural and Food Chemistry*, 2000. **48**(4): p. 1033-1040.
60. Knoester, M., P. De Bruijne, and M. van den Tempel, *The solid-liquid equilibrium of binary mixtures of triglycerides with palmitic and stearic chains*. *Chem.Phys.Lipids*, 1972. **9**: p. 309-319.
61. Humphrey, K.L., P.H.L. Moquin, and S.S. Narine, *Phase behavior of a binary lipid shortening system: From molecules to rheology*. *Journal of the American Oil Chemists Society*, 2003. **80**(12): p. 1175-1182.
62. Sato, K., *Polymorphism of POP and SOS. 1. Occurrence and polymorphic transformation*. *Journal of American Oil Chemists Society*, 1989. **66**: p. 664-674.
63. Sato, K., S. Ueno, and J. Yano, *Molecular Interactions and Kinetic Properties of Fats*. *Prog.Lipid Res.*, 1999. **38**: p. 91-116.

64. Inoue, T., et al., *Phase behavior of binary mixture of palmitoleic acid (cis-9-hexadecenoic acid) and asclepic acid (cis-11-octadecenoic acid)*. *Chemistry and physics of lipids*, 1993. **66**: p. 209-214.
65. Jasperson, H. and A. McKerrigan, *The use of differential curves in the dilatometry of fats*. *J.Sci.Food Agric.*, 1957. **8**: p. 46-54.
66. Lambelet, P. and A. Raemy, *Iso-Solid Diagrams of Fat Blends from Thermal Analysis Data*. *Journal of American Oil Chemists' Society*, 1983. **60**: p. 845-847.
67. Liang, B., Y. Shi, and R. Hartel, *Phase Equilibrium and Crystallization Behavior of Mixed Lipid Systems*. *Journal of the American Oil Chemists' Society*, 2003. **80**(4): p. 301-306.
68. Loisel, C., et al., *Phase transitions and polymorphism of cocoa butter*. *J.Am.Oil Chem.Soc.*, 1998. **75**(4): p. 425-439.
69. Marangoni, A. and R. Lencki, *Ternary phase behavior of milk fat fractions*. *J.Agric.Food Chem.*, 1998. **46**: p. 3879-3884.
70. Minato, A., *Synchrotron Radiation X-ray Diffraction Study on Phase Behaviour of PPP-POP Binary Mixtures*. *Journal of American Oil Chemists Society*, 1996. **73**(11): p. 1567-1572.

71. Minato, A., et al., *Thermodynamic and kinetic study on phase behaviour of binary mixtures of POP and PPO forming molecular compound systems*. J.Phys.Chem.B, 1997. **101**: p. 3498-3505.
72. Rossell, J., *Phase diagrams of triglyceride systems*. Advances in Lipid Research, 1967. **5**: p. 353-408.
73. Rousseau, D., et al., *Restructuring Butterfat Through Blending and Chemical Interesterification 1. Melting Behaviour and Triacylglycerol Modifications*. Journal of American Oil Chemists Society, 1996. **73**(8): p. 963-970.
74. Rousseau, D. and A. Marangoni, *Tailoring the Textural Attributes of Butter Fat/ Canola Oil Blends via Rhizopus arrhizus Lipase-Catalyzed Interesterification. 1. Compositional Modifications*. 1998. **46**: p. 2368-2374.
75. Timms, R., *Computer program to construct isosolid diagrams for fat blends*. Chem.Ind., 1979: p. 257-258.
76. Timms, R., *The Physical Properties of Blends of Milk Fat with Beef Tallow and Beef Tallow Fractions*. The Australian Journal of Dairy Technology, 1979: p. 60-65.
77. Timms, R., *Physical properties of oils and mixtures of oils*. J.Am.Oil Chem.Soc., 1985. **62**(2): p. 241-248.

78. Timms, R.E., *Solubility of Milk-Fat, Fully Hardened Milk-Fat and Milk-Fat Hard Fraction in Liquid Oils*. Australian Journal of Dairy Technology, 1978. **33**(4): p. 130-135.
79. Walker, R.C. and W.A. Bosin, *Comparison of SFI, DSC and NMR Methods for determining solid-liquid ratios in fats*. Journal of American Oil Chemists Society, 1971. **48**: p. 50-53.
80. Humphrey, K.L. and S.S. Narine, *A comparison of lipid shortening functionality as a function of molecular ensemble and shear: Crystallization and melting*. Food Research International, 2004. **37**(1): p. 11-27.
81. Amey, R. and D. Chapman, *Infrared spectroscopic studies of model and natural biomembranes*, in *Biomembrane structure and function, Topics in molecular and structural biology*, D. Chapman, Editor. 1984, Weinheim: Basel.
82. Chapman, D., *Infrared spectroscopy of lipids*. J.Am.Oil Chem.Soc., 1964. **42**: p. 353-371.
83. Freeman, N., *Applications of infrared absorption spectroscopy in the analysis of lipids*. J.Am.Oil Chem.Soc., 1968. **45**: p. 798-809.
84. O'Connor, R., E. DuPre, and R. Feuge, *The infrared spectra of mono-, di-, and triglycerides*. J.Am.Oil Chem.Soc., 1955. **33**: p. 88-93.
85. Yano, J., *Vibrational spectroscopic study on structures and polymorphic transformations of triacylglycerols*. 1998, Osaka University Editor.

86. Yano, J., et al., *Structural analysis of triacylglycerol polymorphs with FT-IR techniques. 2. b'1-form and 1,2-dipalmitoyl-3-myristoyl-sn-glycerol*. The Journal of Physical Chemistry B, 1997. **101**: p. 8120-8128.
87. Yano, J., et al., *Structural analysis of triacylglycerol polymorphs with FT-IR techniques. 1. Assignments of CH₂ progression bands of saturated monoacid triacylglycerols*. The Journal of Physical Chemistry B, 1997. **101**: p. 8112-8119.
88. Chapman, D., *Infrared spectroscopic characterization of glycerides*. J.Am.Oil Chem.Soc., 1960. **37**: p. 73-77.
89. Birker, P. and J. Blonk, *Alkyl chain packing in a b' triacylglycerol measured by atomic force microscopy*. J.Am.Oil Chem.Soc., 1993. **70**: p. 319-321.
90. Arishima, T., et al., *C-13 cross-polarization and magic-angle spinning nuclear magnetic resonance of polymorphic forms of three triacylglycerols*. J.Am.Oil Chem.Soc., 1996. **73**(10): p. 1231-1236.
91. Boceik, S., S. Ablett, and I. Norton, *C-13 NMR study of the crystal polymorphism and internal mobility's of the triglycerides tripalmitin and tristearin*. J.Am.Oil Chem.Soc., 1985. **62**: p. 1261-1266.
92. Calaghan, P. and K. Jolly, *The use of C-13 spin relaxation to investigate molecular motion in liquid tristearin*. J.Chem.Phys.Lipids, 1977. **19**: p. 56-73.

93. Chapman, D., *Nuclear resonance spectra of the polymorphic forms of glycerides*. J.Chem.Soc., 1960: p. 436-444.
94. Gibon, V., F. Durant, and C. Deroanne, *Polymorphism and Intersolubility of some Palmitic, Stearic, and Oleic Triglycerides: PPP, PSP, and POP*. J.Am.Oil Chem.Soc., 1986. **63**(8): p. 1047-1055.
95. Hagemann, J. and J. Rothfus, *Polymorphism and transformation energetics of standard monoacid triglycerides from differential scanning calorimetry and theoretical modeling*. J.Am.Oil Chem.Soc., 1983. **60**: p. 1123-1131.
96. Norton, I., et al., *A calorimetric, NMR and X-ray diffraction study of the melting behavior of tripalmitin and tristearin and their mixing behavior with triolein*. J.Am.Oil Chem.Soc., 1985. **62**: p. 1237-1244.
97. Campos, R., S.S. Narine, and A. Marangoni, *Effect of cooling rate on the structure and mechanical properties of milk fat and lard*. Food Research International, 2002. **35**(10): p. 971-981.
98. Rousseau, D., et al., *Restructuring butterfat through blending and chemical interesterification. 1. Melting behavior and triacylglycerol modifications*. Journal of the American Oil Chemists' Society, 1996. **73**(8): p. 963-972.
99. Timms, R., *Dr. Ralph E. Timms, Consultant-Oil and Fats*. 2003.
100. Koyano, T., et al., *Crystallization Behavior of Ternary Mixtures of POP/POS/SOS*. Yukagaku, 1993. **42**(6): p. 453-457.

101. Ahm, T. and A. Smf, *Solvent flooding displacement efficiency in relation to ternary phase behavior*. Society of Petroleum Engineers Journal, 1972. **12**(2): p. 89.
102. Lv, P. and A. Smf, *Ternary phase behavior at high temperatures*. Society of Petroleum Engineers Journal, 1968. **8**(7): p. 381.
103. Mam, C., et al., *Binary and ternary phase behavior of alpha-pinene, beta-pinene, and supercritical ethene*. Journal of Chemical and Engineering Data, 1996. **41**(5): p. 1104-1110.
104. Gioielli, L.A. and M. Nogueira Oliveria, *Interactions in Binary and Ternary Mixtures of Hydrogenated Fats*. Alimentaria, 1998. **294**: p. 67-73.
105. Braipson-Danthine, S., V. Gibon, and C. Deroanne, *Physiochemical characteristics of Ternary Fat Blends involving low-erucic rapeseed oil*. European Journal of Lipid Science and Technology, 2005. **107**: p. 627-633.
106. Gioielli, L.A., I.S. Simoes, and J.N. Rodrigues, *Crystal morphology and interactions of binary and ternary mixtures of hydrogenated fats*. Journal of Food Engineering, 2003. **57**: p. 347-355.
107. Solis-Fuentes, J.A. and C. Duran-de-Bazua, *Characterization of eutectic mixtures in different natural fat blends by thermal analysis*. European Journal of Lipid Science and Technology, 2003: p. 742-748.

108. Aini, I.N., et al., *Trans-free vanaspati containing ternary blends of palm oil-palm stearin-palm olein and palm oil-palm stearin-palm kernel olein*. Journal of the American Oil Chemists Society, 1999. **76**(5): p. 643-648.
109. Norlida, H.M., A.R.M. Ali, and I. Muhadhir, *Blending of palm oil, palm stearin and palm kernel oil in the preparation of table and pastry margarine*. International Journal of Food Sciences and Nutrition, 1996. **47**(1): p. 71-74.
110. Danthine, S. and C. Deroanne, *Blending of hydrogenated low-erucic acid rapeseed oil, low-erucic acid rapeseed oil, and hydrogenated palm oil or palm oil in the preparation of shortenings*. Journal of the American Oil Chemists' Society, 2003. **80**(11): p. 1069-1075.
111. Chow, M.C. and C.C. Ho, *Rheological Properties of the Palm Oil/Monoglyceride/Water System*, in *Physical Properties of Fats, Oils, and Emulsifiers*, N. Widlak, Editor. 1999, AOCS Press: Champaign, Illinois. p. 186-210.
112. Narine, S.S. and A.G. Marangoni, *Relating structure of fat crystal networks to mechanical properties: a review*. Food Research International, 1999. **32**(4): p. 227-248.
113. Cho, F. and J. de Man, *Physical Properties and Composition of Low Trans Canola/Palm Blends Partially Modified by Chemical Interesterification*. Journal of Food Lipids, 1993. **1**: p. 53-68.

114. deMan, J. and L. deMan. *Formulations for No-trans and Low-trans Margarines and Shortenings*. in *World Congress of the International Society for Fat Research*. 1996. The Hague: ISF.
115. Bell, A., et al., *Effects of Composition on Fat Rheology and Crystallization*. *Food Chemistry*, 2007. **101**: p. 799-805.
116. Dedek, J., et al., *Modified Edible Fats Containing Hydrogenated Erucic Acid-Low Rape Oil*. 1989: Czech. p. 7.
117. Wester, I., *Texturizing Compositions for use in Fat Blends in Foods*, W.I.P. Organization, Editor. 1998: International.
118. Wheeler, E.L., et al., *Low-palmitic, Reduced-trans Margarine and Shortening*, U.S.P. Office, Editor. 1995, Nabisco, Inc.: USA. p. 24.
119. *SansTrans RS39T20*. 2006 [cited 2007 July 1, 2007]; An announcement of a new zero trans, lowered saturates shortening product, SansTrans RS39T20]. Available from: www.croklaan.com.
120. Roberts, B.A., T.A. Scavone, and S. Riedell, P., *Beta-stable low-saturate, low-trans all-purpose shortening*, W.I.P. Organization, Editor. 1995: USA. p. 25.
121. Scavone, T.A., *Beta-prime stable low-saturate, low-trans, all-purpose shortening*, W.I.P. Organization, Editor. 1995: USA. p. 24.

122. Jeyarani, T. and S.Y. Reddy, *Preparation of Plastic Fats with Zero trans FA from Palm Oil*. Journal of the American Oil Chemists' Society, 2003. **80**(11): p. 1107-1113.
123. Kok, L., et al., *Trans-free Margarine from Highly Saturated Soybean Oil*. J.Am.Oil Chem.Soc., 1999. **76**(10): p. 1175-1181.
124. Berger, K.G. and I.N. Aini, *Formulation of Zero-trans Acid Shortenings and Margarines and Other Food Fats with Products of the Oil Palm*. J. Am. Oil Chem. Soc., 2005. **82**(11): p. 775-782.
125. Ullanoormadam, S.R., *Trans free non-hydrogeanted hard structural fat and non-hydrogenated hard palm oil fraction component*, U.S.P. Office, Editor. 2005: USA. p. 22.
126. Neff, W.E., G.R. List, and W.C. Byrdwell, *Effect of Triacylglycerol Composition on Functionality of Margarine Basestocks*. Lebensm.-Wiss. u.-Technol., 1999. **32**: p. 416-424.
127. Chami, A., et al., *Process for the production of micronutrient rich zero-trans shortening by interesterification*, in *United States Patent Office*, W.I.P. Organization, Editor. 2005, Council of Scientific and Industrial Research: India. p. 9.
128. Mayamol, P.N., et al., *A process for the production of zero-trans shortening*, I.P. Office, Editor. 2005: India.

129. Sakaguchi, K., *Hydrogenated-oil Manufacture of Low Trans Acid Contents*, J.P. Office, Editor. 2006: Japan. p. 5.

130. Feron, T., in *Margarine: An Economic, Social and Scientific History, 1869-1969*, J.H. van Stuijvenberg, Editor. 1969, Liverpool University Press: Liverpool. p. 83-121.

2. A Comparison of Lipid Shortening Functionality as a Function of Molecular Ensemble and Shear: Crystallization and Melting

2.1 Introduction

Lipid shortenings are usually composed of a mixture of oils from a number of sources such as un- and variously hydrogenated (both fully and partially) oils, emulsifiers and other additives. The typical oils used are canola, cottonseed, lard, palm, soybean, and tallow. As can be expected, it is difficult to understand the influence of molecular composition, processing conditions, additives and emulsifiers on physical functionality simultaneously, as the number of variables quickly become unmanageable. Efforts in our laboratory are focused on elucidating these complex relationships in a fashion which will ultimately render predictive databases and models to allow the shortening and margarine developer to be able to manipulate the variables at their disposal (type of oil, hydrogenation, interesterification, additives, emulsifiers, processing conditions, hold times, tempering conditions) to produce products with consistent and desirable quality.

We have therefore produced an exhaustive review of the literature related to lipid shortenings [1], and highlighted the relationships and parameters that need to be elucidated, taking into consideration the impressive amount of work that has been done in the lipid crystallization field in general [2-4]. In this communication, we simplify the

A version of this chapter has been published.

Humphrey, K.L. and S.S. Narine, A comparison of lipid shortening functionality as a function of molecular ensemble and shear: Crystallization and melting. *Food Research International*, 2004. 37(1): p. 11-27.

problem in order to examine the effects of molecular composition and shear on the physical functionality of a number of binary lipid systems, purposely excluding partially hydrogenated lipids, emulsifiers, and other additives. This work examines binary lipid systems composed of fully hydrogenated samples of canola, cottonseed, lard, palm, soybean and tallow blended to different percentages with refined, unhydrogenated soybean oil. These systems were chosen for study as they form the normal feedstock in industrial shortenings, and it was felt that the study would suggest ways in which developers can expect these lipid systems to behave. In addition these systems provide a realistic diversity of TAGs in varying proportions.

Five different shortenings sold on the market were also investigated in this study: All Vegetable Shortening (generic), Blue Crisco All Vegetable Shortening, Golden Crisco All Vegetable Shortening, Pure Lard (generic), and Tenderflake Pure Lard. These five products have been related to the simplified binary systems and parallels drawn.

To study the effect of shear on shortening systems, the cooling scheme was kept constant, as was the final storage temperature. With these conditions followed, this study uses DSC measurements to find the melting and crystallization (unsheared samples only) enthalpies, which are indicative of the polymorphic form of crystals and the growth modes of crystals respectively, as well as the system's intersolubility behavior. Since the fatty acid composition within the fat affects the availability of TAGs which in turn determine its range of functionality, it was desirable to know the fatty acid composition of each sample. Therefore, GC determinations of fatty acid content were obtained for

each of the component fats. The commercially available shortenings were also studied using the techniques as described above in order to relate the laboratory findings to those shortenings currently on the market.

2.2 Experimental Procedures

When referring to sample holding temperature as well as cooling and heating rates all temperatures are reported to a certainty of ± 0.5 °C. The six fully hydrogenated fats used (canola, cottonseed, palm, lard, soybean, and tallow) as well as the refined soybean oil was supplied by Bungee Foods Ltd., of Bradley IL.

2.2.1 *Fatty Acid Content of the Fully Hydrogenated Fats*

FAMES were prepared for the soybean oil and all the fully hydrogenated fats using the procedure outlined by Moodie [5]. The Gas Chromatograph (GC) used was Varian's 3500 Capillary Gas Chromatograph – Flame Ionization Detector (GC-FID) equipped with Varian's 8200 Auto Sampler. A BP X 70 column 120 m long with a 0.25 mm internal diameter and a 0.25 μm thick silica wall was used. The GC was controlled with Varian's "Star Chromatography Workstation" software V.5.51. The method used was 107 minutes long with the injector temperature being set at 240 °C. The column flow rate was 1 mL per minute and the temperature was set at 180 °C for 100.00 minutes, and was then raised at 10.0 °C per minute to 250 °C. The detector had a temperature of 300 °C. The FAME standards used in the analysis of the GC spectra were obtained from Sigma Aldridge.

2.2.2 *Sample Preparation*

Each fully hydrogenated fat (canola, cottonseed, palm, lard, soybean, and tallow) was mixed in clean, dry, glass jars with non-hydrogenated soybean oil at concentrations ranging from 10 to 25% (w/w) hydrogenated fat/soybean oil in 5% increments. Each fat mixture was heated to 90 °C and the sample was mixed for 2 minutes by a motorized mechanical stirrer to ensure homogeneity before sampling. The samples were tempered using the following procedure to achieve a constant cooling rate of 10 °C per minute in the unsheared samples and 11 °C per minute in the sheared samples. Note that the cooling rate refers to that of soybean oil. The processing conditions were kept constant but of course due to the differences in crystallization enthalpies of the different systems, actual cooling rates for the systems varied. A 250 mL stainless steel beaker, 8 cm tall, 6 cm in diameter, with 1 mm thick walls, containing 80 g of fat was equilibrated in a water bath at 67 °C. The beaker was then transferred to a 40 °C water bath for 2 minutes before being transferred to a water bath at 20 °C where the sample was sheared (or not for the unsheared samples) with an automated stirring mechanism at no more than 60 rpm for 4 minutes.

Three DSC pans were prepared for each concentration of all the fully hydrogenated fats for both the sheared and unsheared samples (a total of 144 DSC pans. The pans were hermetically sealed. The mass of the fat in the DSC pans was between 15 and 25 mg. Three DSC pans were also prepared for each of the five market shortenings used.

2.2.3 DSC Measurements, Thermal Behavior

The instrument used in the investigations was the “DSC 2920 Modulated DSC” by TA Instruments. The data sampling and temperature control procedures were fully automated and controlled by the “TA Instrument Control” software program, and the output spectra were analyzed with the “TA Universal Analysis” software to find the peak maximum, onset temperatures and enthalpies of crystallization and melt. All resulting curves were normalized to a uniform sample mass of 15 grams. The FWHM of the curves was determined via a manual measurement with vernier rulers.

The cooling and heating rates of the instrument were kept constant at 10 °C per minute and 5 °C per minute respectively. For the sheared samples, one of the prepared pans was immediately placed in the DSC chamber and heated with the other pans being stored at 20 °C and processed after 48 hours. To obtain the melting curve for the sheared samples, the sample was equilibrated at 20 °C then heated to 67 °C where the sample temperature came to equilibrium. The fat sample was then cooled to 20 °C.

Each of the unsheared samples was processed twice in the following manner. The first process measurement was of crystallization and immediate melting of the sample, and the second was crystallization for the purpose of storing the sample. To obtain the crystallization curve and 0 hour melting curve, the sample was heated to 90 °C to remove any crystal memory. Then, the sample was equilibrated at 67 °C for 5 minutes and then cooled to 20 °C. To prepare the sample pans for storage for the 48 hour melting curve, the sample was heated to a temperature of 67 °C for 5 minutes before being cooled to 20

°C at the same rate to ensure that the crystallization is identical; this pan was then stored at 20 °C, and the melting procedure was repeated after 48 hours.

2.3 Results and Discussion

The crystallization of a lipid system is ultimately limited by its molecular ensemble, as the size, number, and nature of the molecules affect the heat and mass transfer within the system and determine the degree of crystallization due to molecular complementarities and concentration effects. The solubility of one type of molecule in another, as well as the related chemical potential between molecules in the solid phase and those in solution affects how and when crystallization can occur. One can also supercool and/or shear a system to induce and/or alter the crystallization process. These factors continue to play a role after initial crystallization has taken place within a system as the lipid goes through a period of growth wherein some crystals may redissolve into the melt, re-crystallize, and/or continue to grow. It is during this step that structural effects of the fat network are determined. That is, the microstructure and the polymorph(s) of the fat are defined, these structural hierarchies also depending directly on the fatty acids and the TAGs in the fat crystal network as they vary with respect to melting points, solubility, chemical potential, etc. After a period of ripening, a 48 hour waiting period in this study, variations in the final physical properties of the fat are often observed. The melting behaviors of the fat networks were observed and interesting trends and deviations are shown in this paper. These trends can be traced back through the entire network formation process, and to the mechanisms of crystallization affected by parameters such as shear and molecular diversity.

The molecular ensemble of the shortening as described by the fatty acid composition as shown in Figure 2.1, and the TAG composition in Figure 2.2, establishes the limits of physical functionality for the final network. Manipulating the crystallization and ripening conditions will affect final functionality, but only to an extent that is ultimately constrained by the molecular ensemble. Understanding the effect of this level of structure is extremely difficult, related in no small part to our inability to accurately vary its complexity in controlled quanta.

All of the fully hydrogenated fats have stearic acid (S) as the main fatty acid present. In fully hydrogenated palm, there are almost equal amounts of palmitic (P at 56%) and stearic (S at 44%) acids. The main fatty acid in soybean oil is linoleic (L) at 53.2%. One can see that the palmitic acid content increases in the fully hydrogenated fats in the order: canola, soybean, cottonseed, lard, tallow, and palm. As the fully hydrogenated oils are composed of only palmitic and stearic acid (any remaining unsaturated fatty acids after hydrogenation were not detectable by our GC method and is probably negligible), one can also observe that the stearic acid content of the fats decreases in the same order that the palmitic acid increases. Therefore, one would expect that as one moves from canola to palm, the changes in behavior would be motivated by the decrease in stearic and the increase in palmitic acid. However, it is important to remember that the fatty acids exist mostly on glycerol backbones, and that the manner in which they are stereospecifically arranged on that backbone will have a tremendous influence in the ensuing crystallization behavior.

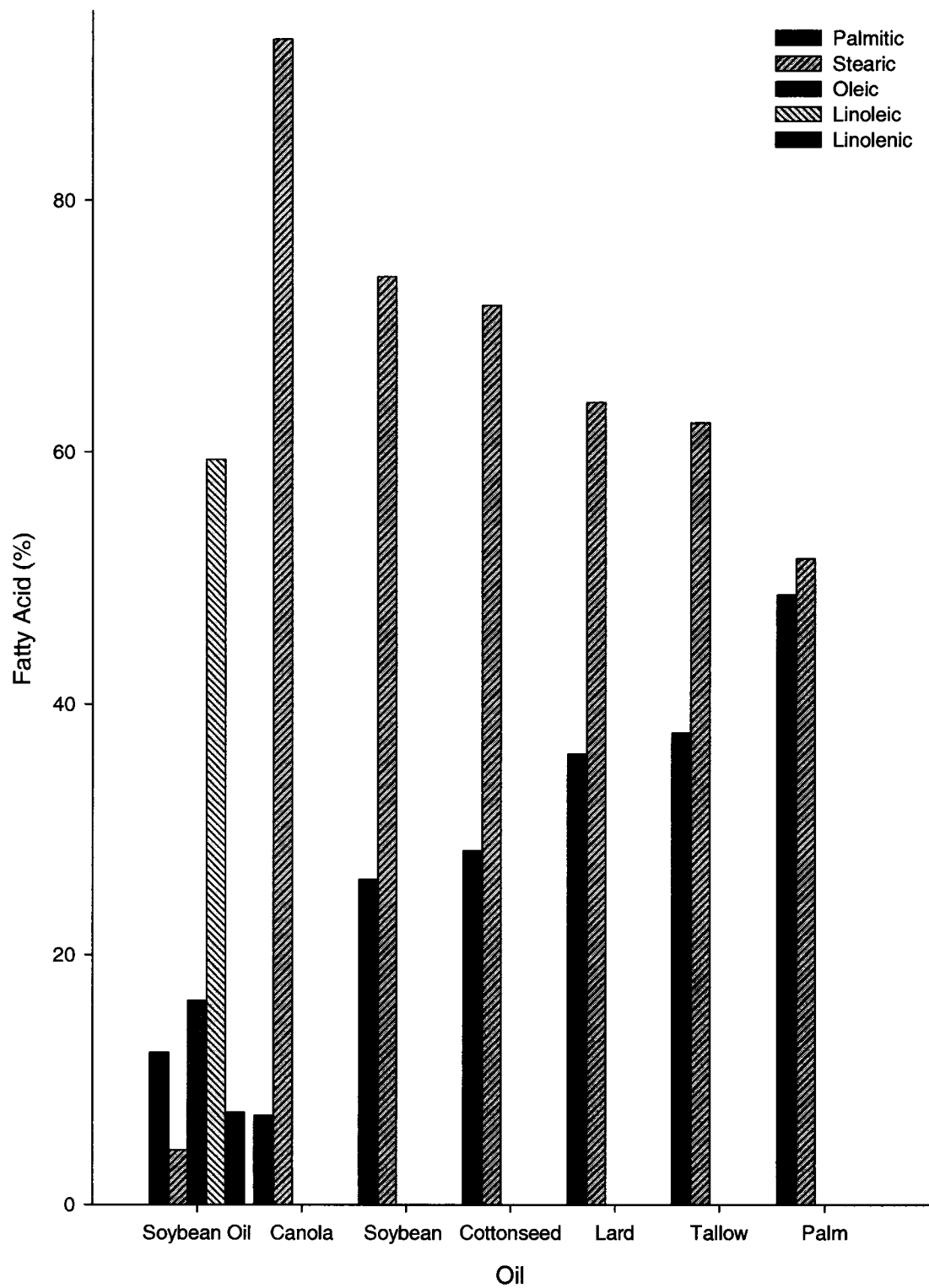


Figure 2.1: Fatty acid composition of the fully hydrogenated fats and soybean oil

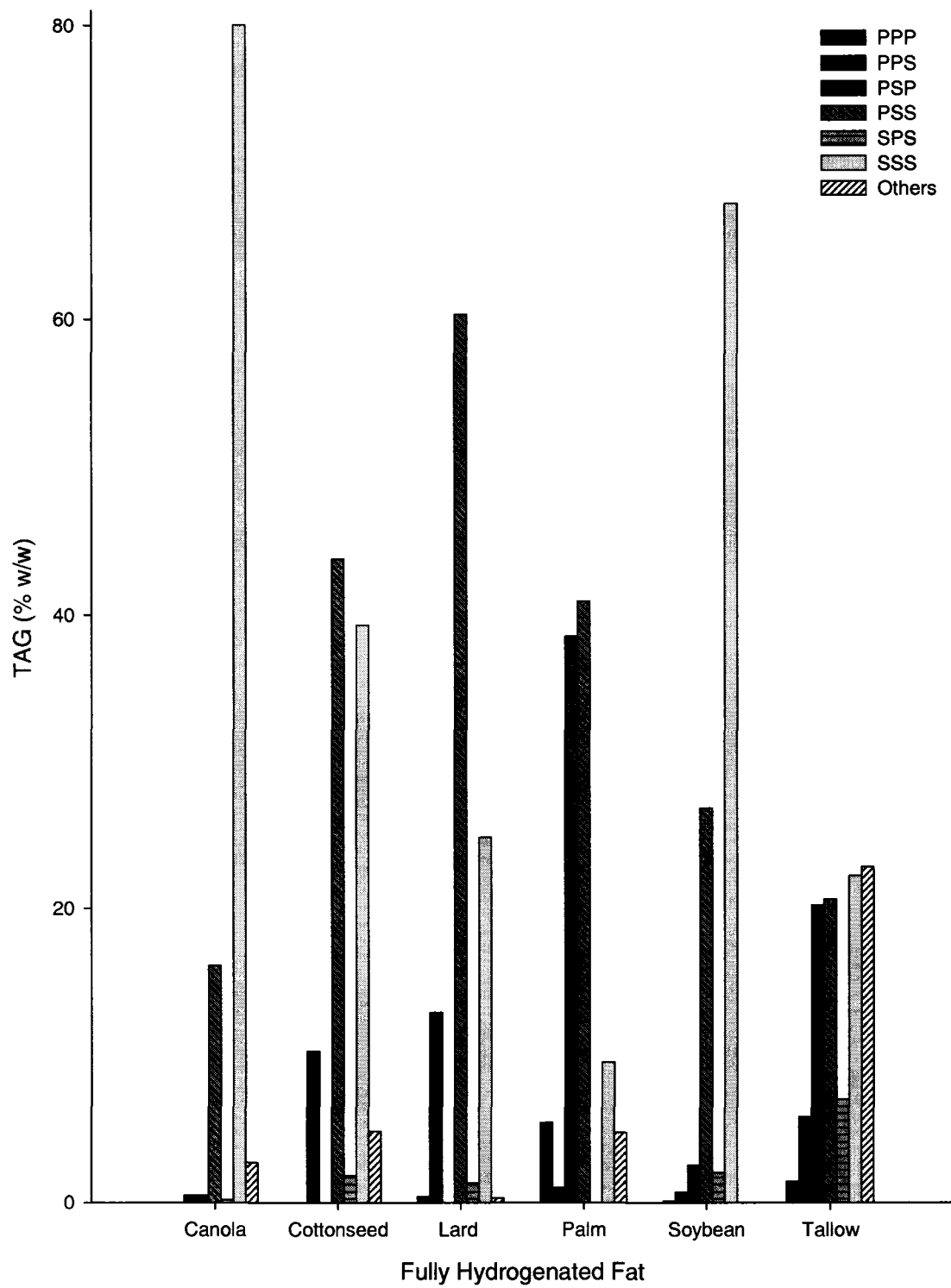


Figure 2.2: TAG composition of the fully hydrogenated fats [6-9]

Tristearin (SSS) is the main TAG in canola, soybean, and tallow. Cottonseed, lard, and palm have palmitic-stearic-stearic (PSS) as the main TAG. Unlike the other fats shown, there is not a single TAG in tallow dominating the solution as palmitic-stearic-palmitic (PSP at 20.2%) and PSS (20.6%) are almost as prominent as SSS (22.2%). Tallow also demonstrates a broader distribution of TAGs than the other fats, consisting of a significant cumulative percentage (22.8%) of TAGs with individual percentages below 2%. The TAG composition of fully hydrogenated palm is different from the other fats, as the main TAGs are PSS and PSP, not SSS and PSS as in canola, cottonseed, lard, and soybean.

As PSS is the major TAG in fully hydrogenated lard (60.3%), one can assume that its functionality may be greatly influenced by the high percentage of PSS in the ensemble of molecules. The same can be said for canola and SSS (80.0%). Palm has the highest percentage of PSP within the fully hydrogenated fats at 38.5%. Thus functionality due to PSP would be most visible within the samples containing palm.

Figure 2.3 shows the TAGs in soybean oil. The major TAG in soybean oil is linoleic-linoleic-oleic (LLO) at 15.6%. As there are no major TAGs (>2%) present in soybean oil which also occur in the fully hydrogenated fats, it is reasonable to expect that increasing the canola in a sample by 5% will increase the SSS in the sample by the same amount as the decrease in soybean oil concentration will not significantly decrease the amount of SSS in the sample. The same would be true of PSS in lard and PSP in palm.

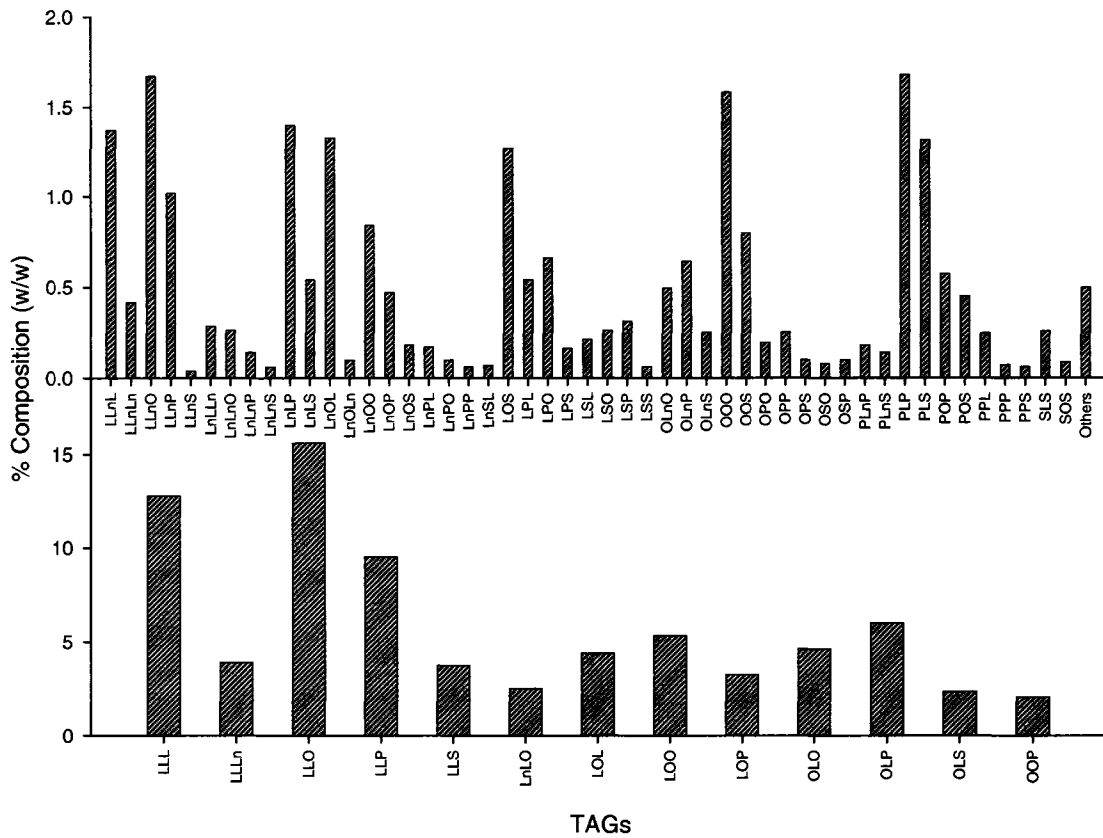


Figure 2.3: TAG composition of soybean oil [9]

Also of importance to mention at this point is the issue of molar concentration versus mass concentration. For molecular intersolubility inferences, it is important to have a sample containing 25% fully hydrogenated fat by mole interacting with 75% soybean oil by mole. However, to simplify sample preparation, the samples were prepared (w/w) with 25% fully hydrogenated fat by mass interacting with 75% soybean oil by mass. This could cause the interaction of greater than or less than 75 moles of soybean oil with less than or greater than 25 moles of fully hydrogenated fat. However, if one calculates the mass of one mole of each of the fully hydrogenated fats and soybean oil based on the information in Figures 2.1 and 2.3 respectively, it is found that the percent molar concentration and the percent mass concentration are essentially the same, within $\pm 0.01\%$.

Table 2.1 shows the ingredients of the market shortenings as listed on the packaging. Two similar shortenings were Blue Crisco – All Vegetable Shortening and Golden Crisco – All Vegetable Shortening; which both contain partially hydrogenated soybean and palm oils, hydrogenated modified palm oil, mono and diglycerides, and artificial flavor, with added color being present in Golden Crisco. All Vegetable Shortening contains hydrogenated vegetable oils (canola and/or soybean and/or palm), mono and diglycerides, BHA, BHT, and citric acid. The final two systems are Pure Lard, and Tenderflake Pure Lard, both of which listed the same ingredients on the package. As the listed ingredients are similar, one would expect Blue Crisco and Golden Crisco to exhibit similar properties, as well as Tenderflake and Pure Lard. Any differences found between the market shortenings made with animal fats (and again between the Golden

Table 2.1: Ingredients of the five market shortenings used, as listed on the shortenings' packaging

	All Vegetable Shortening	Blue Crisco	Golden Crisco	Pure Lard	Tenderflake
Lard (may be hydrogenated)				X	X
Partially hydrogenated canola oil	X				
Partially hydrogenated soybean and palm oil	X	X	X		
Hydrogenated modified palm oil		X	X		
Mono and diglycerides	X	X	X		
Artificial flavor		X	X		
Color			X		
BHA, BHT, and citric acid	X			X	X

Crisco and Blue Crisco) may be due to the variances in (w/w) composition and/or the tempering of the product.

The temperatures at which the crystallization curves reach their peak maximum for all unsheared systems are shown in Figure 2.4. For samples containing the same fully hydrogenated fat, the temperature at which the DSC crystallization curve reaches a maximum increases with increasing hard fat in the sample. This is to be expected as fully hydrogenated fats contain saturated fatty acids which have higher melting points than the unsaturated fatty acids which are found in soybean oil. Thus as the amount of hard fat in the sample increases, there are higher melting compounds formed in the sample, and the bulk of the sample then melts at a higher temperature. The canola samples consistently had the highest peak maxima with the exception of the 25% sample, where the peak max of the soybean sample occurred at a higher temperature (35.2 ± 0.1 °C) than that for the canola sample (34.4 ± 0.1 °C). This variation may be due to intersolubility effects between SSS and PSS (67.9% and 26.8%) within the fully hydrogenated soybean samples which would not occur in the canola samples due to the dominance of SSS (93% S and 7% P). Of the six hard fats used, the palm samples consistently reached the crystallization peak maxima at the lowest temperatures with the exception of the 20% concentration where the peak maximum for tallow occurred at a lower temperature (27.8 ± 0.1 °C versus 28.9 ± 0.1 °C for the 20% palm sample). It was expected that the palm samples would have the lowest crystallization peak maximum as fully hydrogenated palm contains only 51% S which is lower than that for all other samples (Figure 2.1). Tallow has the closest fatty acid composition to palm (62% S), and thus if one fully

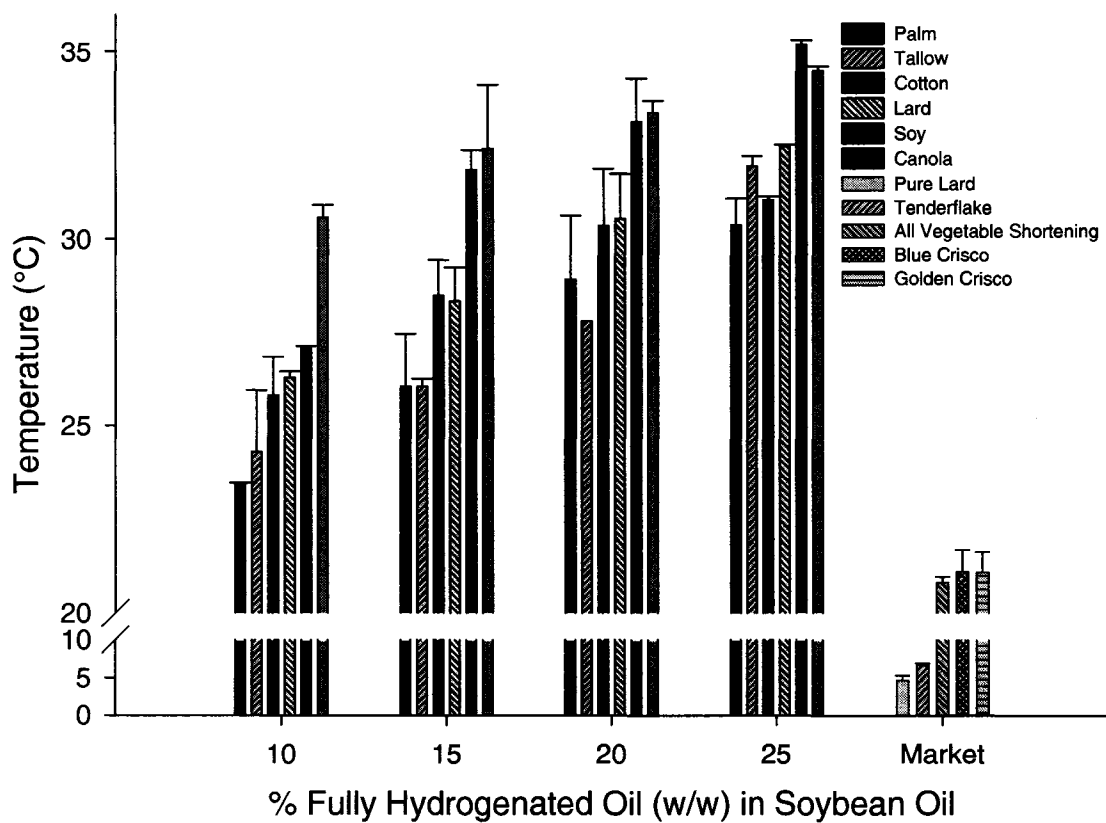


Figure 2.4: Crystallization peak maximum versus concentration for unsheared mixtures

hydrogenated fat were to interrupt the pattern of palm samples having the lowest peak maxima, the tallow samples would be suspect. Within each fat type, the crystallization peak max increases linearly as the concentration of the fully hydrogenated fat in soybean oil increases, as seen in a previous study [10].

The crystallization peak maxima are also shown for the market shortening samples. The crystallization curve for the Pure Lard sample reached its maximum at a temperature lower than that of all other samples measured (4.3 ± 0.1 °C) whilst All Vegetable Shortening, Blue Crisco, and Golden Crisco all shared the same crystallization peak maximum (20.7 ± 0.1 °C). Tenderflake and Pure Lard had peak maxima less than 10 °C; lower than that of all other samples measured. All of the crystallization curves for the market shortenings reached their peak maximum at lower temperatures than the binary lipid samples measured. The trends in crystallization peak maximum for the market shortenings mimic the trends shown by samples made of their composite oils (partially and fully hydrogenated). Pure Lard and Tenderflake have lard as a main ingredient. The crystallization peak maximum for the binary lard samples is consistently less than that for the canola and soybean samples. Thus it is reasonable to find that the peak maxima for All Vegetable Shortening, Blue Crisco, and Golden Crisco occurs at a greater temperature as they are composed of partially hydrogenated soybean and palm oils (as well as partially hydrogenated canola oil in All Vegetable Shortening, and hydrogenated modified palm oil in both Blue Crisco and Golden Crisco).

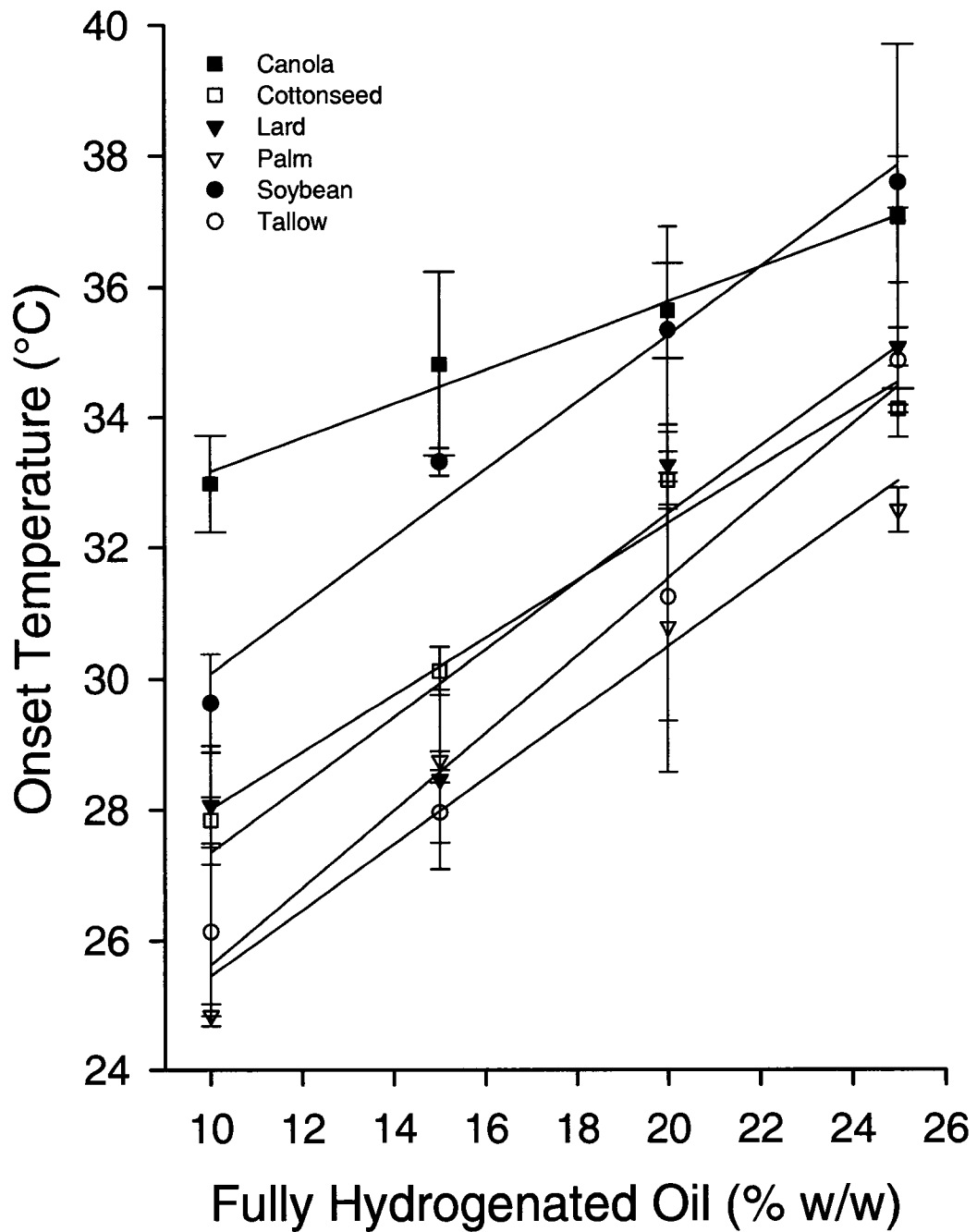


Figure 2.5a: Crystallization onset temperatures versus concentration for unsheared mixtures

The onset temperature of crystallization as a function of the concentration of the samples is shown in Figure 2.5a with each curve representing the crystallization onset temperatures of a different hard fat at varying concentrations. All of the systems demonstrated increasing onset temperatures as the amount of hard fat in the sample increased. This is to be expected as increasing amounts of high melting species are added to the samples resulting in increasingly higher melting molecular compounds being crystallized at successively higher onset temperatures. With greater amounts of high melting TAGs in the sample, the sample would crystallize at a higher temperature.

Figure 2.5b is a graph representing the slopes of the lines in Figure 2.5a as obtained using the “Linear Regression” function in Sigma Plot v.8.0. It can be seen that as one increases the amount of fully hydrogenated fat in a sample, the onset temperature of crystallization also increases. The rate of increase of temperature of crystallization, shown by the slope of the line (or height of the bar in Figure 2.5b), is greatest for tallow. Canola has the smallest slope, significantly smaller than the average slope of the other fats shown.

The tallow shortening system demonstrates the steepest onset of crystallization increase as the amount of hard fat increases. A steep slope is indicative of a greater amount of interaction between the molecules in the melt, as the onset of crystallization is significantly affected as one increases the complexity of the molecular ensemble in such a manner as to produce molecular compounds which have higher melting points and therefore crystallize at a higher onset temperature. Fully hydrogenated tallow also has

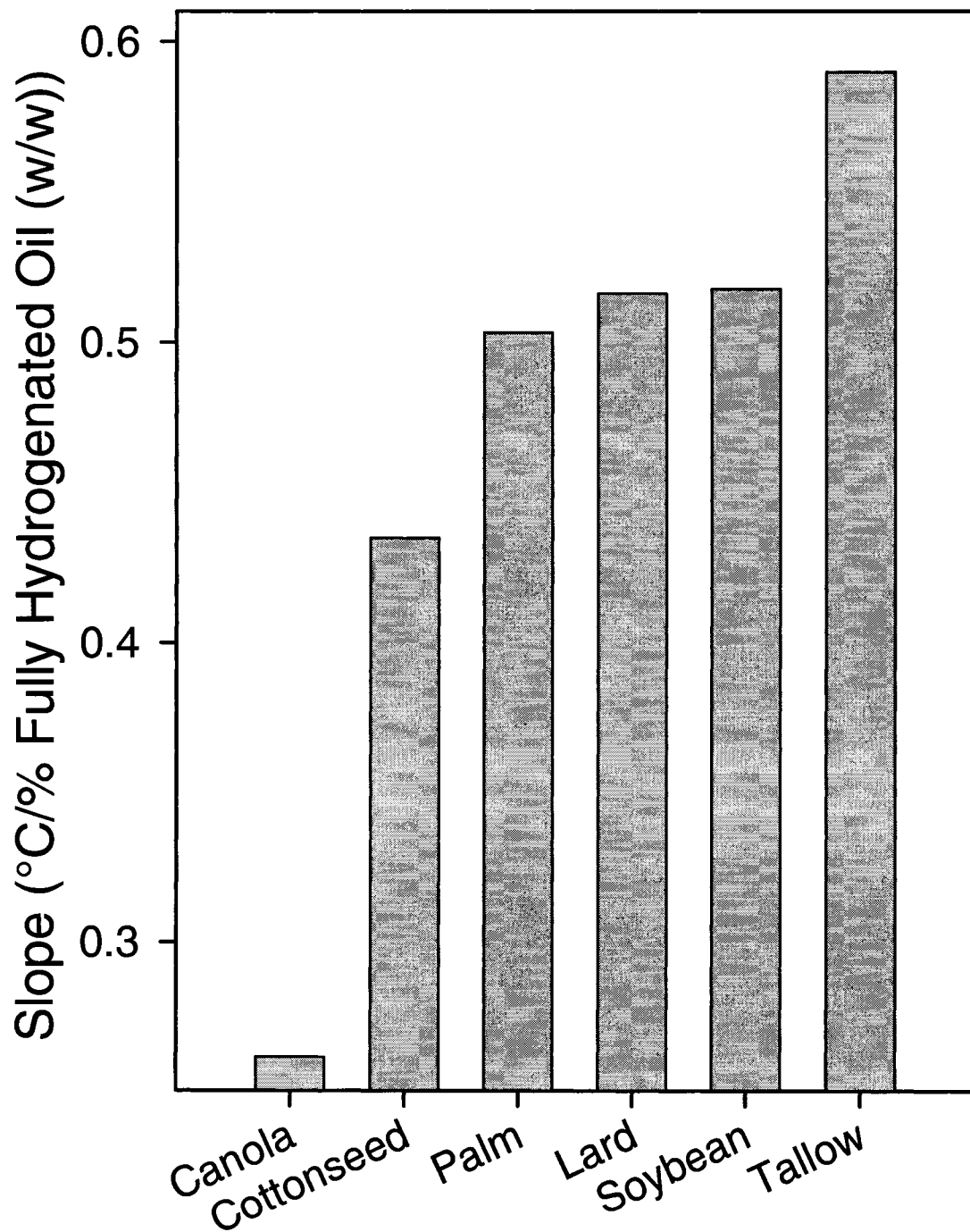


Figure 2.5b: Slope of line of best fit for all hard fat crystallization onset temperature curves

approximately 20% of each SSS, PSS and PSP, with approximately 6.5% of SPS and PPS, and a small amount of PPP (~2%), but with ~20% of minor components. The equivalent amounts of SSS, PSS, PSP and minor components, coupled with the linear and steep increase in the onset time of crystallization suggests that the intersolubility of SSS, PSS, and PSP is excellent, leading to the formation of successively higher melting molecular compounds as the relative amounts of these molecules increase.

Fully hydrogenated canola has approximately 80% SSS, and 16% PSS, with all other TAGs being minor, as shown in Figure 2.2. As one increases the amount of fully hydrogenated canola, one is essentially increasing those mixed compounds formed with PSS, whilst adding mainly SSS. Therefore, Figure 2.5b suggests that by adding SSS alone, one does not significantly increase the onset of melt. In the case of tallow the mixed compounds formed creates much higher melting entities that significantly increase the onset of melt. This clearly indicates that adding the highest melting TAG (SSS) does not necessarily increase melt. However, by exploiting the molecular complementarities of TAGs such as PSS, and PSP, one can increase onset significantly. Also suggested here, is that the molecular compounds formed when PSP is present with PSS and SSS as with tallow, the solution behavior is very different from when just PSS and SSS are present as with canola. The fact that the presence of PSP would create higher melting crystal entities is surprising, and suggests that the phase behavior of PSP with PSS and SSS is of immense importance to shortening systems.

The fully hydrogenated palm, soybean and lard systems demonstrated approximately the same steepness in increase of onset even though each fat has a unique complement of TAGs. Fully hydrogenated palm has ~40% of PSP and PSS and ~10% of SSS. Fully hydrogenated soybean has ~27% PSS and ~70% SSS. This suggests that increases in PSS in the presence of SSS significantly increases the amount of high-melt mixed crystals when compared with canola at 16% PSS and 80% SSS. Finally, fully hydrogenated lard had ~ 13% PPS, 60% PSS and 25% SSS. As each of these three fully hydrogenated fats exhibits the same steepness in increase in onset while possessing PSS and SSS in different concentrations, it is further suggested here that the phase behavior of PSP, PSS, SSS, and PPS are of equivalent importance.

Fully hydrogenated cottonseed has ~15% more SSS than lard, yet it demonstrates less steep an increase in onset temperature as the amount of hard cottonseed is increased. Cottonseed also has ~10% PPS and ~44% PSS. These two facts again suggest that PPS, PSS, and SSS together form mixed crystals of significantly higher melting points than those with a preponderance of solely SSS. Therefore PPS, PSS, SSS, and PSP should be carefully investigated with respect to phase behavior as blends of the fats examined in this study are typically encountered in lipid shortening systems.

Figure 2.6 compares the onset times of crystallization for each fully hydrogenated fat by concentration. Figure 2.7 compares the onset time of crystallization for different binary systems at the same concentrations. All of the concentrations follow the same patterns except for the 15% concentration. The samples of canola have the highest onset

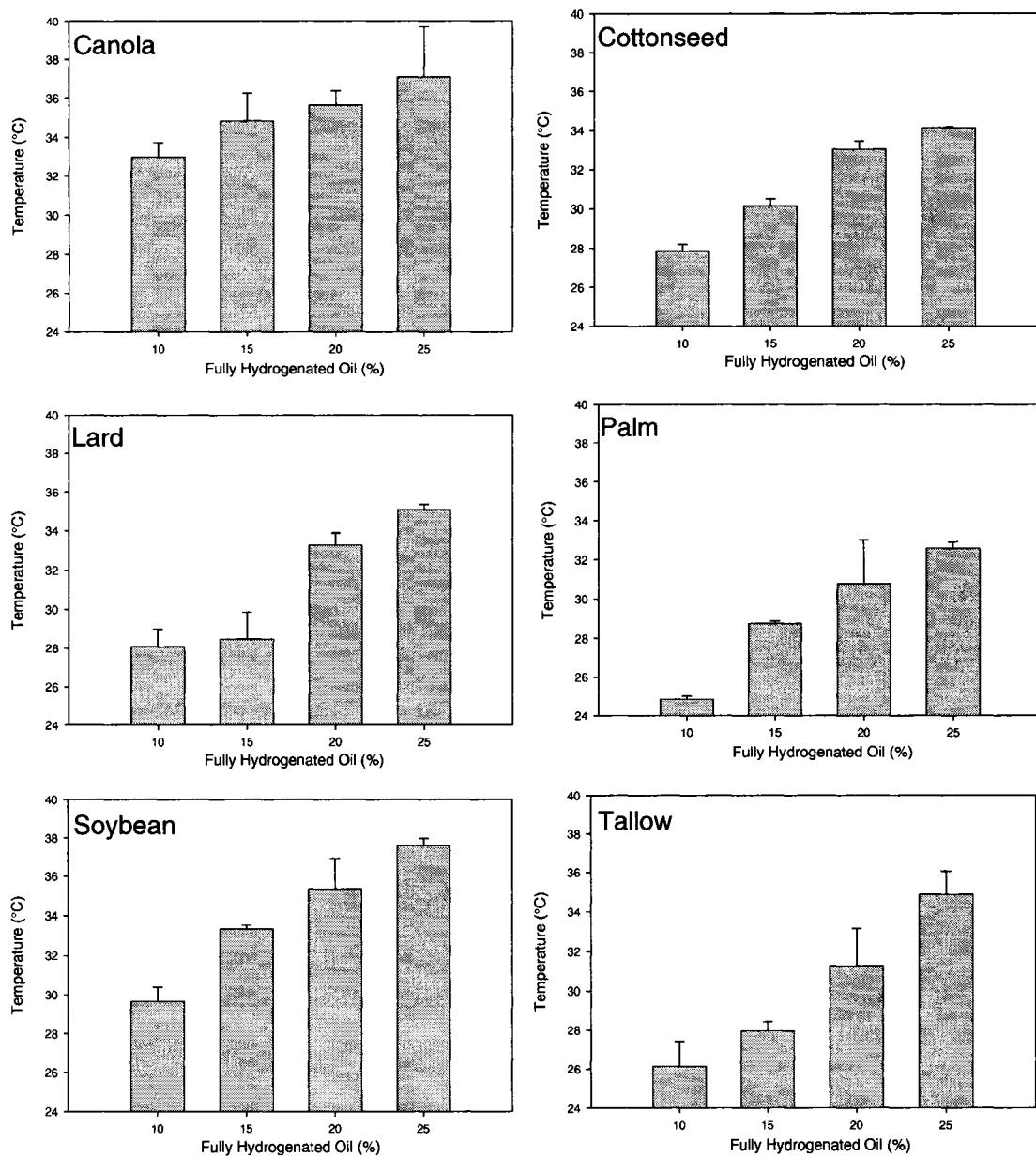


Figure 2.6: Crystallization onset temperatures versus concentration for unsheared mixtures arranged by fully hydrogenated fat

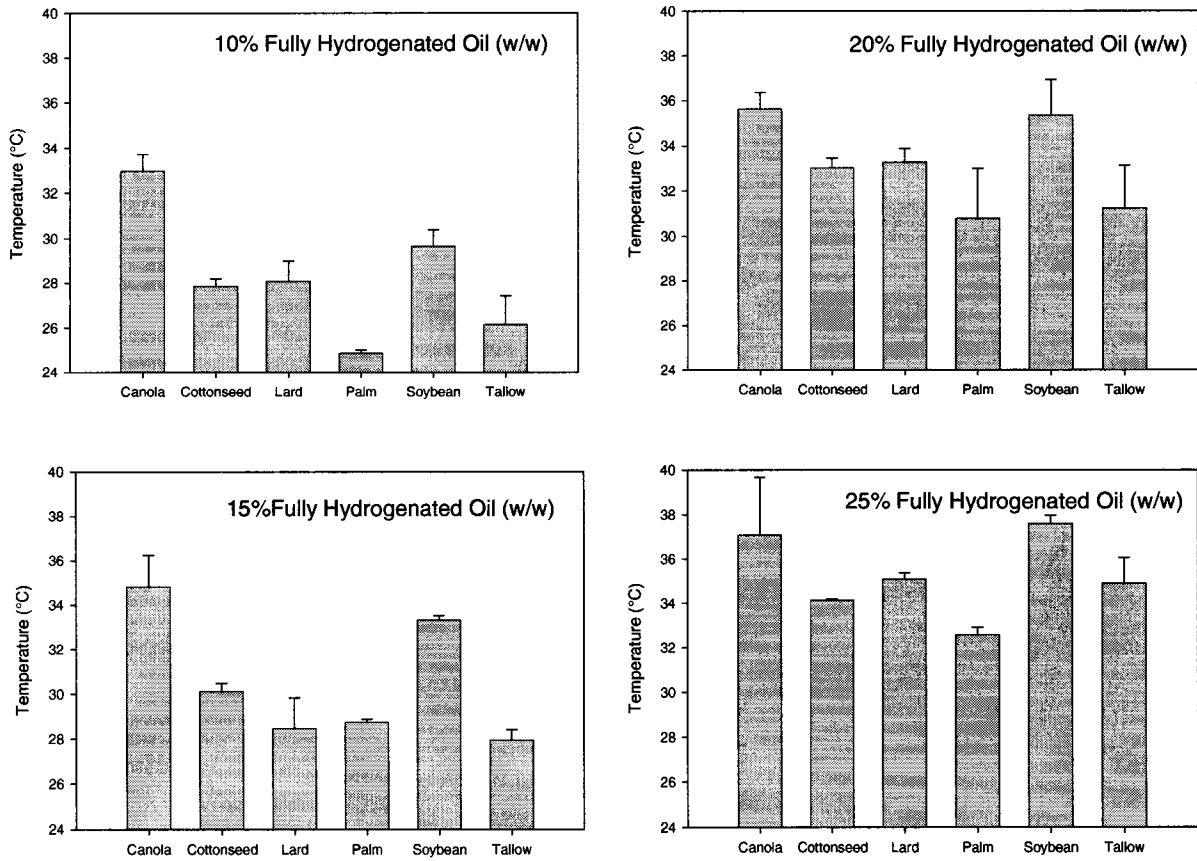


Figure 2.7: Crystallization onset temperatures versus fully hydrogenated fat for unsheared mixtures arranged by concentration

temperature meaning that it crystallizes earliest. Palm samples have the lowest onset temperature of crystallization. Tallow samples have an onset between palm, and that of lard and cottonseed which have similar onset temperatures. The soybean samples have higher onsets than both cottonseed and lard, but lower than canola. Greater percentages of stearic acid in a compound lead to a greater onset temperature of crystallization. From Figure 2.6 and Figure 2.7, as the amount of fully hydrogenated fat is increased, the onset temperature of the soybean samples gets closer to and then exceeds that of the canola samples for the 25% concentration. Furthermore, with an increase in fully hydrogenated fat, the lard samples begin to crystallize at a significantly higher temperature than those for cottonseed, and tallow begins to crystallize at a lower temperature than cottonseed.

If one compares the SSS content to the crystallization onset temperature at the 10% concentration for all fats (Figure 2.7), a good correlation can be seen with the exception of cottonseed and lard. Cottonseed has more SSS than lard (39.3% versus 24.8%), but it begins to crystallize at a lower temperature than lard (27.8 °C versus 28.1 °C). This is not surprising as stearic acid is the highest melting TAG. However, as concentrations increase, the trends are no longer explainable by just the SSS variation, thus the other components such as PPS, PSP, PSS become of significance.

The crystallization peak maximums in Figure 2.4 tell the same story as the onset temperatures from Figure 2.5a, although not as dramatically. Furthermore, the position and height of the peak maximums are also influenced by the growth mode of the fat, whilst the onset temperature just indicates the temperature at which crystallization begins.

The growth mode of a lipid crystal network is the collection of decisions which direct the formation of a hierarchy of structure which produces the final network. Crystal aggregation, re-melt into solution, and polymorphic transformation are possible routes a fat structure may pursue within the limits of heat and mass transfer and as such are contributing factors to the growth mode of the network. The starting ensemble of molecules within the melt is not controlled by the environmental conditions, and is therefore not a decision in the growing process, but obviously the initial mixture of TAGs is influential with respect to the final network formed.

The market shortenings also shown in Figure 2.4 have much lower peak maximums of crystallization due to the effect of having partially as opposed to fully hydrogenated fats and also to the effect of the emulsifiers. Although the market shortenings all have much lower peak maximums of crystallization, the relative peak maximums of the canola/soy/palm shortening systems compared to the lard systems is what we would expect, given the results of the studies on the model systems shown in Figure 2.4. Pure Lard has the lowest enthalpy of crystallization peak maxima, followed by Tenderflake, All Vegetable Shortening, and Golden Crisco which has the same maximum as Blue Crisco. The peak maximum for Pure Lard is close to that of Tenderflake (4.6 °C versus 6.6 °C), and that of Blue Crisco is the same as that of Golden Crisco (21.1 °C). This is as expected given the similar ingredients in both of these pairs of products as shown in Table 2.1.

The crystallization curves as obtained by DSC are shown in Figures 2.8 and 2.9. Each graph within Figure 2.8 contains the curves for samples containing the same fully hydrogenated fat with the 10% curve being the lowest curve on the graph, and the 25% curve being the uppermost. These curves are shown again in Figure 2.9, this time organized by concentration, with each graph exhibiting curves of the same concentration, but different binary systems. Within each graph in Figure 2.9, the curves are organized top to bottom: tallow, soybean, palm, lard, cottonseed, and canola. Obvious trends within a fully hydrogenated fat system include the trends illustrated in Figures 2.4 and 2.5a. One can also note that while the area under the enthalpy curve increases as the percentage of hard fat in the sample increases, the general shape of each line within a fat system remains the same. As one adds more fully hydrogenated fat to a sample, the initial rise in the enthalpy curve becomes steeper and the fall from the peak maximum becomes steeper as well. This is due to the increase in high melting TAGs within the samples which tend to crystallize at once, causing thermal energy to be released instantaneously as seen by full width half maximum data (not shown). Enthalpy curve for samples with 10% fully hydrogenated fat appear as a smooth broad curve rather than a sharply peaked curve due to the gradual increase and subsequent decrease in enthalpy. This is expected due to the absence of a large portion of high melting compounds, thus instead of the samples crystallizing quickly, the 10% concentration samples crystallize over a longer period of time which results in a wider enthalpy of crystallization peak.

An increase in the amplitude of the start of the enthalpy of crystallization curve as the concentration of fully hydrogenated fat in a sample increases is to be expected. As

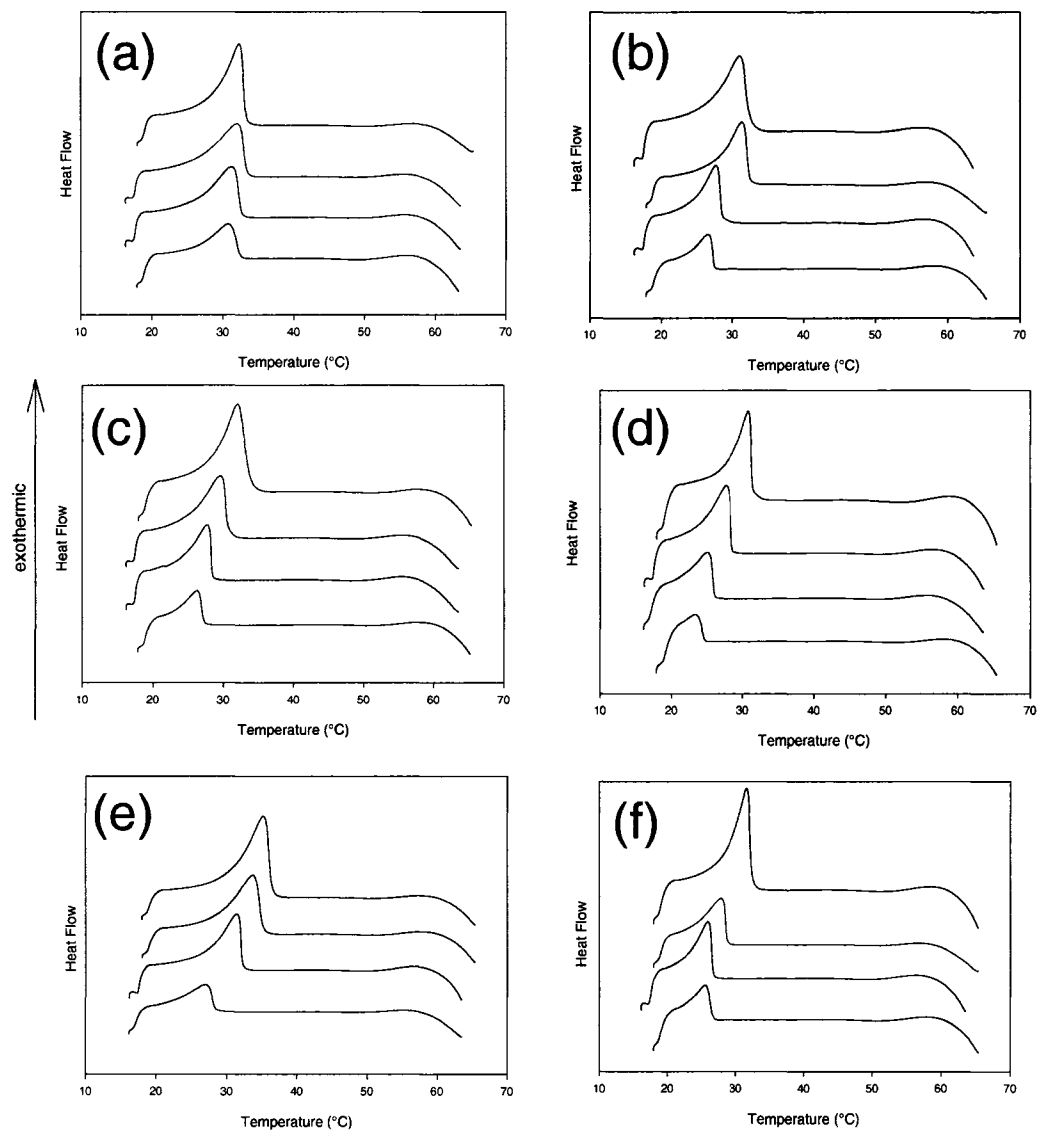


Figure 2.8: Crystallization curves for unsheared systems arranged by increasing concentration of hard fat (a) canola, (b) cottonseed, (c) lard, (d) palm, (e) soybean, (f) tallow

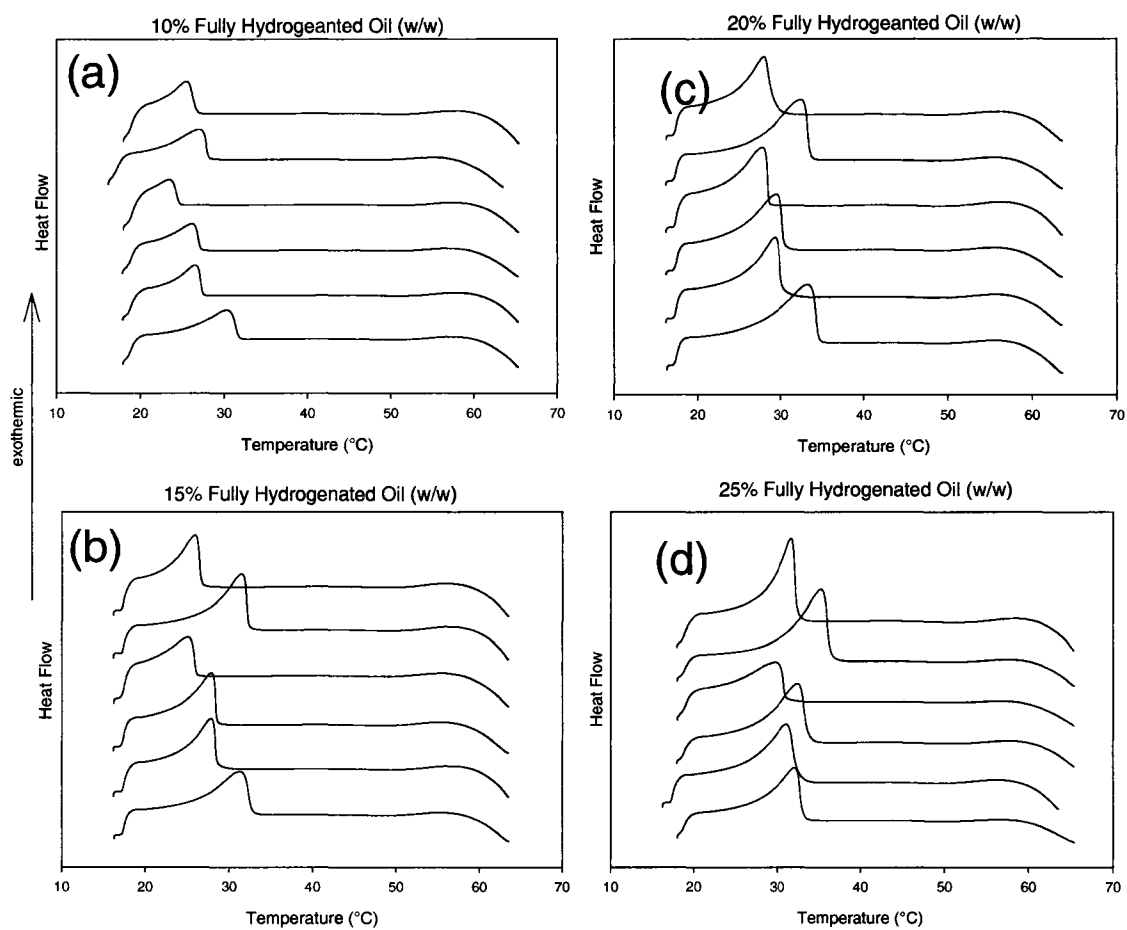


Figure 2.9: Crystallization curves for unsheared systems arranged by concentration (a) 10%, (b) 15%, (c) 20%, (d) 25%

the concentration of fully hydrogenated fat increases, there is a larger fraction of the hard fat, with a higher melting point, to be crystallized. Thus when crystallization begins within a sample, all of the hard fat will immediately crystallize, and heat will be released. The greater the number of molecules involved in crystallization at one point would cause a greater amount of energy to be released into the system. Thus, a 25% fully hydrogenated fat sample will initially release more energy during crystallization than a 10% fully hydrogenated fat sample. This accounts for the steep onset to crystallization as seen in the 25% concentration graph in Figure 2.9, as well as for the increase in amplitude as the amount of fully hydrogenated fat in the sample increases. The growth mode of a fat network is illustrated by the enthalpy of crystallization curves as these curves depict the heat transfer to/from the system. Changes in the shape of the enthalpy of crystallization curves, for example the steep onset to crystallization on the 25% concentration graph in Figure 2.9, indicate a change in the growth mode of the network. Steep narrow curves indicate an abundance of crystallization activity as this process is exothermic. Wider enthalpy of crystallization peaks indicate a slower growth of the network, with re-melt of the crystals occurring more often. Thus, in general, the growth mode of all of the fully hydrogenated fats at each concentration is similar.

The crystallization curves for the market shortenings are shown in Figure 2.10. The curves for the Tenderflake and Pure Lard samples differ from the other crystallization curves as each curve has a large peak, with a small shoulder peak occurring at a slightly (5 ± 1 °C) higher temperature. The peak maxima for the Tenderflake and Pure Lard curves occur at 7 and 5 ± 0.1 °C respectively. The

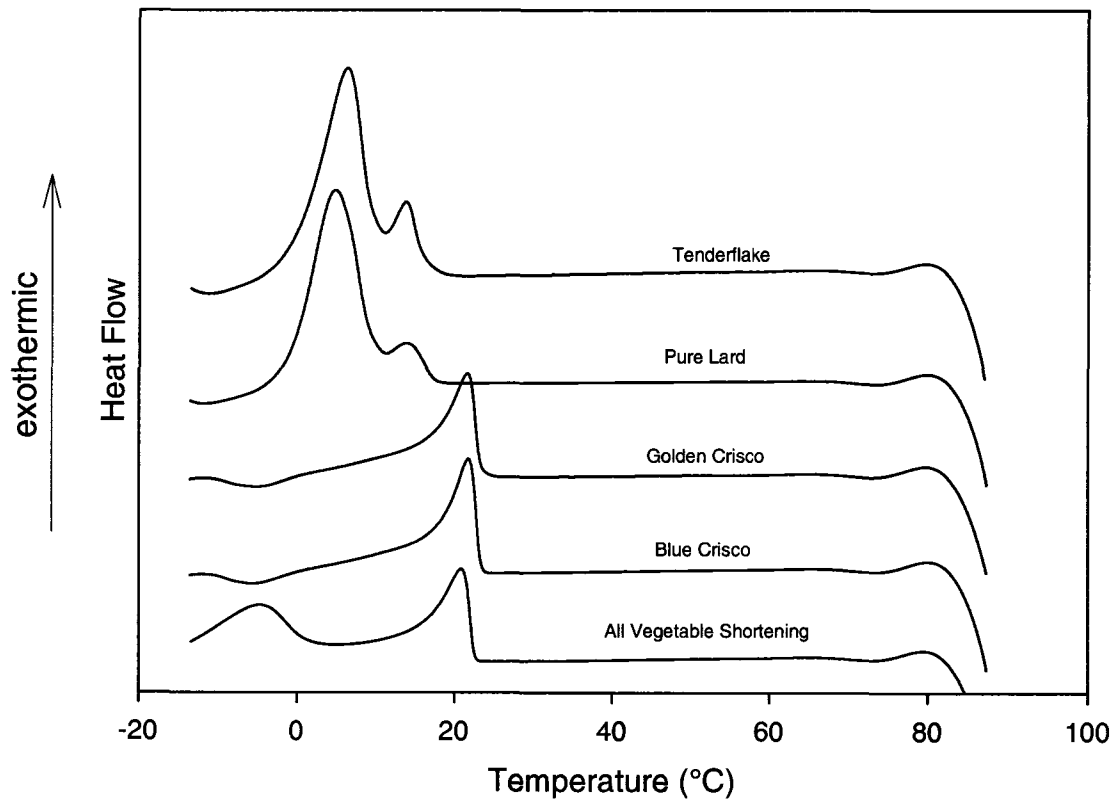


Figure 2.10: Market shortening crystallization curves

crystallization curves for the remaining market shortenings have similar shapes, location of peak maxima (20 ± 1 °C) and onset temperatures of crystallization. However, the All Vegetable Shortening, whilst initially appearing as Blue Crisco and Golden Crisco, differs as there is another peak maximum at -5 °C. This is not a true separated peak as the enthalpy curve does not reach zero prior to the appearance of this second, smaller peak.

From Figure 2.10, one can infer that the crystallization and growth modes of Tenderflake and Pure Lard are quite similar as the crystallization curves are similar. This is as one would expect, as from Table 2.1, one can see that the ingredients of Tenderflake and Pure Lard as listed on the product's packaging are the same. Thus any differences noted could be due to minor compositional variances, or differences in the processing of the shortening. Figure 2.10 also indicates that the crystallization and growth modes of Golden Crisco and Blue Crisco are similar. Table 2.1 indicates that the products have a similar composition, with the exception of added color in Golden Crisco. Initially appearing to be similar to Blue Crisco and Golden Crisco, All Vegetable Shortening possesses the second peak, indicating a second occurrence of crystallization. This could be due to the presence of partially hydrogenated canola oil and/or the absence of hydrogenated modified palm oil and artificial flavor in All Vegetable Shortening, as shown by Table 2.1. These observations therefore further strengthen the argument that lipid systems with similar molecular identities will crystallize and melt in very similar fashions, particularly samples which have sat on the shelf for a while. Certainly large

differences in crystallization and melting can be procured from processing, but over time the structures revert to their molecularly induced thermodynamic minima.

Figure 2.11 shows the temperature at which the maxima of the DSC melting curves occur for all sheared samples; this is the predominant temperature at which melting is observed. For samples containing the same fully hydrogenated fat at varying concentrations, it can be seen that as one increases the amount of hard fat in the sample, the temperature at which the maximum of the melting curve occurs increases. One exception to this trend is the 10% fully hydrogenated canola sample, which has its peak maximum at 58.3 ± 0.1 °C, which is higher than that for the 15% sample (58.0 ± 0.1 °C). The cause of this exception baffles the authors. The samples containing fully hydrogenated palm consistently have melting peak maxima occurring at lower temperatures than that for the other five fully hydrogenated fat samples. The samples containing fully hydrogenated canola have the melting peak maxima occurring at the highest temperatures with the exception of the 15% concentration (58.0 ± 0.1 °C) where the soybean sample peak maximum occurs at a higher temperature (58.6 ± 0.1 °C). In this instance, the compounds in the soybean samples have higher melting points than those in the 15% canola samples. Within samples containing the same hard fat there is little variation in location of melting peak maxima (less than 5 °C). Thus, the choice of fully hydrogenated fat, not the amount of the hard fat in the sample is important in determining the melting peak maxima for the sheared concentrations.

Also shown in Figure 2.11 are the melting peak maxima for the market shortening

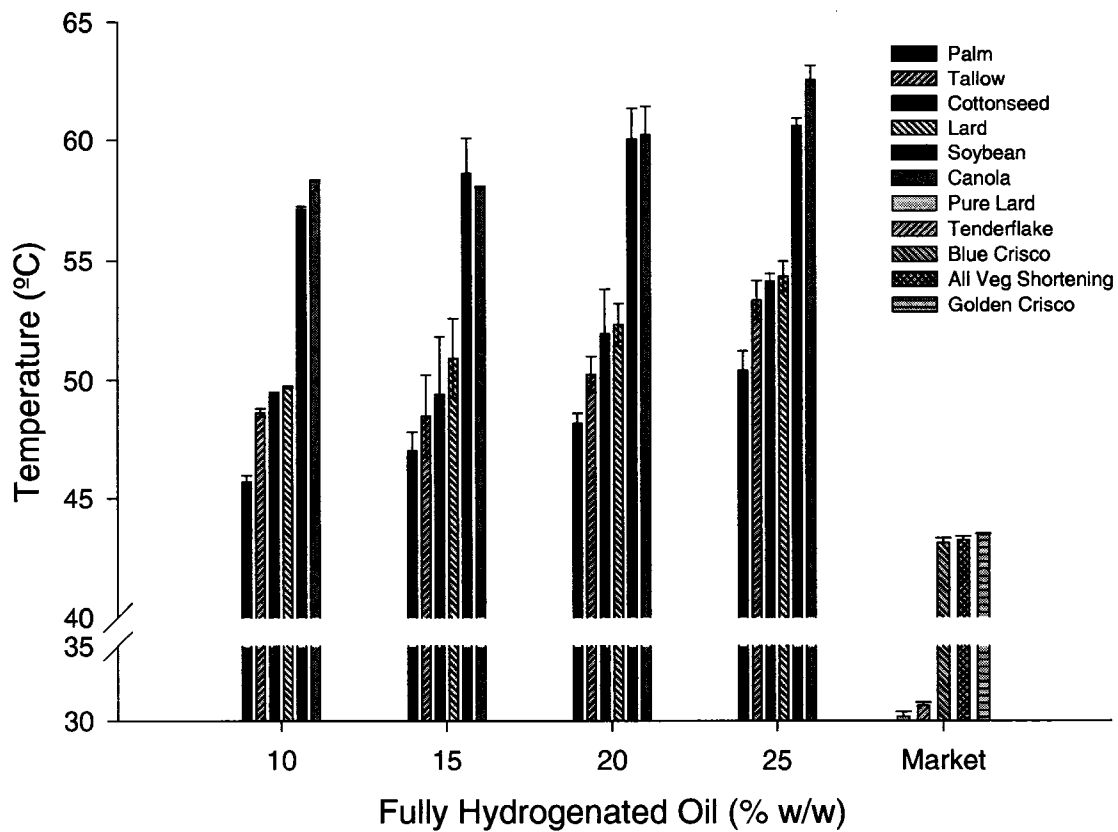


Figure 2.11: Enthalpy of melt peak maximum versus concentration for sheared samples

samples. As with the crystallization peak maxima, the melting peak maxima for the market shortenings occur at lower temperatures than that for the samples with varying concentrations of the six hard fats. Again, the peak maximum of melting of Pure Lard is at the lowest temperature, and highest temperature of peak maximum is with Golden Crisco, Blue Crisco, and All Vegetable Shortening which occur at roughly the same temperature ($43.2\text{ }^{\circ}\text{C} \pm 0.2\text{ }^{\circ}\text{C}$). Given that the compositions of Golden Crisco, Blue Crisco, and All Vegetable Shortening from Table 2.1 are quite similar it is interesting to note that the melting peak maxima occur at the same temperature. This would be an indication that the molecular ensemble of the market shortenings is a major factor in determining the melting point of the sample.

Figure 2.12 shows the temperatures at which the melting peak maxima occur for all unsheared samples. As with Figures 2.4 and 2.11 there is an increasing trend for samples containing the same fully hydrogenated fat as one increase the amount of hard fat in the samples. The samples containing fully hydrogenated palm have the peak maxima occurring at consistently lower temperatures than for all other samples with hard fat at the same concentration, suggesting that fully hydrogenated palm has a lower melting point. More importantly, the trends for the sheared and unsheared values of melting peak maxima are the same. As well, the samples containing fully hydrogenated soybean oil have the peak maxima occurring at higher temperatures than for all other samples of the other fully hydrogenated fats at the same concentrations with the exception of the 25% cottonseed sample ($63.9\text{ }^{\circ}\text{C}$). The authors do not know the cause of this exception. Shearing switches the position of the canola and soybean peak maxima.

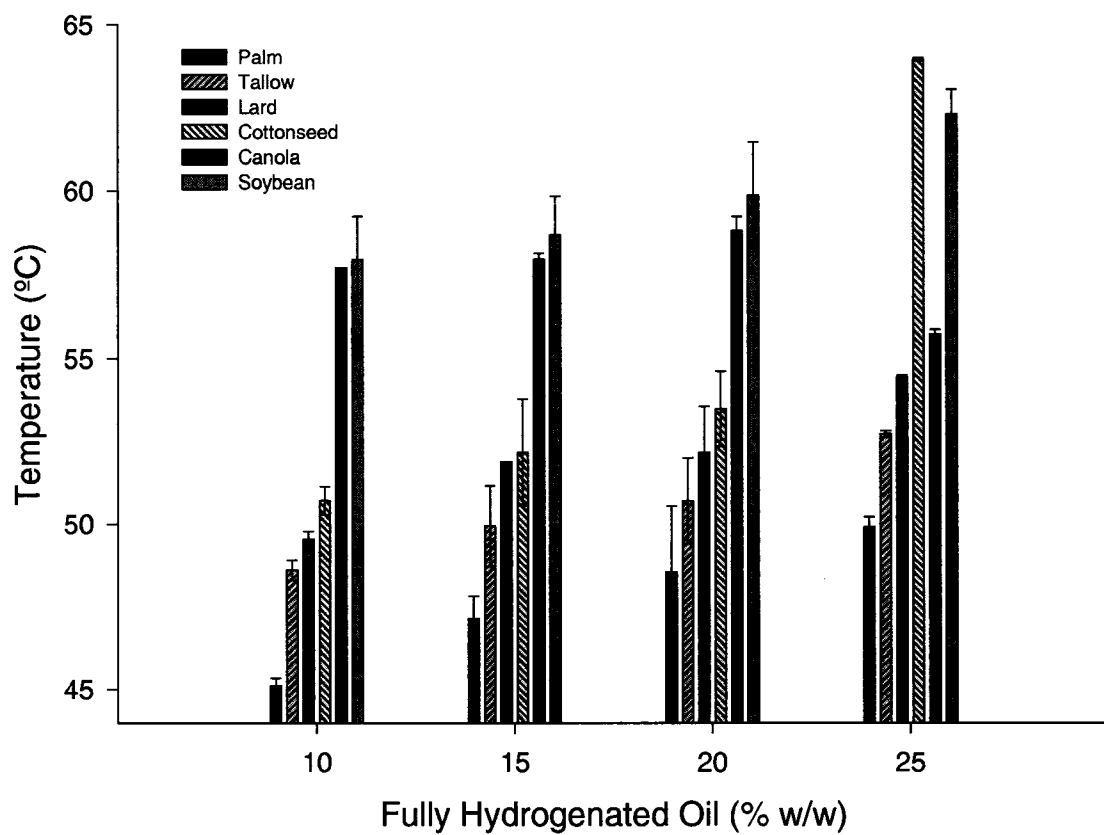


Figure 2.12: Enthalpy of melt peak maximum versus concentration for unsheared samples

Also, cottonseed is higher than lard in the unsheared samples, but that trend is reversed with the sheared samples. However, as with the sheared samples, the melting peak maxima for the unsheared samples are relatively unchanged (less than 5 °C) when comparing samples with the same fully hydrogenated fat. Again, this is an indication that the choice of fully hydrogenated fat determines the melting peak maxima more-so than the percentage of fat used in the sample. However, it is also clear here that performance can be optimized for a particular lipid ensemble by manipulating processing conditions such as shear.

The onset temperature of melting, indicating a shortening's tendency to "oil off", is shown in Figure 2.13. Each line within a graph in Figure 2.13 represents a different fully hydrogenated fat system. The sheared samples containing canola consistently had the highest onset temperature and the largest variance in onset temperature between samples of canola at varying concentrations. Canola samples therefore have the highest oiling off point of all the samples tested, and this point is greatly affected by the amount of canola in the samples. The melting onset temperature for all the other sheared samples was restricted to a melting range of 25 ± 3 °C. Lard demonstrated an increase in onset of melt at 25% probably due to higher melting crystals being formed at higher percentages of PPS, PSS, and SSS. The melting onset temperatures for the unsheared samples varied a great deal, with no one fully hydrogenated fat consistently demonstrating the highest or lowest melting temperature or the greatest change in melting temperature across all concentrations. Thus for the unsheared samples, little importance in terms of melting point is placed on the molecular ensemble within the samples – the variations in melting

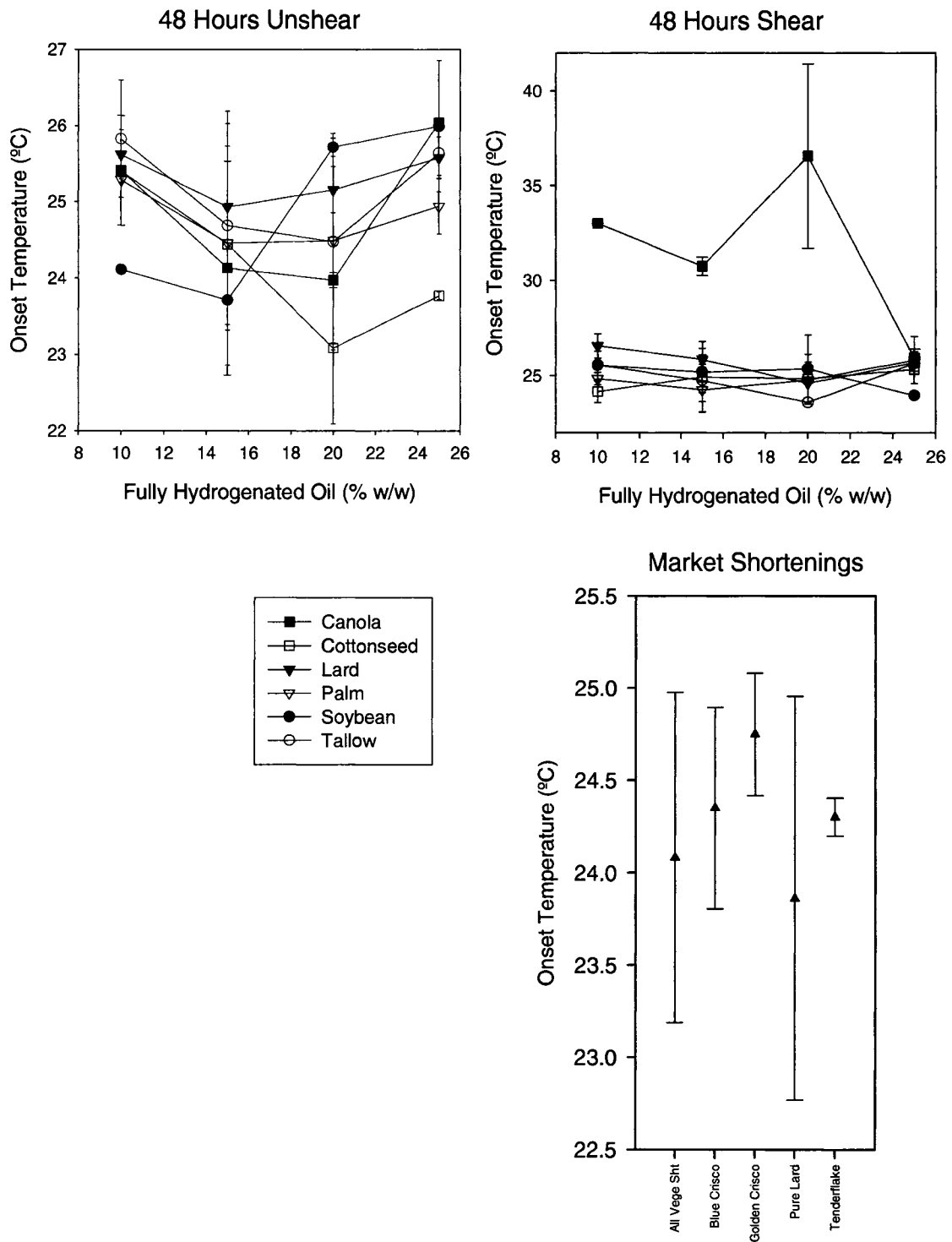


Figure 2.13: Melting onset temperatures versus concentration for sheared and unsheared mixtures at 0 and 48 hours with inset market shortenings onset of melt graph

onset must be due to the polymorphic forms or the networks formed during the crystallization process. In the unsheared samples, the onset of crystallization varied by 2.91 °C across all samples, unlike the sheared samples which varied by 12.61 °C across all samples. The main variants in the onset of melting in the sheared samples were the canola samples whose onsets ranged from 25.9 °C to 36.5 °C. This increase in onset of melting in the canola samples indicates that the sample is composed of high melting compounds. This is likely due to the large percentage of the TAGs SSS and PSS in the sample as shown by Figure 2.2. In the case of the canola samples, shear promotes the formation of a more thermodynamically stable form by increasing the heat and mass transfer within the system.

Inset in Figure 2.13 is the onset of melt temperature for the market products. These values are within the same range as the onset temperatures of the six binary fat mixtures used with Pure Lard having the lowest, and Golden Crisco having the highest melt onset temperature. Thus, the structures formed by the market shortenings have the same melting onset. The onset of melting for the market shortenings is within the same range as that of the composite binary samples. For example, the oiling off point for Blue Crisco is 24.3 °C, and that for its composite fats (palm and soybean), is 25.0 °C ± 0.8 °C (accounting for the different concentrations) and 24.5 °C ± 0.9 °C respectively. However, from Figure 2.6, the melting peak maxima of the market shortenings are consistently lower than that of the binary mixtures. Thus the network formed during crystallization of the market shortenings is quickly altered with the addition of thermal energy whereas the

structures within the binary mixtures are more resistance to the addition of heat. Thus, the microstructures must be significantly different.

The enthalpy of melt curves of the sheared and unsheared samples are shown in Figures 2.14 and 2.15 respectively. Each graph shows the curves for a different hard fat, in increasing concentration with the 10% sample being represented by the lowest curve in the graph, and the 25% sample represented by the uppermost curve in the graph. Figures 2.16 and 2.17 exhibit the same curves illustrated by Figures 2.14 and 2.15, organized by concentration, instead of by fully hydrogenated fat. The curves within each graph in Figures 2.16 and 2.17 are stacked (upper to lower) as: tallow, soybean, palm, lard, cottonseed, and canola with Figure 2.16 illustrating the sheared samples, and Figure 2.17 the unsheared samples. As the amount of hard fat in the sample increases, the size of the peak also increases, as supported by enthalpy and full width half maximum data obtained (not shown) for both the sheared and unsheared samples. Therefore, the addition of more fully hydrogenated fat to a sample increases the enthalpy of melt of that sample. This is expected as the fully hydrogenated fats are composed of higher melting TAGs than the soybean oil. Thus with an increase in thermal energy, there is a greater amount of heat absorbed by each sample as one increases the percentage of fully hydrogenated fat.

The DSC melting curves for the market shortenings are shown in Figure 2.18. The enthalpy curve for All Vegetable Shortening has a small shoulder peak occurring 22 ± 0.1 °C after the large melting peak which is at 43 ± 1 °C. The curves for the Golden Crisco and Blue Crisco samples are nearly identical with the peak maxima, and onset

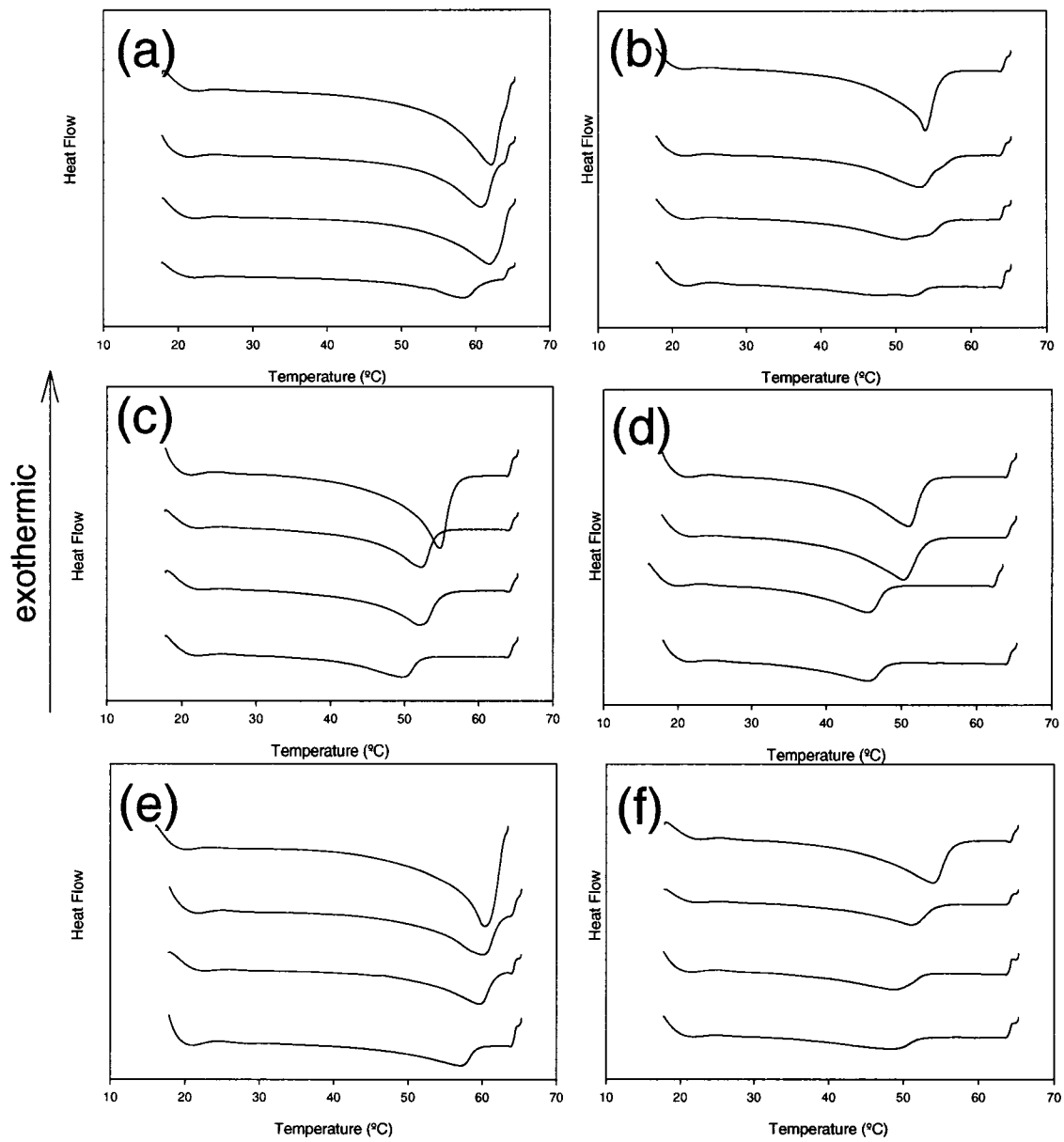


Figure 2.14: Enthalpy of melt curves for sheared samples arranged by increasing concentration of hard fat (a) canola, (b) cottonseed, (c) lard, (d) palm, (e) soybean, (f) tallow

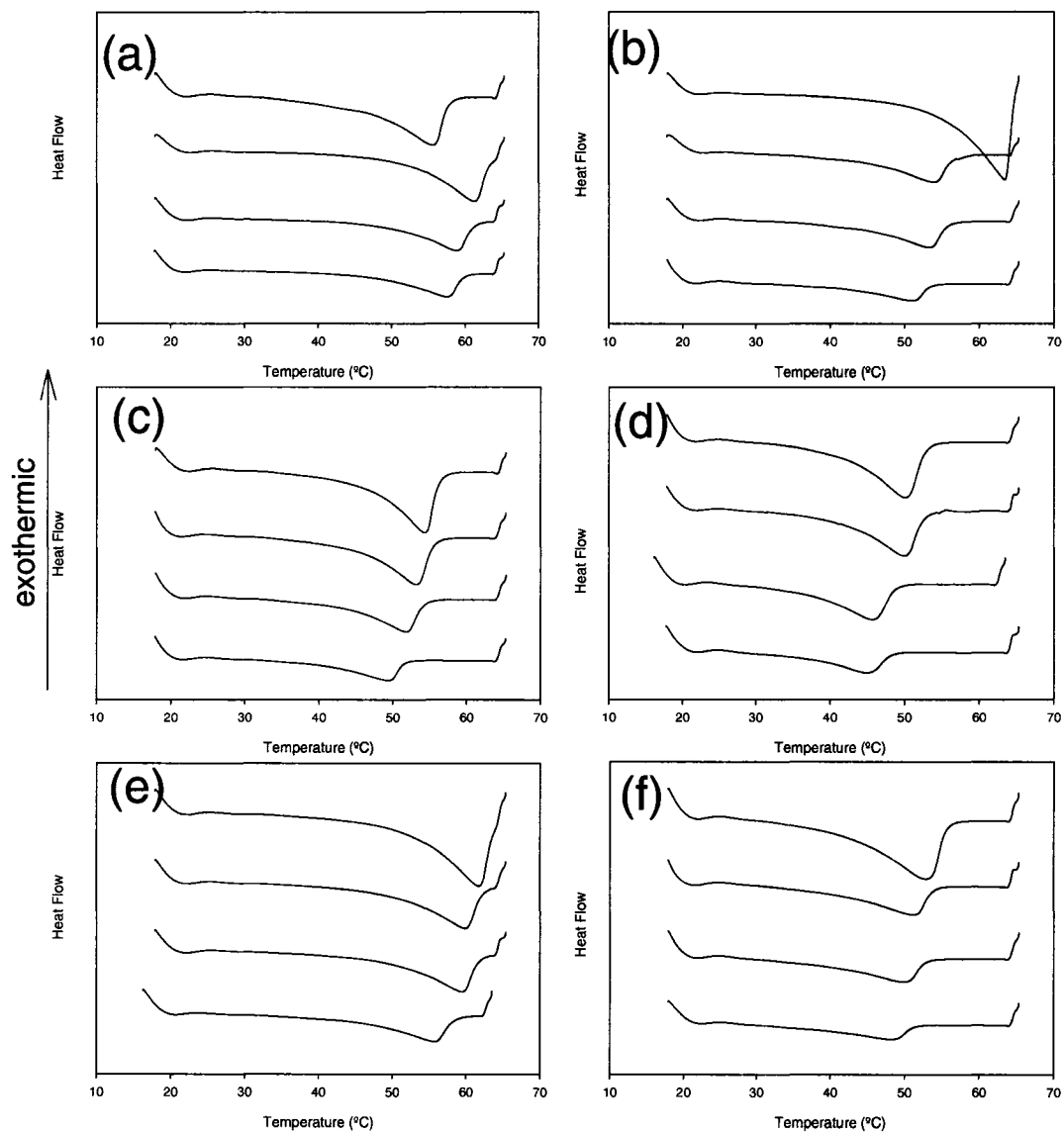


Figure 2.15: Enthalpy of melt curves for unsheared samples arranged by increasing concentration of hard fat (a) canola, (b) cottonseed, (c) lard, (d) palm, (e) soybean, (f) tallow

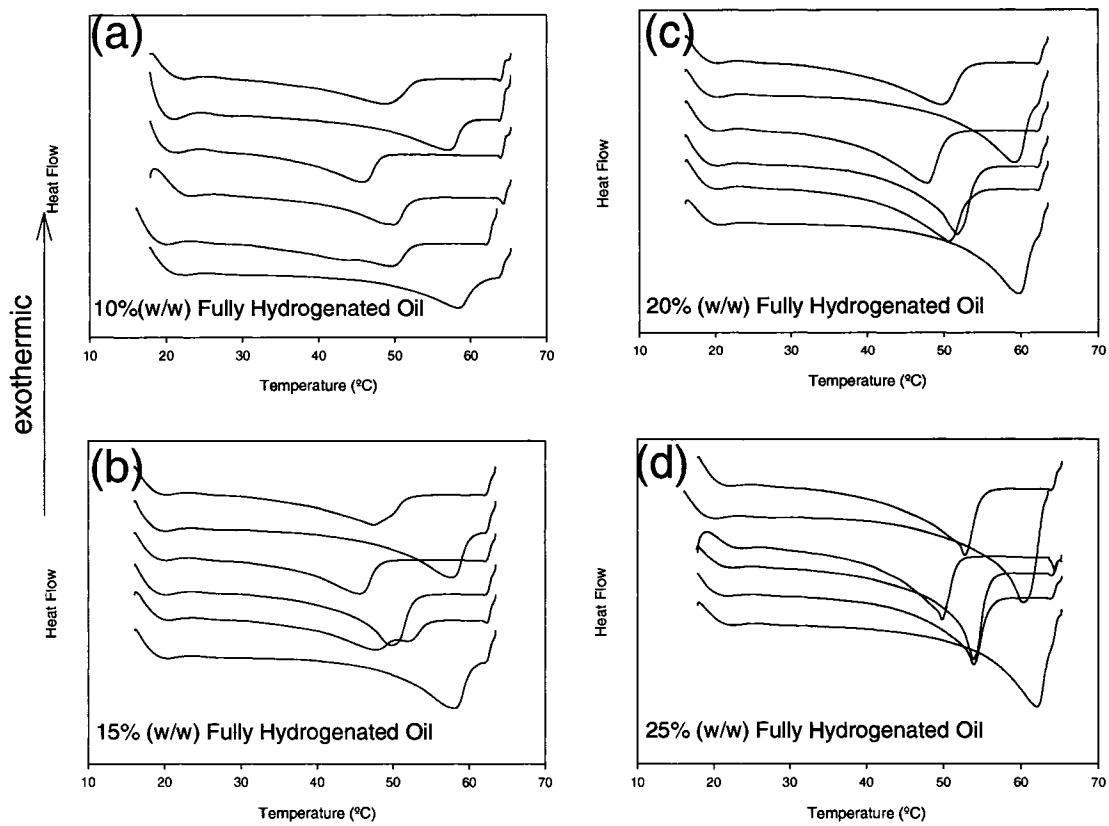


Figure 2.16: Enthalpy of melt curves for sheared samples arranged by concentration (a) 10%, (b) 15%, (c) 20%, (d) 25%

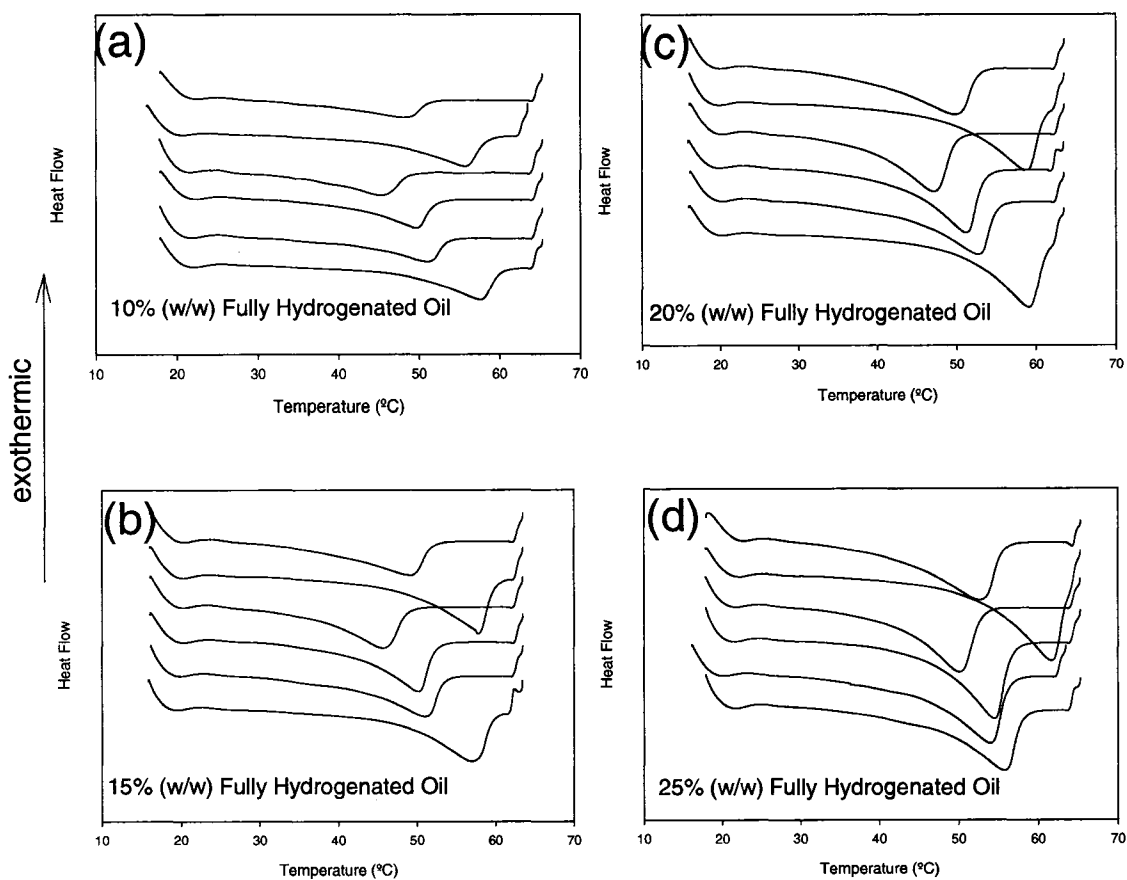


Figure 2.17: Enthalpy of melt curves for unsheared samples arranged by concentration

(a) 10%, (b) 15%, (c) 20%, (d) 25%

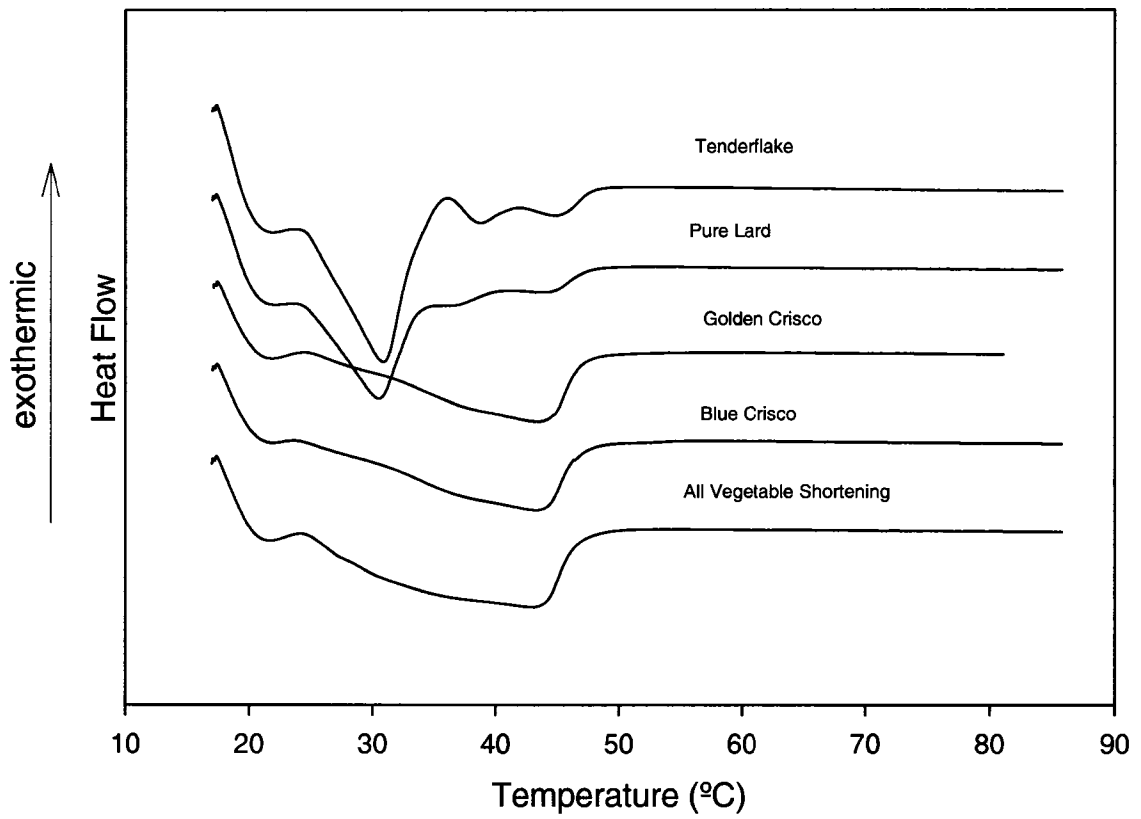


Figure 2.18: Enthalpy of melt curves for the market shortenings

occurring at the same temperature. Again, given the composition of both of these shortenings from Table 2.1 as well as the similarities found between these shortenings in Figures 2.4, 2.10, and 2.11, the similarities found between the enthalpy of melt curves is to be expected. As with the crystallization enthalpy curves, the Pure Lard and Tenderflake melt curves are similar as they each have a small peak at a higher temperature (10 ± 1 °C) above the main melting peak (at 30 ± 1 °C). As with Golden Crisco and Blue Crisco, the enthalpy of melt curve for the Pure Lard sample was projected to be akin to that for the Tenderflake sample.

Therefore, selection of molecular ensemble, and the presence/absence of shear processed with a constant cooling scheme do lead to changes in the crystallization growth mode, and enthalpies of crystallization and melt. The market shortenings used in this study were found to have properties similar to the composite partially and fully hydrogenated fats. Blue Crisco and Golden Crisco as well as Pure Lard (generic) and Tenderflake were found to be similar with respect to enthalpies of crystallization, and melt.

2.4 References

1. Ghotra, B.S., S.D. Dyal, and S.S. Narine, *Lipid shortenings: a review*. Food Research International, 2002. **35**(10): p. 1015-1048.
2. Hartel, R.W., *Crystal Growth*, in *Crystallization in Foods*. 2001, Aspen Publishers, Inc: Gaithersburg, Maryland. p. 192-232.
3. Hartel, R.W., *Nucleation*, in *Crystallization in Foods*. 2001, Aspen Publishers, Inc: Gaithersburg, Maryland. p. 145-191.
4. Narine, S.S. and A. Marangoni, *Structure and Mechanical Properties of Fat Crystal Networks*, in *Physical Properties of Lipids*, A. Marangoni and S.S. Narine, Editors. 2002, Marcel Dekker Inc: New York. p. 63-83.
5. Moodie, G.E.E., et al., *Influence of Egg Characteristic on Survival, Growth, and Feeding in Larval Walleye (Stizostedion vitreum)*. Canadian Journal of Fisheries and Aquatic Sciences, 1989. **46**: p. 516-521.
6. Bockisch, M., *Animal Fats and Oils*, in *Fats and Oils Handbook*. 1998, AOCS Press: Champaign, Illinois. p. 154.
7. Neff, W.E., et al., *Triacylglycerol structure of animal tallows, potential food formulation fats, by high performance liquid chromatography coupled with mass spectrometry*. J.Liq.Chrom.& Rel.Technol., 2002. **25**(6): p. 985-998.

8. Neff, W.E., et al., *Oxidative Stability of Purified Canola Oil Triacylglycerols with Altered Fatty Acid Compositions as Affected by Triacylglycerol Composition and Structure*. J.Am.Oil Chem.Soc., 1994. **71**(10): p. 1101-1109.
9. Wang, T., *Soybean Oil*, in *Vegetable Oils in Food Technology; Composition, Properties and Uses*, F.D. Gunstone, Editor. 2002, CRC Press LLC: Boca Raton, Florida. p. 21-22.
10. Humphrey, K.L., P.H.L. Moquin, and S.S. Narine, *Phase behavior of a binary lipid shortening system: From molecules to rheology*. Journal of the American Oil Chemists Society, 2003. **80**(12): p. 1175-1182.

3. A Comparison of Lipid Shortening Functionality as a Function of Molecular Ensemble and Shear: Microstructure, Polymorphism, Solid Fat Content and Texture

3.1 Introduction

Lipid shortenings are important industrial food ingredients, which are manufactured from a mixture of oils from a number of sources, variously processed (fully and partially hydrogenated, interesterified, etc.), and emulsifiers and other additives. In an effort to begin an approach to a comprehensive description of the fundamental relationships between molecular ensemble, processing conditions, additives, and emulsifiers on final physical functionality of shortening crystal networks, a detailed study of the relationships between molecular profile, crystallization, and melting of a series of binary lipid shortening-like systems and a number of over-the-counter market shortenings has been performed in Chapter 2 [1]. This work examined binary lipid systems composed of fully hydrogenated samples of canola, cottonseed, lard, palm, soybean and tallow blended to different percentages with refined, unhydrogenated soybean oil under constant cooling conditions and varying conditions of shear. These systems were chosen for study as they form the normal feedstock in industrial shortenings, and it was felt that the study would suggest ways in which developers can expect these lipid systems to

A version of this chapter has been published.
Narine, S.S. and K.L. Humphrey, A comparison of lipid shortening functionality as a function of molecular ensemble and shear: microstructure, polymorphism, solid fat content and texture. Food Research International, 2004. 37(1): p. 28-38.

behave. In addition, these systems provide a realistic diversity of TAGs in varying proportions. The market shortenings investigated in this study [1] were All Vegetable Shortening (generic), Blue Crisco All Vegetable Shortening, Golden Crisco All Vegetable Shortening, Pure Lard (generic), and Tenderflake Pure Lard.

However, the crystallization and melting behavior of these systems, while offering a wealth of information and inferences on the relationships sought, are but a subset of the physical parameters that can be measured and related to molecular ensemble, processing conditions, and final physical functionality. Much endeavor has been recorded on efforts to relate phase behavior [2, 3], polymorphism [2, 4], microstructure [4-6], processing conditions, and texture [3] of lipid crystal networks. Very few such studies have however, involved scrutiny of molecular ensemble, crystallization and melting behavior, crystal structure and polymorphism, microstructure, SFC, and texture under variable conditions of shear.

In many instances, crystallization and melting behavior may not indicate changes in polymorphism of the samples and certainly does not impart any but indirect information on SFC, and absolutely no information on microstructure; all structural parameters that are important to predicting final physical functionality. Furthermore, it is important to relate *all* of the structural levels to final hardness, as for example relying on SFC alone to predict hardness has been shown to be unreliable [7-9]. In this study, we report findings, relying heavily on the data communicated by Humphrey and Narine [1], of relationships between the effects of molecular ensemble and shear on SFC,

polymorphism, microstructure, and final hardness of the shortening networks studied by Humphrey and Narine [1].

3.2 Experimental Procedures

When referring to sample holding temperature as well as cooling and heating rates all temperatures are reported to a certainty of ± 0.5 °C. All measurements were performed with a stage temperature of 20 °C ± 1 °C, and the samples were stored at 20 °C. The six fully hydrogenated fats used (canola, cottonseed, palm, lard, soybean, and tallow) as well as the refined soybean oil was supplied by Bunge Foods Ltd., of Bradley IL.

Samples of each fully hydrogenated fat (canola, cottonseed, palm, lard, soybean, and tallow) were prepared and tempered as indicated by Humphrey and Narine [1].

3.2.1 *Sample Preparation*

Three precooled (20 °C) NMR tubes were prepared for both the sheared and the unsheared samples. Hardness samples were also prepared by transferring 36.0 ± 0.5 g of the prepared fat into 3 precooled (20 °C) stainless steel pans (diameter 6.4 ± 0.1 cm). Three XRD tubes were prepared for each mixture by pressing a precooled (20 °C) glass capillary tube into the hardness sample after a 48 hour time period (after all of the hardness measurements had been taken).

The five market shortenings were prepared in the following manner. For hardness measurements, a uniform slice of each sample 3.0 ± 0.5 cm thick was cut and placed on wax paper. Three NMR tubes were precooled ($20\text{ }^{\circ}\text{C}$) and the open end was pushed into the shortening. The tubes were then vibrated so that the sample moved to the bottom of the NMR tubes. Three precooled ($20\text{ }^{\circ}\text{C}$) DSC pans were prepared for each of the market shortenings. Microscope slides of the market shortenings were prepared in two ways. The first was by heating a portion of the shortening to $90\text{ }^{\circ}\text{C}$ and then cooling it in a Linkam 350 temperature controlled microscope stage at $10\text{ }^{\circ}\text{C}$ per minute to $20\text{ }^{\circ}\text{C}$, as the unsheared samples were prepared. Another set of slides was prepared by taking a thin slice of the sample and placing it on the slide, which had been precooled ($20\text{ }^{\circ}\text{C}$). This second batch of slides was not tempered in the Linkam, but rather held at $20\text{ }^{\circ}\text{C}$ for the pictures. Three XRD tubes were prepared by pressing a pre-cooled tube into the market-shortening hardness sample.

3.2.2 NMR Measurements, SFC Determination

The instrument used in the investigations was the ‘minispec mq SFC analyzer’, which is a pulse magnetic resonance spectrometer with a temperature controlled measurement chamber. The data sampling procedure was fully automated, and the SFC was calculated and displayed by computer software [10-13].

Immediately after being prepared, the samples were measured in the NMR. The sample tube was then stored for 48 hours when another SFC reading was acquired.

3.2.3 Relative Hardness Measurements

The instrument used in the investigation was the 'Instron 4201' with a temperature controlled stage. The software package "Instron Series IX Automated Materials Tester V. 7" controlled the instrument and the following procedure was used. Using a 5.00 kg maximum load cell a steel penetration cone of mass 45 ± 0.5 g and angle 22.5° was applied to a penetration depth of 8.00 mm. The position of the penetration cone was controlled by the software, and it moved downward at a rate of 120.00 mm per minute with a data sampling rate of 20 points per second. The hardness measurements were acquired after 48 hours.

The outputs of the hardness measurements were made into displacement-force graphs with the slope of the graph being an indication of the relative hardness of the sample. The slope of the line was calculated, and the slopes were plotted against the composition of the mixture using a log scale on the vertical axis.

3.2.4 Microstructure Determination

A high resolution polarized light microscope, equipped with a high resolution "Hamamatsu Digital Camera", and a "Linkam LTS 350" temperature controlled stage was used. The microscope/camera assembly was controlled by "Openlab 3.0.8" software.

The slides of the unsheared samples were processed in the temperature controlled stage by heating the slide to 90°C , holding at of 67°C for 5 minutes, then cooling at a

rate of 10 °C per minute to the final temperature of 20 °C which was held for 12.5 minutes. The pictures were taken immediately after the 12.5 minute holding period and the samples were held to allow for pictures 48 hours after slide tempering. Pictures were taken immediately after preparation of the slides for the sheared samples, which were stored at 20 °C for pictures 48 hours after slide tempering.

3.2.5 XRD Measurements, Polymorphism

The 'Bruker AXS X-ray diffractometer' was used in this study. The procedure was automated and commanded by Bruker's 'General Area Detector Diffraction System V 4.1.08' (GADDs) software with a measurement time of 450 seconds and a maximum display count of 127.

3.3 Results and Discussion

Figure 3.1 shows increasing SFC with increasing concentration of fully hydrogenated fats within sheared samples containing the same fully hydrogenated fat. The error bars represent the standard deviation between three replicates. This trend is evident for all concentrations measured. This is expected, as the addition of fully hydrogenated fat should increase the SFC of the sample since more of the sample is solid at 20 °C due to the addition of the higher melting fat as well as the formation of successively higher melting compounds as described by Humphrey and Narine [1]. The market shortening's SFCs are also shown in Figure 3.1. One can see that Tenderflake has

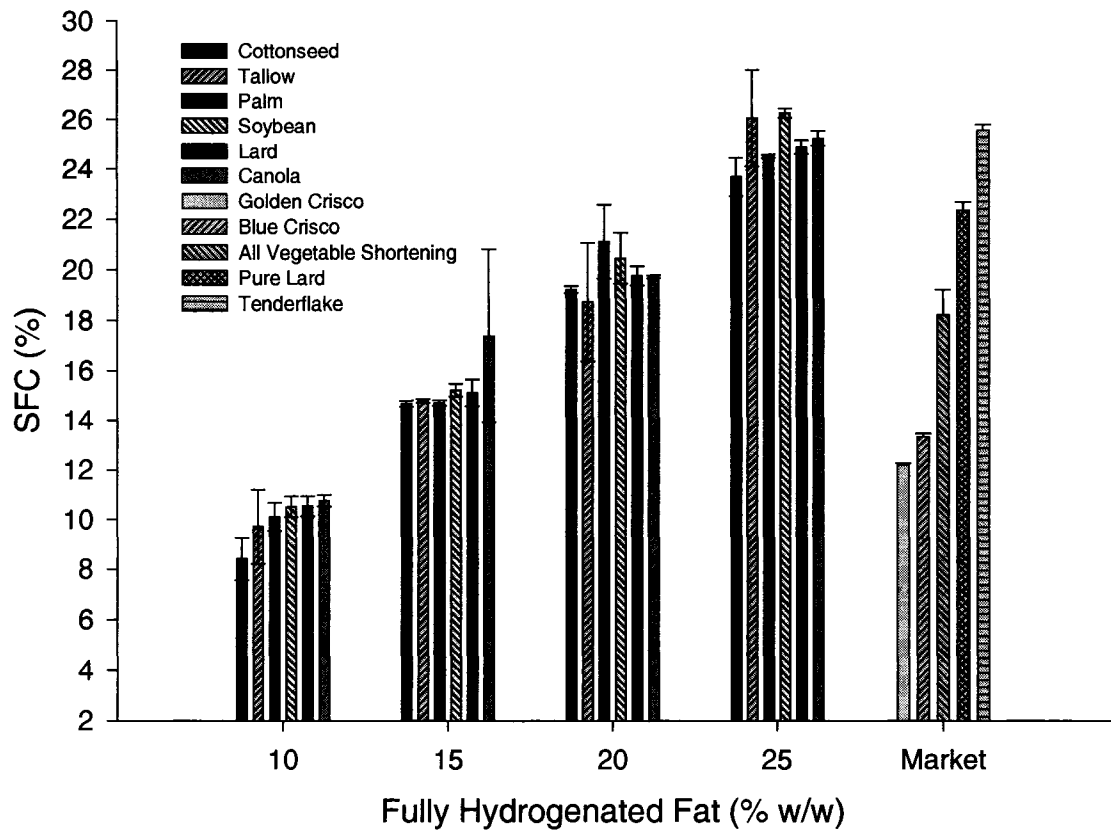


Figure 3.1: SFC versus concentration for sheared systems 48 hours after tempering

the highest SFC, and Golden Crisco the lowest. The range of SFC for the market shortenings is within the range of the SFC for the sheared binary concentrations. This is interesting as the crystallization peak maxima and melting peak maxima of these market shortenings are lower than that for the corresponding binary systems [1]. Therefore, even though the bulk of a market shortening melts at a lower temperature than the binary shortenings, the SFC is still close to that of the binary shortenings. Tenderflake, for example, has an SFC of $(25.5\% \pm 0.2\%)$ and a melting peak maxima of $(31.0\text{ °C} \pm 0.2\text{ °C})$ whilst the sheared 25% lard sample has an SFC of $(24.8\% \pm 0.2\%)$ and a melting peak maximum of $(54.3\text{ °C} \pm 0.6\text{ °C})$. This is an example of how SFC measurements used as a means to compare fat systems can be flawed. Obviously, the reason the binary systems have similar SFCs to the corresponding market systems in this case is due to the fact the fats were all stored at 20 °C, a temperature lower than the melting points of both systems. However, this alludes to a structural difference in the network of the market shortenings and the network of the binary shortenings. The important structural level here is the crystal level. This is not surprising as the market shortenings have significantly different molecular ensembles compared to their binary counterparts.

Figure 3.2 shows the SFC for unsheared samples. There is a trend of increasing SFC with increasing percent fully hydrogenated fat within the samples containing the same fat. The SFC of the samples at each concentration are also typically within a 4% range with the exception of the 10% fully hydrogenated lard sample which has a SFC of 3.8%, well out of the 7.6 - 9.6% SFC range within which the rest of the 10% samples lie.

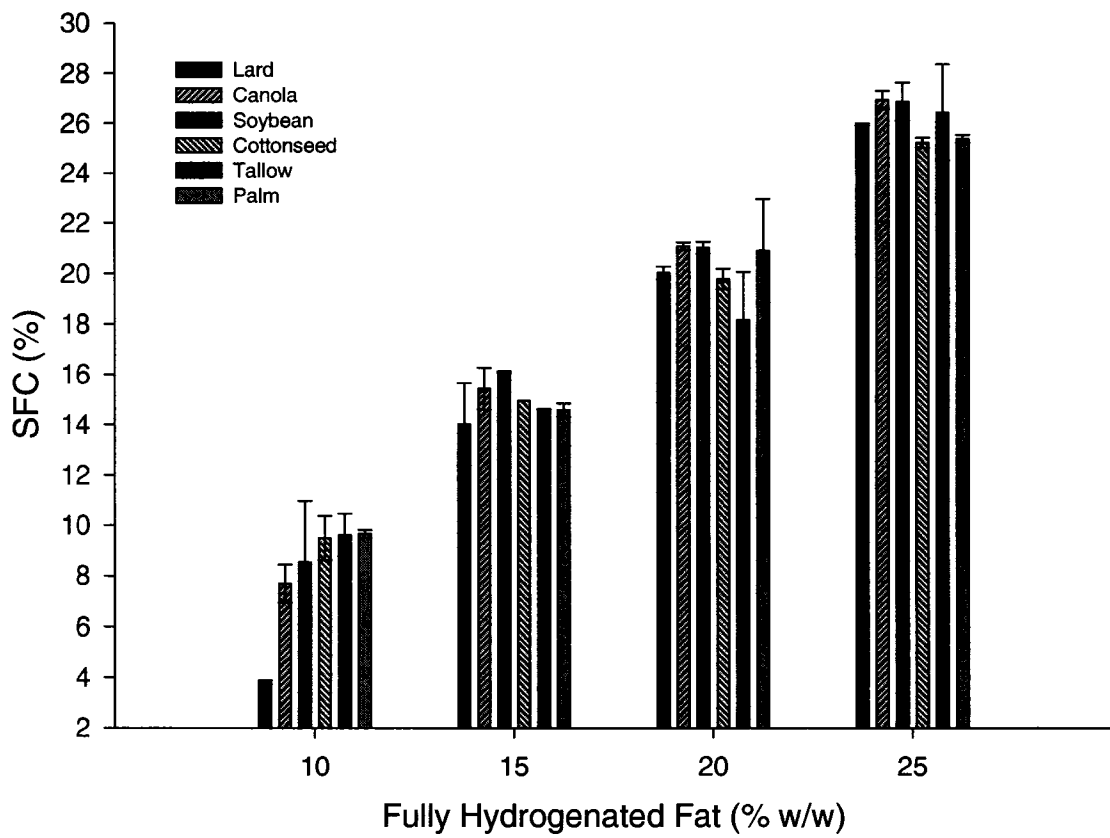


Figure 3.2: SFC versus concentration for unsheared systems 48 hours after tempering

With the exception of the 10% lard, 10% canola, and 10% soybean samples, the SFC of the unsheared concentrations are within the same range as the SFC of the sheared concentrations (10 – 28%).

Figure 3.3 shows the smoothed XRD spectra for the 25% concentrations of the hard fats, sheared and unsheared samples, as well as that for the market shortenings. The unsheared sample's spectra are the lower curve in each fully hydrogenated fat "pair" in the graph. The output spectra from the XRD were smoothed using the "Bisquare smoothing method" which is a function of "Sigma Plot v.8.0". A smoothing method was used as it reduces the noise of the signal. The Bisquare smoothing method was selected as once applied it did not eliminate shoulder peaks from the curve. Also in Figure 3.3 is a graph of average d versus the sample measured; the error bars represent the standard deviation between the three replicates. The peaks fall into the beta-prime polymorph range as indicated by the solid lines ($0.37 < \beta' < 0.40$ nm and $0.42 < \beta' < 0.43$ nm) with significant variations occurring within the range. These variances indicate that although the samples are all of form Beta-prime, the samples differ significantly within the Beta-prime polymorph. There are also a great number of samples demonstrating reflections at 0.45 nm. This spacing does not fall into α , β' , or β classifications. The authors have taken this spacing to indicate a "modified" β' form since all of the fats demonstrating this spacing observed reflections in the β' region. More work is needed to investigate the exact nature of this reflection at 0.45 nm. However, for the present discussion, it is sufficient to understand that this reflection represents a different structure from the reflections at 0.42, 0.39 and 0.38 nm.

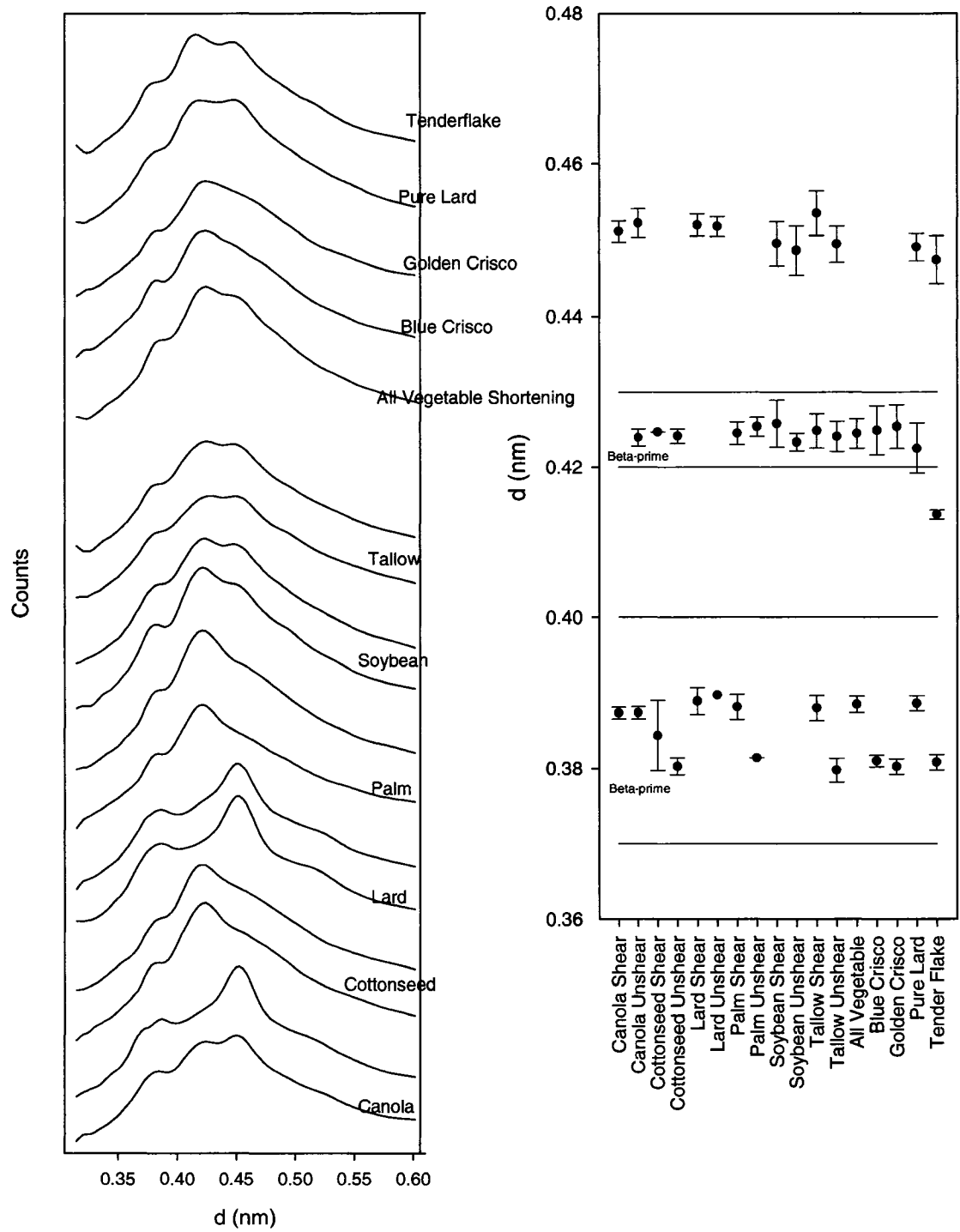


Figure 3.3: Composite diagram of smoothed X-ray diffractometry curves for 25% fully hydrogenated fats both unsheared (lower) and sheared (upper), and market shortenings with distance versus sample graph (right)

The unsheared cottonseed and the Tenderflake samples do not have a peak within the 0.42 thru 0.43 nm range. However, all samples do have a peak within the 0.37 thru 0.40 nm range. Although Tenderflake and Pure Lard are composed of mainly lard, the XRD spectra of the samples are not similar in shape. The 25% lard sheared and 25% lard unsheared samples have peaks at 0.45 and 3.9 nm whilst the Tenderflake sample has peaks at 0.45 and 0.38 nm, and the pure lard sample has peaks at 0.45, 0.42 and 0.39 nm. Similarly, the reflections of the All Vegetable Shortening, Blue Crisco, and Golden Crisco XRD samples are quite different than those of the canola and palm samples. This disparity between the crystal structure of the market shortenings and the corresponding binary systems therefore accounts for the differences seen in their crystallization behavior and is reflected by the discussed differences in melting [1]. The differences observed are probably influenced by the presence of partially hydrogenated TAGs and emulsifiers in the market shortenings.

The soybean samples reflections are characterized by a ~ 0.012 nm full width half maximum of the main peak, with a small shoulder peak occurring to the left of the main peak. The Golden Crisco and Blue Crisco samples also have this shoulder peak. Thus, the polymorphs of the Golden Crisco and Blue Crisco samples are strongly influenced by the presence of fully (or partially) hydrogenated soybean oil in the mixture.

In some cases, there are large differences observed in the XRD reflections between sheared and unsheared samples. There is a striking difference observed between the sheared and unsheared canola samples. Sheared canola samples have reflections at

0.45 and 0.39 nm, whilst unsheared canola samples have reflections at 0.45, 0.42 and 0.39 nm. Furthermore, the sheared sample has its major peak at 0.45 nm, while the unsheared samples have broad reflections equally at 0.45, 0.42, and 0.39 nm.

There is also a striking difference observed between sheared and unsheared palm samples, with sheared samples having reflections at 0.42 and 0.39 nm, and unsheared samples having reflections at 0.42 and 0.38 nm.

Tallow is the only other fat that demonstrated differences in XRD reflections between sheared and unsheared samples, with shear samples having reflections at 0.45, 0.42, and 0.39 nm and unsheared samples having reflections at 0.45, 0.42, and 0.38 nm.

Molecular arguments can be made for the differences in crystal structure between sheared and unsheared samples of canola and palm. Canola has a preponderance of stearic acid (~92.7%) and palm has a preponderance of palmitic acid (~ 48.5%) [1]. These are the fatty acids which are the highest melting and therefore form the TAGs which crystallize earliest. From Humphrey and Narine [1], we know that SSS and PPP do form mixed compounds with the other mixed TAGs such as PPS, PSP, and PSS. In an unsheared crystallization process, SSS and PPP in canola and palm would crystallize first, and would probably crystallize in isolation due to reduced mass transfer preventing other species such as PPS, PSP and PSS being in adequate amounts at the growing surface to result in mixed crystal formation. Therefore, crystal structure would be strongly influenced by a template of SSS or PPP initially crystallizing in isolation.

Furthermore, this crystal structure would be deficient in mixed crystal structures. However, under sheared crystallization conditions, a sufficient supply of mixed TAGs may be available to the growing surfaces due to increased mass transfer, resulting in an overall crystal structure dominated by mixed crystal formation between PPP, SSS, PSP, PPS and PSS. While tallow does not have a preponderance of any high-melting TAGs, molecular arguments may also be made to explain the differences in XRD reflection between sheared and unsheared samples. Tallow, of all the fully hydrogenated fats studied, has the largest amount of minor TAGs (TAGs not present individually at percentages below 2%). In fact, a full 22.8% of the TAGs found in tallow are made up of individual species present at levels lower than 2%. It is therefore not inconceivable that without good mass transfer coefficients, the participation of the minor TAGs in crystal structure will be compromised. Therefore, it is not surprising that there are differences between the sheared and unsheared crystal structures. It is important to note that none of the remaining fully hydrogenated systems have either such large percentages of minor TAGs or an overwhelming preponderance of a higher-melting TAG.

The microstructure of the 25% sheared samples is shown in Figure 3.4 at 500 X magnification. Due to the difficulties in preparing slides using crystallized shortenings, bubbles, up to $\sim 100\ \mu\text{m}$ in diameter, are visible in all pictures.

Figure 3.5 shows the microstructure of the unsheared 25% fully hydrogenated fat samples. Unlike Figure 3.4, there are no large bubbles, and the Maltese crosses are clearly visible. Canola, cottonseed, and palm exhibit like microstructures, with

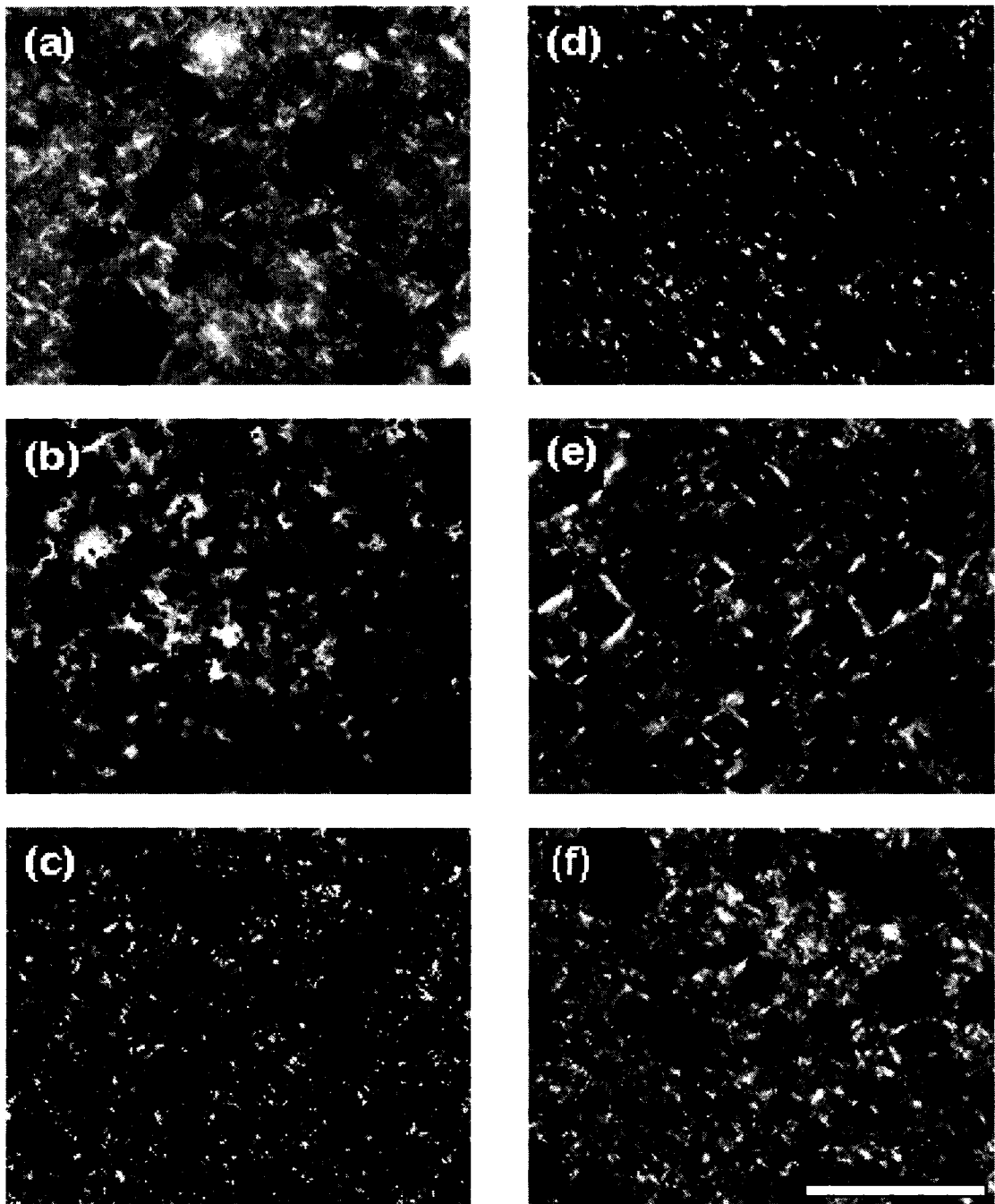


Figure 3.4: Composite diagram of the microstructure of sheared samples at 25% concentration after 48 hours. The samples vary with respect to fully hydrogenated fat: (a) canola (b) cottonseed (c) lard (d) palm (e) soybean (f) tallow (bar = 500 μm)

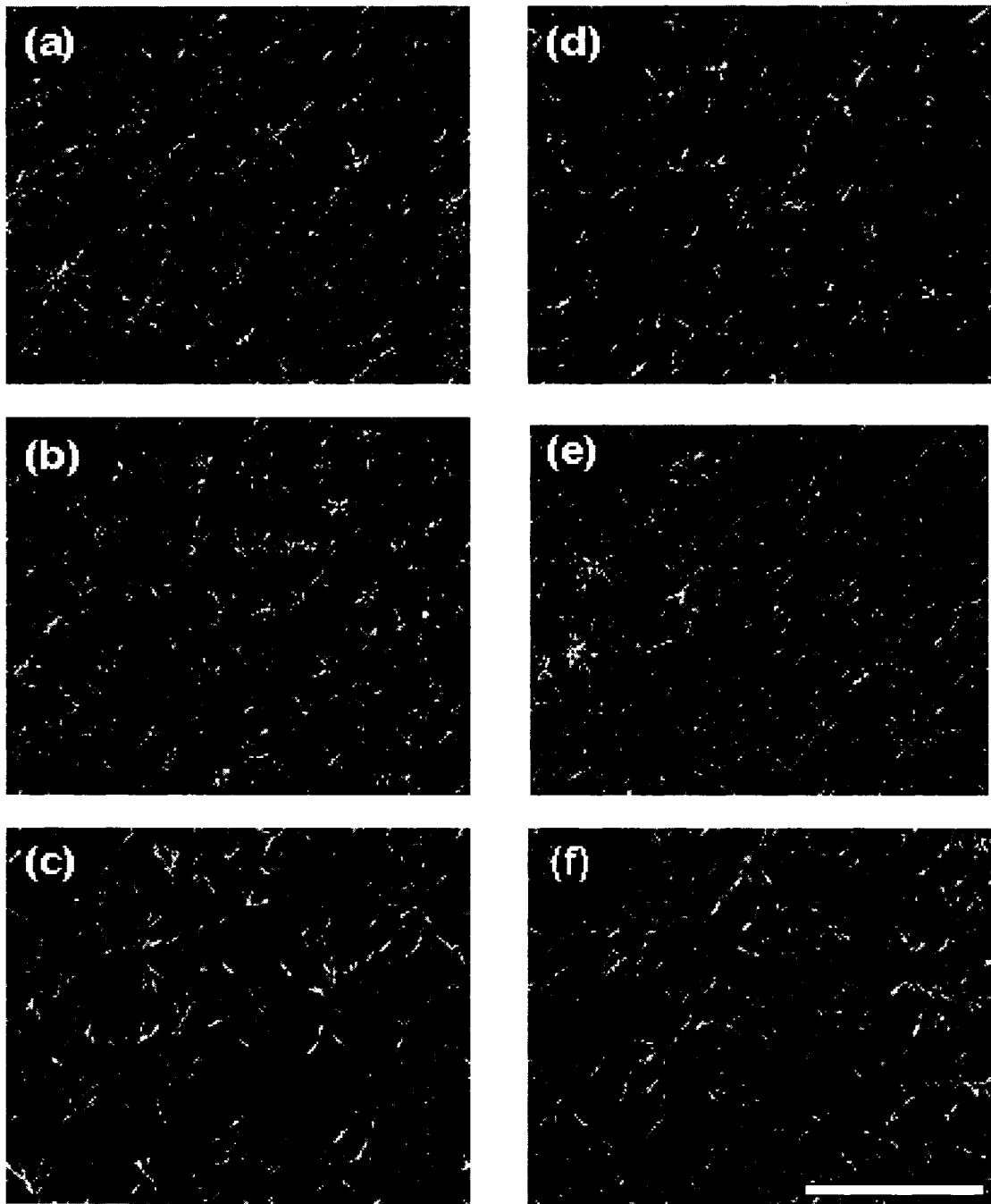


Figure 3.5: Composite diagram of the microstructure of unsheared samples at 25% concentration after 48 hours. The samples vary with respect to fully hydrogenated fat: (a) canola (b) cottonseed (c) lard (d) palm (e) soybean (f) tallow (bar = 500 μm)

spherulites of the same relative size (approximately 100 μm in diameter) and same relative spacing (approximately 20 – 50 μm) between spherulites. Note that spherulite here refer to microstructures [14]. Although the microstructures are similar, the crystal structure of canola is quite different from that of palm and cottonseed. Cottonseed and palm both demonstrate XRD reflections at 0.42 and 0.38 nm for unsheared samples, whilst canola demonstrated reflections at 0.45, 0.42, and 0.39 nm. Canola's crystal structure is however, dominated by tristearin, so it is not surprising that its crystal structure is different from that of palm and cottonseed which are dominated by tripalmitin and by PSS respectively.

The lard and tallow samples have much larger spherulites (approximately 300 μm in diameter) which are tightly packed with very little space showing between adjacent spherulites. It is expected that the tallow and lard samples would produce microstructures or spherulites of similar size as the fatty acid compositions [1] of tallow (38% P, 62% S) and lard (36% P, 64% S) are similar. Also, for unsheared 25% concentrations, the crystallization peak maximum of the tallow (31.9 $^{\circ}\text{C}$) sample is similar to that of the lard (32.4 $^{\circ}\text{C}$) sample [1]. The same is true for the melting peak maxima (54.5 $^{\circ}\text{C}$ for lard, and 52.7 $^{\circ}\text{C}$ for tallow [1] and for the SFC of lard (25.9%) and tallow (26.4%) at 25%. However, from Figure 3.3, one can see differences in the shapes of the XRD curves for the unsheared lard and tallow samples. Unsheared tallow has XRD reflection at 0.45, 0.42, and 0.38 nm, while unsheared lard has XRD reflections at 0.45, and 0.39 nm. More importantly, unsheared lard has a very strong reflection at 0.45 nm (the “modified” β' polymorph); while unsheared tallow demonstrated no dominant

reflections. Therefore, while the microstructures of these fats are similar, the crystal structures are very different, motivated most likely by the differences in starting molecular ensemble [1].

The microstructure of the market shortenings are shown in Figure 3.6. Samples a-e are the industrially processed shortenings as sold in the store. Large bubbles are visible in the All Vegetable Shortening, Blue Crisco, and Golden Crisco samples. The Pure Lard and Tenderflake samples are characterized by the long white crystals which indicate the presence of large structures. It is interesting to note in these sheared samples, that the micrographs of the All Vegetable Shortening, Blue Crisco, and Golden Crisco appear similar as the compositions of these market shortenings are similar. The same is true for the Pure Lard and Tenderflake micrographs. The samples f-j were melted and cooled in the same manner as the unsheared samples in this experiment. The unsheared Tenderflake and Pure Lard samples show densely packed microstructures with few spaces between them. The structures shown are like those in Figure 3.5 for the lard and tallow samples as the structures are densely packed. However, the market shortening samples have smaller structures than the binary mixtures, possibly due to the presence of emulsifiers (BHA, BHT) [1]. The Golden Crisco sample shows well defined microstructures (approximately 100 μm in diameter) with small spaces (approximately 10 μm) between structures. These structures are of the same size as those in the unsheared palm and soybean samples, with fewer spacings between structures than in the palm sample. This is interesting as Golden Crisco is composed of (partially and fully hydrogenated) palm and soybean oils [1]. The structures shown in the All Vegetable

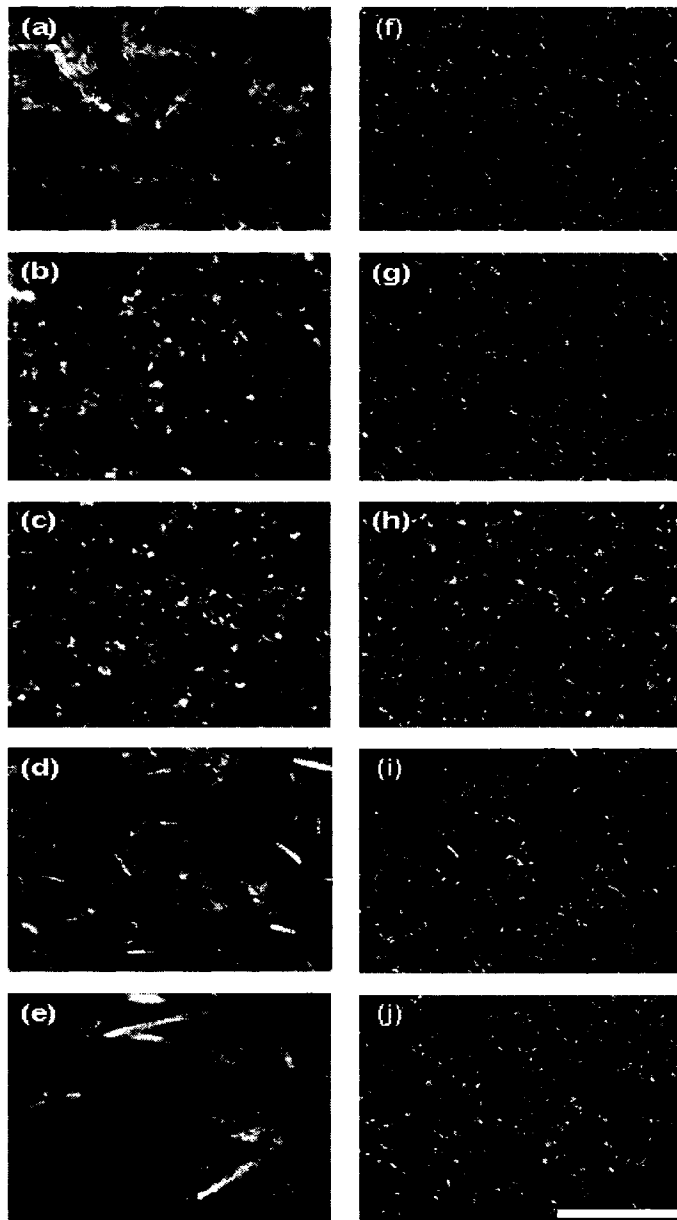


Figure 3.6: Composite diagram of microstructure of market shortenings. The samples a-e were taken of the shortenings as purchased in the store, and the samples in f-j were melted and cooled at a rate of 10 °C/min. (a) All Vegetable Shortening (b) Blue Crisco (c) Golden Crisco (d) Pure Lard (e) Tenderflake (f) All Vegetable Shortening (g) Blue Crisco (h) Golden Crisco (i) Pure Lard and, (j) Tenderflake (bar = 500 μm)

Shortening and Blue Crisco samples are of similar size as the Golden Crisco sample, but the microstructure are not as well defined, and the spaces between adjacent structures are not as prominent. Again, these micrographs are similar to those for the canola, palm and soybean samples shown in Figure 3.5.

Figure 3.7 shows the hardness of the sheared systems as well as for the market products. The 10% samples were too soft to be measured for hardness with the Instron cone penetrometer [15]. The hardness of samples containing the same fully hydrogenated fat increases with increasing percentage of hard fat in the sample. This correlates well with Figures 3.1 and 3.2 as the SFC of the samples increased with increasing percentage of hard fat in the sample. However, unlike Figures 3.1 and 3.2, the increase in hardness is not linear like the increase in SFC. This variability in hardness (within the increasing trend) is due to the variance in structures that are formed during crystallization as it is possible for two samples to have the same SFC value but for them to have quite different crystal structures and microstructures, as seen above. The only exceptions to this increasing trend are the 15% palm sample which is harder (0.003 kgf/mm) than the 20 and 25% palm samples (0.0002 and 0.0005 kgf/mm respectively) and the soybean samples for which the hardness remains relatively the same (9.1×10^{-5} kgf/mm $\pm 0.5 \times 10^{-5}$ kgf/mm). The hardness of the soybean samples is not predicted by the SFC values for these samples, as the SFC increases with increasing percentage of hard fat in the sample. As our data set does not include microstructures and polymorphic information on the 15 and 20% (w/w) concentrations, we are unable to infer a structural reason for these changes.

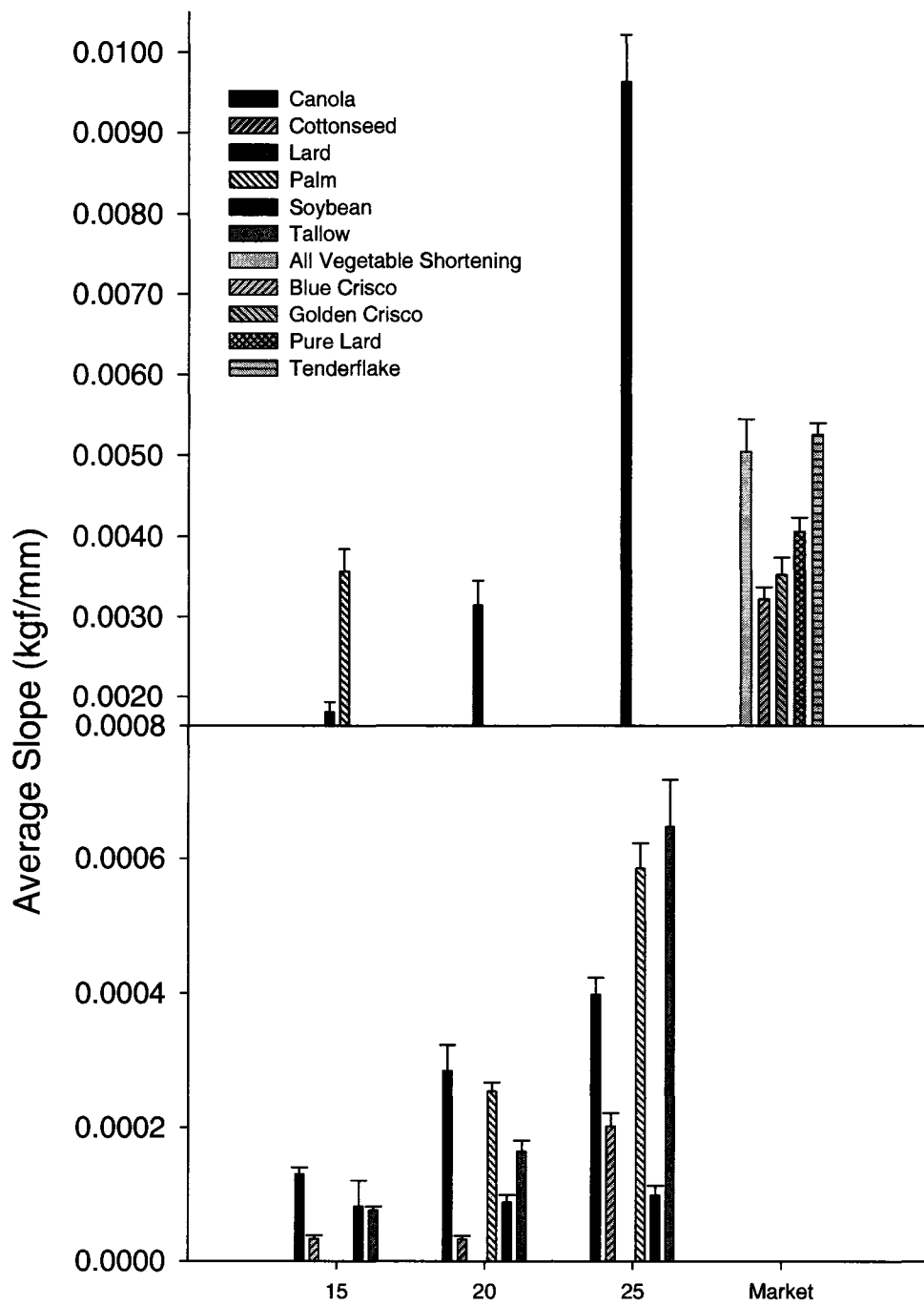


Figure 3.7: Variation in the hardness of sheared systems for the 15-25% (w/w) concentrations of the local fats and the market shortenings

The hardness values for the market shortenings are also shown in Figure 3.7. Blue Crisco was found to be the softest (0.003 kgf/mm) and Tenderflake Lard the hardest (0.005 kgf/mm). The market shortenings are harder than all of the other samples except for the 15% palm (0.003 kgf/mm) and 25% lard (0.009 kgf/mm) samples. It is interesting that the market shortenings are harder than most binary systems as the SFC value (Figure 3.1) lies within the same range as that for the binary systems. It is interesting to note that the Pure Lard and Tenderflake samples are softer (4.0530×10^{-3} kgf/mm and 5.2580×10^{-3} kgf/mm) than the 25% lard sample (9.6280×10^{-3} kgf/mm) but have similar SFC values (Pure Lard 22.3%, Tenderflake 25.5%, lard sample 24.8%), and similar microstructures (Figures 3.5 and 3.6). The crystallization and melting peak maximum locations for the Pure Lard and Tenderflake samples are much less than those for the 25% lard samples, indicating that there are higher melting compounds being formed in the 25% lard sample. Furthermore, as mentioned earlier, the polymorphism of the lard samples is very different from the Pure Lard and Tenderflake samples. Therefore, the differences in crystallization behavior of these systems, leading to very diverse crystal structures are responsible for the differences in hardness as opposed to microstructure or SFC. This lends some credence to the generally accepted notion that the crystal structure significantly affects the forces of attraction (and therefore hardness) between crystallites, through such parameters such as the Hamaker's constant, shape, size, and inter-crystalline distance of the network [14].

Figure 3.8 shows the hardness of the unsheared samples for all concentrations except for the 10% concentration which was too soft to measure with the Instron [15].

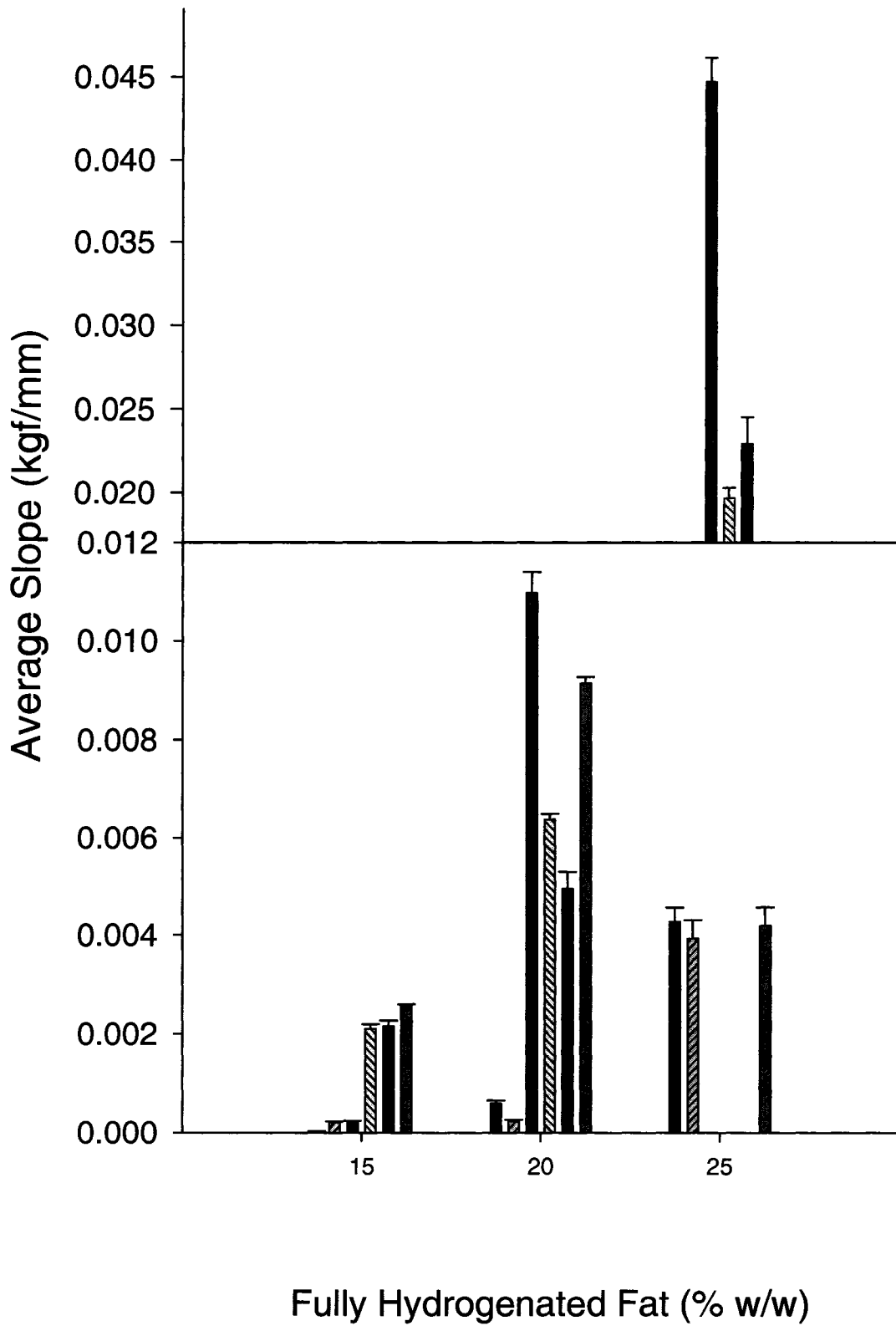


Figure 3.8: Variation in the hardness of unsheared systems for the 15-25% (w/w) concentrations of the local fats

As in Figure 3.7, increasing the amount of fully hydrogenated fat in a sample causes an increase in the hardness of the sample. Again, this increasing trend is no surprise as the percentage of fully hydrogenated (i.e. hard) fat in each sample is also increasing. The 25% cottonseed sample (0.004 kgf/mm) deviates from this trend as it is softer than the 20% cottonseed sample (0.009 kgf/mm). The enthalpy of melt curve peak maxima for the 20 and 25% cottonseed samples are at 54.1 °C and 63.9 °C respectively [1]. As the peak maxima for the 10 and 15% cottonseed samples are at 50.8 °C and 52.7 °C respectively, the peak max of the 25% cottonseed sample is a large jump from that of the other cottonseed samples. This indicates that in the 25% cottonseed sample, there is a greater amount of high melting compounds than in the 20% cottonseed sample. Comparing Figures 3.7 and 3.8, one can see that the unsheared samples are generally an order of magnitude harder than the sheared samples. This is due to the large air bubbles present in the sheared mixture as seen in Figure 3.4 as opposed to the unsheared mixtures in Figure 3.5.

As outlined above, samples containing fully hydrogenated lard and tallow demonstrated very similar microstructures for unsheared 25% (w/w) concentration samples, but differ significantly in their polymorphism. It is also interesting to note that tallow is one order of magnitude harder than lard for 25% unsheared samples. For sheared samples, while it is not entirely clear from Figure 3.4 whether there are differences in microstructure, we know from our previous discussion on XRD measurements that the polymorphism of tallow samples changes under shear. This change is reflected in the hardness measurement, where for sheared systems, lard

becomes harder than tallow by two orders of magnitude. Therefore, there is a total reversal of the relative hardness of these two networks under the influence of shear.

Recall that palm, canola, and cottonseed showed similar microstructures. For sheared samples at 25% concentration, palm is harder than canola; which is harder than cottonseed samples. However, for unsheared systems at 25% concentration, although palm is still the hardest of the three, cottonseed is harder than canola. This is however not surprising given the changes in polymorphism of canola between sheared and unsheared samples.

Therefore, shear and molecular ensemble play a significant role in determining the final hardness of a lipid crystal network, but in a way which can be predicted by structural changes at the crystalline and or microstructural levels.

3.4 References

1. Humphrey, K.L. and S.S. Narine, *A comparison of lipid shortening functionality as a function of molecular ensemble and shear: Crystallization and melting*. Food Research International, 2004. **37**(1): p. 11-27.
2. Norton, I., et al., *A calorimetric, NMR and X-ray diffraction study of the melting behavior of tripalmitin and tristearin and their mixing behavior with triolein*. J.Am.Oil Chem.Soc., 1985. **62**: p. 1237-1244.
3. de Man, L., J.M. de Man, and B. Blackman, *Physical and Textural Evaluation of Some Shortenings and Margarines*. Journal of the American Oil Chemists Society, 1989. **66**(1): p. 128-132.
4. Chawla, P., J.M. de Man, and A.K. Smith, *Crystal Morphology of Shortenings and Margarines*. Food Structure, 1990. **9**: p. 329-336.
5. Heertje, I., *Microstructural Studies in Fat Research*. Food Structure, 1993. **12**: p. 77-94.
6. Juriaanse, A.C. and I. Heertje, *Microstructure of Shortenings, Margarine and Butter - A Review*. Food Microstructure, 1988. **7**: p. 181-188.
7. Narine, S.S. and A. Marangoni, *Factors Influencing the Texture of Plastic Fats*. Inform, 1999. **10**(6): p. 565-570.

8. Narine, S.S. and A.G. Marangoni, *Relating structure of fat crystal networks to mechanical properties: a review*. Food Research International, 1999. **32**(4): p. 227-248.
9. Narine, S.S. and A.G. Marangoni, *Microscopic and rheological studies of fat crystal networks*. Journal of Crystal Growth, 1999. **199**: p. 1315-1319.
10. *Standard Methods for the Analysis of Oils, Fats, and Derivatives*, in *International Union of Pure and Applied Sciences*. 1979.
11. *Solid Content Determination in Fats by Low Resolution Nuclear Magnetic Resonance v. 2.150*, in *International Union of Pure and Applied Sciences*. 1987.
12. *Determination of Solid Fat Content by Pulsed NMR Method*, in *International Standard, Animal and Vegetable Fats and Oils*. 1991.
13. *AOCS Method Cd 16b-93*, in *Official and tentative methods of the American Oil Chemists' Society*, W.E. Link, Editor. 1998, AOCS Press: Champaign, IL.
14. Narine, S.S. and A. Marangoni, *Structure and Mechanical Properties of Fat Crystal Networks*, in *Physical Properties of Lipids*, A. Marangoni and S.S. Narine, Editors. 2002, Marcel Dekker Inc: New York. p. 63-83.
15. Humphrey, K.L., P.H.L. Moquin, and S.S. Narine, *Phase behavior of a binary lipid shortening system: From molecules to rheology*. Journal of the American Oil Chemists Society, 2003. **80**(12): p. 1175-1182.

4. Using 1 – palmitoyl, 2,3 – distearoyl – sn - glycerol (PSS) as a structural enhancer so as to decrease the level of saturates in zero-trans shortenings

4.1 Introduction

The health-related risks introduced by *trans* fatty acids in foods have already been discussed in Chapter 1. However the removal of *trans* fats from a shortening product is not without difficulties. *Trans* fat free products tend to have a liquid like viscosity (or a softer solid nature) and a lower melting point than those containing *trans* fat [1]. If the melting point of the fat is too low, the product may run, bleed, or melt at typical handling temperatures [2]. There are an increasing number of patents which offer formulation solutions for *trans* fat free shortenings products, but very few which addresses both the removal of *trans* fatty acids as well as the reduction of saturated fatty acids. A summary of these solutions is found in Chapter 1.

Shortenings are composed of a mixture of a solid hard lipid fraction and liquid lipid fraction, with or without selected emulsifiers. The solid hard fat fraction is typically composed of fully and/or partially hydrogenated canola, cottonseed, palm, and soybean oil, and/or palm oil or a combination of such oils. A comprehensive understanding of the

A version of this chapter has been included in a patent application.
Narine, S., K. Humphrey, and F. Kincs, *Shortenings and Methods of Making and Using Thereof*. 2007,
Scanlon, S. Weiss, S.: United States Patent and Trademark Office. 60953609 p. 38.

influence of molecular composition, processing conditions, additives and emulsifiers on the physical functionality of a particular shortening has not been established. Significant work has been done with shortening systems containing fully hydrogenated oils in refined soybean oil in exclusion of partially hydrogenated oils, emulsifiers and additives [3, 4]. The work by Humphrey and Narine [3, 4], detailed in Chapters 2 and 3 specifically points to the beneficial effects on crystallization and melting of shortening type systems containing percentages of the fully hydrogenated TAGs: PSS, PSP, PPS, and SPS. The work summarized in these previous chapters strongly suggests that PSS in particular, as well as the other TAGs mentioned above, has a major influence on the onset temperature of crystallization of a shortening system. This effected change in crystallization behavior could be extended beyond just the onset temperature as the presence of PSS, via the affectation of onset, would either promote or inhibit the crystallization of the remainder of the system. Scrutiny of the effect of enhancement of these TAGs in shortening products is therefore proposed by the work detailed in Chapters 2 and 3. Given the interest in *trans* free shortening products with lowered saturates, this investigation was carried out from the perspective of potential exploitation of the mechanisms of crystallization modification introduced by these potential structural enhancers, to reduce saturates in shortenings whilst still allowing the product to deliver expected measurements of texture and melting.

The functionality of a shortening is affected by three basic factors 1) the oil and saturated fat mixture as well as the emulsifiers and other additives of which the shortening is made of, 2) the cooling, shear and other environmental parameters during

the crystallization of the shortening, and 3) the tempering conditions during which the crystals can further crystallize and ripen within the shortening [5, 6]. In this study we address the first of these factors, the shortening composition. The formulation of a typical all purpose shortening, using a hard component which was fully hydrogenated (therefore containing practically no *trans* fat) was altered via enrichment with PSS either in pure form or as a component of added fully hydrogenated cottonseed oil.

4.2 Experimental Procedures

The shortening samples used in this study were composed of fully hydrogenated canola (FHC) and fully hydrogenated cottonseed (FHCo) hard fats and soybean oil all supplied by Bunge Oils (Bradley IL., USA) as well as pure (97% by GC) PSS synthesized by the Alberta Lipid Utilization Program at the University of Alberta, Edmonton, Alberta. Four different types of samples (each with five levels of total added saturates: 15.0, 17.5, 20.0, 22.5, and 25.0 %) were created and studied in this portion of the PSS Study. These types are (1) FHC mixed with Soybean oil (control, No Added PSS), (2) 5% Pure PSS and FHC mixed with Soybean oil (5% PSS), (3) 5% FHCo and FHC mixed with Soybean oil (5% Cottonseed), and (4) a blend of FHCo and FHC oil mixed with Soybean oil in which the percentage of PSS and SSS is matched to the levels found in the 5% PSS in Canola and Soybean oil sample (PSS/SSS Match). The total added saturated fat in the PSS/SSS Match samples was slightly (approximately 2%) higher than that for the corresponding sample (5% PSS) with the molar ratio of PSS to SSS in these samples ranging from $x = 0.51$ for the 27.1% hard fat sample to $x = 0.83$

for the 17.1% hard fat sample (where $x = \frac{\%PSS}{\%SSS}$). The sample compositions of all 20 samples used in this study are shown in Table 4.1.

Sample cooling and heating rates of 10.0 °C/min and 5.0 °C/min respectively were used and all temperatures are reported to a certainty of ± 0.1 °C/min unless otherwise noted. The hardness, final SFC, XRD, and microscope measurements were performed at a stage temperature of 20.0 ± 0.5 °C. All measurements were performed in triplicate ($n = 3$) and the mean values are reported with their subsequent standard deviations.

4.2.1 Sample Preparation

Samples were heated to 90 °C and stirred with a mechanical stirrer for 2 minutes to destroy crystal memory and to ensure homogeneity and then transferred to the appropriate container (aluminum pans for DSC and hardness, appropriate tubes for NMR and XRD) for analysis. Microscope slides of each sample were also prepared.

4.2.2 Relative Hardness Measurements

The molten sample was transferred into aluminum DSC pans. The samples were processed in the pans using a “Linkam LTS 350” temperature controlled stage (Linkam Scientific Instruments, Tadworth, Surrey, United Kingdom). After thermal processing, the samples were stored for 2, 4, 6, 8, 10, and 13 days at 20 °C. A TA.XT.plus Texture Analyzer (Stable Microsystems, Surrey U.K.) fitted with a 1.0 kg load cell was used to

Table 4.1: Compositions of the 20 samples used in this study

Sample Type	Total Added Saturated Fat (%)	Soybean Oil (%)	Fully Hydrogenated Canola (%)	Fully Hydrogenated Cottonseed (%)	Pure PSS (%)	SSS (%)	PSS (%)
No Added PSS (Control)	15.0	85.0	15.0			12.0	2.4
	17.5	82.5	17.5			14.0	2.8
	20.0	80.0	20.0			16.0	3.2
	22.5	77.5	22.5			18.0	3.6
	25.0	75.0	25.0			20.0	4.0
5% PSS	15.0	85.0	10.0		5.0	8.0	6.6
	17.5	82.5	12.5		5.0	10.0	7.0
	20.0	80.0	15.0		5.0	12.0	7.4
	22.5	77.5	17.5		5.0	14.0	7.8
	25.0	75.0	20.0		5.0	16.0	8.2
5% Cottonseed	15.0	85.0	10.0	5.0		10.0	3.8
	17.5	82.5	12.5	5.0		12.0	4.2
	20.0	80.0	15.0	5.0		14.0	4.6
	22.5	77.5	17.5	5.0		16.0	5.0
	25.0	75.0	20.0	5.0		18.0	5.4
PSS/SSS Match	17.1	82.9	3.1	14.0		8.0	6.6
	19.6	80.4	5.6	14.0		10.0	7.0
	22.1	77.9	8.1	14.0		12.0	7.4
	24.6	75.4	10.6	14.0		14.0	7.8
	27.1	72.9	13.1	14.0		16.0	8.2

obtain hardness measurements in this study. During testing, the stage temperature was maintained by an Autotune CAL 9300 (CAL Controls Ltd., Herts U.K.) temperature controlled chamber fitted to the texture analyzer. Sample penetration and data acquisition were controlled by the Texture Exponent 32 (Version 2.0.0.7, www.SaxSoft.com) software. The TA was fitted with a stainless steel ball probe with diameter 3.175 ± 0.001 mm (provided by Texture Technologies Corp., probe number TA 8A) and a penetration depth of 1.5 ± 0.1 mm and speed of 0.5 ± 0.1 mm/s. The maximum force of the force displacement graph obtained was used as the measure of relative hardness [7].

4.2.3 DSC Measurements, Thermal Behavior

A “DSC 2920 Modulated DSC” by TA Instruments was used in the non-modulated DSC mode for thermal measurements. The sample was pipetted in consistent amounts (10 to 15 mg each) into three aluminum DSC pans which were then hermetically sealed. An empty aluminum pan was used as a reference. The samples were held isothermally at 90 °C for 5 minutes and then cooled at 10 °C/min down to 20 °C where they were equilibrated for 45 minutes to allow crystallization to complete. The sample was then immediately heated to 90 °C at a constant rate of 5 °C/min to obtain the 0H melting curve. Each sample was then recrystallized using the same conditions and stored to obtain the 48H melting curve and the 13 day melting curve.

The data sampling and temperature control procedures were fully automated and controlled by the “TA Instrument Control” software program. The data was analyzed

using the “TA Universal Analysis” software and a method developed by our group [7]. All curves were normalized to a uniform sample mass of 15 milligrams.

4.2.4 XRD measurements, Polymorphism

“Bruker’s AXS X-ray diffractometer” equipped with a filtered Cu-K α radiation source ($\lambda = 0.1542$ nm) was used for XRD analysis. The procedure was automated and commanded by Bruker AXS’ “General Area Detector Diffraction System” (GADDS V 4.1.08) software. The XRD samples were prepared by filling glass capillary tubes with the molten sample. The tubes were tempered at 10 °C/min to the final holding temperature of 20 °C in a “Linkam LTS 350” temperature controlled stage described above. The sample was held isothermally in the Linkam for 30 minutes at this final temperature. The sample tube was then fitted with the brass holder and then quickly transferred for analysis to the XRD stage where the temperature was maintained at 20 °C \pm 0.5 °C via the “Air Jet” cooling system (Kinetics-Thermal Systems, New York, USA). The XRD frames, obtained after 450 seconds exposure to a monochromatic Cu-K α X-ray beam, were processed using GADDS software and the resulting spectra were analyzed using Bruker AXS’s “Topas V 2.1” software.

4.2.5 NMR measurements, SFC determination

SFC data was acquired using the pulse magnetic resonance spectrometer “Minispec mq SFC Analyzer” (Bruker Instruments, Milton, Ontario, Canada), equipped with a temperature controlled measurement chamber. The data sampling procedure was

fully automated, and the SFC was calculated and displayed by the “Minispec v2.20 Rev.01/NT” software [8-11].

The NMR tubes were filled with molten fat to a height of 3.5 ± 0.1 cm. To achieve the cooling rate of 10 °C/min, the samples were first heated to 90 °C and held there for 5 minutes before being transferred through a series of water baths, separate from the NMR, at prescribed times. The sample was then held isothermally 20 °C. The SFC was measured after 1 hour, 2 days and 13 days. The reported SFC value is the average of the SFC values provided by the NMR software for each of the 3 NMR tubes filled with the sample.

To determine the growth rate and growth mode of the fat crystal network, SFC versus time curves for each sample were fitted with modified form of the Avrami equation [12]. Thus, the crystallization of a series of crystallization events ($i = 1, 2, \dots, p$), each with its own A_i and m_i is given by [12]:

$$F(t) = \sum_{i=1}^p F(t_i)$$

$$\theta(t_i) = \frac{F_i(t)}{F_{i\infty}} = 1 - e^{-A_i(t-t_i)^{m_i}}$$
(1)

where $F_i(t)$ is the absolute crystallinity at time t , $F_{i\infty}$ is the crystallinity at some time when the growth rate or the nucleation conditions change, and t_i is the induction time for

the crystallization of the sample. Upon applying Equation 1 to a crystallization growth curve which is a single sigmoid ($i = p = 1$), Equation 1 collapses to the original Avrami [13] equation given by:

$$\theta(t) = \frac{F(t)}{F_{\infty}} = 1 - e^{-At^m} \quad (2)$$

where $\theta(t)$ is the relative crystallinity at time t , $F(t)$ is the absolute crystallinity at time t , F_{∞} is the final absolute crystallinity, A is the crystallization rate constant containing the nucleation and growth rates, and m is the Avrami index or exponent. To that end each sample was also cooled at a rate of 3 °C/min from 90 °C to 20 °C with the sample being inside the NMR while being cooled from 67 °C to 20 °C (using equipment described previously [14]) and held isothermally for 1 hour in order to acquire crystallization growth curves.

4.2.6 Microstructure Determination

A high resolution polarized light microscope with a 10x eyepiece lens and a 10x objective lens, equipped with a “Hamamatsu Digital Camera”, and a “Linkam LTS 350” was used. The microscope assembly was controlled by “Openlab 3.0.8” software (Improvision, Coventry, United Kingdom). Pictures were taken 1 hour, 2 days and again 13 days after tempering.

The sample slides were processed in the Linkam temperature controlled stage (described above) by heating the slide to 90 °C and holding at of 90 °C for 5 minutes,

then cooling at a rate of 10 °C per minute to the final temperature of 20 °C. The micrographs were taken after 1 hour, 2 days and 13 days

4.3 Results and Discussion

As discussed, the phase behavior studies in Chapters 2 and 3 suggested that added PSS (either in pure form or as a constituent of other oils) will beneficially modify crystallization of a shortening sample to create structural and functional improvements.

4.3.1 *Relative Hardness*

Figures 4.1ai thru 4.1av show the relative hardness as a function of sample type for each level of total added saturated fat of all of the shortening samples after they have been stored for 13 days. Clearly, as one increases the amount of total added saturated fat within a sample the relative hardness of the shortening increases, as is to be normally expected.

The sample with the PSS/SSS match ($x = 0.70$) has a total of 19.6% saturated fat, and demonstrates the same level of hardness as the 25% saturated fat sample with no added PSS after 13 days. This indicates that hardness can be maintained whilst reducing the level of saturated fat by 5.4%, when the PSS is used as a structural enhancer with targeted levels referenced to the level of SSS in the sample ($x = 0.83$). Clearly, since the samples with 5% Cottonseed added (which represents an added 1.4% PSS over the sample with No Added PSS and $x = 0.35$ at 17.5% total added saturates) does not exhibit

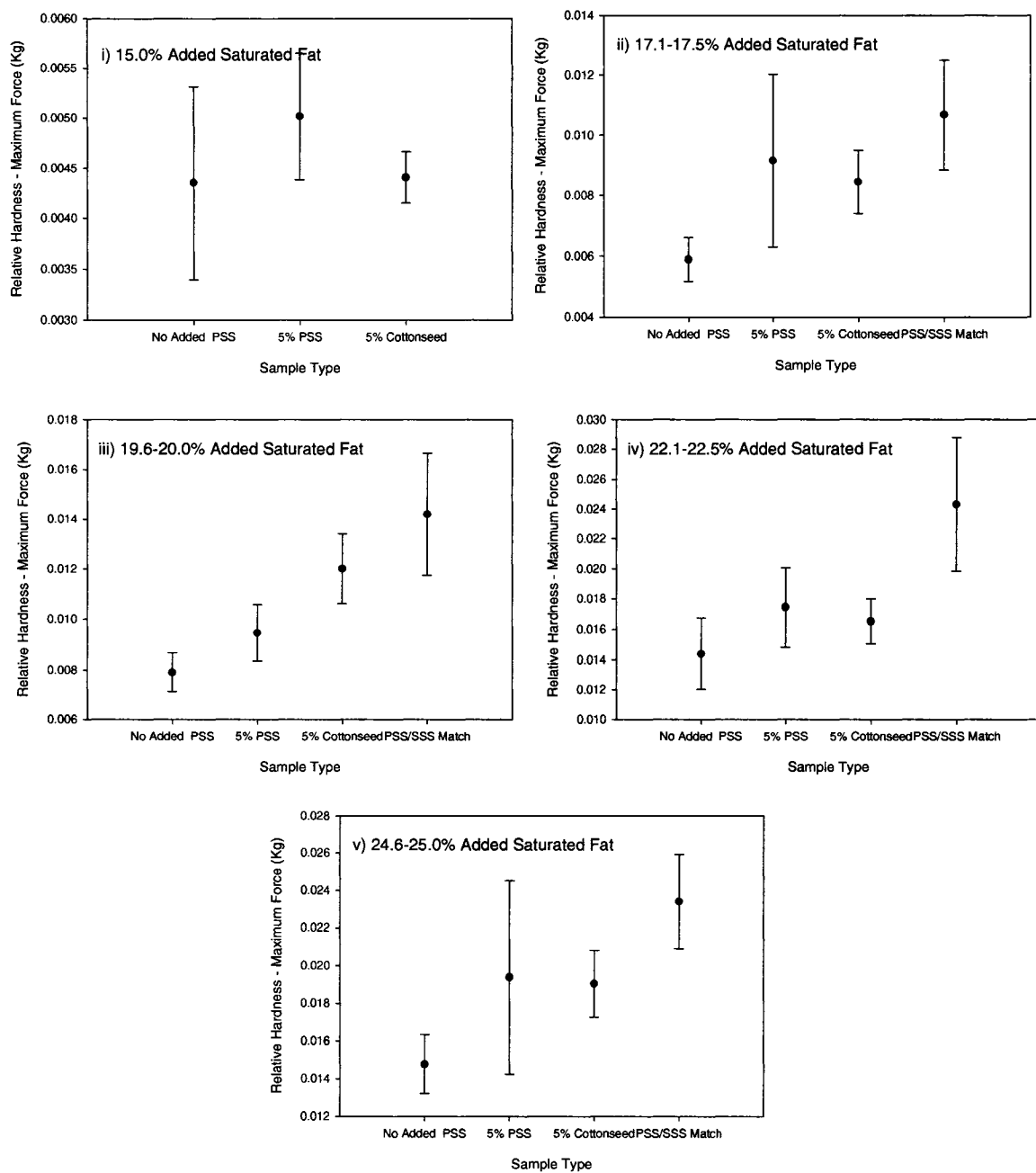


Figure 4.1a: Relative hardness of the shortening samples after 13 days as a function of sample types at with total added saturated fat of i) 15.0%, ii) 17.1-17.5%, iii) 19.6-20.0%, iv) 22.1-22.5%, and v) 24.6-25.0%

the same increase in hardness, the balance of PSS and SSS is of importance. Thus the careful blending of PSS and SSS as constituents of FHC and FHCo is required to promote the hardness of the shortening blend, and not just solely the introduction of cottonseed.

The evolution of hardness over time is shown in Figure 4.1b for the 17.5% hard fat samples and 17.1% fully saturated fat for PSS/SSS Match. It is clear that the hardness for all samples tends to decrease slightly (a maximum of 4% of the hardness after 2 days) as the storage time increases. As the control sample shortening (No Added PSS) also exhibits a softening effect after storage, this is not seen to be an issue which challenges the beneficial effects of the PSS enriched samples.

4.3.2 Polymorphism

The polymorphic form of the crystals within the shortening is important as it has an effect on the melting properties of the shortening, and the different polymorphs have different morphologies, which has an effect on the physical functionality of the product. Furthermore, the stability of the different polymorphic forms are of importance, as unless the polymorphic form is stabilized in the product, it can continue to evolve as a function of time, leading to melting, morphological and functional changes in the shortening.

For discussion purposes the XRD spectral range is divided into the short spacing ($3.0 \text{ \AA} \leq d \leq 5.0 \text{ \AA}$) and long spacing ($d \geq 5.0 \text{ \AA}$) regions. In the long spacing region, there are two peaks present for all samples. The angle of tilt, θ , of the lamellar repeat unit

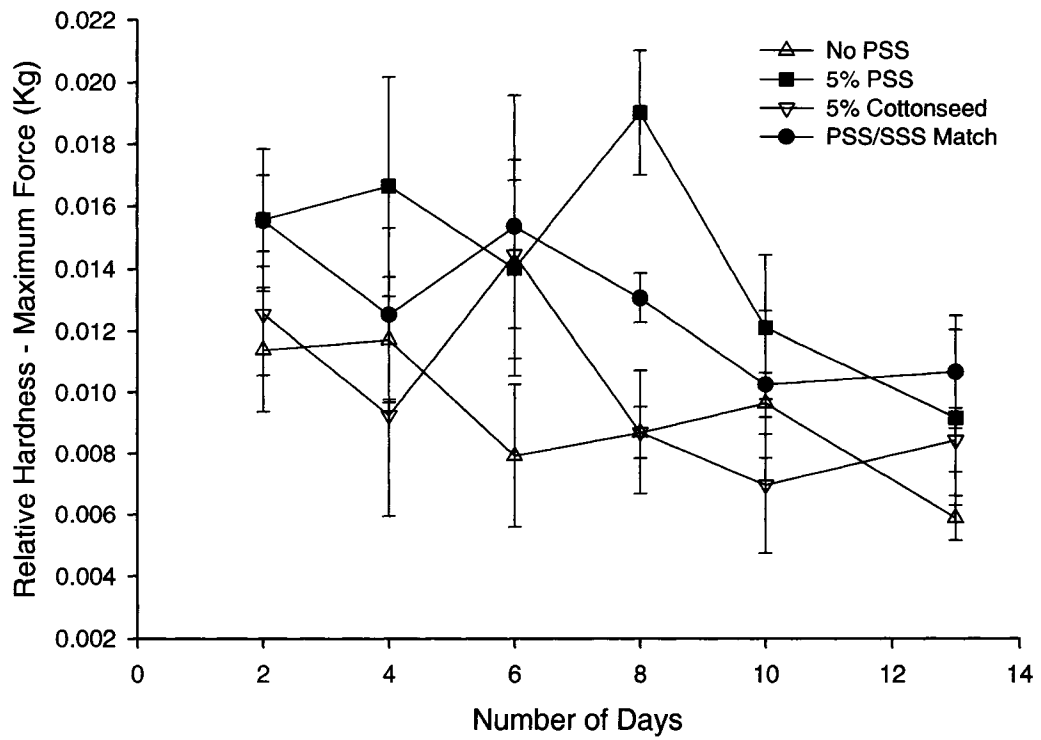


Figure 4.1b: Relative hardness versus time of shortening samples of all types with 17.1% (PSS/SSS Match) to 17.5% (No Added PSS, 5% PSS, and 5% Cottonseed) total added saturates

has been determined from the parallel and perpendicular spacings using basic trigonometry. After 1 hour, the angle of tilt for the PSS/SSS Match sample ($\theta = 47.8 \pm 0.4^\circ$) is different than that for the other three sample types ($\theta = 54 \pm 1^\circ$). The long spacings and thus the angles of tilt were the same for all sample types after 2 and 13 days ($\theta = 53 \pm 2^\circ$).

The short d-spacings after 2 days are shown in Figure 4.2 with three peaks in the XRD spectra for each sample within the short spacing range. The d-spacings for the No Added PSS, 5% PSS, and 5% Cottonseed samples, like the angle of tilt, θ , do not change over time. The short d-spacings for the PSS/SSS Match sample changes after 1 hour and remain the same for 2 and 13 days. Thus, the short d-spacings after 2 days are shown for all samples (Figures 4.2a-c), while the evolution in d-spacing over time is shown for the PSS/SSS Match sample (Figure 4.2d). In the short spacing region, the alpha polymorph is characterized by a reflection at 4.2 Å and the beta by strong reflections at 4.6 Å and 3.8 Å [15]. The beta prime polymorph exhibits either two spacings at 3.8 Å and 4.2 Å or three spacings at 4.3 Å, 4.0 Å and 3.7 Å [15].

In Figures 4.2a, 4.2b, and 4.2c, the d-spacings of No Added PSS, 5% PSS, 5% Cottonseed and PSS/SSS Match samples two days after crystallization are shown. Three d-spacings are evident for the four sample types: 3.8 ± 0.3 Å, 4.2 ± 0.2 Å and 4.5 ± 0.2 Å. The first two short spacings are suggestive of the beta prime polymorph, while the third short spacing persists just below the 4.6 Å beta spacing. This has been seen before, but

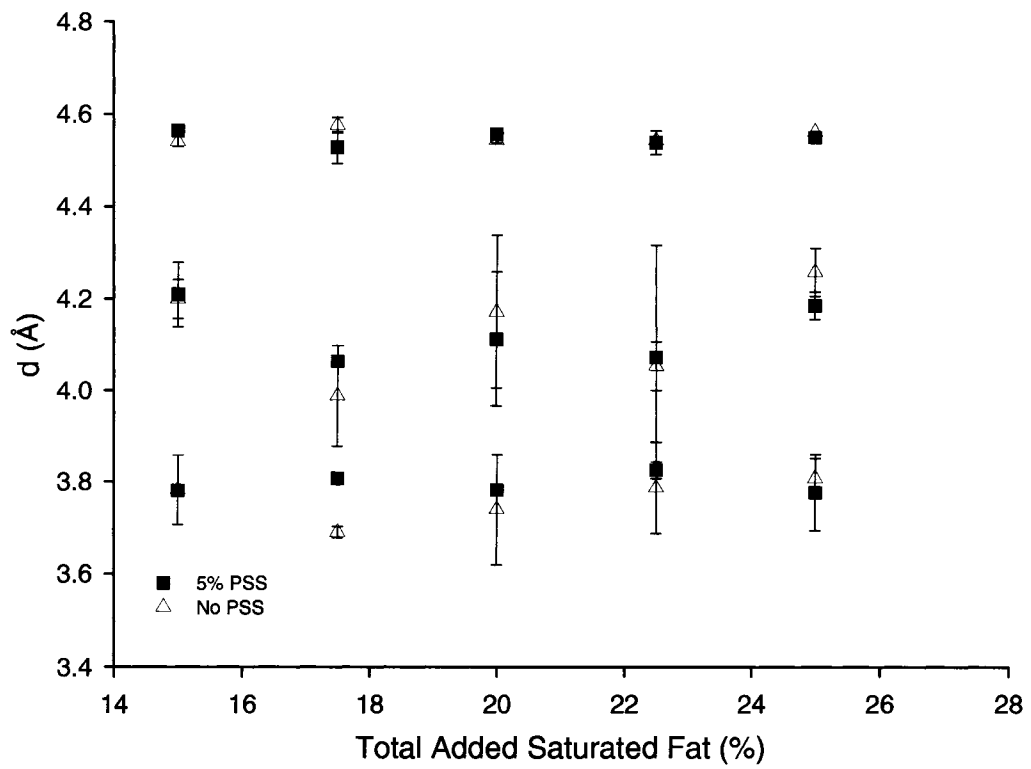


Figure 4.2a: Polymorphism of the shortening samples after 2 days for the No Added PSS sample compared with the 5% PSS sample

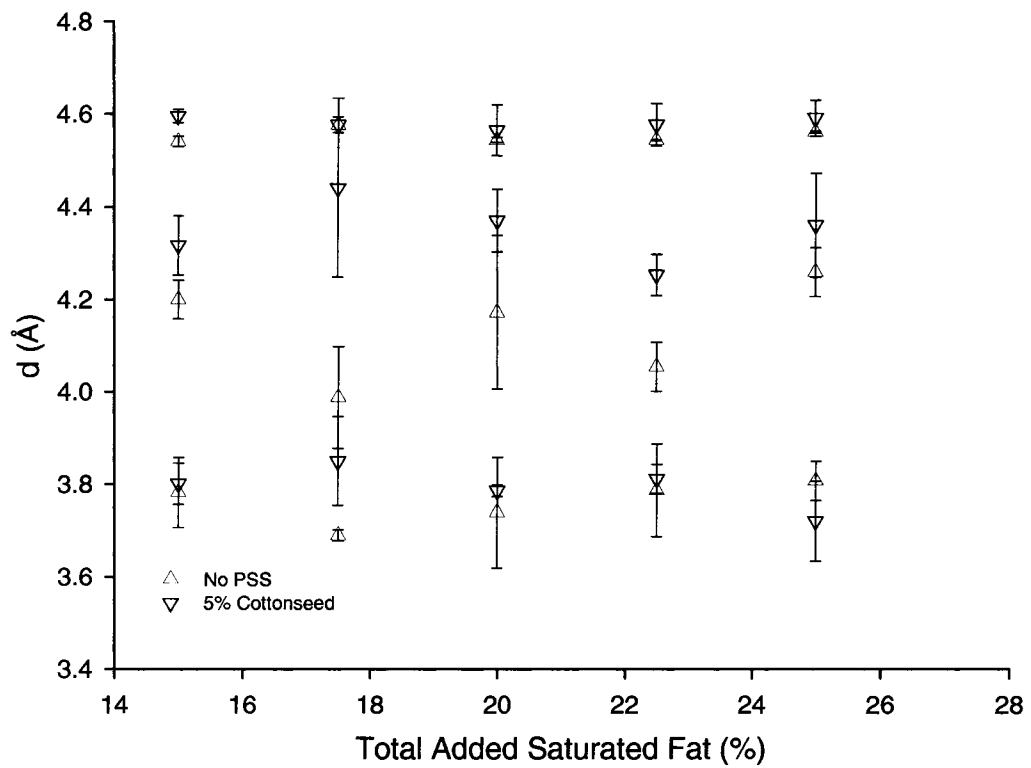


Figure 4.2b: Polymorphism of the shortening samples after 2 days for the No Added PSS sample compared with the 5% Cottonseed sample

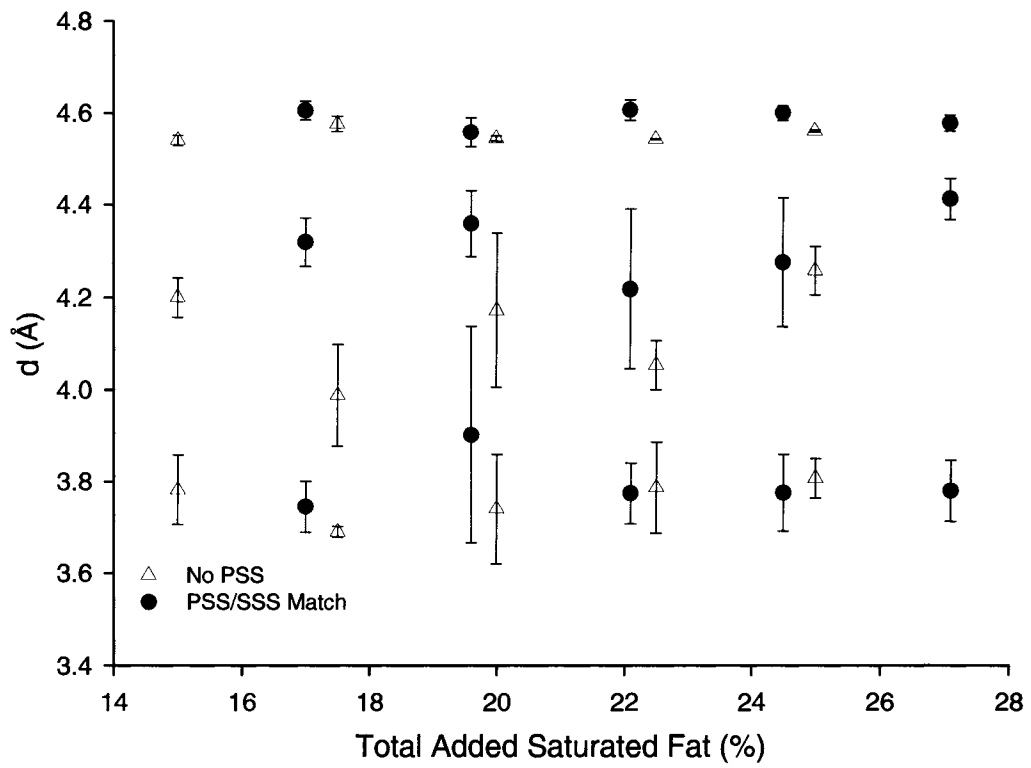


Figure 4.2c: Polymorphism of the shortening samples after 2 days for the No Added PSS sample compared with the PSS/SSS Match sample

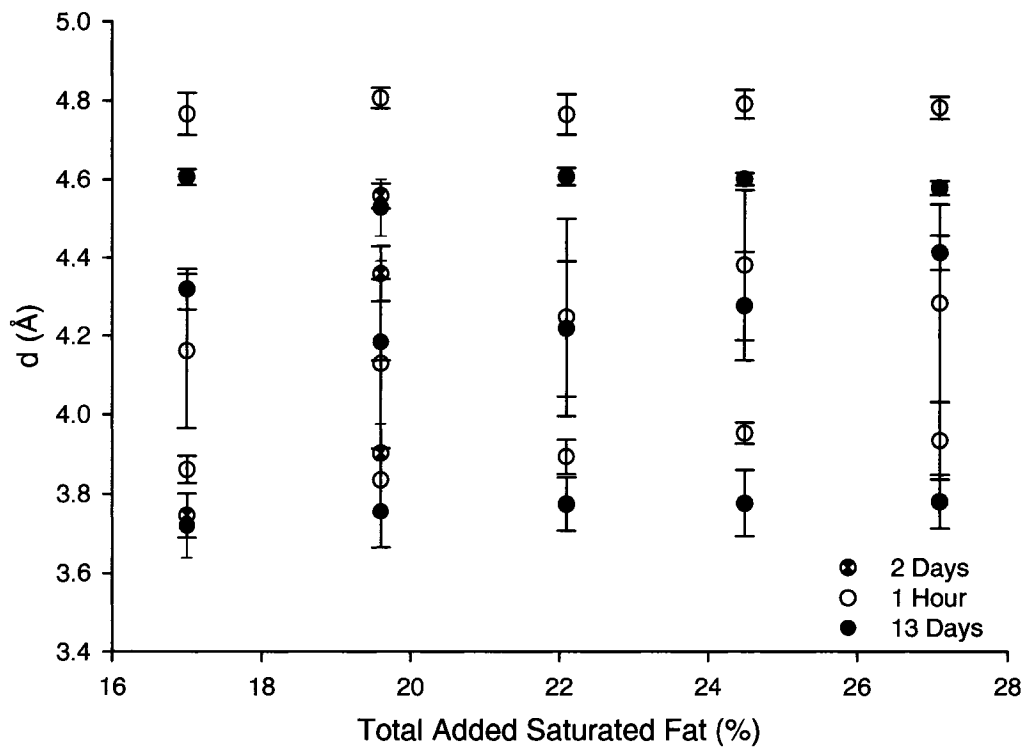


Figure 4.2d: The effect that storage has on polymorphism for the PSS/SSS Match sample after 1 hour, 2 days, and 13 days

has yet to be well explained [4]. Thus all the shortening samples are a mixture of beta and beta prime polymorphs, which is typical for a shortening product [15].

The evolution of polymorphism over time for the PSS/SSS Match sample is shown in Figure 4.2d. After one hour the PSS/SSS match samples has short d-spacings at $3.9 \pm 0.2 \text{ \AA}$, $4.2 \pm 0.2 \text{ \AA}$, and $4.8 \pm 0.1 \text{ \AA}$. The reflection at $4.8 \pm 0.1 \text{ \AA}$ is not evident in the d-spacings after 2 and 13 days, as the peak in the XRD spectra is shifted to a lower d-spacing value of $4.6 \pm 0.1 \text{ \AA}$. This suggests that the persisting polymorphic form 2 days after crystallization takes some time to develop as it is not present after 1 hour. As the hardness evolves over time (Figure 4.1b) the PSS/SSS Match sample becomes harder than the No Added PSS sample (as discussed above). This harder product may be due to the formation of the polymorph evident after 2 days. This further suggests that in an industrial setting some sort of tempering to allow this polymorph to form is required to achieve the polymorphic transition and thus the desired increase in hardness. For all other sample types, there are no changes in the XRD d-spacings as a function of storage of the sample.

4.3.3 Solid Fat Content

The final SFC of all the shortening samples after (a) 1 hour, (b) 2 days, and (c) 13 days is shown in Figure 4.3. SFC increases linearly as a function of the amount of saturated fat for all samples, as is shown in all of the figures. The PSS/SSS Match sample has a lower SFC for the same amount of total added saturates than the control sample (No Added PSS), 5% PSS, and 5% Cottonseed. Comparing between Figures

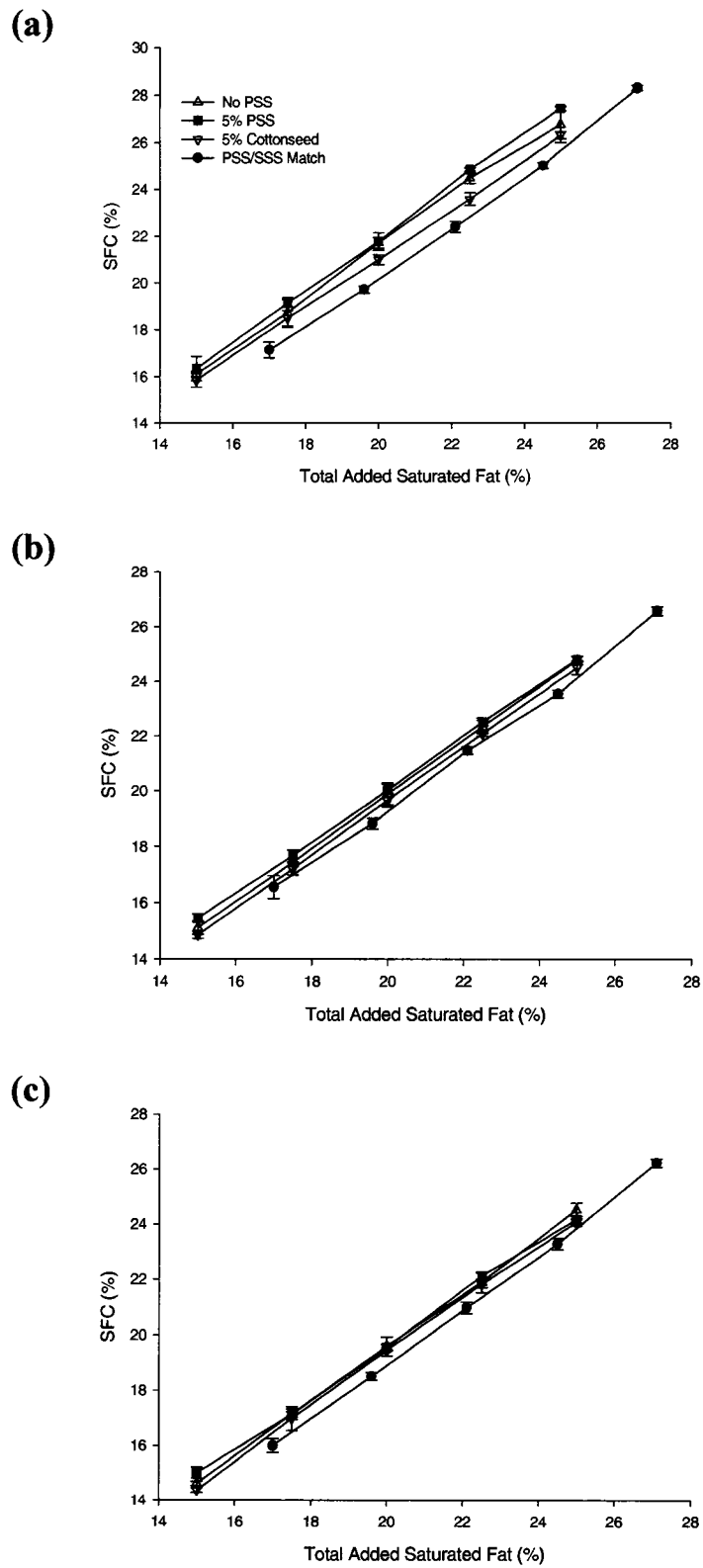


Figure 4.3: SFC of the shortening samples as a function of total added saturated fat after a) 1 hour, b) 2 days and c) 13 days

4.3a, 4.3b and 4.3c, one can see that as the storage time increases, the percent SFC for all samples decreases as does the difference between the SFC of the PSS/SSS Match sample and the other sample types investigated. However, even after 13 days of storage, the SFC of the PSS/SSS Match samples are lower at all levels of added saturated fat. At the same time, these samples are harder, which suggests that the effect of the structural enhancer in the appropriate proportions to SSS results in the development of a unique network structure which is harder, without the development of increased solid content.

The continuous crystallization curves obtained by crystallizing the samples within the NMR at a rate of 3 °C/min were fitted with Equation 1 and the rate constant and Avrami exponent were obtained. Due to the nature of the growth curve, it was found that ($i = p = 1$). The Avrami constant as a function of the total added saturated fat is shown in Figure 4.4a. Clearly there is a decrease in the rate constant (from 0.014 ± 0.001 for 5% Cottonseed with 15% total added saturates to 0.0029 ± 0.0002 for 5% Cottonseed with 25% total added saturates), and thus in the rate of crystallization as the total added saturated fat is increased. This suggests that the added saturated fat results in a retardation of crystallization, potentially due to the increase in higher melting components found in the saturated fat causing decreases in the rate of mass transfer due to increased viscosity effects, or due to the inability of the cooling conditions to adequately remove the heat of crystallization. The No Added PSS, 5% PSS and PSS/SSS Match samples have similar A values (ranging from 0.008 ± 0.001 to 0.0031 ± 0.0002 for 15 and 25% total added saturated fat samples respectively). The A value of the 5% Cottonseed sample (0.014 ± 0.002) is much higher than that of the other three samples

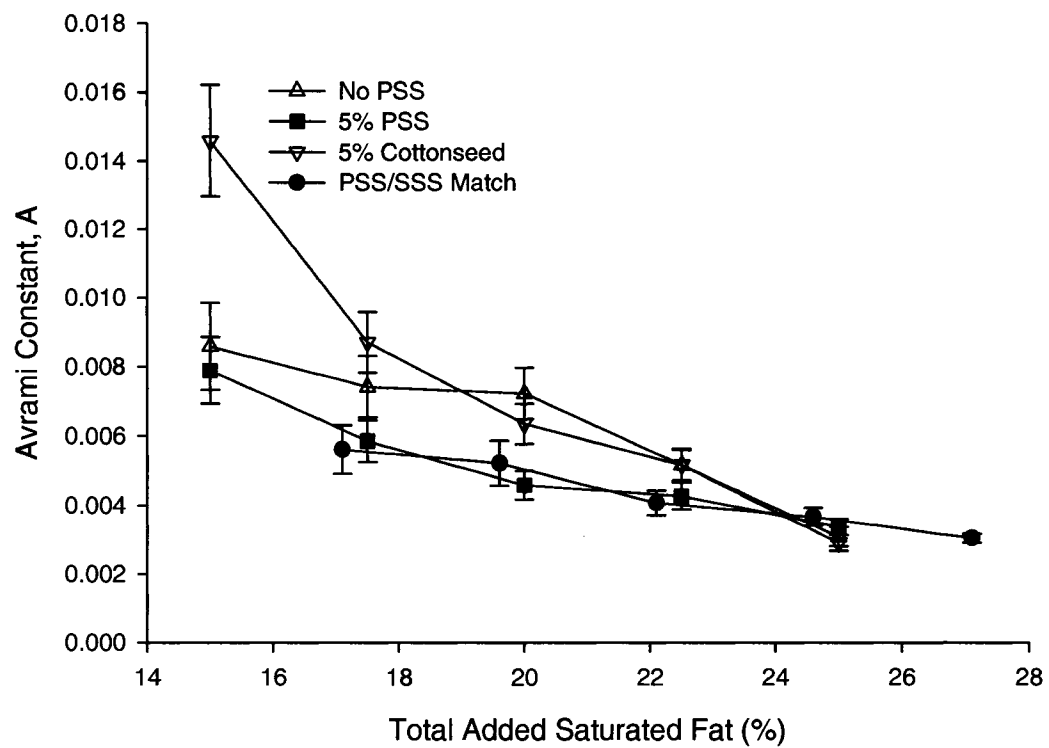


Figure 4.4a: Avrami Constant obtained by fitting continuous NMR growth curves with the Avrami equation as a function of the total added saturated fat

(0.008 ± 0.001) at 15.0% total added saturates indicating an increase in the crystallization rate of this sample. The difference between the A values of the 5% Cottonseed and the other samples is much smaller at higher levels of total added saturated fat due to the similar levels of SSS and PSS in the 5% Cottonseed samples with higher levels of total added saturates and those in the No Added PSS Samples (Table 4.2).

The Avrami exponent gives details about the geometry of the crystallizing system. Figure 4.4b shows the trend in m as a function of the total added saturated fat. It can be seen that the Avrami exponent increases slightly (0.90 ± 0.02 for the 5% Cottonseed sample with 15% total added saturates to 1.17 ± 0.01 for the PSS/SSS Match sample with 27.1% total added saturates) as the total added saturated fat increases. The m value for the No Added PSS sample is lower (1.02 ± 0.03) than that for the 5% PSS and PSS/SSS Match samples (1.03 ± 0.02 to 1.11 ± 0.02) for samples with 20% or less total added saturated fat. The m value of the 5% Cottonseed samples is slightly lower than that of the other sample types at low level of added saturated fat. For the maximum amount of total added saturated fat (25.0% for the No Added PSS, 5% PSS, and 5% Cottonseed and 27.1% for the PSS/SSS Match samples), all samples tend to have similar m values. The similarity in m suggests that the geometry of all the crystallizing samples tends to be the same. An m value of 1 suggests rod-like growth from instantaneous nuclei [16].

Whilst it is not immediately obvious why a harder sample (Figures 4.1a and 4.1b) would have a lower SFC (Figure 4.3), it suggests that the structure built by the

Table 4.2: TAG composition of the samples at all levels of total added saturated fat as a percentage of both the total sample and the total added saturated fat

Sample Type	Total Added Saturated Fat (%)	As a Percentage of the Total Sample		As a Percentage of the Total Added Saturated Fat	
		SSS (%)	PSS (%)	SSS (%)	PSS (%)
No Added PSS	15.0	12	2	80	16
	17.5	14	3	80	16
	20.0	16	3	80	16
	22.5	18	4	80	16
	25.0	20	4	80	16
5% PSS	15.0	8	7	53	44
	17.5	10	7	57	40
	20.0	12	7	60	37
	22.5	14	8	62	35
	25.0	16	8	64	33
5% Cottonseed	15.0	10	4	66	25
	17.5	12	4	68	24
	20.0	14	5	70	23
	22.5	16	5	71	22
	25.0	18	5	72	22
PSS/SSS Match	17.1	8	7	47	39
	19.6	10	7	51	36
	22.1	12	7	54	34
	24.6	14	8	57	32
	27.1	16	8	59	30

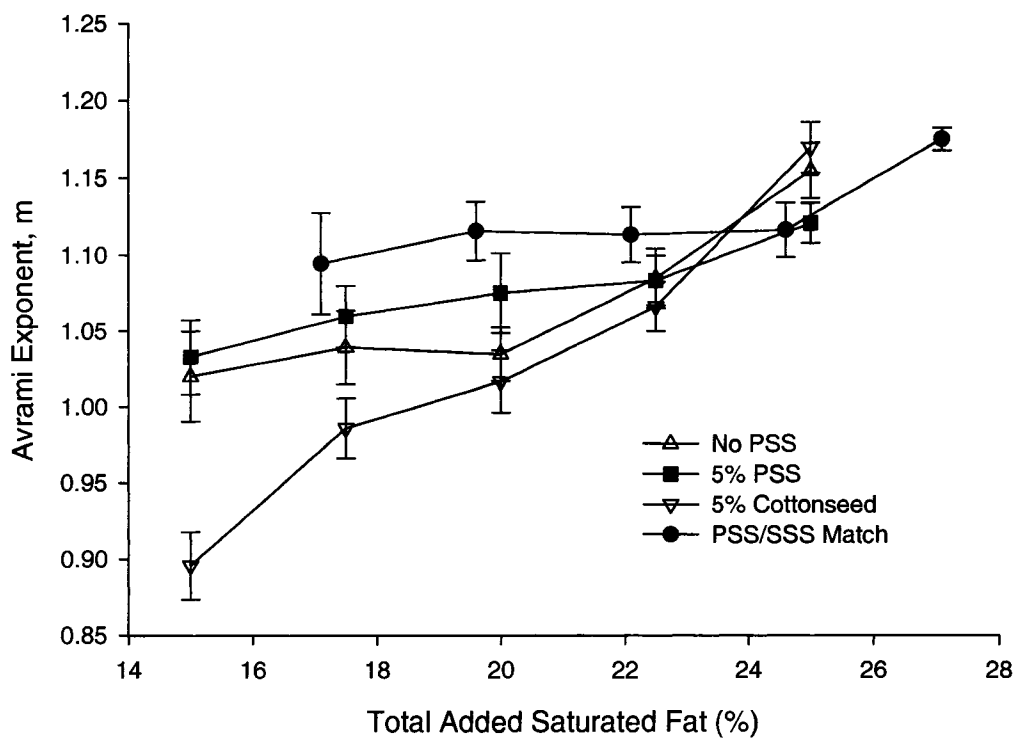


Figure 4.4b: Avrami Exponent obtained by fitting continuous NMR growth curves with the Avrami equation as a function of the total added saturated fat

crystallizing system is not solely due to an increase in the solid fat within the system, but rather due to the types of packing occurring.

Molecular packing within the β polymorphic form occurs in a double chain length structure. The lamella, which consists of TAGs in the chair conformation with height equal to the 'd' spacing and with an angle of tilt (θ) as shown in Figure 4.5a. The predominating forces between the TAGs are van der Waals forces. Given that the magnitude of these forces is inversely proportional to x^8 , the distance between interacting molecules is integral to the strength of the network as the forces become much weaker with incremental increases in the distance between molecules.

Packing models suggestive of the possible molecular interactions of PSS and SSS (in both pure form and in a mixture) are shown in Figures 4.5 b-d. The close packing of SSS-SSS (Figure 4.5b) shows how the fatty acid in the *sn*-2 position, being the chain which protrudes furthest from the center of the TAG, prohibits close packing of the subsequent layer of TAGs. Potentially, the gap between the *sn*-1 and *sn*-2 fatty acids is almost as large as two carbon-carbon single bond lengths (one carbon to carbon single bond is 153 pm) while the gap between the *sn*-3 fatty acids is larger than two single bond lengths.

PSS aids in the close packing as palmitic acid in the *sn*-1 position allows room for the protruding stearic acid (*sn*-2) chain to lie so the glycerol backbones of the interacting TAGs draw nearer in the lamellar structure as shown for PSS-PSS in Figure 4.5c.

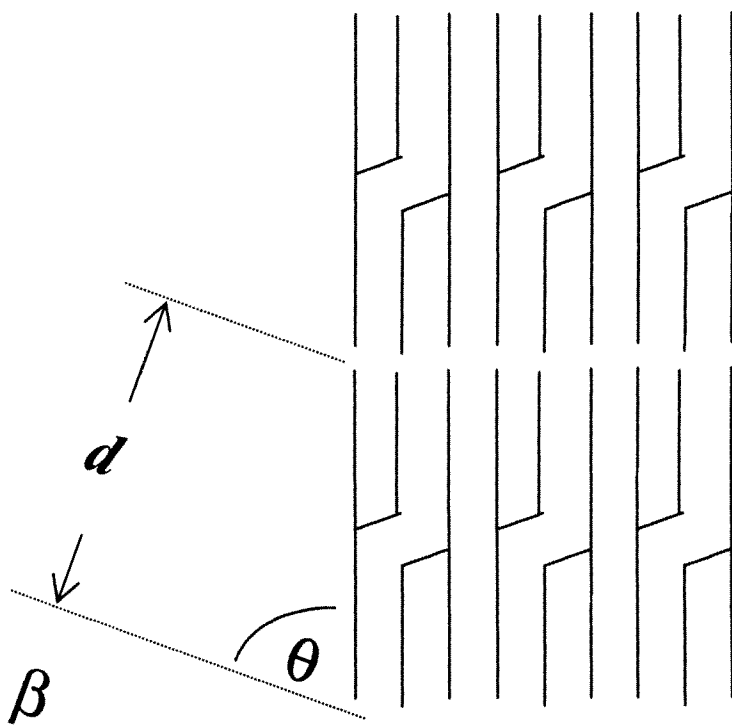


Figure 4.5a: Schematic of the double length TAG packing at an angle θ

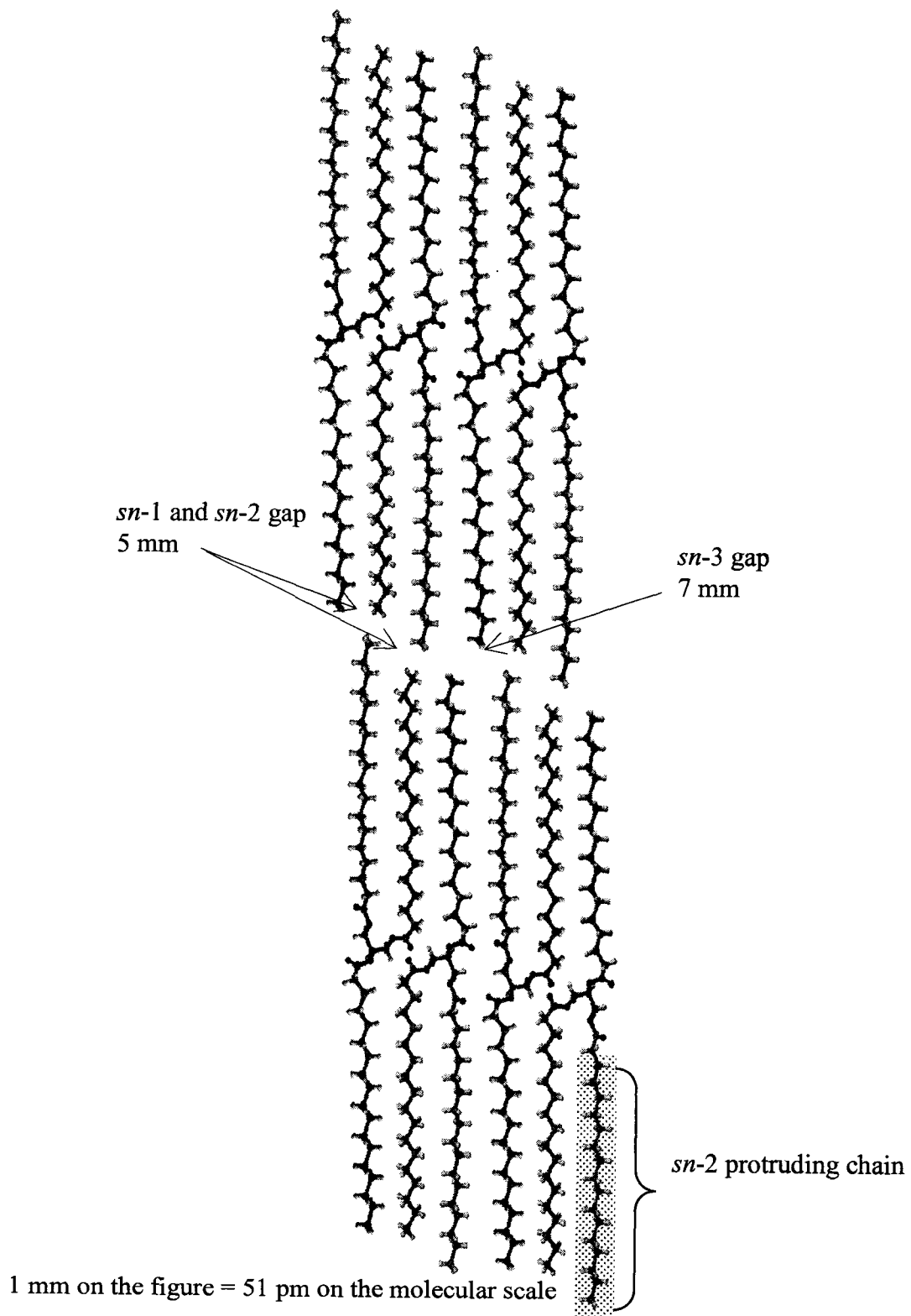


Figure 4.5b: Schematic of the TAG packing of the SSS-SSS system

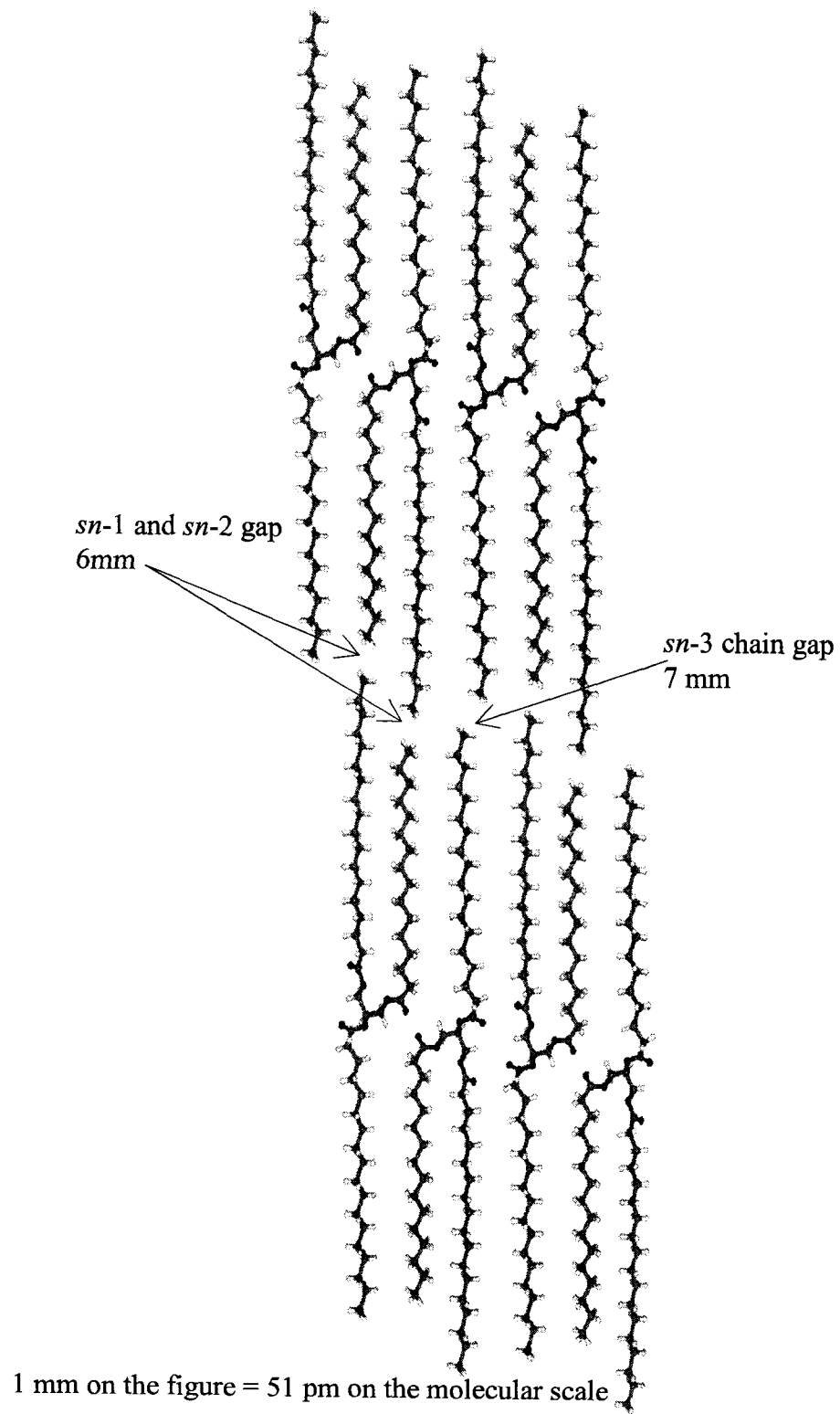


Figure 4.5c: Schematic of the TAG packing of the PSS-PSS system

Possibly, the gap between the *sn*-3 stearic acid chains is quite large (greater than two single bond lengths), and that between the *sn*-1 and *sn*-2 fatty acids is also as large as two single bond lengths. Therefore, the interactions between the PSS-PSS layers would be weaker than in the SSS-SSS system as the magnitude of the van der Waals forces decreases greatly with incremental increases in the separation of the interacting species.

Figure 4.5d illustrates the potential packing of PSS and SSS. The shorter palmitic acid in the *sn*-1 position of the PSS molecule allows for close packing with the protruding stearic acid chain in the *sn*-2 position of the subsequent layers. The gap between the interacting *sn*-1 and *sn*-2 chains ranges from one single bond length to greater than two bond lengths (as illustrated in Figure 4.5d). Clearly in this situation, the shorter palmitic fatty acid, allows for transverse interactions of the stearic acids (*sn*-2 position), and thus a larger number of interacting species (4 carbon atoms) than that in the case of interacting chain ends (2 carbon atoms). The possibility for transverse interactions (i.e. PSS-SSS) which are absent in the packing allowed between SSS-SSS and PSS-PSS results in a higher magnitude of van der Waals forces than when the end carbon on each chain is responsible for the interactions (i.e. SSS-SSS) as there are two times the number of interacting groups.

It is further suggested herein that the close interaction between neighboring TAGs due to the van der Waals forces acting over a short distance scale to the macroscale as the microstructural elements join together to form microstructures. The TAGs at the edges of the microstructural elements will also interact as illustrated in Figures 4.5b-d. Thus the

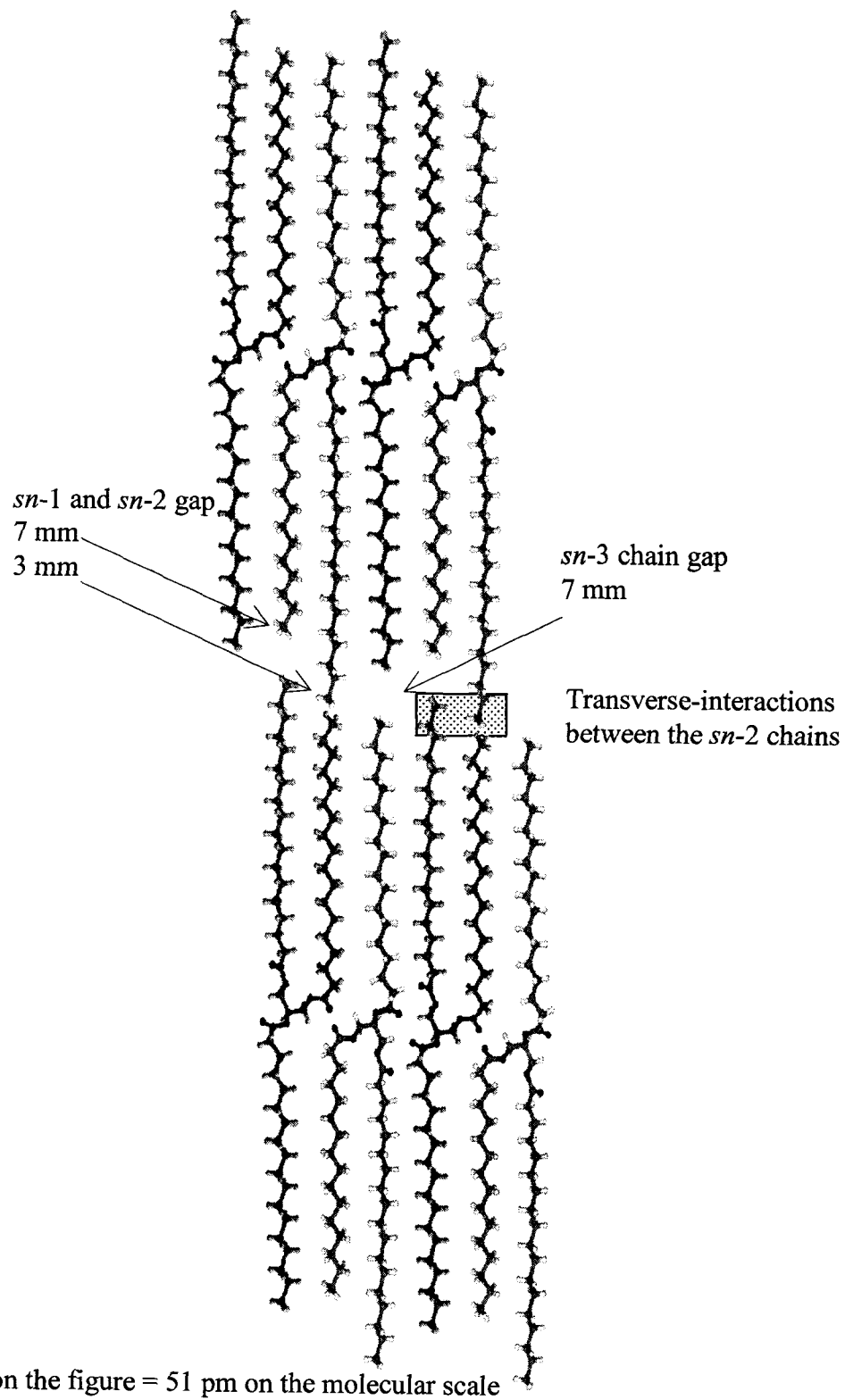


Figure 4.5d: Schematic of the TAG packing of the PSS-SSS system

closer packed TAGs result in stronger van der Waals forces holding together the microstructures. As a system with equal parts PSS and SSS has twice as many interacting carbon atoms (when compared with the SSS-SSS or PSS-PSS systems) the van der Waals interaction forces increase by 50%. Given that each carbon atom has a radius (σ) of 3.92 Å, a potential well depth (ϵ) of 72 K, and a closest interaction distance (R) of 4.25 Å [17], an estimation of the Lennard-Jones potential (U) can occur using Equation 1:

$$U(R) = 4\epsilon \left[\left(\frac{\sigma}{R} \right)^{12} - \left(\frac{\sigma}{R} \right)^6 \right] \quad (1)$$

Thus in a sample containing 1 mole of PSS and 1 mole of SSS (mass of 1.754 kg), the transverse interacting carbon atoms (as illustrated in Figure 4.5d) contributes approximately 1343 J/mole greater than that which is present in the PSS-PSS or the SSS-SSS systems. Therefore, this extra interaction energy provides strength to the PSS-SSS system on the molecular level, as well as on the microstructural level, resulting in a harder lipid crystal network when both PSS and SSS are incorporated into the sample.

4.3.4 Melting Enthalpy

The peak maximum of the enthalpy of melt curve as a function of the total added saturated fat after 48 hours is shown in Figure 4.6a. As is expected, as the amount of saturated fat in samples increases, the melting peak maximum also increases. Comparing between sample types, one can see that the control sample (No Added PSS) has the highest melting peak maxima at all levels of total added saturated fat (59.0 ± 0.1 °C to 62.4 ± 0.1 °C). Thus, there is a preponderance of high melting compounds formed in this

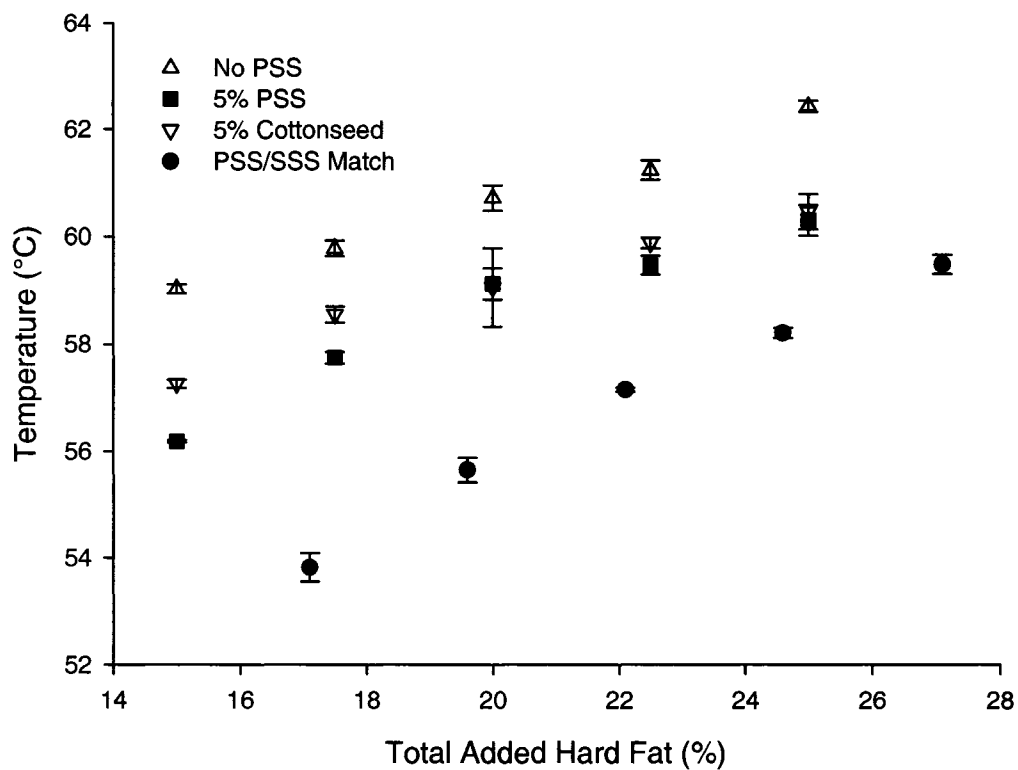


Figure 4.6a: Peak maximum of melting by DSC as a function of the total added saturated fat

sample (No Added PSS) as compared to the PSS/SSS Match sample for which the melting peak maxima are found at lower temperatures (53.8 ± 0.2 °C to 59.5 ± 0.2 °C). Since the melting peak maxima of the 5% PSS sample (56.1 ± 0.0 °C to 60.3 ± 0.3 °C) is lower than that of the control, the inclusion of PSS into the shortening blend must aid in creating a preponderance of correspondingly lower melting compounds. However, this does not mean that the PSS/SSS Match sample does not contain higher melting compounds; rather it suggests that the bulk of the compounds formed during the crystallization process tend to melt at a lower temperature than the bulk of the compounds formed during the crystallization of the No Added PSS samples. The melting peak maxima of the 5% Cottonseed sample (57.2 ± 0.1 °C to 60.4 ± 0.3 °C) is somewhat lower than that of the No Added PSS sample, yet not as low as the 5% PSS or the PSS/SSS Match samples. As this sample has a lower amount of SSS (66 to 72%) when compared to the No Added PSS sample (80%) (as shown in Table 4.2) at the same levels of total added saturated fat, one can hypothesize that this lack of the higher melting compound may lead to the lowering of the melting point of the majority of the compounds formed. The melting peak maxima of the 5% PSS sample is not as low as that of the PSS/SSS Match sample potentially due to the lower levels of the higher melting TAG SSS in the 5% PSS sample type (53 to 64% versus 47 to 59% in the PSS/SSS Match sample).

While the location of the peak maximum of melt gives an indication of the temperature at which a large amount of compounds within the sample melt, the FWHM suggests a temperature range over which the melting event occurs, which further suggests variance

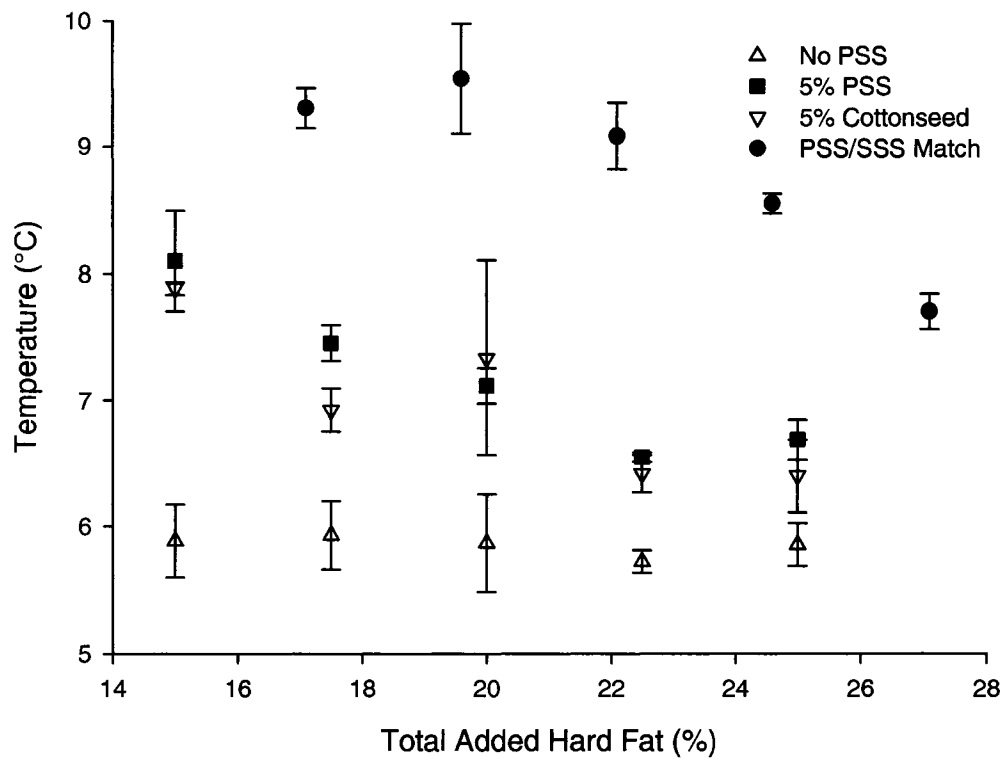


Figure 4.6b: FWHM of DSC melting peak as a function of the total added saturated fat

in the types of compounds created within the sample during the crystallization process. The FWHM of the enthalpy of melt curves obtained by DSC 48 hours after tempering is shown in Figure 4.6b as a function of total added saturated fat. Clearly, the No Added PSS sample type consistently melts over a narrow range (5.5 to 6.3 °C for all concentrations of saturated fat), whilst the samples enriched with added PSS tend to melt over a wider range of temperatures, with the FWHM decreasing as the amount of total added saturated fat increases. The FWHM of the 5% PSS sample is 8.1 ± 0.4 °C at 15% hard fat, and decreases to 6.7 ± 0.2 °C when the hard fat is increased to 25%. The FWHM of the 5% Cottonseed samples decreases from 7.9 ± 0.0 °C to 6.4 ± 0.3 °C as the hard fat is increased from 15 to 25%. The FWHM of the PSS/SSS Match sample decreases from 9.3 ± 0.2 °C to 7.7 ± 0.1 °C (17.1% to 27.5%). Clearly, as the total amount of added saturated fat increases, there is a tendency for the compounds within the sample to melt over an increasingly similar temperature span. Seeing as the SSS and PSS concentrations as a function of the total added fat for the 5% Cottonseed (72 and 22% respectively) and No Added PSS (80 and 16% respectively) samples tend to be more similar at higher values of total added hard fat, one could propose that the similarities in the melting FWHM are due to the molecular compositions of the samples.

A high FWHM value suggests a wide variety of different melting compounds being melted and therefore created during crystallization or ripening. The converse is also true for a low FWHM value suggesting a narrow variety of compounds being created. Therefore, in the control sample, there are very similar compounds being formed which tend to melt at 59.0 ± 0.1 °C to 62.4 ± 0.1 °C for the samples with total added hard

fat of 15 to 25% respectively. The PSS/SSS Match sample, which exhibits high values of FWHM, is composed of compounds with a wide range of melting temperatures with a bulk of the melting occurring at 53.8 ± 0.2 °C to 59.5 ± 0.2 °C (17.1 to 25% added hard fat). Thus, augmenting the shortening sample with PSS either in pure form or as a constituent of a saturated fat, leads to an increase in the types of compounds formed during crystallization. This increase in the number of types of compounds formed could be due to PSS-PSS or PSS-SSS interactions due to the significant increase in PSS in the enriched samples (Table 4.2). As the range of FWHM for the No Added PSS <1 °C compared to a decrease of >1 °C for the 5% PSS, 5% Cottonseed and PSS/SSS Match samples, and given the TAG composition of each sample type, Table 4.2, one can suggest that the majority of the cause of the increase in FWHM of the 5% Cottonseed sample is due to an increase in PSS-SSS interactions. Therefore, one can assume that, for the 5% PSS and the PSS/SSS Match samples, the increased FWHM is due to the variance in the melting points of the compounds formed during crystallization, and as the amount of PSS is significantly increased in these samples, this increase is due to PSS-SSS interactions but is also influenced greatly by PSS-PSS interactions due to the increased levels of PSS in these samples. Thus the PSS/SSS Match sample tends to melt over a wide temperature range, but the bulk of the sample tends to melt at a lower temperature, further suggesting that there are an increased number of compounds formed with the lower melting TAG PSS as opposed to SSS-SSS interactions.

As with the melting peak maxima and FWHM, the onset temperature of melt is affected by the types of compounds formed during crystallization and ripening as a lower

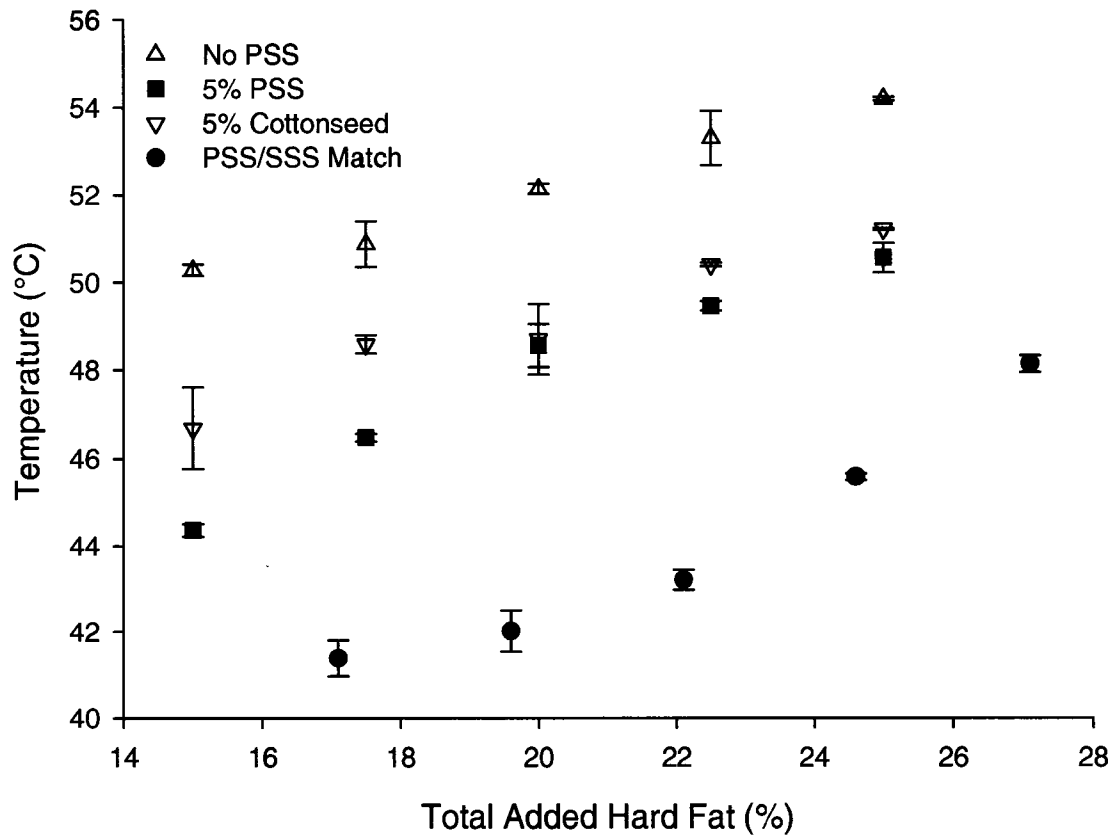


Figure 4.6c: Melting onset after 2 days as a function of the total added saturated fat

onset temperature suggests the existence of lower melting compounds in the sample, and a higher onset temperature suggesting the absence of these compounds. The onset of the enthalpy of the 48 hour melt curve is shown in Figure 4.6c. One can see that this data closely mimics that for the peak maxima of enthalpy of melt (Figure 4.6a). Clearly, the PSS/SSS Match sample begins to melt (41.4 ± 0.4 °C to 48.1 ± 0.2 °C) at a much lower temperature than the No Added PSS sample (50.2 ± 0.1 °C to 54.2 ± 0.0 °C), with the peak maxima of the PSS/SSS Match sample at 17.1% saturates being at the same temperature as the onset of melt for the 15% saturated No Added PSS sample. The high onset of melt temperatures of the No Added PSS sample could be due to the high percentage of the high melting TAG SSS (which melts at 71-73 °C) within the sample (80%, Table 4.2), whilst the lower melting TAG (PSS melts at 60-62 °C) is only present in small amounts (15%) compared with 47% SSS and 39% PSS in the PSS/SSS Match sample. The same trends in melting peak maxima, FWHM and onset to melt are evident after 0 hours and 13 days (data not shown).

4.3.5 Crystallization Enthalpy

Figures 4.7a and 4.7b show the start and onset temperatures of crystallization respectively as a function of the total added saturated fat in a sample. There is an increase in both the start and the onset temperatures of crystallization as the amount of total added hard fat is also increased, is as expected and has been seen before [3]. It is interesting to note that the start and onset temperatures of the PSS/SSS Match sample are lower than that of the No Added PSS, 5% PSS and 5% Cottonseed samples at all percentages of total added hard fat. A lower onset and start to crystallization temperature

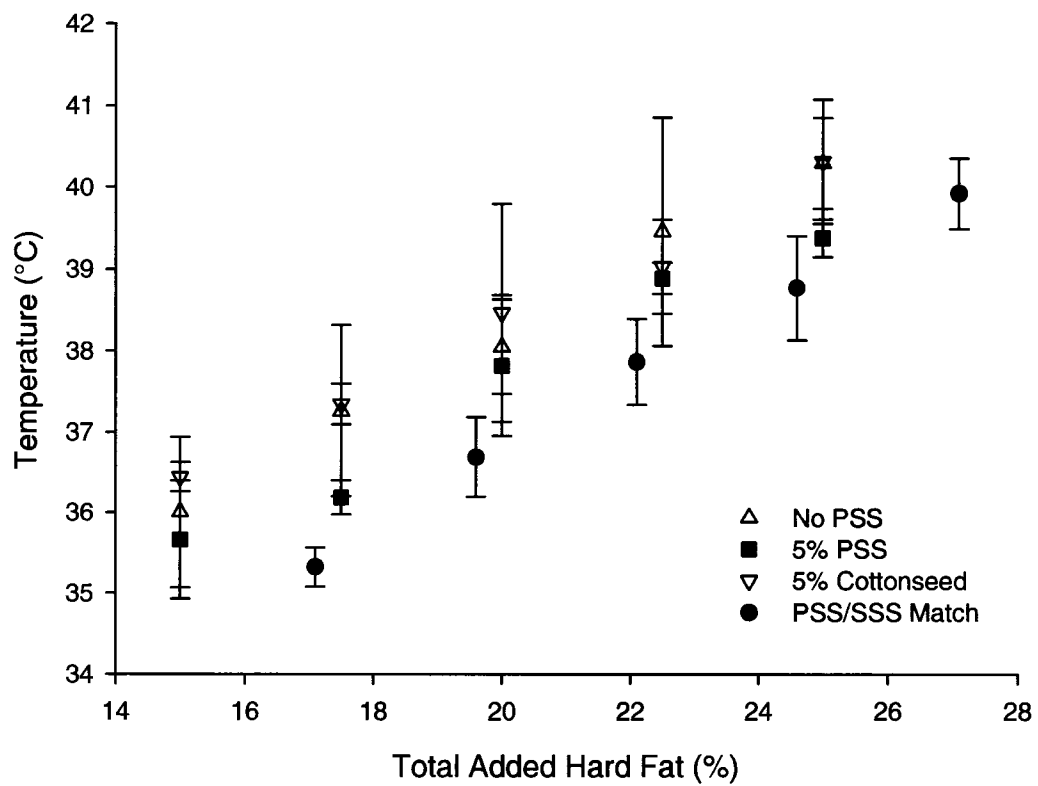


Figure 4.7a: Start of enthalpy of crystallization curves versus total added saturates

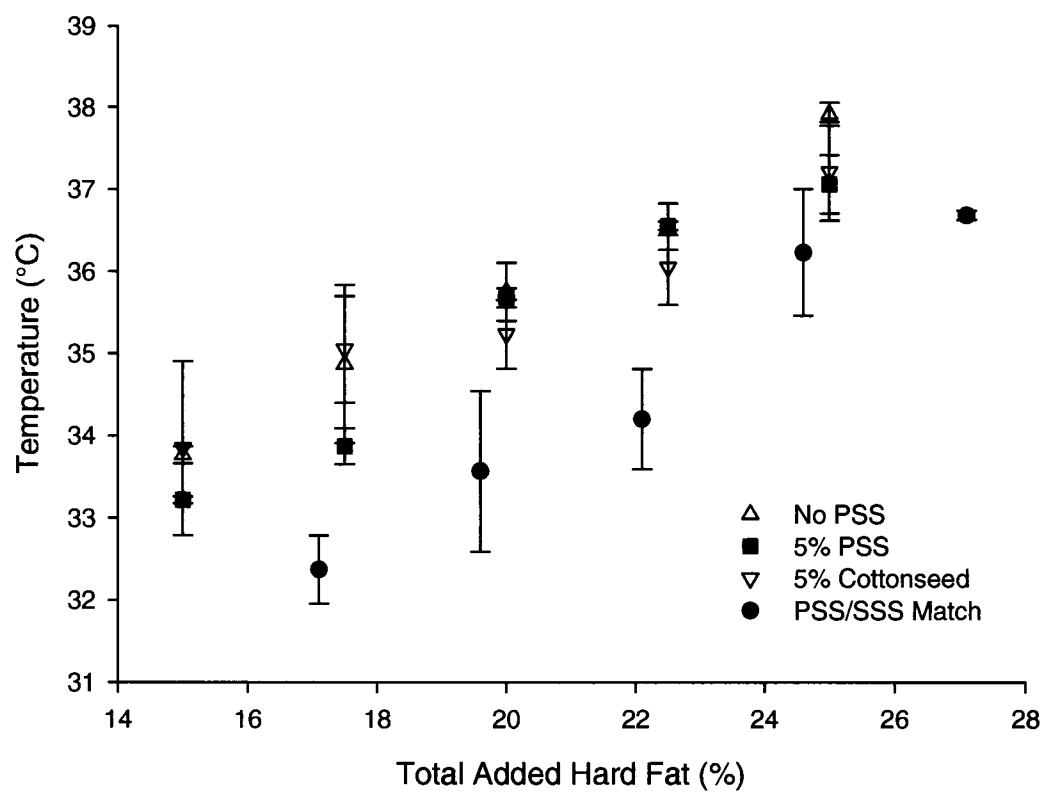


Figure 4.7b: Onset of enthalpy of crystallization curves versus total added saturates

suggests that more time is required prior to crystallization for the molecules within the sample to achieve the preferred alignment and concentration prior to crystallization. Recall that in Figure 4.6c the onset of melt was lower for the PSS/SSS Match sample at all levels of total added saturated fat. Thus, this lower onset and start of melt may be due to the formation of lower melting compounds within the sample, due to both the reorganization time prior to crystallization and the increase in the concentration of the lower melting TAG PSS within the sample itself.

The peak maxima of the enthalpy of crystallization curves obtained via DSC is shown in Figure 4.7c as a function of total added saturated fat. As the amount of added hard fat is increased, the temperature at which the peak maxima occur for all samples also increases. The PSS/SSS Match sample has a lower temperature of peak maxima than the three other sample types (30.8 ± 0.3 °C to 35.5 ± 0.3 °C for the PSS/SSS Match sample as compared to a window of 31.5 to 36.7 °C for the other three sample types). Thus, the bulk of the crystallization within the PSS/SSS Match sample occurs at a lower temperature than in the No Added PSS, 5% PSS and 5% Cottonseed samples. This again suggests that a greater driving force to crystallization is required to fully crystallize the sample. As SSS has the higher melting point of the two TAGs in question, and as the PSS/SSS Match sample has a lower percentage of SSS (47 to 59%, Table 4.2), the lower melting point of the PSS would allow the PSS/SSS Match sample to crystallize at a lower temperature. Another possible explanation for the lower peak maxima of the PSS/SSS Match samples would be due to the asymmetry of the TAG PSS. It has been suggested

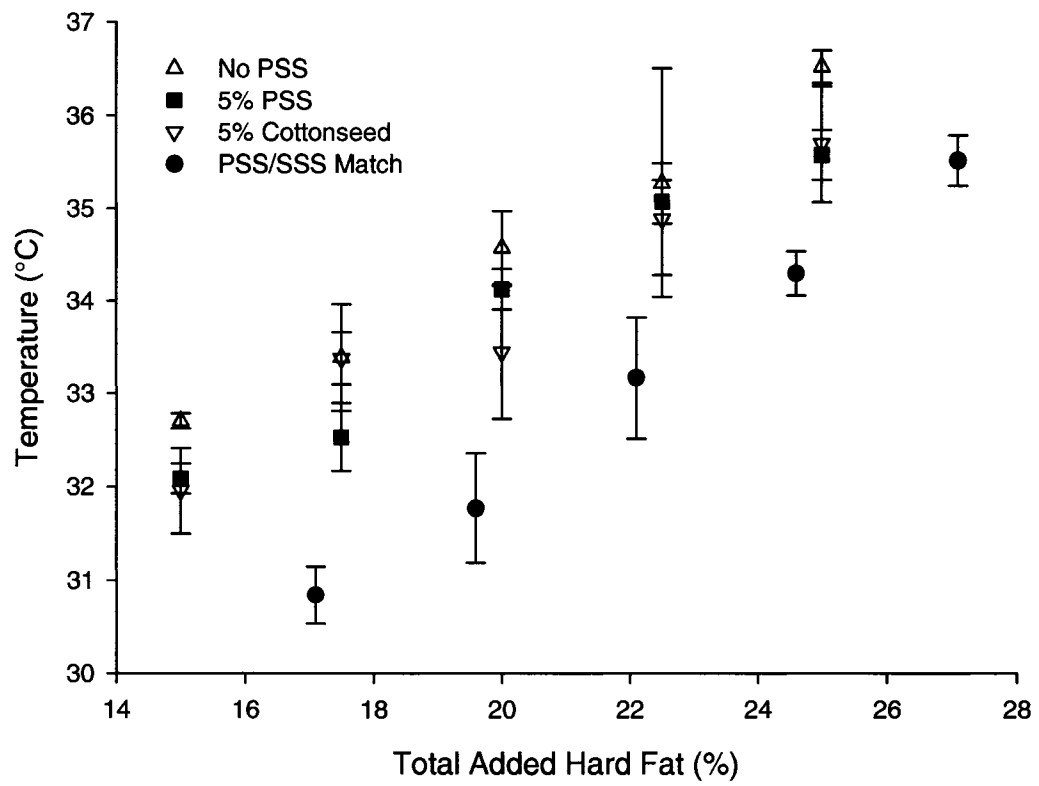


Figure 4.7c: Crystallization peak maximum versus total added saturates

by Roussett et al [18] that asymmetric TAGs “require more time to attach in the right position to the solid phase”, and as such apply a “brake” to the crystallization process. This trend was also highlighted by the start and onset temperatures of crystallization (Figures 4.7a and 4.7b, respectively). This also agrees with the melting peak temperatures shown in Figure 4.6a where the PSS/SSS Match samples had lower melting peak maxima than the other three sample types in this study.

The enthalpy of crystallization by DSC for all samples is shown in Figure 4.7d as a function of increasing total added saturated fat. As the percent total added hard fat is increased, the enthalpy of crystallization also increases. All samples tested of all types fit into this increasing trend, suggesting that regardless of the compounds being formed, the heat evolved during the crystallization process depends on the concentration hard fat within the sample and not necessarily on the molecular composition of this hard fraction.

4.3.6 Microstructure

The microstructure of each of the sample types ((a) No Added PSS, (b) 5% PSS, (c) 5% Cottonseed, and (d) PSS/SSS Match) 1 hour after processing is shown in Figure 4.8. The control samples, No Added PSS (Figure 4.8a), demonstrated small spherulites ($> 10 \mu\text{m}$) evenly distributed throughout the field of view. The 25% No Added PSS sample had well defined large Maltese crosses indicating the presence of spherulites of diameter $\sim 20 \mu\text{m}$, mostly likely due to the high concentration of saturated fat within the sample as well as the high level of SSS (80%, Table 4.2) which aids in the early construction of a solid crystal network upon which the remainder of the sample can form.

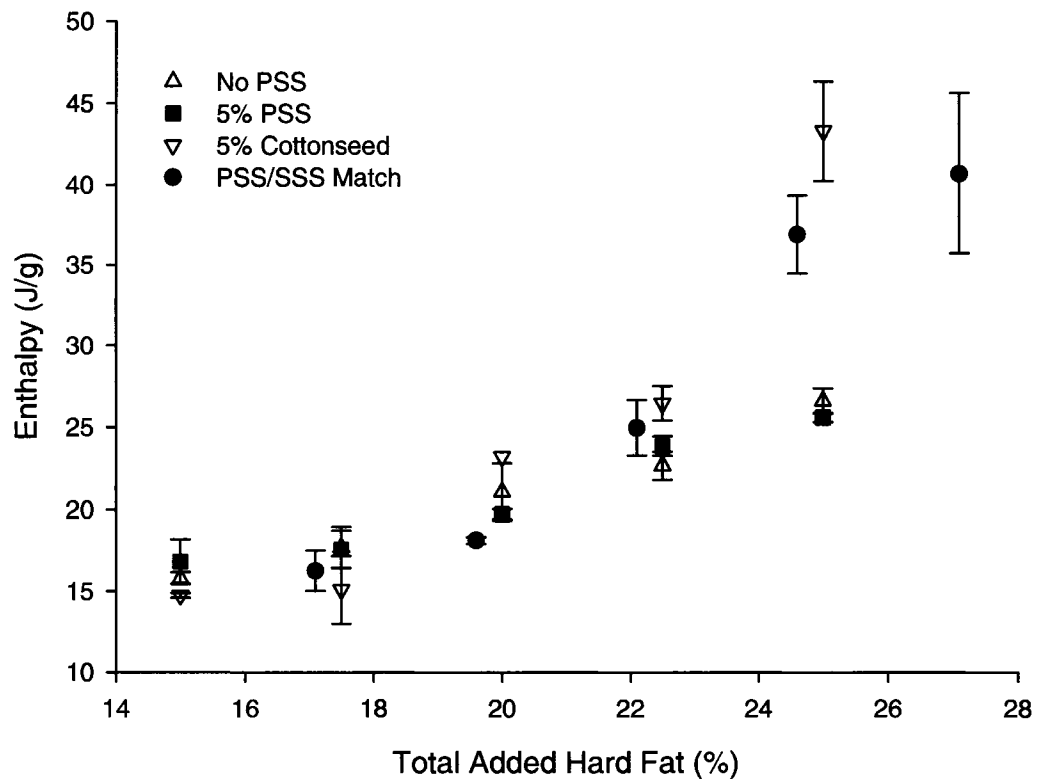


Figure 4.7d: Crystallization enthalpy versus total added saturates

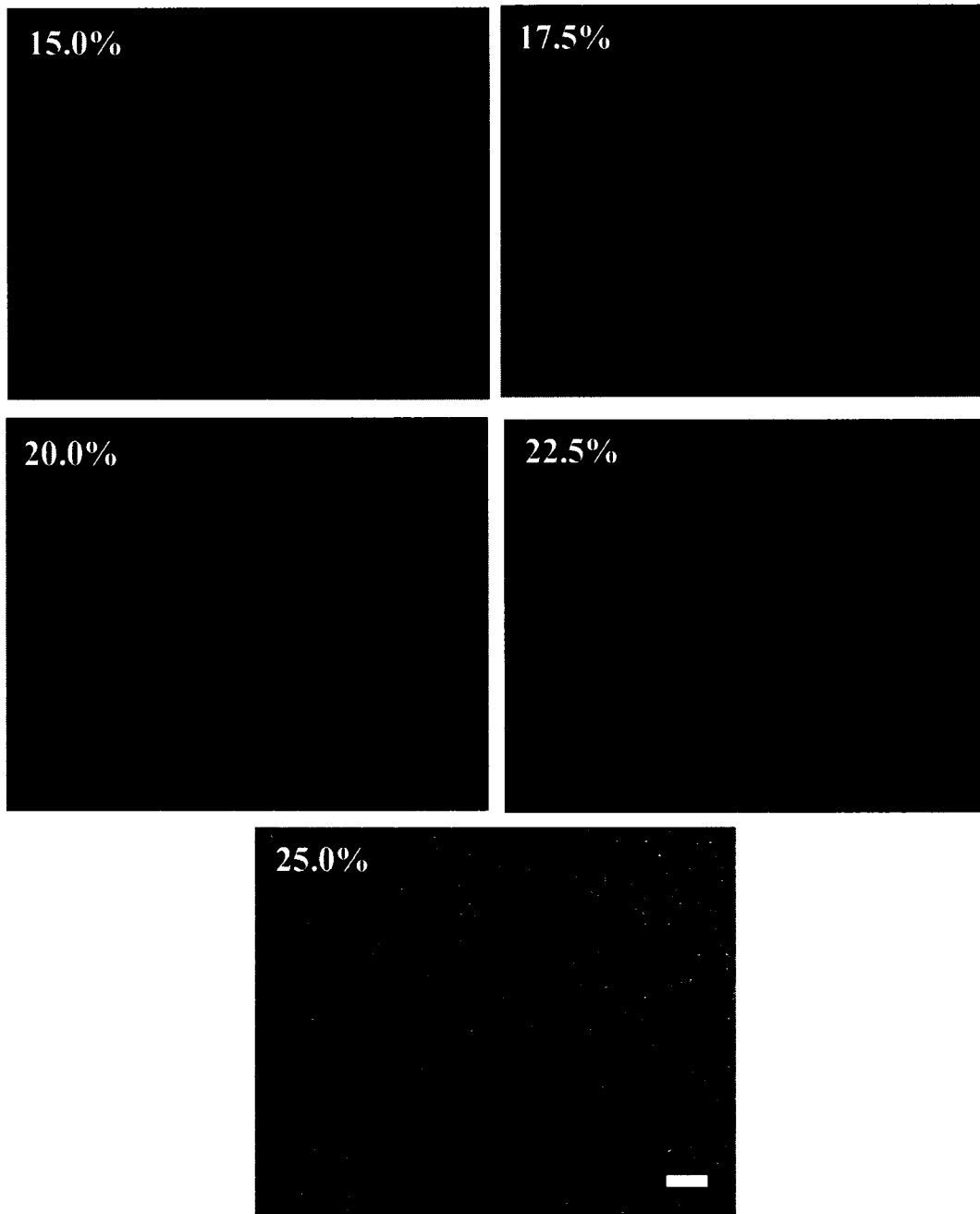


Figure 4.8a: Microstructure of the No Added PSS samples 1 hour after processing.
(White bar = 100 μm)

The microstructures in the 5% PSS samples are shown in Figure 4.8b, with small spherulites ($\sim 15 \mu\text{m}$) visible for all concentrations of total added saturated fat up to 22.5% and spherulites of diameter $< 10 \mu\text{m}$ for the 25.0% total added saturated fat sample. The larger spherulites visible in the samples of type 5% PSS may be due to the higher concentrations of PSS within the hard fat of the sample (35 thru 44% PSS compared with 33% PSS for the 25% hard fat sample). Therefore it is suggested that after two days PSS will work to modify the crystal network (pinning) of a sample of which it is a minor component, and this effect is most easily seen in the sample with the highest concentration of PSS, the 5% PSS samples with $< 22.5\%$ total added saturated fat.

Figure 4.8c shows the microstructure of the 5% Cottonseed samples. The samples all exhibit small spherulites ($< 10 \mu\text{m}$) in the network structure, with the 15% total added hard fat sample having slightly larger spherulites ($\sim 12 \mu\text{m}$) than the other samples of this type.

Finally, the microstructure of the PSS/SSS Match samples is shown in Figure 4.8d. Yet again, the dominate feature is the existence of spherulites at all concentrations (approximately 5 to 8 μm). Even though the concentration of TAGs within the hard fat fraction of each of the samples as a function of the total sample composition is the same as that in the 5% PSS samples, the same feature of larger spherulites being present for higher concentrations of PSS is not seen here. This is potentially due to the presence of other TAGs at low concentrations being present due to the combination of FHCo to

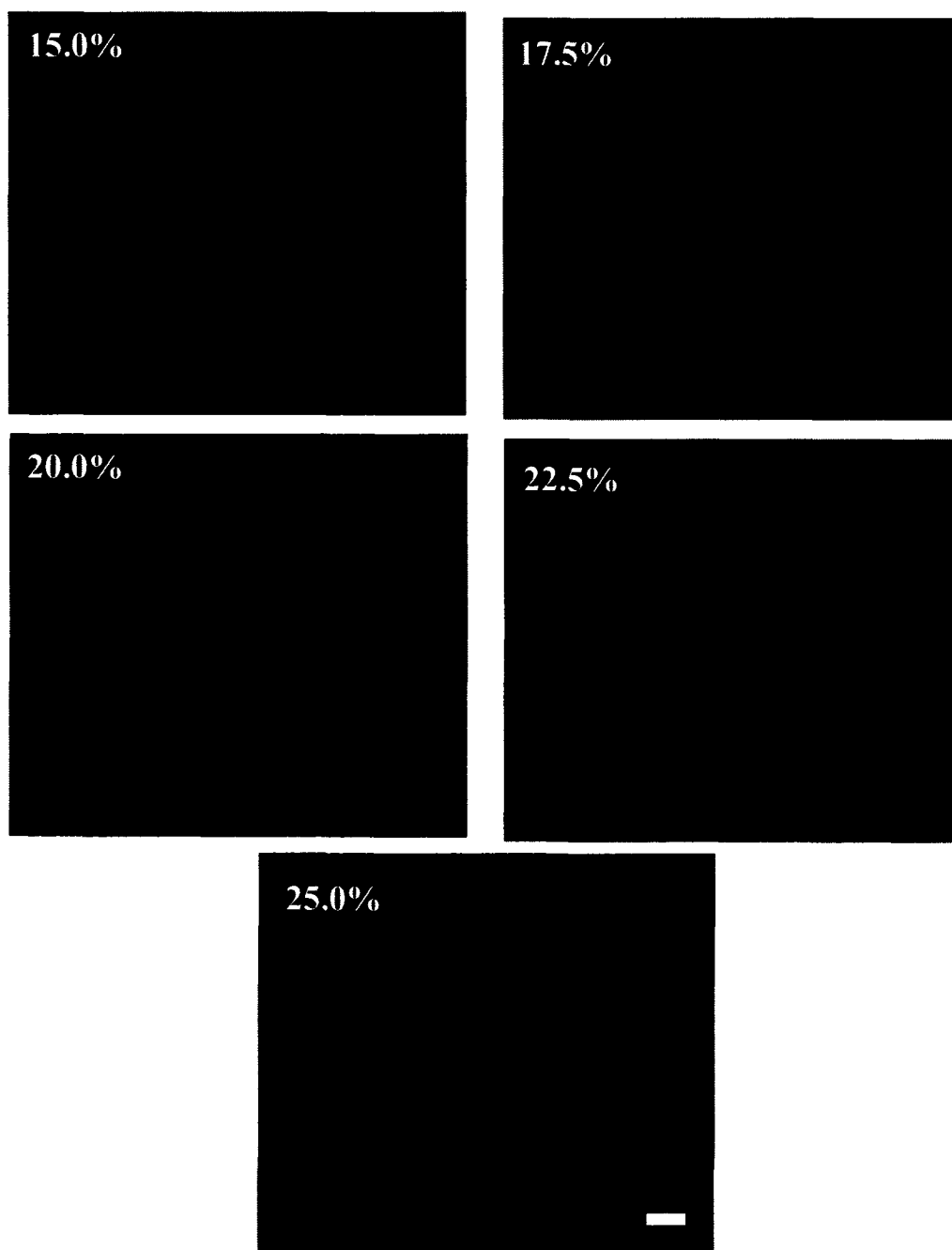


Figure 4.8b: Microstructure of the 5% PSS samples 1 hour after processing. (White bar = 100 μm)

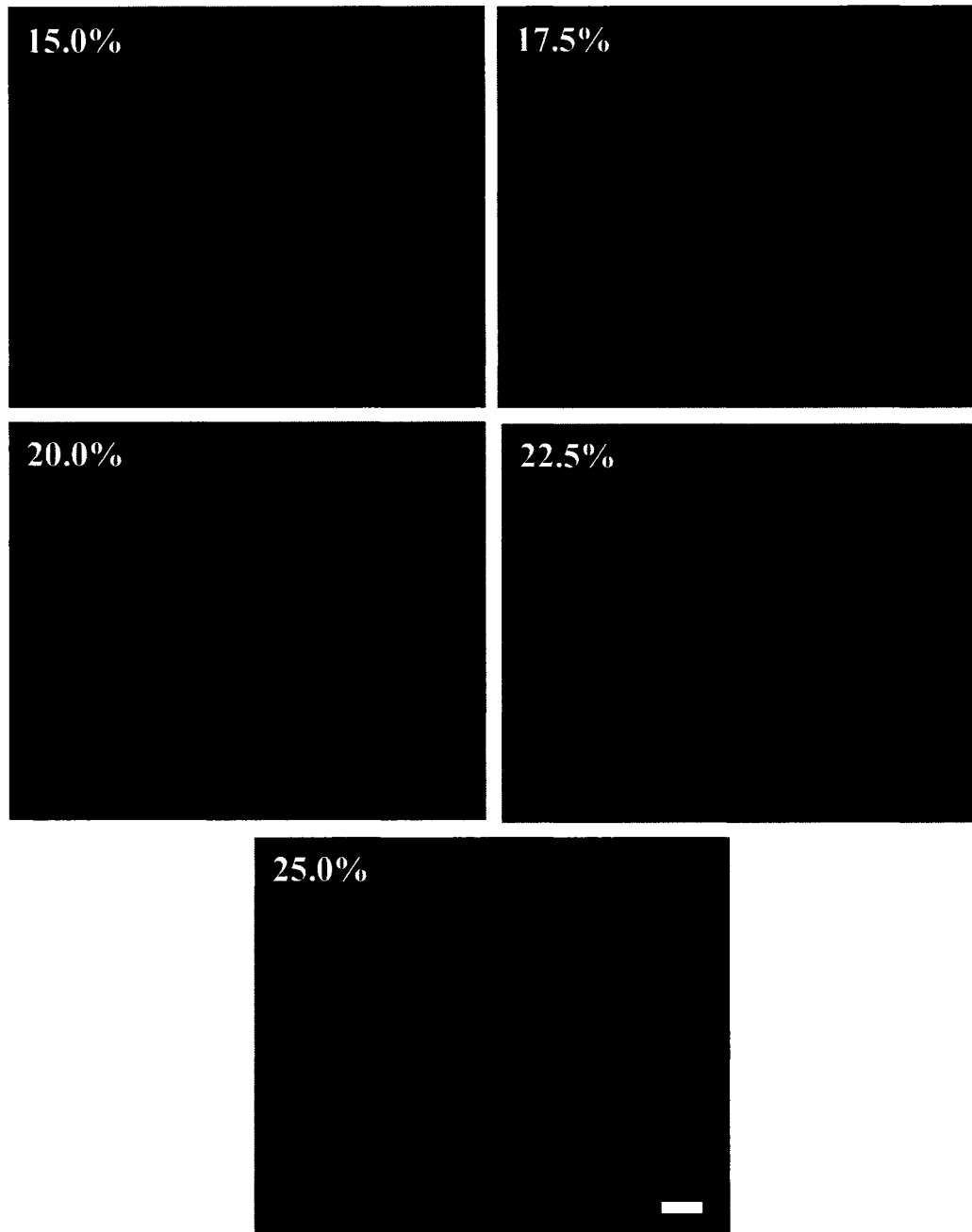


Figure 4.8c: Microstructure of the 5% Cottonseed samples 1 hour after processing.
(White bar = 100 μm)

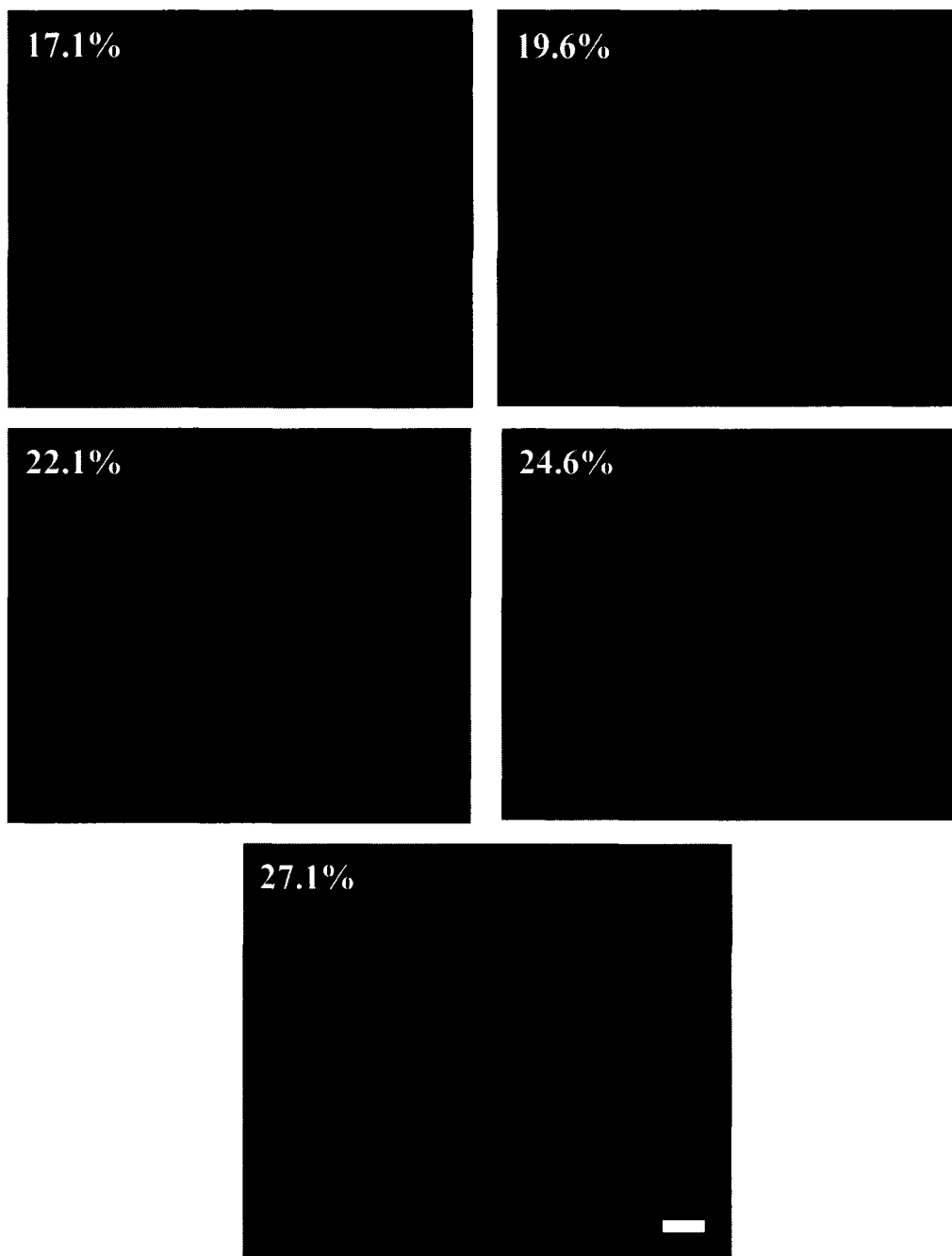


Figure 4.8d: Microstructure of the PSS/SSS Match samples 1 hour after processing.
(White bar = 100 μm)

replace the pure PSS leading to a reduction in the SSS and PSS percentages as a function of the total added saturated fat (Table 4.2).

For all of Figure 4.8, it is clear that there is no rod-like growth occurring as suggested by the Avrami fitting (Figure 4.4b). This could be due to the change in the rate of cooling at which the samples were processed, however an investigation into the microstructure of each sample crystallized at 3 °C/min revealed similar microstructure to that shown in Figure 4.8. Thus, the rod-like growth predicted by the Avrami fitting was not seen in the microscope pictures obtained.

4.4 Conclusions

Clearly, the fat crystal network of a canola based shortening system can be modified by the addition of PSS both in pure form and as a component of FHCo. The change in the crystal networks formed due to the incorporation of PSS is reflected in the lowered crystallization peak max as well as in the increase in FWHM with the addition of PSS. The Avrami treatment of the SFC growth curves reveals that the PSS enrichment of the samples did not affect the growth mode of the crystal network and that the greatest effect on the growth rate was due to the amount of total added saturates, not on the composition of the saturated fat. Therefore, the modification of the canola based shortening samples with PSS affects only specific levels of structure, resulting in a stable shortening which is harder for commensurate levels of saturated fat, without significant deleterious effects on the melting and polymorphism of the shortening.

4.5 References

1. Bell, A., et al., *Effects of Composition on Fat Rheology and Crystallization*. Food Chemistry, 2007. **101**: p. 799-805.
2. Higgins, N.W., *Low Trans-Stereoisomer Shortening Systems*, U.S.P.a.T. Office, Editor. 2004: USA. p. 12.
3. Humphrey, K.L. and S.S. Narine, *A comparison of lipid shortening functionality as a function of molecular ensemble and shear: Crystallization and melting*. Food Research International, 2004. **37**(1): p. 11-27.
4. Narine, S.S. and K.L. Humphrey, *A comparison of lipid shortening functionality as a function of molecular ensemble and shear: microstructure, polymorphism, solid fat content and texture*. Food Research International, 2004. **37**(1): p. 28-38.
5. O'Brien, R.D., *Shortenings: Types and Formulations*, in *Edible Oil and Fat Products: Products and Applications*, F. Shahidi, Editor. 2005, John Wiley & Sons, Inc. p. 125-157.
6. O'Brien, R.D., *Shortening Technology*, in *Introduction to Fats and Oils Technology*. 2000. p. 421-451.
7. Bouzidi, L., et al., *Use of first and second derivatives to accurately determine key parameters of DSC thermographs in lipid crystallization studies*. Thermochemica Acta, 2005. **439**: p. 94-102.

8. *Standard Methods for the Analysis of Oils, Fats, and Derivatives*, in *International Union of Pure and Applied Sciences*. 1979.
9. *Solid Content Determination in Fats by Low Resolution Nuclear Magnetic Resonance v. 2.150*, in *International Union of Pure and Applied Sciences*. 1987.
10. *Determination of Solid Fat Content by Pulsed NMR Method*, in *International Standard, Animal and Vegetable Fats and Oils*. 1991.
11. *AOCS Method Cd 16b-93*, in *Official and tentative methods of the American Oil Chemists' Society*, W.E. Link, Editor. 1998, AOCS Press: Champaign, IL.
12. Narine, S., K. Humphrey, and L. Bouzidi, *Modification of the Avrami Model for Application to the Kinetics of the Melt Crystallization of Lipids*. *J. Am. Oil Chem. Soc.*, 2006. **83**(11): p. 913-921.
13. Avrami, M., *Kinetics of Phase Change. II. Transformation-Time Relations for Random Distribution of Nuclei*. *Journal of Chemical Physics*, 1940. **8**: p. 212-224.
14. Narine, S.S. and K.L. Humphrey, *Extending the capability of pulsed NMR instruments to measure solid fat content as a function of both time and temperature*. *J. Am. Oil Chem. Soc.*, 2004. **81**(1): p. 101-102.
15. de Man, L., et al., *Polymorphic Stability of Some Shortenings as Influenced by the Fatty Acid and Glyceride Composition of the Solid Phase*. *J. Am. Oil Chem. Soc.*, 1992. **69**(3): p. 246-250.

16. Sharples, A., *Overall Kinetics of Crystallization*, in *Introduction to Polymer Crystallization*. 1966, Edward Arnold: London. p. 44-59.
17. Roth, M.W., C.L. Pint, and C. Wexler, *Phase Transitions in Hexane Monolayers Physisorbed onto Graphite*. *Physical Review B*, 2005. **71**(155427): p. 1-13.
18. Rousset, P., M. Rappaz, and E. Minner, *Polymorphism and Solidification Kinetics of the Binary System POS-SOS*. *J.Am.Oil Chem.Soc.*, 1998. **75**(7): p. 857-864.

5. Using 1 – Palmitoyl, 2,3 – Distearoyl – sn - Glycerol (PSS) as a Structural Enhancer so as to Decrease the Level of Saturates in Zero-Trans Shortenings: Pilot Scale Studies

5.1 Introduction

In Chapter 4, we investigated, at the laboratory scale, the effects of addition of PSS to an all purpose shortening sample composed of a hard fat with predominantly stearic acid (fully hydrogenated canola oil) and soybean oil. It was found that crystalline structure was significantly altered, as well as the kinetics of crystallization. Furthermore, the work demonstrated that when PSS is present in specific ratios with SSS, the resulting network is significantly harder, even though its melting point is somewhat decreased as well as its solid content. However, the decreases in solid content and melting ranges are not undesirable features, and therefore it is suggested that PSS addition to such shortening systems can be used as a means of reducing saturates whilst still delivering a product which meets expected textural, thermal and plastic expectations. However, at the laboratory scale, it is difficult to predict how such structural enhancers would work within a scraped-surface heat exchanger. Therefore, in this study, we report pilot trials of the same concept. In this study, we also investigate the effects of the controllable parameters of a scraped surface heat exchanger on the final functionality of the enhanced

A version of this chapter has been included in a patent application.
Narine, S., K. Humphrey, and F. Kincs, *Shortenings and Methods of Making and Using Thereof*. 2007,
Scanlon, S. Weiss, S.: United States Patent and Trademark Office. 60953609 p. 38.

product as well as controls, and we also report on a series of application tests when utilizing the shortening made in the production of icings.

5.2 Experimental Procedures

5.2.1 *PSS enrichment at the pilot plant scale and the effect of processing conditions and tempering*

The shortening samples used in this study were composed of fully hydrogenated Canola and Cottonseed hard fats, and soybean oil all supplied by Bunge Oils (Bradley IL., USA). The sample compositions of the three types of samples used in this study are listed in Table 5.1. These types are (1) FH Canola mixed with Soybean oil (control), (2) 5% FH Cottonseed and FH Canola mixed with Soybean oil ($x = \frac{\%PSS}{\%SSS} = 0.35$), and (3) a blend of FH Cottonseed and FH Canola oil mixed with Soybean oil in which the percentage of PSS and SSS is matched to the levels found in a 5% PSS in Canola and Soybean oil sample ($x = \frac{\%PSS}{\%SSS} = 0.83$) [1].

5.2.1.a Sample Preparation

The molten samples were processed in a scraped surface heat exchanger system, specifically a Gerstenburg Pilot Plant Type 3x57 (Copenhagen, Denmark) and a schematic diagram of the crystallizer is shown in Figure 5.1. The pump speed (high or low), fill temperature (medium or low), and perfector revolutions per minute

Table 5.1: Sample compositions of all 5 sample mixtures used in this study

Sample Type	Total Added Saturated Fat (%)	Soybean Oil (%)	Fully Hydrogenated Canola (%)	Fully Hydrogenated Cottonseed (%)
No Added PSS (Control)	15.0	85.0	15.0	
	20.0	82.5	20.0	
	25.0	75.0	25.0	
5% Cottonseed	17.5	82.5	12.5	5.0
PSS/SSS Match	17.1	82.9	3.1	14.0

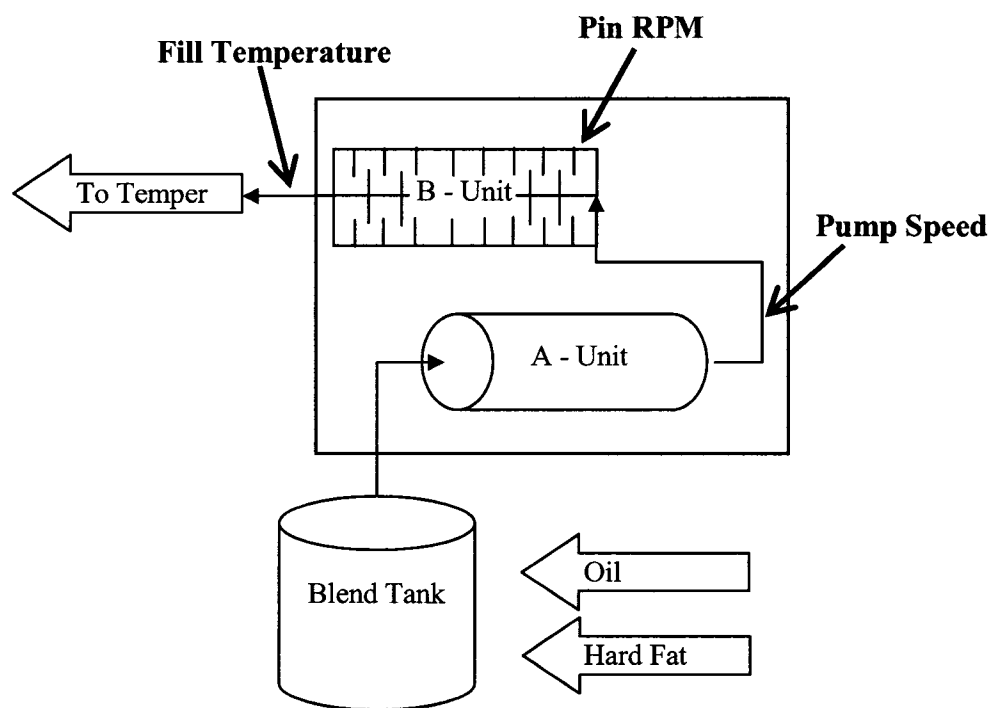


Figure 5.1: Schematic diagram of a pilot plant shortenings crystallizer with Pin RPM, Pump Speed, and Fill Temperature indicated on corresponding units

(RPM) (high) within the scraped surface heat exchanger were modified (Table 5.2). The crystallized sample was poured from the scraped surface heat exchanger into 3 lb plastic tubs, 8" in diameter, which were then sealed with a plastic lid. Each sample was stored at 85 °F for 2 days before being stored at 70 °F, and a duplicate sample was immediately stored at 70 °F. Thus, for each sample listed in Table 5.1, 4 different processing regimes and 2 tempering conditions resulted in each sample being processed 8 different ways (and 2 tubs were produced for each of these 40 unique samples).

5.2.1.b Relative Hardness Measurements

A TA Texture Analyzer was used for hardness measurements. Each tub was penetrated with a spherical ball probe with diameter 1/8 inch. The depth of penetration was 1.5 mm and the speed of penetration was 0.5 mm/s. The maximum force of penetration was taken as the relative hardness of the sample. Each tub was penetrated four times proceeding radially inward at 1/2 inch steps starting 1/2 inch from the exterior of the tub. Given that there were 2 tubs for each sample at each processing and tempering condition, this resulted in 8 penetrations for each sample. Measurements were reported as an average and standard deviation of the 8 penetrations. Measurements were taken 7 and 14 days after processing. Not only do such measurements evaluate the texture of the shortening product, it also measures the consistency of the product, due to the radial measurements – i.e. ensuring that there are no variations in the texture/hardness within the sample itself.

Table 5.2: Processing conditions for pilot scale samples in this study

Sample ID	Pump Speed (% Capacity)	Fill Temperature (°F)	Perfector RPM	Tempering (° F)
LMH 70	Low (50%)	Medium (67)	High (100)	70
LMH 85	Low (50%)	Medium (67)	High (100)	85
LLH 70	Low (50%)	Low (50)	High (100)	70
LLH 85	Low (50%)	Low (50)	High (100)	85
HMH 70	High (70%)	Medium (67)	High (100)	70
HMH 85	High (70%)	Medium (67)	High (100)	85
HLH 70	High (70%)	Low (50)	High (100)	70
HLH 85	High (70%)	Low (50)	High (100)	85

5.2.1.c NMR Measurements, SFC Determination

SFC data was acquired using a pulse magnetic resonance spectrometer equipped with a temperature controlled measurement chamber. The data sampling procedure was fully automated, and the SFC was calculated and automatically printed out by the NMR [2-5].

NMR tubes were filled with the solid sample from each plastic tub at the time of measurement after 7 and 14 days. The sample was either spooned into the top of the NMR tube (very soft sample) or a plug of solid sample (very firm samples) was inserted into the tube. The bottom of the tube was then tapped on the table until the sample rested at the bottom of the tube. The sample tubes were filled with the processed shortenings to a height of $3.5 \text{ cm} \pm 0.1 \text{ cm}$. The tube was then inserted in to the NMR and a measurement was taken immediately. 3 tubes were filled for each sample. The SFC is reported as the average and standard deviation of the 3 SFC's recorded.

5.2.2 Applications testing of PSS enriched samples

Shortening samples created and tested in Section 7.2.1 of this study were made into icings in this part of the study. The same sample notations as that in Table 5.1 are used. Vrest, an all purpose mono-diglyceride emulsifier supplied by Bunge Oils, was added to each of the test shortenings as outlined below. Three control shortenings: Vreamay, Vreamay Right, Vreamay NT, supplied by Bunge Oils were also made into icings.

5.2.2.a Sample Preparation

Each shortening sample was made into cream icing using the Cream Icing Test Method (17-73) (Appendix 3). 5.5% (w/w) of each test shortening (not the control shortenings) was replaced by the all purpose emulsifier. All icing ingredients were weighed into a 10 quart bowl and mixed on low for 30 seconds and the excess material on the sides of the bowl and beater was scraped down into the bulk of the icing. The icing was then creamed at the first mixer speed for 15 minutes, scraping again after 3 minutes.

5.2.2.b Trench Score

The trench score of each sample, an in-house test designed at Bunge's headquarters to quantify the ability of the shortening product to maintain its structural integrity and shape, was determined according to the directions in Cream Icing Test Method (17-73). A trench almost to the bottom of the bowl is cut into the finished icing with a 1 inch wide metal spatula. A score is assigned relating to the length of time for the plastic deformation due to the weight of the icing to close the trench. Digital pictures of each sample's trench were taken 2 minutes after creating the trench.

5.2.2.c Specific Gravity

The specific gravity of each prepared icing was measured directly after the Trench Score and photos of the trench were taken. An aluminum moisture dish 2.25 inches in

diameter and 2.25 inches tall with 200 cc capacity was filled with the prepared icing. The mass of the contents (in grams) of the dish was divided by 200.0 g to obtain the specific gravity of the icing.

5.2.2.d Slump-Slide Tests

Immediately following the specific gravity measurement, the slump test, an in-house test developed at Bunge's headquarters to measure the plasticity of the shortening and resistance to flow from a vertical application, was performed. Following Slump-Slide Test Method (1-88), developed by Bunge Oils (Appendix 4), the instrument box as shown in Figure 5.2 (all dimensions ± 0.05 cm unless otherwise noted) was filled with icing, the excess was scraped off the top of the box with a metal spatula from the bottom to the top of the box. A small knife was run between the icing and the top of the box and the box was immediately placed in the leveled base with the edge of the box even with the zero line on the base. The slump (horizontal displacement over onto the base) and slide (vertical displacement down the back of the box) of the icing was measured (in millimeters) after 10 minutes.

5.2.2.e One Week Observations

Each icing sample was stored in sealed 3 lb plastic containers at room temperature for one week. At this time the appearance of each icing sample was recorded for the sample at the top and bottom of each container.

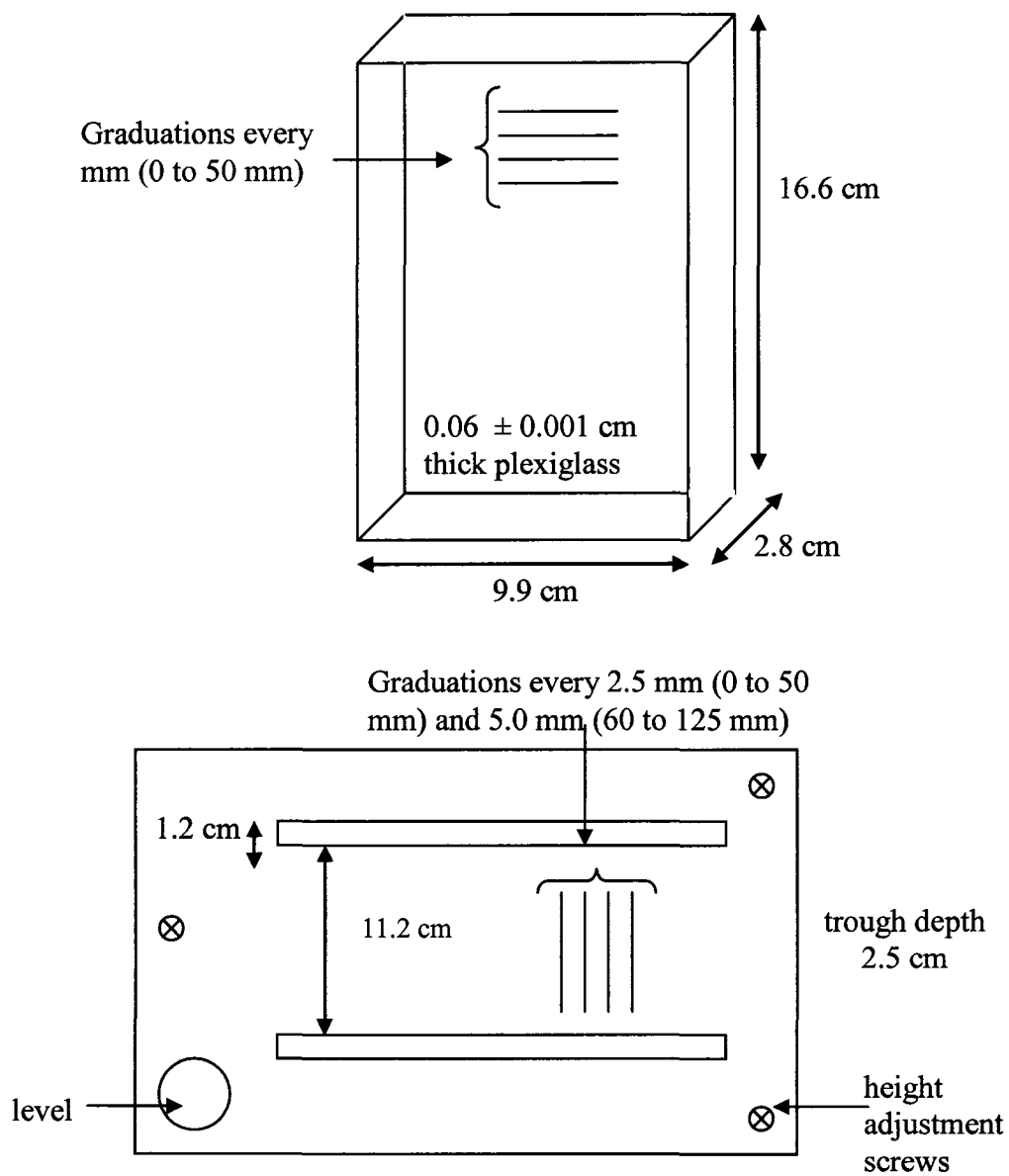


Figure 5.2: Dimensions of the apparatus used to measure the plasticity of the icings and resistance to flow (Slump-Slide Box Dimensions)

5.3 Results and Discussion

In Chapter 4, we suggested that PSS, either in pure form or as a constituent of fully hydrogenated Cottonseed oil or another carrier, will interact within a shortening sample with SSS to form a structure enhancer [1, 6, 7]. It is further suggested here that by altering the parameters of cooling and shear during the crystallization process one will be able to further promote this structure enhancing effect, and that the resulting reduced saturates, zero *trans* samples could potentially be suitable for use in cream icing formulations.

5.3.1 PSS enrichment at the pilot plant scale and the effect of processing conditions and tempering

The processing conditions that each sample undergoes will also affect the types and concentrations of the crystallizing species formed. Figure 5.3 shows the effect of fill temperature and pump speed on the cooling rate and degree of undercooling. A higher fill temperature (M) would result in the feedstock being subject to a lower degree of undercooling (ΔT) where ΔT is given by:

$$\Delta T = T_{Start} - T_{Fill(M)}$$

where T_{Start} is the temperature of the mixture entering the scraped surface heat exchanger and $T_{Fill(M)}$ is the medium fill temperature of the crystallized shortening when it is expelled from the heat exchanger. A lower ΔT suggests that the molecules within the sample would have greater mobility during crystallization and prior to temper,

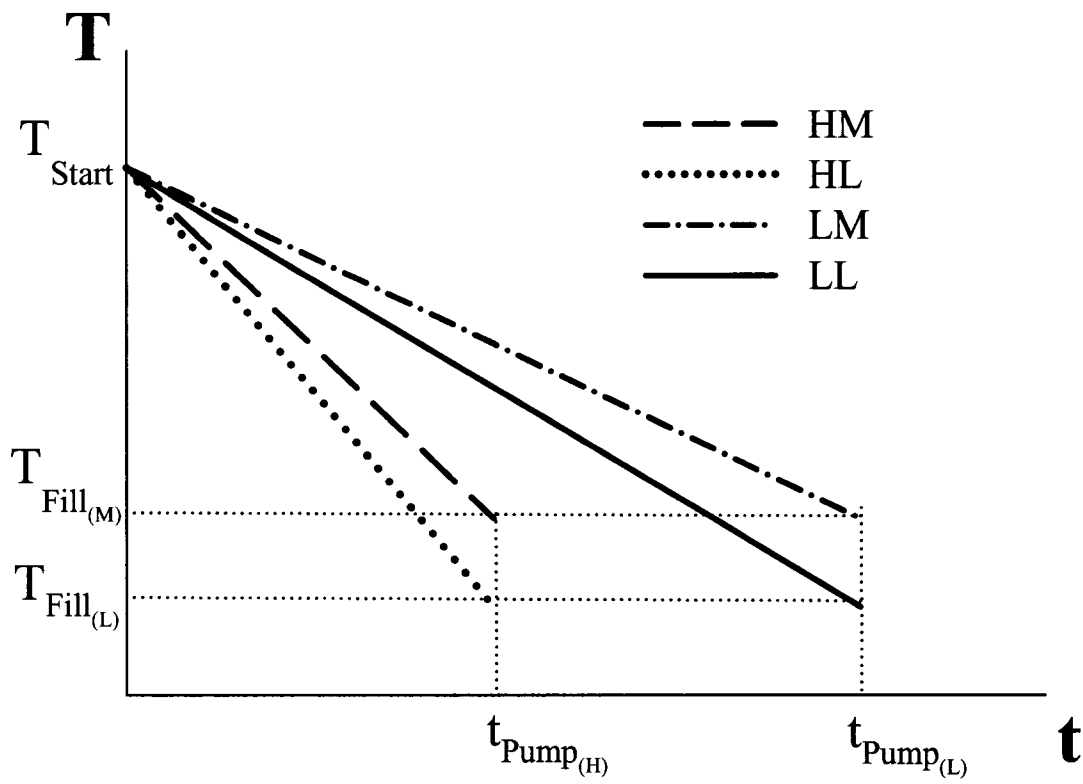


Figure 5.3: Effect of pump speed and fill temperature on the rate of cooling and effective undercooling within a shortening crystallizer

but with the crystallization requirements for fewer of the components being met. A lower fill temperature (L) would be due to a higher ΔT taking place prior to temper. The samples crystallized with a lower fill temperature will have less molecular mobility during crystallization and temper due to a greater number of components within the shortening having their crystallization requirements met, and thus the free liquid oil content of the shortening immediately after exiting the crystallizer is low, thus the heat and mass transfer is hampered at this point.

A high pump speed (H) would cause the sample to spend less time within the scraped surface heat exchanger than a low pump speed (L) and a high pump speed is indicative of a higher rate of cooling. This would mean that there would be less time for shear and less exposure to the heat exchange system. Given a low pump speed, the sample would spend a greater amount of time within the system, allowing more shear time under a slower rate of cooling.

The perfector RPM is a measure of the speed at which the sample is sheared within the heat exchanger. It has been suggested that mechanical mixing or shear promotes the formation of the more stable polymorphic forms [8], potentially due to the increase in mass and heat transfer within the crystallizing product thereby allowing for the favored form to be achieved. For this study the shear rate was kept constant (high, H) in order to facilitate good mass and heat transport.

The tempering scheme also affects the final stages of structure building within the shortening samples. Holding the sample at 85 °F for two days prior to long term storage at 70 °F allows for more molecular mobility within the sample which facilitates drastic changes in the structure of the shortening. Moving the sample directly to long term storage at 70 °F provides a greater driving force for continued crystallization but with less molecular mobility within the sample due to higher viscosity.

The hardness of the shortening samples after 7 days is shown in Figure 5.4a for all samples tempered at (i) 70 °F and (ii) 85 °F. One can see that the PSS/SSS Match sample (represented by the black circle) is consistently as hard as or harder than the 5% Cottonseed sample (represented by the white triangle). Tempering the samples at 85 °F increases the hardness of the PSS/SSS Match samples and decreases the hardness of the 25% fully hydrogenated Canola oil (No Added PSS) shortening (represented by the height of the dark grey bar). For the HMH, LLH, and LMH processing schemes, the PSS/SSS Match sample is harder than all the other shortening blends tested, highlighting an increase in hardness with an 8% reduction in total added saturates.

The hardness of the shortening samples after 14 days is shown in Figure 5.4b for all samples tempered at (i) 70 °F and (ii) 85 °F. The No Added PSS samples are represented by the bars, while the black circles represent the PSS/SSS Match samples and the white triangles represent the 5% Cottonseed samples. After 14 days, the PSS/SSS Match samples are consistently harder than the 5% Cottonseed samples. Again tempering at 85 °F causes the PSS/SSS Match samples to be much harder than those

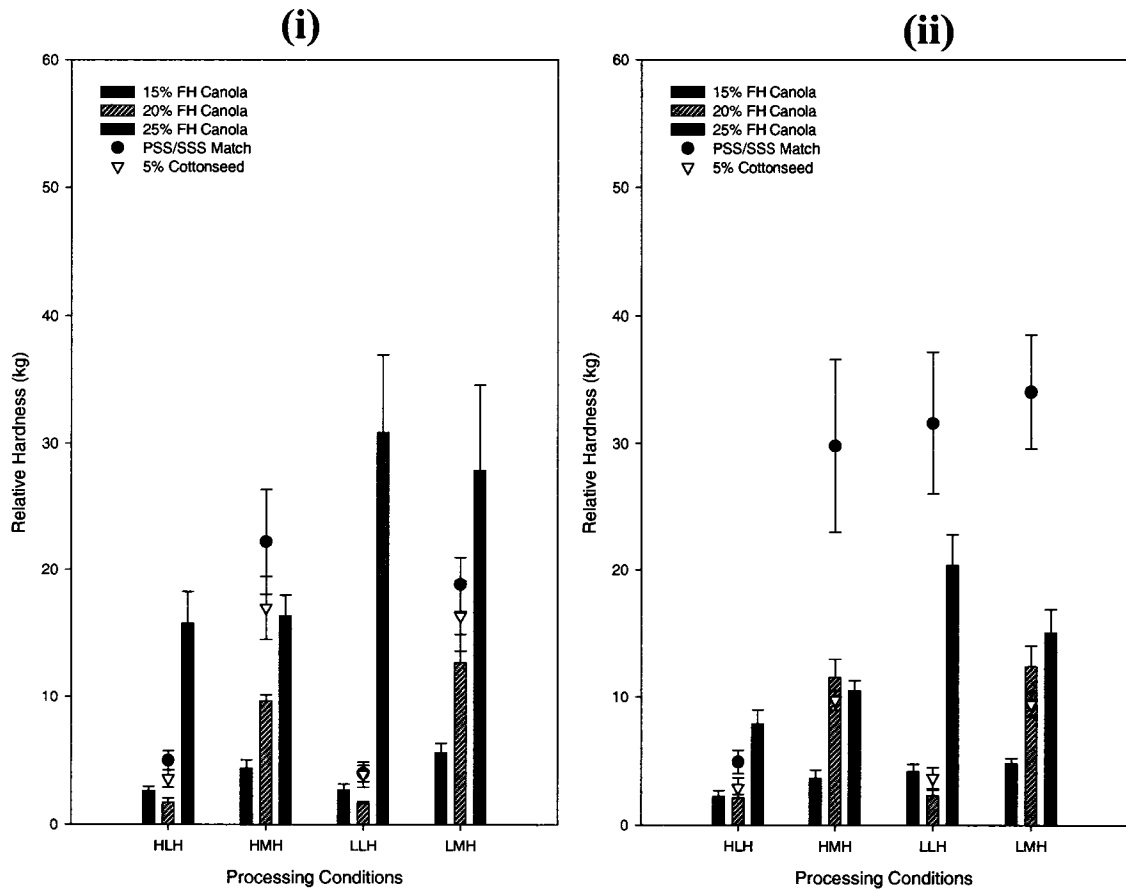


Figure 5.4a: Relative hardness of the shortening samples after 7 days as a function of the processing condition. Hardness for samples tempered at (i) 70 °F and (ii) 85 °F is shown. The vertical bars represent the hardness of the shortening samples with No Added PSS, the white triangles represent that of the 5% Cottonseed samples and the black circles represent that of the PSS/SSS Match samples.

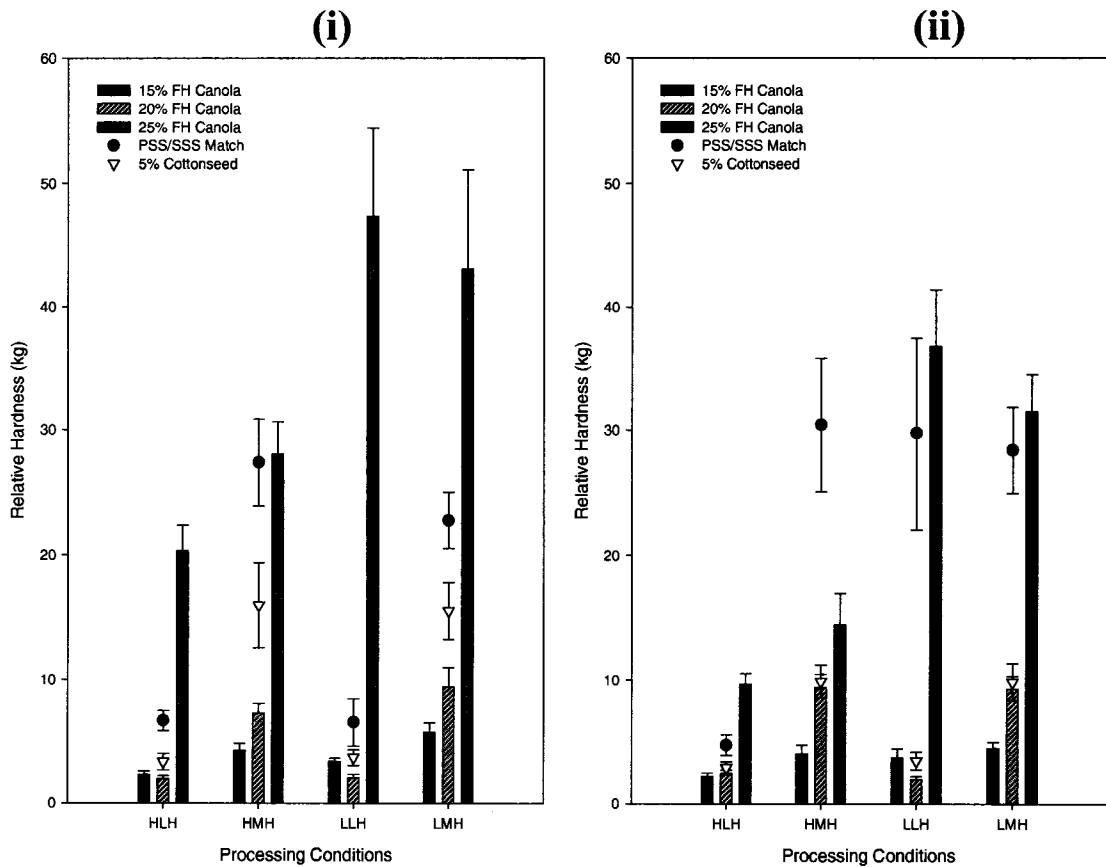


Figure 5.4b: Relative hardness of the shortening samples after 14 days as a function of the processing condition. Hardness for samples tempered at (i) 70 °F and (ii) 85 °F is shown. The vertical bars represent the hardness of the shortening samples with No Added PSS, the white triangles represent that of the 5% Cottonseed samples and the black circles represent that of the PSS/SSS Match samples.

tempered at 70 °F while decreasing the hardness of the 25% fully hydrogenated Canola (No Added PSS) shortening samples. As with the shortening samples 7 days after processing, 14 days after processing, the PSS/SSS Match sample tempered at 85 °F and processed with the regimes HMH, LLH, and LMH are harder than those tempered at 70 °F and those processed with HLH. For the processing regime HMH and tempering at 85 °F the PSS/SSS Match sample is harder than the 25% fully hydrogenated Canola (No Added PSS) sample after 14 days, even with an 8% decrease in total added saturates in the PSS/SSS Match shortening sample.

The SFC of the shortening samples after 7 days is shown in Figure 5.5a for all samples tempered at 70 °F (i) and 85 °F (ii). For the samples with 15, 20 and 25% fully hydrogenated Canola; one can see that as the amount of added saturated fat increases, the percent SFC also increases. The blended samples each containing 17.1% (PSS/SSS Match) and 17.5% (5% Cottonseed) total added saturated fat have a lower SFC than the 20% total added saturated fat (No Added PSS) sample. Thus the fully hydrogenated Cottonseed in the samples must work to build a structure with less solid fat incorporated. This suggests that the PSS content of fully hydrogenated Cottonseed, works to disrupt the structure, building a harder crystal network with entrapped oil. While there is little effect on SFC after 7 days with changing the tempering regime of the shortening, one can see that tempering at 85 °F lowers the SFC of the PSS/SSS Match samples at all processing conditions tested. Thus during the time the shortening is held at a higher temperature, the molecules within the PSS/SSS Match sample builds a crystal network structure which leads to a harder shortening (Figure 5.4a), while not increasing the SFC of the shortening.

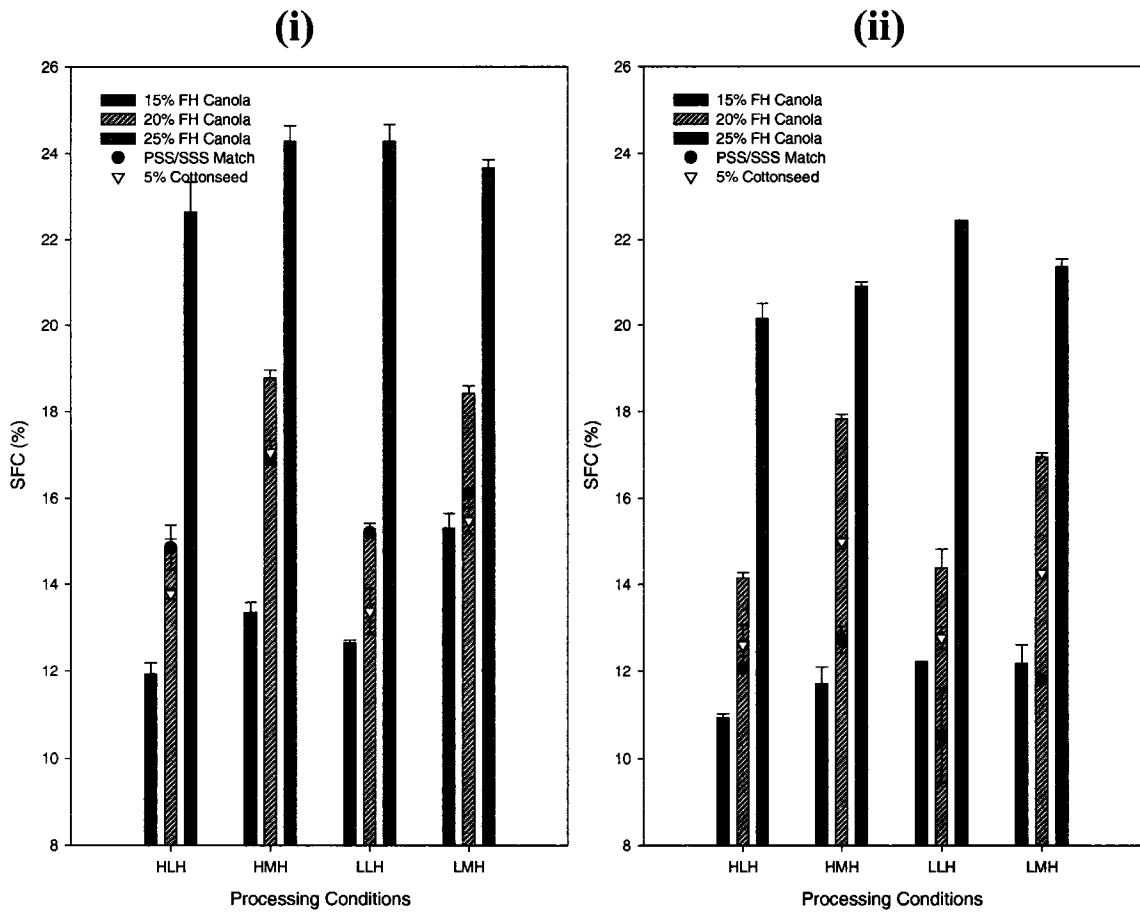


Figure 5.5a: SFC of the shortening samples after 7 days. The SFC for samples tempered at (i) 70 °F and (ii) 85 °F is shown. The vertical bars represent the SFC of the shortening samples with No Added PSS, the white triangles represent that of the 5% Cottonseed samples and the black circles represent that of the PSS/SSS Match samples.

Figure 5.5b shows the SFC data after 14 days for the samples tempered at (i) 70 °F and (ii) 85 °F. As with the SFC after 7 days (Figure 5.5a), the SFC of the No Added PSS samples increases as the amount of total added saturates increases. With the exception of LLH tempered at 70 °F, all of the shortening samples with fully hydrogenated Cottonseed included (17.1 and 17.5% total added saturates in PSS/SSS Match and 5% Cottonseed samples respectively) have a lower SFC than the 20% Canola (No Added PSS) sample, again implying that the entrapped oil has not been crystallized after a holding time of 14 days.

After 14 days all samples tempered at 85 °F have a lower SFC than those tempered at 70 °F. Again this suggests that holding the shortening samples at a higher temperature provides sufficient energy to the crystallizing system to build a harder crystal structure which has a low SFC (Figure 5.4b).

The melting peak maximum by DSC after 7 (a) and 14 (b) days for samples tempered at 70 °F (i) and 85 °F (ii) is shown in Figure 5.6. Clearly upon increasing the amount of added saturated fat in the No Added PSS samples the melting peak maximum also increases. The PSS/SSS Match sample peak maxima are all lower than that of the 5% Cottonseed shortening samples as well as that of any of the No Added PSS samples. A lower peak melting maxima suggests that the bulk of the crystallized shortening is melted at a lower temperature than that of a sample with a higher peak maximum. This in turn suggests that there are more lower melting TAGs in the starting lipid or that more lower melting compounds are formed during the crystallization of the shortening. The

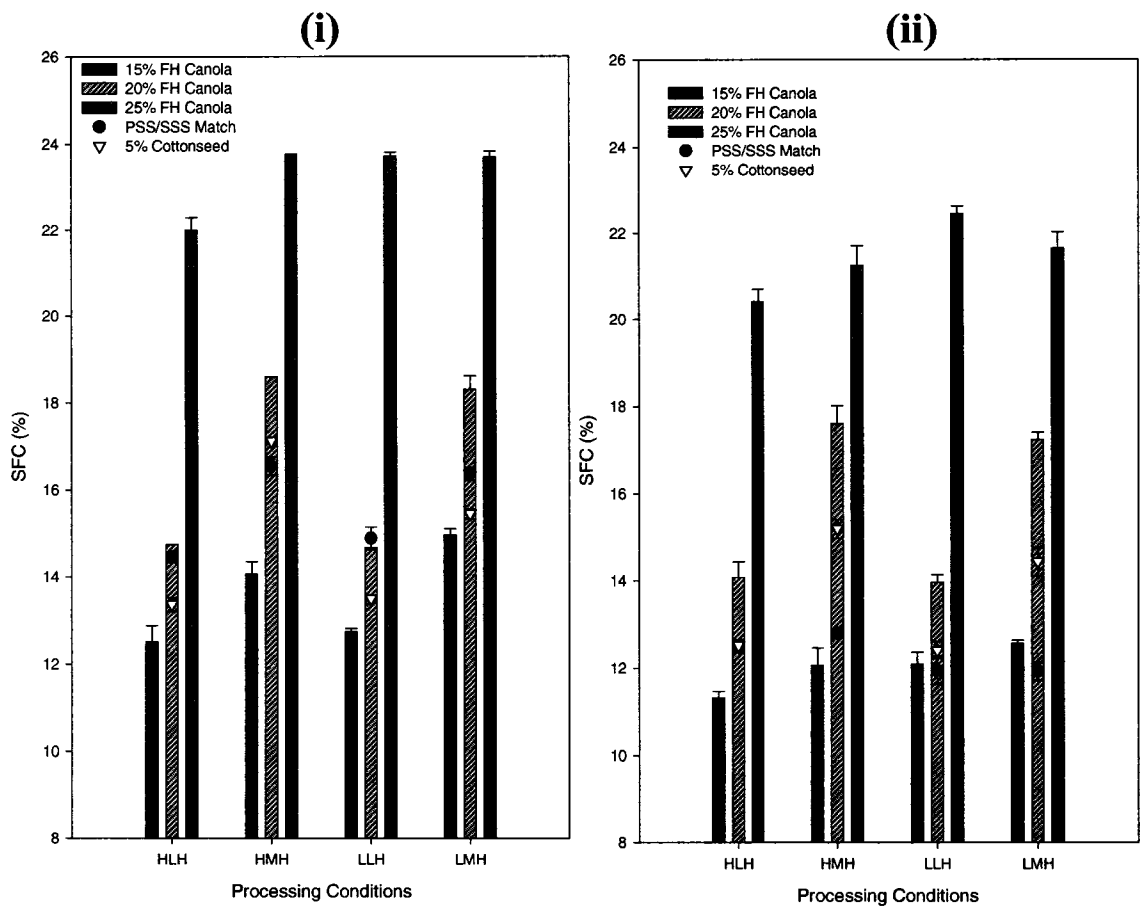


Figure 5.5b: SFC of the shortening samples after 14 days. The SFC for samples tempered at (i) 70 °F and (ii) 85 °F is shown. The vertical bars represent the SFC of the shortening samples with No Added PSS, the white triangles represent that of the 5% Cottonseed samples and the black circles represent that of the PSS/SSS Match samples.

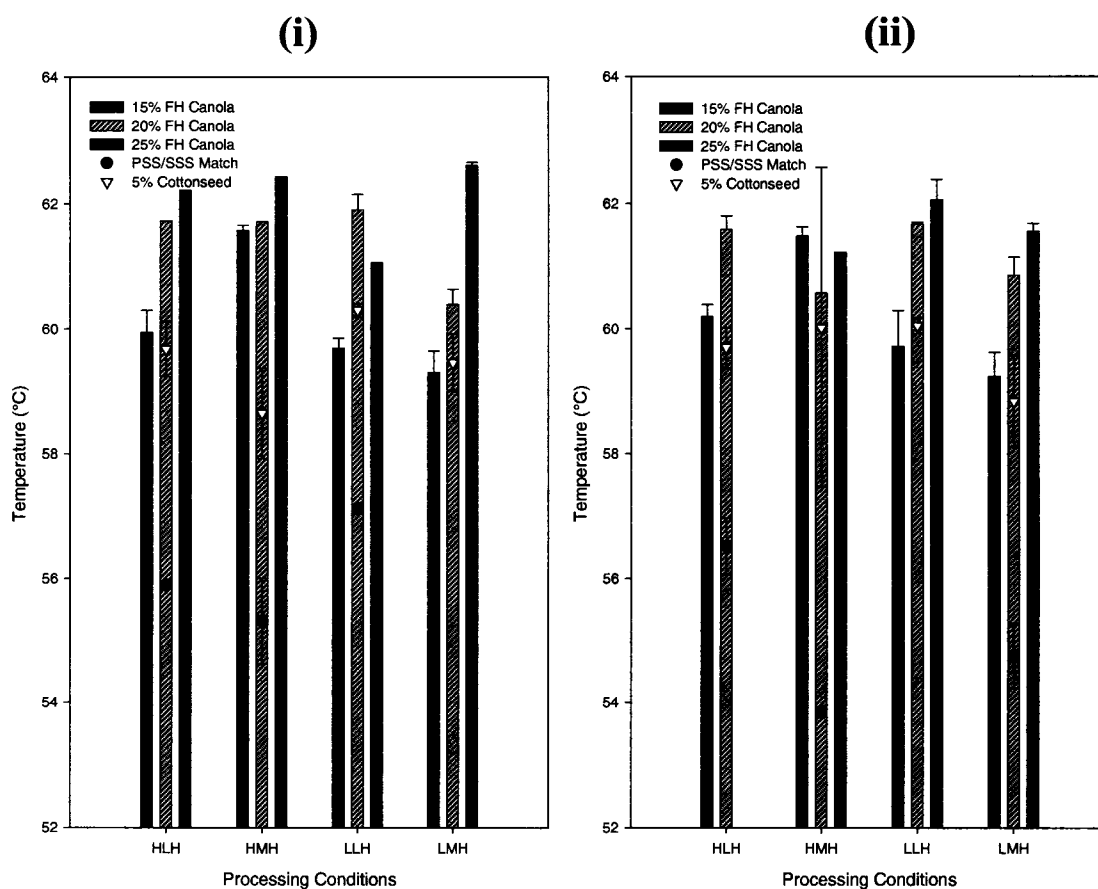


Figure 5.6a: Peak maximum of DSC melting curves after 7 days tempered at 70 °F (i) and 85 °F (ii). The vertical bars represent the melting peak maxima of the shortening samples with No Added PSS, the white triangles represent that of the 5% Cottonseed samples and the black circles represent that of the PSS/SSS Match samples.

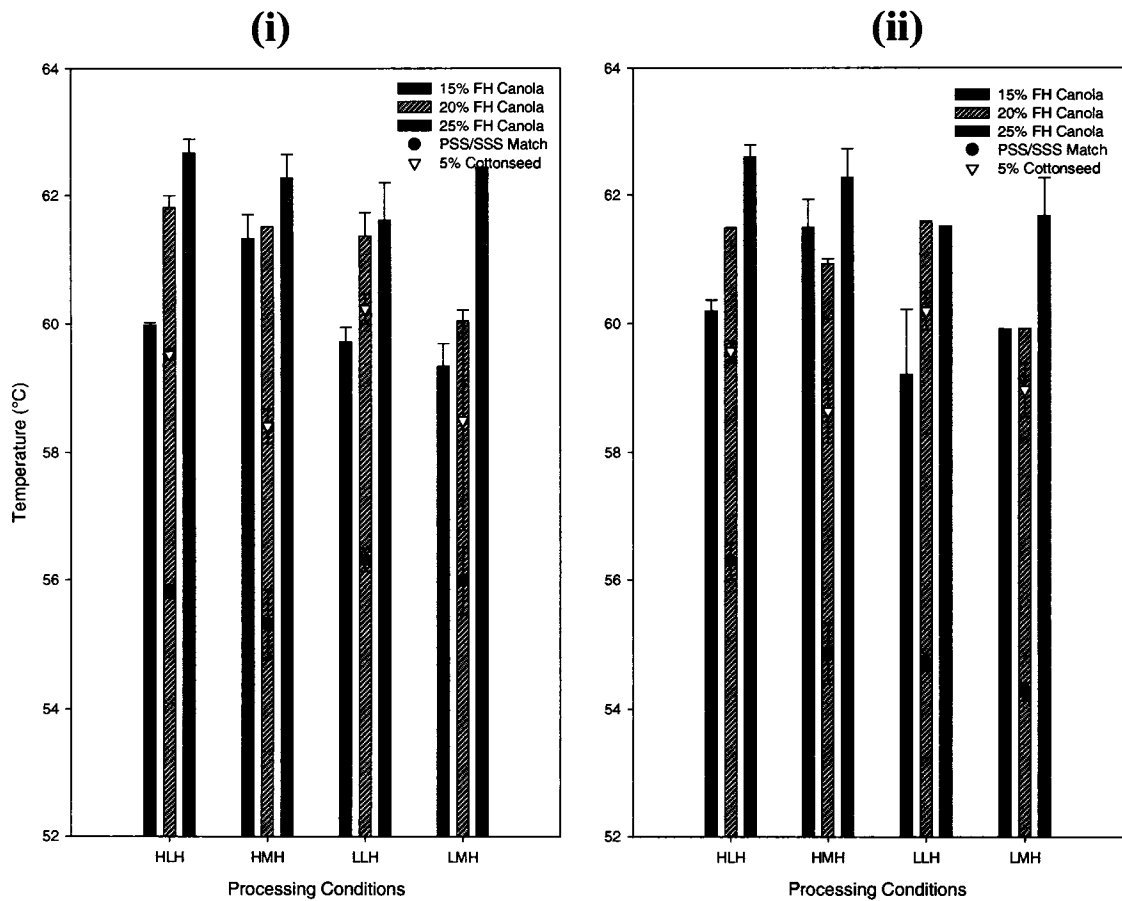


Figure 5.6b: Peak maximum of DSC melting curves after 14 days tempered at 70 °F (i) and 85 °F (ii). The vertical bars represent the melting peak maxima of the shortening samples with No Added PSS, the white triangles represent that of the 5% Cottonseed samples and the black circles represent that of the PSS/SSS Match samples.

bulk of each shortening is the same in all samples (soybean oil), however, the TAG composition of the fully hydrogenated oil(s) that also make up the shortening do differ depending on the sample. Given though that the TAG composition of the fully hydrogenated oils is well known [9-11] it is suggested that the peak maxima of the PSS/SSS Match sample is lower than that of the 5% Cottonseed and No Added PSS samples due to the lowered amount of the high melting TAG SSS present (47% of the total added saturated fat) in the PSS/SSS Match sample (compared with 68-80% for the other samples) [1].

Altering the processing conditions of a set of shortening samples greatly influences the hardness, SFC and melting characteristics of those samples. Clearly, the hardness of the PSS/SSS Match and 5% Cottonseed samples was maximized if the samples, tempered for two days at 85 °F, were crystallized with both a high pump speed and medium fill temperature, or with a low pump speed. This suggests that the advantage of using PSS to enrich shortening samples is not fully utilized if a high pump speed and low fill temperature are used, potentially due to the combined reduction in mass transfer ability due to the steep temperature gradient that this processing parameter combination would result in. Whilst it is also evident that the hardness of the No Added PSS blends at 70 °F temper is equivalent to that of the PSS enriched shortenings at 85 °F temper, the reduction (7.9 and 7.5%) in total added saturates within the PSS enriched shortenings make them a more useful product given current consumer demand for lower saturates, zero *trans* products.

5.3.2 Applications testing of PSS enriched samples

The body of the icing was tested by doing a trench score test and the trench scores for the test icings are shown in Table 5.3. Two of the three control icings (Vreamay NH and Vreamay Right) had trench scores of 4 while the third control icing (Vreamay) had a trench score of 0. With the exception of the test icings containing 5% Cottonseed and the PSS/SSS match each processed with HMH and tempered at 85 °F which had an average (n=2) trench score of 0.5, all other test icings had a trench score of zero. Thus the test icings were not very stable, and thus would not be very useful for creating stable icing based elements (such as roses on cakes, or filling in a sandwich type cookie) without further optimization work.

The specific gravity of the icings was also tested, and typically a low specific gravity is desired in an icing. Each of the control icings had a specific gravity ranging from 0.75 ± 0.02 (for the icing made with Vreamay Right) to 0.79 ± 0.01 (Vreamay) as shown in Table 5.4. The specific gravity of each of the test icings is shown as a function of tempering temperature in Figure 5.7 for the processing conditions (a) HMH, (b) LMH, (c) HLH, and (d) LLH as a function of the tempering. Tempering at 85 °F tends to reduce the specific gravities of the icings made from the 5 shortenings processed with each of the four regimes. There are a few exceptions to this reduction in specific gravity at a higher tempering temperature, and these increases in specific gravity for samples tempered at a higher temperature can be for samples not containing the fully hydrogenated Cottonseed oil and processed at LLH (15% + 0.06, 25% + 0.02), HMH (20% + 0.08), LMH (20% + 0.05), and HLH (25% + 0.08). The specific gravities of all

Table 5.3: Cream icing trench scores

Average Trench (n=2)						
Processing	Temper	PSS/SSS Match	5% Cottonseed	15% Hard Fat	20% Hard Fat	25% Hard Fat
HLH	70	0	0	0	0	0
HLH	85	0	0	0	0	0
HMH	70	0	0	0	0	0
HMH	85	0.5	0.5	0	0	0
LLH	70	0	0	0	0	0
LLH	85	0	0	0	0	0
LMH	70	0	0	0	0	0
LMH	85	2	0	0	0	0
Controls						
				Vreamay	0	
				Vreamay NH	4	
				Vreamay Right	4	

Table 5.4: Specific gravities, slide, and slump values for the control icings

Control Sample	Specific Gravity	Slide	Slump
Vreamay	0.79 ± 0.01	16 ± 3	7.5 ± 0.0
Vreamay Right	0.75 ± 0.02	8 , 42	5.0, 27.5
Vreamay NH	0.76 ± 0.00	19, >50	10.0, 30.0

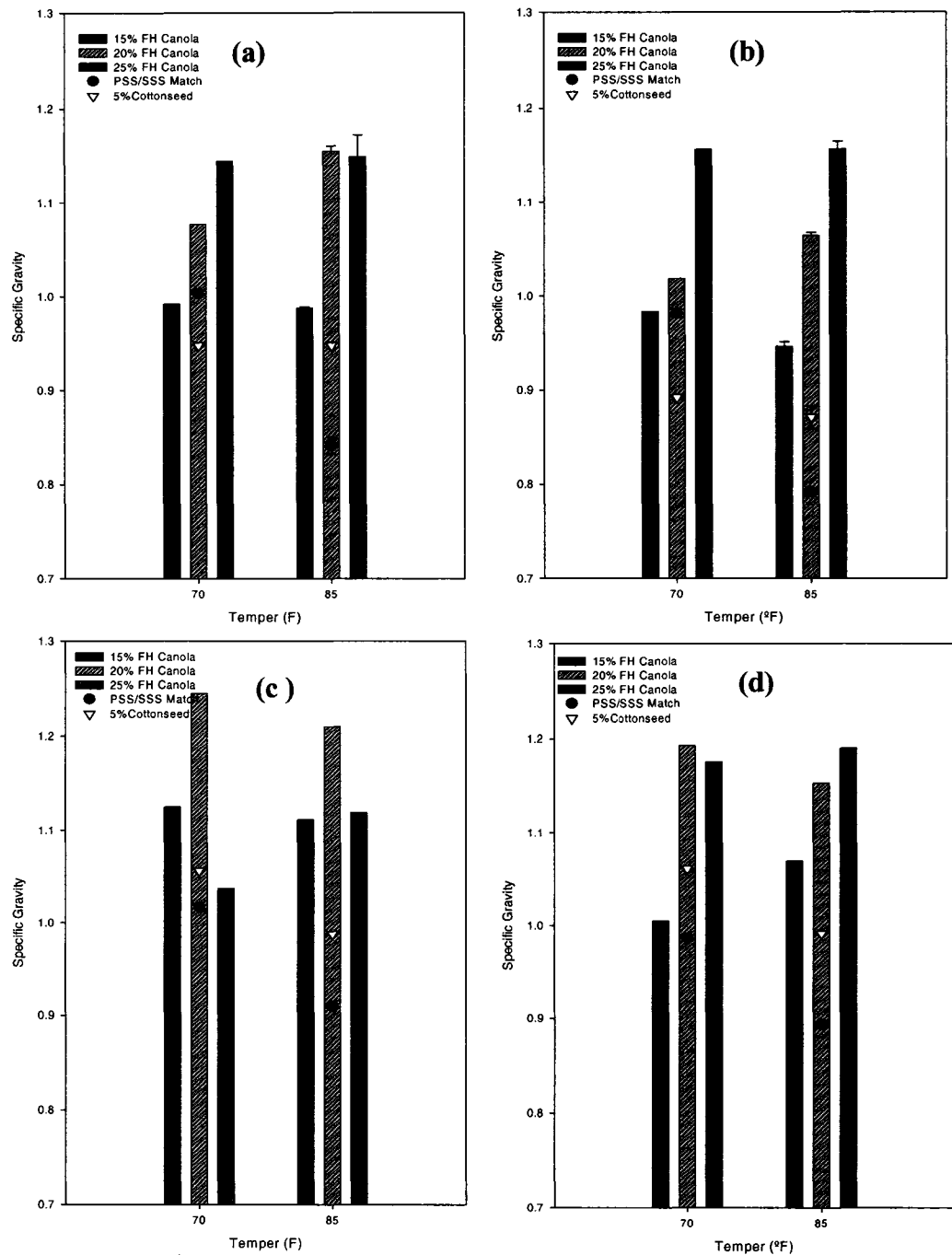


Figure 5.7: Specific gravities of each of the test icings processed with the conditions (a) HMH, (b) LMH, (c) HLH, and (d) LLH. The vertical bars represent the specific gravities of the icings made from the No Added PSS shortenings, the white triangles represent that of the 5% Cottonseed samples and the black circles represent that of the PSS/SSS Match samples.

icings made from the 20 and 25% fully hydrogenated Canola (No Added PSS) shortenings at all processing conditions and tempering are greater than 1.01 with the specific gravities of the 15% sample ranging from 0.94 (LMH 85 °F) to 1.13 (HLH 70 °F). The icing samples made from the 5% Cottonseed shortenings have specific gravity values ranging from 0.87 (LMH 85 °F) to 1.06 (LLH 70 °F). The PSS/SSS Match shortening produced icings with specific gravities ranging from 0.79 (LMH 85 °F) to 1.02 (HLH 70 °F). Clearly, the PSS/SSS Match sample has the lowest specific gravities when used in cream icings, and the specific gravity of the sample processed with LMH and tempered at 85 °F (0.79) is very similar to that of the control Vreamay (0.79 ± 0.01).

The slump test was performed on the icing samples to predict how the icing would stand up in vertical applications (such as on the side of a cake). Typically a slump of less than 30 mm is desired for these applications. The slump scores of each of the test icings are shown in Figure 5.8 for samples tempered at (a) 70 °F and (b) 85 °F with 125 mm being the maximum recordable value. The slump and slide values for the control samples are shown in Table 5.4. The slump scores for the control samples ranged from 5.0 mm to 30.0 mm. The slump values for the test samples tempered at 70 °F range from 70 mm (5% Cottonseed HMH) to >125 mm (5% Cottonseed, PSS/SSS Match, 15 and 20% fully hydrogenated Canola (No Added PSS) each processed at HLH and LLH, and 15% fully hydrogenated Canola processed at HMH). For the icings made from shortenings tempered at 85 °F, the slump values range from 42.5 mm (PSS/SSS Match LMH) to >125 mm (5% Cottonseed, 15 and 20% fully hydrogenated Canola (No Added PSS) each processed at HLH and LLH). This suggests that HMH and LMH processing

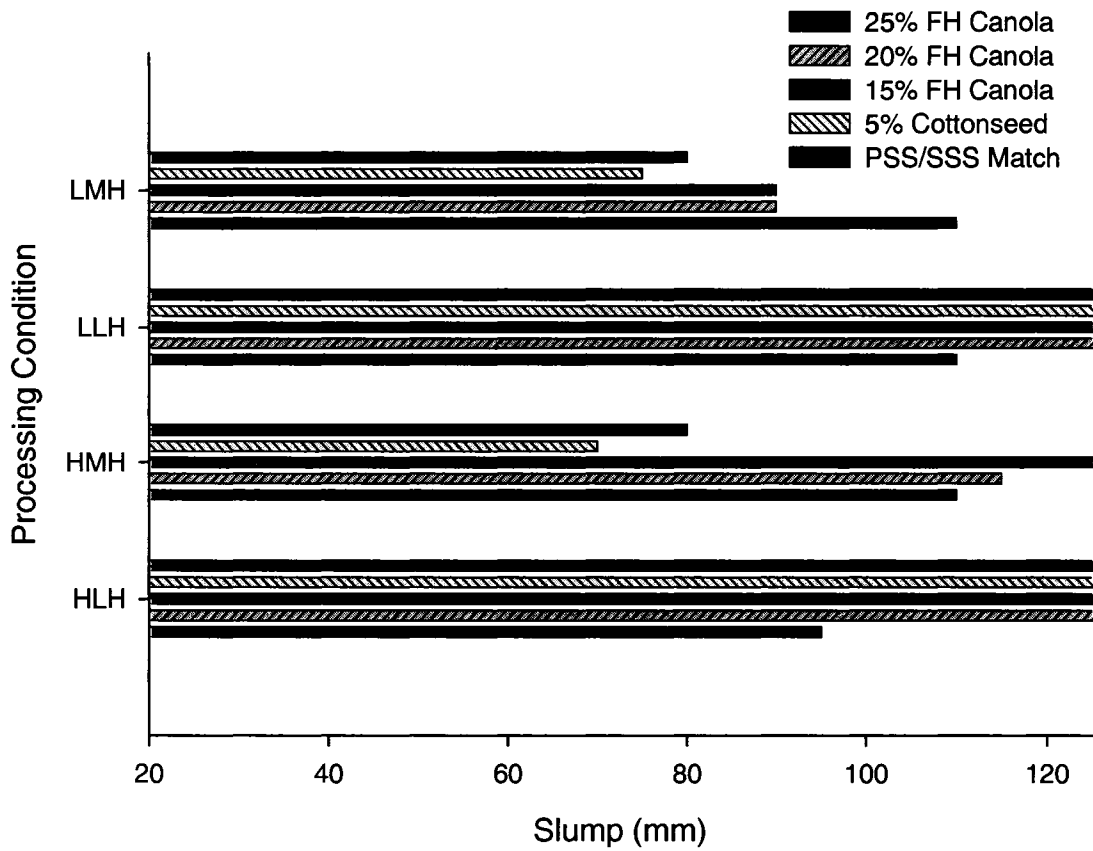


Figure 5.8a: Amount of horizontal slump of each of the test icings made from the shortenings tempered at 70 °F as a function of processing conditions

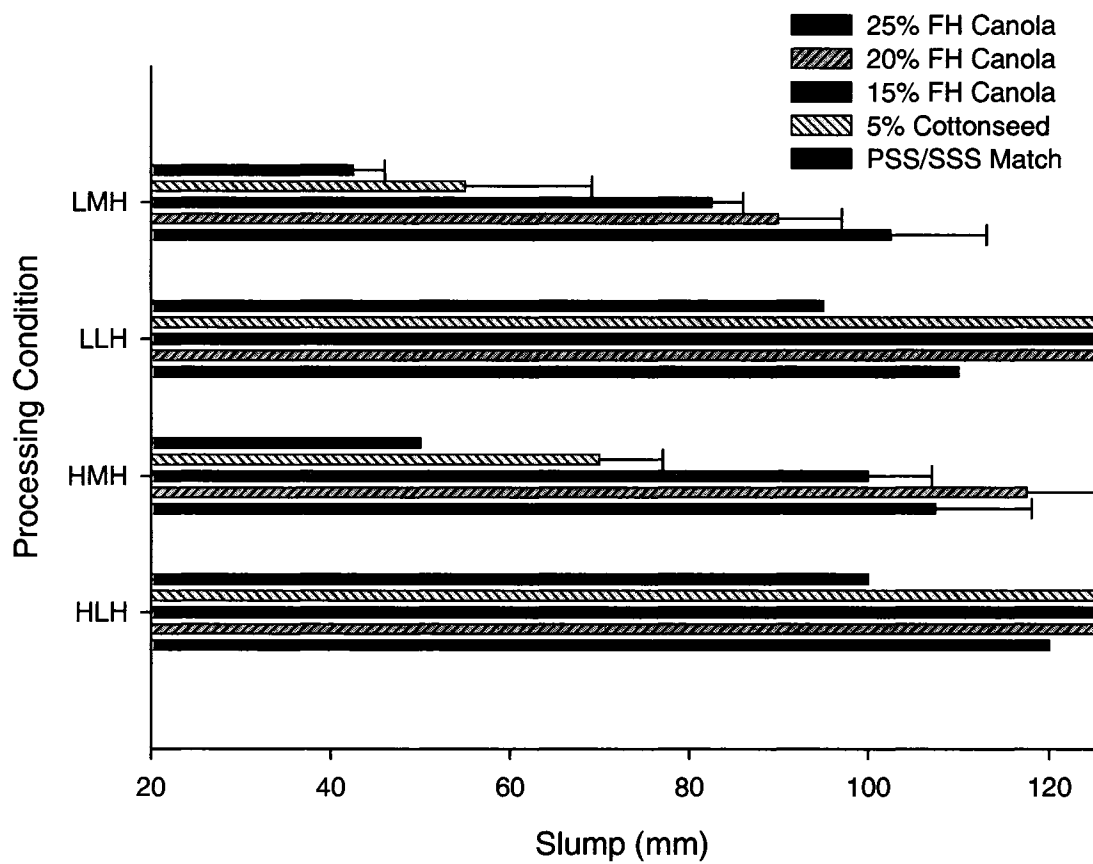


Figure 5.8b: Amount of horizontal slump of each of the test icings made from the shortenings tempered at 85 °F as a function of processing conditions

regimes are more beneficial to reducing the slump in the cream icing and while there is not much change in the Canola/soybean binary shortenings, the performance of the PSS/SSS Match and 5% Cottonseed shortenings can be affected by the processing scheme chosen at both tempering regimes. However, it was shown in Figure 5.7, for 70 °F tempering, that the HMH and LMH processing of the PSS/SSS Match sample resulted in a cream icing with a higher specific gravity than that obtained via the HLH and LLH processing regimes. This is counter intuitive, as one would expect a light and airy icing (with a low specific gravity) to resist slump in a vertical application, but it was shown in Figure 5.8, when comparing with Figure 5.7 between processing schemes that this is not the case. However, if one compares the specific gravities and slump values between tempering regimes, the results are as expected. For the 85 °F tempering, the specific gravities (Figures 5.6a, 5.6b, 5.6c, and 5.6d) of the PSS/SSS Match sample were found to be lower than that at 70 °F, and these cream icings do slump less in vertical applications than their 70 °F counterparts (Figures 5.7a, and 5.7b).

The slide values for the control samples range from 8 mm to greater than 50 mm, the test samples all reported slide values of greater than 50 mm, and are thus not shown as they ran beyond the scale of the apparatus. The slide test on the control samples did not prove to be reproducible as slide values of 8 mm and 42 mm were found for Vreamay Right, and 19 mm and >50 mm were found for Vreamay NH.

It was also observed that the PSS/SSS Match samples also tended to slide within the apparatus in the same manner as the control samples (the icing pulled away from the

apparatus, and even held a rectangular shape at the top while it was sliding, whilst the 5% Cottonseed and the three No Added PSS blends tended to coat the vertical apparatus box while sliding) even though their slump and slide scores were much higher than the control.

Each of the sample icings was stored in the lab for one week, and was then visually observed at both the top of the container, and the bottom of the container based on the “homogeneity” and “airiness” of the icings. These observations are summarized in Table 5.5. While the control samples maintained their homogeneity and airiness on the top and bottom of the icing container, very few test samples did the same. The 25% fully hydrogenated Canola sample tended to separate into oil and water phases at the top of the container whilst maintaining an airy consistency. The PSS/SSS Match sample processed at LMH with tempering at 85 °F was the only sample which maintained an airy consistency and did not separate.

Figure 5.4 showed that the PSS/SSS Match shortenings processed with HMH, LMH, and LLH and each tempered at 85 °F had similar hardness measurements. While the specific gravities (Figure 5.7) of the icings made from these shortenings are similar, the trench scores (Table 5.3) and slide and slump values for the shortenings with of different processing conditions are quite different (Figure 5.8). Clearly, shortening hardness is not an accurate predictor of shortening performance in cream icings with respect to trench score, specific gravity, slump-slide measurements, and stability over time. However, lower SFC values of the shortening (Figure 5.5) tended to result in lower

Table 5.5: Visual observations of the icings after one week

Sample	Processing Condition	Top		Bottom	
		Homogenous	Airy	Homogenous	Airy
PSS/ SSS Match	HLH 70	X			
	HLH 85		X		
	HMH 70		X	X	X
	HMH 85	X		X	X
	LLH 70				
	LLH 85		X		X
	LMH 70		X		X
	LMH 85	X	X	X	X
5% Cotton- seed	HLH 70				
	HLH 85				
	HMH 70				
	HMH 85				
	LLH 70				
	LLH 85				
	LMH 70				
	LMH 85		X	X	
15% FHC	HLH 70				
	HLH 85				
	HMH 70				
	HMH 85				X
	LLH 70		X		
	LLH 85		X		X
	LMH 70		X		X
	LMH 85	X			X
20% FHC	HLH 70				
	HLH 85				
	HMH 70		X		X
	HMH 85		X		X
	LLH 70				
	LLH 85				
	LMH 70		X		X
	LMH 85		X		X
25% FHC	HLH 70		X		X
	HLH 85		X		X
	HMH 70		X		X
	HMH 85		X	X	X
	LLH 70		X	X	X
	LLH 85		X	X	X
	LMH 70		X	X	X
	LMH 85		X	X	X
	Vreamay	X	X	X	X
Vreamay Right	X	X	X	X	
Vreamay NH	X	X	X	X	

specific gravities of the cream icing (Figure 5.7) as seen for the PSS/SSS Match sample with processing LLH at 85 °F, and with similar trends for all other sample types. The melting point of the shortening sample might be predictive of the icing performance as the PSS/SSS Match shortening processed at HMH and tempered at 85 °F was one of the hardest shortenings measured, had a low melting peak maximum (Figure 5.6) and was the shortening which produced the best performing cream icings. The same trends are also evident for the PSS/SSS Match shortening processed at LMH and tempered at 85 °F. The binary shortening types tended to have much higher melting points, SFC and were softer than the PSS/SSS Match sample. The specific gravities of the icings made with these shortenings tended to be much higher than 1, and did not perform well in the trench test, and in maintaining homogeneity over time.

Clearly, the test icings did not match up with the control icings produced in this study. It has been suggested that further optimization work (such as the careful selection of an emulsifier to complement the shortening as well as the application), one might be able to produce an icing with the functionality of the control icings produced in this application testing. However, it has become apparent that the shortenings processed by HMH and LMH and tempered at 85 °F have the greatest potential as a functional shortening for icings, and the PSS/SSS Match samples having the lowest specific gravities, some non-zero trench scores, and were observed to slump and slide in the same manner as the control samples. The one week observations of the PSS/SSS Match samples processed by HMH and LMH and tempered at 85 °F are also promising,

suggesting that an airy icing after one week may be possible with this shortening formulation.

5.4 Conclusions

Clearly the modification of a canola based shortening system with added PSS as a component of fully hydrogenated cottonseed aids in increasing hardness of a shortening sample whilst limiting the added saturates at the pilot plant scale in addition to the lab scale as discussed in Chapter 4. PSS/SSS Match shortenings tempered at 85 °F were up to twice as hard as the No Added PSS shortenings processed in the same manner even with a reduction in saturates in the enriched samples of 8%. The modification of the canola based shortenings also lowered the melting points of the shortenings regardless of tempering, but did not greatly influence the SFC of the final crystal network as a function of the total added saturates. Tempering however did affect the performance of the PSS/SSS Match shortenings with higher tempered shortenings being more functional as a component of cream icings while the functionality of the No Added PSS and the 5% Cottonseed samples were not greatly affected by the tempering scheme. Therefore, the incorporation of PSS into a canola based shortening sample at a preferred ratio of $x = 0.83$, in addition to the use of preferential crystallizer and tempering variables results in a zero trans, reduced saturates shortening with the same functionality of that with 8% more saturates.

5.5 References

1. Humphrey, K. and S. Narine, *Decreasing Trans and Saturated Fatty Acids: A New Generation of Shortenings - The PSS Study - Lab Scale*. 2007 (to be submitted): p. 29.
2. *Standard Methods for the Analysis of Oils, Fats, and Derivatives*, in *International Union of Pure and Applied Sciences*. 1979.
3. *Solid Content Determination in Fats by Low Resolution Nuclear Magnetic Resonance v. 2.150*, in *International Union of Pure and Applied Sciences*. 1987.
4. *Determination of Solid Fat Content by Pulsed NMR Method*, in *International Standard, Animal and Vegetable Fats and Oils*. 1991.
5. *AOCS Method Cd 16b-93*, in *Official and tentative methods of the American Oil Chemists' Society*, W.E. Link, Editor. 1998, AOCS Press: Champaign, IL.
6. Humphrey, K.L., P.H.L. Moquin, and S.S. Narine, *Phase behavior of a binary lipid shortening system: From molecules to rheology*. *Journal of the American Oil Chemists Society*, 2003. **80**(12): p. 1175-1182.
7. Narine, S.S. and K.L. Humphrey, *A comparison of lipid shortening functionality as a function of molecular ensemble and shear: microstructure, polymorphism, solid fat content and texture*. *Food Research International*, 2004. **37**(1): p. 28-38.

8. Widlak, N.R., *Formulation and Production of Fluid Shortenings*. Proceedings of the World Conference on Oilseed Processing Utilization, 2001. **2001**(2000): p. 39-43.
9. Przybylski, R. *Canola Oil: Physical and Chemical Properties*. 2004 [cited 2007 May 30, 2007]; Available from: <http://www.canola-council.org/pubs/oilkit.html>.
10. Neff, W.E., G.R. List, and W.C. Byrdwell, *Effect of Triacylglycerol Composition on Functionality of Margarine Basestocks*. *Lebensm.-Wiss. u.-Technol.*, 1999. **32**: p. 416-424.
11. Humphrey, K.L. and S.S. Narine, *A comparison of lipid shortening functionality as a function of molecular ensemble and shear: Crystallization and melting*. *Food Research International*, 2004. **37**(1): p. 11-27.

6. Conclusions

6.1 General Discussion

As *trans* fats and saturated fat have been shown to be detrimental to human health the shortenings industry is challenged with the task of removing *trans* fats, whilst simultaneously controlling the level of saturated fat in an edible oil product [1]. Clearly, shortening products are affected by their composition, crystallization, and tempering conditions [2]. Removing *trans* fats and reducing saturated fat from a shortenings product is not a trivial problem. *Trans* fats, due in part to their higher melting temperatures, contribute to the hardness promoting structure within a fat crystal network [3]. Therefore, when designing a shortening blend without *trans* fats and decreases in saturated fat, one must find alternative ways of building a structural network which uses less of both of these problematic materials. The use of structural enhancers such as PSS has been shown in this work to be of immense value in building such networks.

Through the use of comprehensive studies (Chapters 3 and 4), possible structure enhancing components of common fully hydrogenated vegetable oil were identified. These structure enhancers, blends of PSS and SSS, were utilized in the production of a canola based shortening system with no added *trans* fats, and up to 10% less saturates than a shortening of comparable hardness. The functionality of this “new generation” shortening was enhanced by careful processing at the pilot plant scale and was found to be acceptable for use in cream icings, particularly by enhancing with emulsifiers.

6.2 Future Prospects

This thesis contains more than the design for the formulation for a single shortening. Rather this work provides the framework for utilizing all the TAGs in fully hydrogenated vegetable oils to promote the required crystal structure. Four TAGs also identified in Chapters 3 and 4, aside from PSS, interact with SSS in a shortening system (Table 6.1). Preliminary studies on a canola based shortening enriched with pure PPS and PSP have yielded promising results with respect to relative hardness (Figure 6.1). Furthermore, enriching a shortening sample with PSP as a component of fully hydrogenated palm has also been shown to increase the hardness of a canola based shortening considerably more than the carefully blended hard canola and cottonseed discussed in Chapters 4 and 5 (Figure 6.2). This suggests that there is promise in further lowering the level of saturates within a shortening system whilst preserving the hardness of the crystal network. Due to the TAG profiles of fully hydrogenated canola, soybean, palm and cottonseed oils, only the PSP/SSS and PSS/SSS TAG combinations are attainable without interesterifying fully hydrogenated feedstocks to increase the levels of PPS, SPS and PPP within the blend. The most promising aspect is that *trans* free shortenings can be designed utilizing common shortening feedstocks: fully hydrogenated canola, cottonseed, palm and soybean oils.

Furthermore it is clear from the hardness data shown in Figure 6.1 that enriching the shortening samples with PPS or its symmetric isomer PSP rather than PSS increases its hardness. Thus it is suggested that TAGs containing two palmitic (and one stearic)

Table 6.1: TAG profiles of fully hydrogenated vegetable oils (% w/w)

	SSS	PSS	PSP	PPS	SPS	PPP
Canola	80.0	16.1	0.5	0.5	0.2	~0
Cottonseed	39.3	43.8	~0	10.3	1.8	~0
Palm	9.5	40.9	38.5	1.0	~0	5.4
Soybean	67.9	26.8	2.5	0.7	2.0	0.1

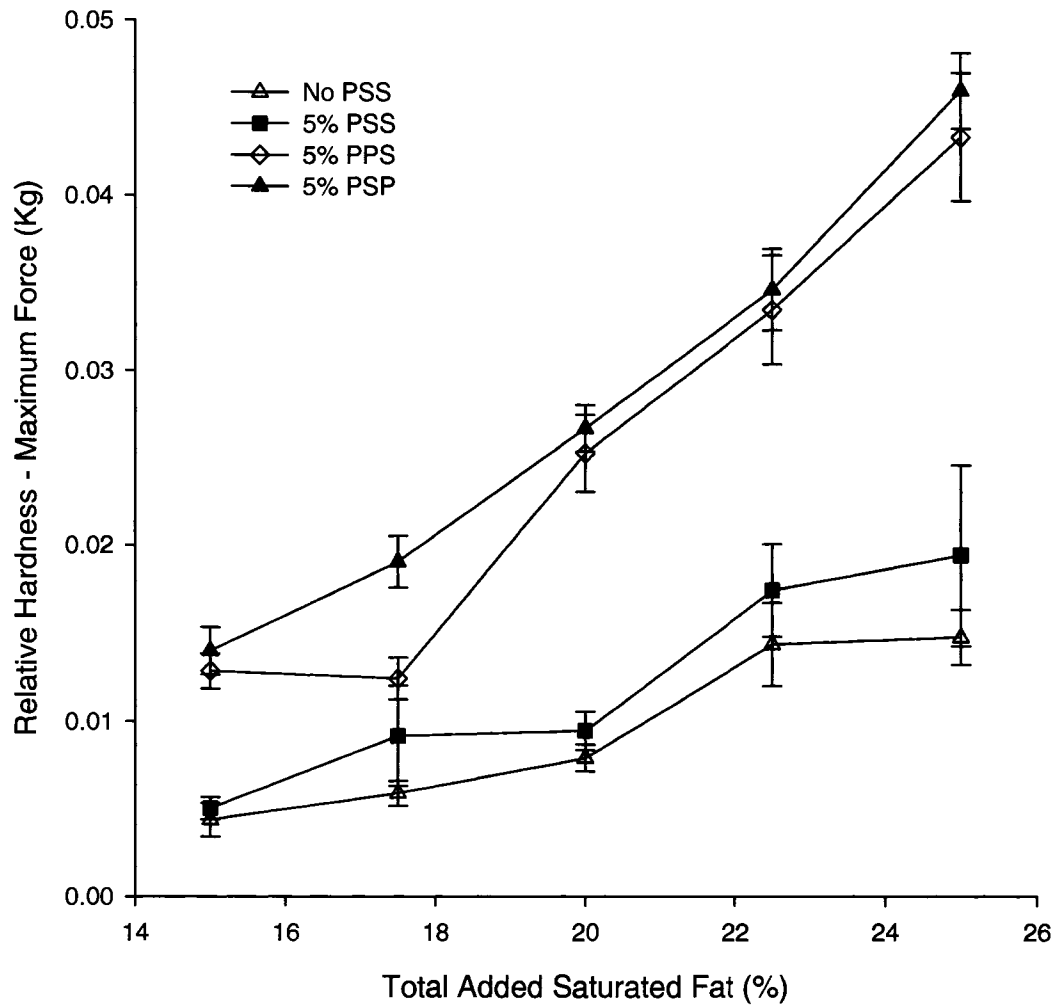


Figure 6.1: Hardness of samples enriched with pure PSS, PSP, and PPS as a function of total added saturates

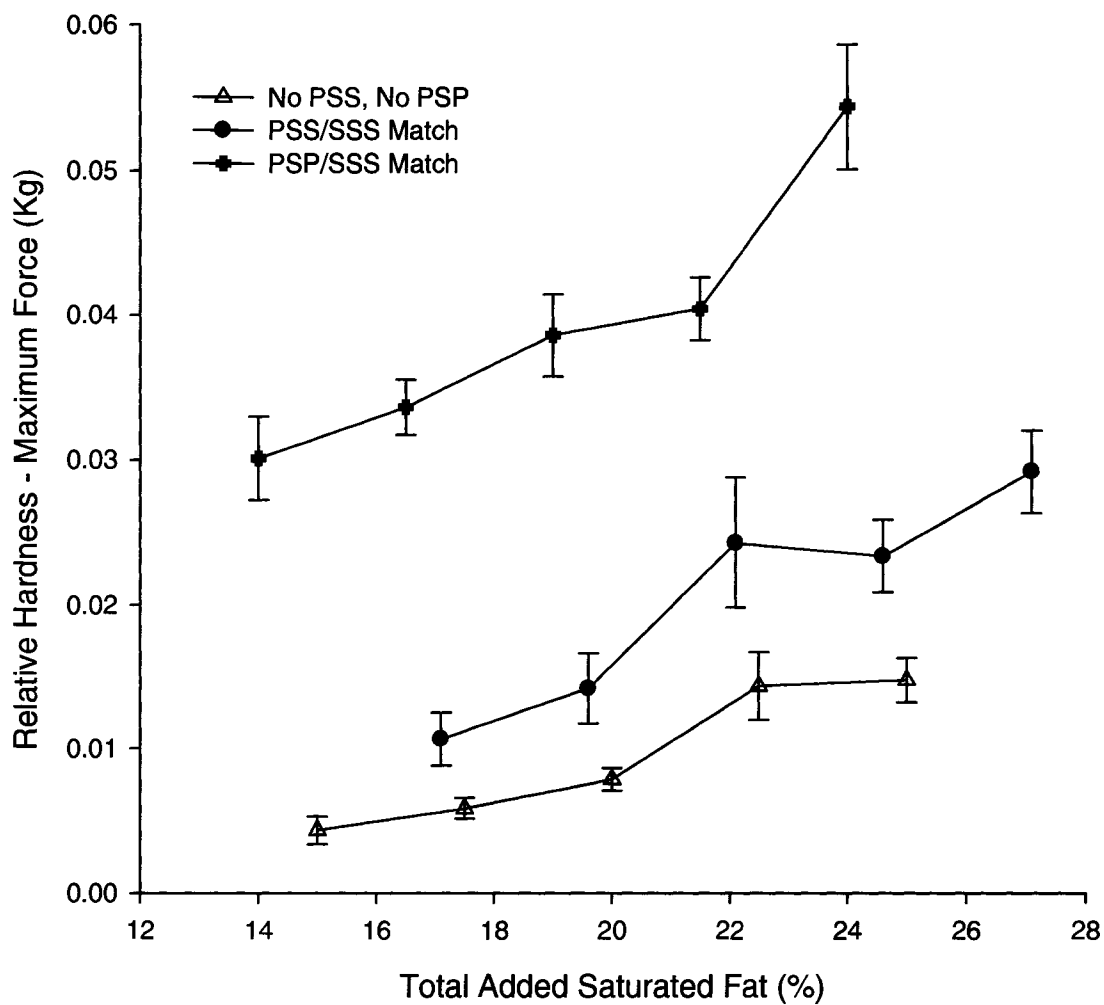


Figure 6.2: Hardness of samples enriched with PSS, and PSP as components of cottonseed and palm oil respectively

acids may interact with SSS to form a considerably harder fat crystal network than that created by TAGs with only one palmitic acid. It is further hypothesized for positional isomers that the presence of a stearic acid in the *sn*-2 position on the enriching TAG might result in a slightly harder shortening than enriching with a TAG with palmitic acid in the *sn*-2 position, although the investigation of SPS enriched samples is necessary to justify this prediction. Clearly, there is a preponderance of TAGs in fully hydrogenated vegetable oils with stearic acid, not palmitic acid in the *sn*-2 position (Table 6.1). Thus, longer chain fatty acid (stearic) is preferentially placed in the *sn*-2 position frequently. TAGs with stearic acid in the *sn*-2 position are harder than those with palmitic acid in the *sn*-2 position, then the availability of these TAGs occurring in fully hydrogenated vegetable fats promises to ensure readily available hardstock for the most efficient hardness promoting structure enhancers within the fat crystal network.

6.3 General Discussion and Conclusions

Chapters 2 and 3 demonstrated the effect of altering sample composition utilizing a range of readily available fully hydrogenated fats, and the effect of shear on the crystal network developed [4-6].

Utilizing the variations in composition of a shortening blend, a structure enhancer based on the relative amounts of SSS and PSS within a shortening blend, was proposed in Chapter 4. It was found that through carefully blending of common shortening feedstocks, one can achieve predetermined ratios of specific TAGs within a complex shortening blend. Enriching samples in this way, and through the use of highly valuable

pure TAGs, resulted in the formation of a crystal network lower in saturates and *trans* than a binary shortening blend of comparable relative hardness.

Furthermore, the carefully blended shortening was also found to maintain hardness when produced on the pilot plant scale, as shown in Chapter 5. The effect of the structure enhancing TAG ratio in the carefully blended shortening could be further enhanced by altering the fill temperature, and pump speed of the scraped surface heat exchanger. The effect of tempering on the shortening blend was also determined and it was found that storage at higher temperatures (85 °F) was advantageous in the formation of the fat crystal network.

In Chapter 5, we also discussed the functionality of the shortenings, produced at the pilot plant scale, in a cream icing product. Whilst the icings made with the carefully blended shortenings did not demonstrate the same amount of plastic deformation or flow as the control samples, the icings made with the shortening with the preferred TAG ratio were found to perform better than the binary shortening counterparts.

The formation of a hard crystal network in a shortening, made of canola/cottonseed hardstock, with zero *trans* and lowered total added saturates, is a suitable solution for the removal of *trans* fatty acids as it does not require expensive or difficult to manage hydrogenation schemes [3]. As well, the proposed formulation utilizes current shortening feedstock and processing equipment thereby aiding in the immediate usefulness to the shortenings industry. Additionally, the basis of the

shortening formulation being on TAGs, the altering of the blend based solely on matching TAG profiles of the shortening formulation proposed (in Chapter 4) without numerous trial and error attempts is possible.

In conclusion, the TAG profiles of commonly used vegetable oil hardstock for shortening manufacture may be utilized through the use of blending, along with carefully selected processing and tempering conditions, to produce vegetable shortenings with zero *trans*, lowered saturates and all the functionality of a canola based product. The shortening product developed, was found to be comparable to the binary blend of fully hydrogenated canola in soybean base oil with respect to the polymorphism, solid fat content, melting profile, and microstructure. Additional work in our laboratory is underway to determine the contribution of each TAG to the final crystal network through the use of phase behavior studies on the pure TAGs. The current study provides one formulation for a low saturates, zero *trans* shortening.

6.4 References

1. Canada, H. *TRANSforming the Food Supply*. 2006 [cited 2007 February 7, 2007]; Available from: http://www.hc-sc.gc.ca/fn-an/nutrition/gras-trans-fats/tf-ge/tf-gt_rep-rap_e.html.
2. Ghotra, B.S., S.D. Dyal, and S.S. Narine, *Lipid shortenings: a review*. Food Research International, 2002. **35**(10): p. 1015-1048.
3. Higgins, N.W., *Low Trans-Stereoisomer Shortening Systems*, U.S.P.a.T. Office, Editor. 2004: USA. p. 12.
4. Humphrey, K. and S. Narine, *Diminishing marginal utility of cooling rate increase on the crystallization behavior and physical properties of a lipid sample*. Journal of the American Oil Chemists' Society, 2007. **84**: p. 709-716.
5. Humphrey, K.L. and S.S. Narine, *A comparison of lipid shortening functionality as a function of molecular ensemble and shear: Crystallization and melting*. Food Research International, 2004. **37**(1): p. 11-27.
6. Narine, S.S. and K.L. Humphrey, *A comparison of lipid shortening functionality as a function of molecular ensemble and shear: microstructure, polymorphism, solid fat content and texture*. Food Research International, 2004. **37**(1): p. 28-38.

A1. Phase Behavior of a Binary Lipid Shortening System

A1.1 Introduction

A phase is a domain, homogenous with respect to chemical composition and physical state [1]. A natural fat is an example of a system of coexisting homogeneous domains in equilibrium. The relationship and occurrence of phase change in a fat system is referred to as the phase behavior of the fat. Phase behavior, obtained through the study of the solid fat content (SFC), is important in optimizing production processes and maintaining production quality, and has been used to predict important attributes such as mouth-feel and hardness in fat-containing food products. Studies on phase behavior also help to gain a better understanding of the ways in which fat blends interact; an important understanding as the large scale industrial production of shortenings, and other fat-containing products often require blending of lipids from many different sources.

Phase behavior as observed from iso-solid lines is important in illustrating some aspects of inter-solubility behavior, but is ultimately limited in scope. In many instances, iso-solid line behavior may not indicate changes in polymorphism of the samples and certainly does not impart information beyond the prediction of hardness by SFC, a method that has been shown to be imperfect [2-4]. On the other hand, DSC phase measurements can reflect changes in polymorphism as well as intersolubility. However,

A version of this chapter has been published.

Humphrey, K.L., P.H.L. Moquin, and S.S. Narine, Phase behavior of a binary lipid shortening system: From molecules to rheology. *Journal of the American Oil Chemists Society*, 2003. 80(12): p. 1175-1182.

257

such changes are not attributable to either polymorphic or inter-solubility effects in isolation utilizing purely DSC data. Therefore, it is important to study phase behavior using a number of different techniques such as X-Ray Diffraction [5], microstructure analysis, GC, and cone penetrometry.

The fat systems used in this study are mixtures of fully hydrogenated canola and soybean oils. These two lipids were selected for study as they form a solution which was yet to be studied, and the oils provided a good complement of TAGs. Due to the large supply of canola and soybean oils in North America, the oils are easily obtainable and economical. Furthermore, there is a potential demand for the use of hard canola in soybean oil as shortening due to the low *trans*-fatty acid content which would comprise a healthier consumer product.

The purpose of this study is to establish a relationship between phase behavior, structural network and mechanical properties of the canola-soybean lipid system, and to provide methodology to study similar shortening systems.

A1.1 Experimental Procedures

When referring to sample holding temperature as well as cooling and heating rates all temperatures are reported to a certainty of ± 0.5 °C.

A1.1.1 *Sample Preparation*

Fully hydrogenated canola was mixed with non-hydrogenated soybean oil at concentrations ranging from 0 to 100% (w/w) canola in 5% increments. Jars containing fat mixtures were tightly covered and stored at -5 °C to minimize auto-oxidation. Each fat mixture was completely melted to 90 °C before being stirred for 2 minutes using a motorized mechanical stirrer. Three samples of approximately equal mass were prepared for each measurement technique. The samples were tempered by equilibrating the sample at 90 °C for 5 minutes and then cooling to 15 °C at a rate of 10 °C per minute. The samples were stored at 15 °C and all instruments were temperature controlled at 15 °C. The XRD tubes were filled with sample from the Instron pans 48 hours after tempering.

A1.1.2 NMR Measurements

The instrument used in the investigations was the ‘minispec mq SFC analyzer’, which is a pulse magnetic resonance spectrometer with a temperature controlled measurement chamber. The data sampling procedure was fully automated, and the solid fat content (SFC) was calculated and displayed by computer software [6-9].

A1.1.2.a SFC Determination

The samples were placed into a 15 °C bath for 15 minutes. Sample tubes were inserted into the NMR probe. After the SFC measurement the sample tube was replaced into the 15 °C bath. This was repeated for all the other sample tubes and then the temperature of the bath containing the samples was increased by 5 °C and equilibrated for

15 minutes. Like-wise, the SFC for all sample tubes was measured for temperatures ranging from 25 to 70 °C. The samples were then re-tempered as described above. The SFC measurement was repeated, this time decreasing the temperature in 5 °C increments from 15 °C to 0 °C.

A1.1.2.b SFC Analysis

Obtained SFCs were used to construct iso-solid diagrams in three different ways. The first method consisted in plotting the average of the actual results using a method outlined by Rossell [10] to construct iso-dilatation diagrams. The second method consisted of using a quadratic interpolation [11]. The SFC was plotted versus temperature for each concentration in the third method. This graph was then interpolated for temperature for a given SFC using the “GraphPad - Prism” software and a multiple line graph of temperature versus composition was made, where each line represented one SFC value [12]. The interpolation graph is presented.

A1.1.2.c Crystallization Onset Measurement

The SFC of each NMR tube was measured for 7 minutes during which time the sample was tempered as described above using a cooling system which allowed the temperature within the chamber to be decreased or increased at specific rates. This apparatus is described in a letter submitted to the editor of the Journal of the American Oil Chemists Society by Narine and Humphrey [13]. The time at which the SFC increased above 1% was recorded as the onset of crystallization.

A1.1.3 DSC Measurements, Thermal Behavior

The instrument used in the investigations was the “DSC 2920 Modulated DSC” by TA Instruments. The data sampling and temperature control procedures were fully automated and controlled by the “TA Instrument Control” software program, and the output spectra were analyzed with the “TA Universal Analysis” software to find the peak maximum of crystallization and melting, as well as respective enthalpies. All samples were normalized to a uniform sample mass of 15 grams.

A1.1.3.a Tempering DSC Samples

The prepared pans were processed twice, once for crystallization and immediate melting of the sample, and the second was crystallization for the purpose of melting after 48 hours. To obtain the crystallization curve, the sample was tempered as described above. To obtain the melting curve, the sample was equilibrated for 2 minutes at 15 °C prior to increasing the temperature to 90 °C at 10 °C per minute. The melting procedure was repeated after 48 hours and again after 7 days.

A1.1.4 Relative Hardness Measurements

The instrument used in the investigation was the ‘Instron 4201’. The software package “Instron Series IX Automated Materials Tester V. 7” controlled the instrument. A 5.00 kg maximum load cell a steel penetration cone of mass $44.962 \pm 0.0001\text{g}$ and angle 31° was applied to a penetration depth of 8.00 mm. The position of the penetration

cone was software controlled, and it was moved downward at a rate of 120.00 mm per minute with a data sampling rate of 20 points per second.

A1.1.4.a Analysis of Instron Samples

48 hours after tempering, 2 measurements were taken from each pan. The slope of the displacement-force graph produced is an indication of the hardness of the sample.

A1.1.5 XRD Measurements, Polymorphism

The 'Bruker AXS X-ray diffractometer' was used in this study. The procedure was automated and commanded by Bruker's 'General Area Detector Diffraction System V 4.1.08' (GADDs) software with a measurement time of 450 seconds and a maximum display count of 127.

A1.1.6 Microstructure Determination

A high resolution polarized light microscope, equipped with a "Hamamatsu Digital Camera", and a "Linkam LTS 350" was used. The microscope assembly was controlled by "Openlab 3.0.8" software. Pictures were taken 15 minutes, 48 hours and again 7 days after tempering.

A1.2 Results and Discussion

All of the studied samples are solutions of many different TAGs. These TAGs are in motion within the sample; this motion is affected by the limitations due to heat transfer and the viscosity of the sample, and the limits to molecular diffusivity due to conformation of the molecule. The interaction between the TAGs depends on the TAGs present in the solution and the conformation of growing surfaces. If certain molecules are in the required orientation and concentration, and if there is an external driving force applied to the system, then the molecules will associate to form an embryo. The driving force may be an increase in pressure or the concentration of the species leading to supersaturation, or it may be a decrease in temperature causing supercooling to occur within the system. If the embryo increases to the critical size from which growth will continue spontaneously without the continuous application of a driving force, then nucleation has occurred.

A nucleus of critical size will possess attributes of a particular polymorphic or polytypic form. The polymorphism of a sample refers to the packing arrangement assumed by the molecules within the crystals. The alpha polymorphic form has the lowest thermodynamic stability, but the potential to mature into the more stable beta prime, or beta forms [14]. The formed nuclei will grow to form crystallites at the sub micrometer level. The continued formation and growth of these crystals, as well as the development of the microstructure of the system, requires molecules to move towards the structure at the same time as the heat of fusion disperses from the structure. As a greater percentage of the sample crystallizes, the movement of mass throughout the system is

slowed due to the increase in viscosity caused by the lack of free material within which a molecule can flow. The flow of heat will also be reduced due to a lack of liquid oil to conduct it away from the structure. In the case where heat is not conducted away from the structure, melting may occur. Under similar constraints, the crystallites continue to aggregate under heat and mass transfer limitations and form micro-structural elements (1-10 μm), and further aggregation of such elements result in the formation of microstructures (50-140 μm) [15]. The growth mode of the final structure is the collection of decisions that the structures make which produce the final network.

Crystallization is the growth and aggregation of the nuclei into crystalline structures that can be detected with NMR, PLM, and XRD (among other) methods. After nucleation, it is possible for the molecules to re-enter the melt, the structure to ripen, and polymorphic changes to occur, with the events after nucleation being not necessarily sequential. The total crystallization process affects the SFC of the sample and it is possible for two samples with the same SFC value to possess very different polymorphic forms as well as diverse microstructure. A change in the temperature of the fat will typically cause a change in the SFC value of the fat if the change is within the melting range of the fat. However, Figure A1.5 (*vide infra*) shows that at 60 °C the SFC is less temperature dependent, as it mainly depends on the relative amount of solidified saturated fat fractions from canola, thus a temperature change in this case has relatively little effect on the SFC value of the sample. However, the SFC of a fat sample alone does not impart information on the functional properties of a lipid network and thus this paper undertakes further investigation into these functional properties.

As shown in Table A1.1, the dominant TAG in fully hydrogenated canola (SSS 79.6%) is not the same as the dominant TAG in soybean oil (LLL 12.8%). Thus, as one increases the concentration of canola by 5%, the percentage increase of the assortment of canola-contributed TAGs within the sample is essentially 5%. As there are no common TAGs of significant proportion in both the hard canola and soybean oil, one cannot draw conclusions that relate the concentration of a particular TAG to the specific microstructure assumed by the system or the functional properties it displays. However, as one increases the percentage of canola in the blend, the number of different molecules present in significant proportion decreases as canola has fewer TAGs than soybean oil. Thus as the samples tend to 100% canola, the relative molecular diversity of each sample decreases.

Figure A1.1 shows the crystallization curves of each sample, as determined by DSC. A wider peak in a crystallization curve in Figure A1.1 implies that the final crystals will have grown from a large number of “types” of nuclei as nucleation occurred over a longer time span. A large nucleation window may also point to the existence of an inhibitor to nucleation – be it viscosity of the sample, heat diffusion constraints, or molecular diversity. A more narrow crystallization peak suggests that all crystals within the sample nucleated at approximately the same time. This would suggest the presence of a single type of nuclei which grows into crystals. If the peak width (which indicates the temperature range over which the sample crystallizes), or the enthalpy (which is the total heat released per gram of sample), for all samples is consistently increasing, then

Table A1.1: Relative percentages of the TAGs in soybean oil [16] and fully hydrogenated canola oil [17]

TAG	Soybean Oil	Fully Hydrogenated Canola Oil	TAG	Soybean Oil	Fully Hydrogenated Canola Oil
LLL	12.8		LSL	0.2	
LLLn	3.9		LSO	0.3	
LLnL	1.4		LSP	0.3	
LLnLn	0.4		LSS	0.1	
LLnO	1.7		OLnO	0.5	
LLnP	1.0		OLnP	0.6	
LLnS	0.0		OLnS	0.3	
LLO	15.6		OLO	4.6	
LLP	9.5		OLP	6.0	
LLS	3.7		OLS	2.3	
LnLLn	0.3		OOO	1.6	
LnLnO	0.3		OOP	2.1	
LnLnP	0.1		OOS	0.8	
LnLnS	0.1		OPO	0.2	
LnLO	2.5		OPP	0.3	
LnLP	1.4		OPS	0.1	
LnLS	0.5		OSO	0.1	
LnOL	1.3		OSP	0.1	
LnOLn	0.1		PLnP	0.2	
LnOO	0.8		PLnS	0.1	
LnOP	0.5		PLP	1.7	
LnOS	0.2		PLS	1.3	
LnPL	0.2		POP	0.6	
LnPO	0.1		POS	0.5	
LnPP	0.1		PPL	0.2	
LnSL	0.1		PPP	0.1	negligible
LOL	4.4		PPS	0.1	0.5
LOO	5.3		PSP		0.5
LOP	3.3		PSS		16.3
LOS	1.3		SLS	0.3	
LPL	0.5		SOS	0.1	
LPO	0.7		SPS		0.2
LPS	0.2		SSS		79.6
			Others	0.5	2.9

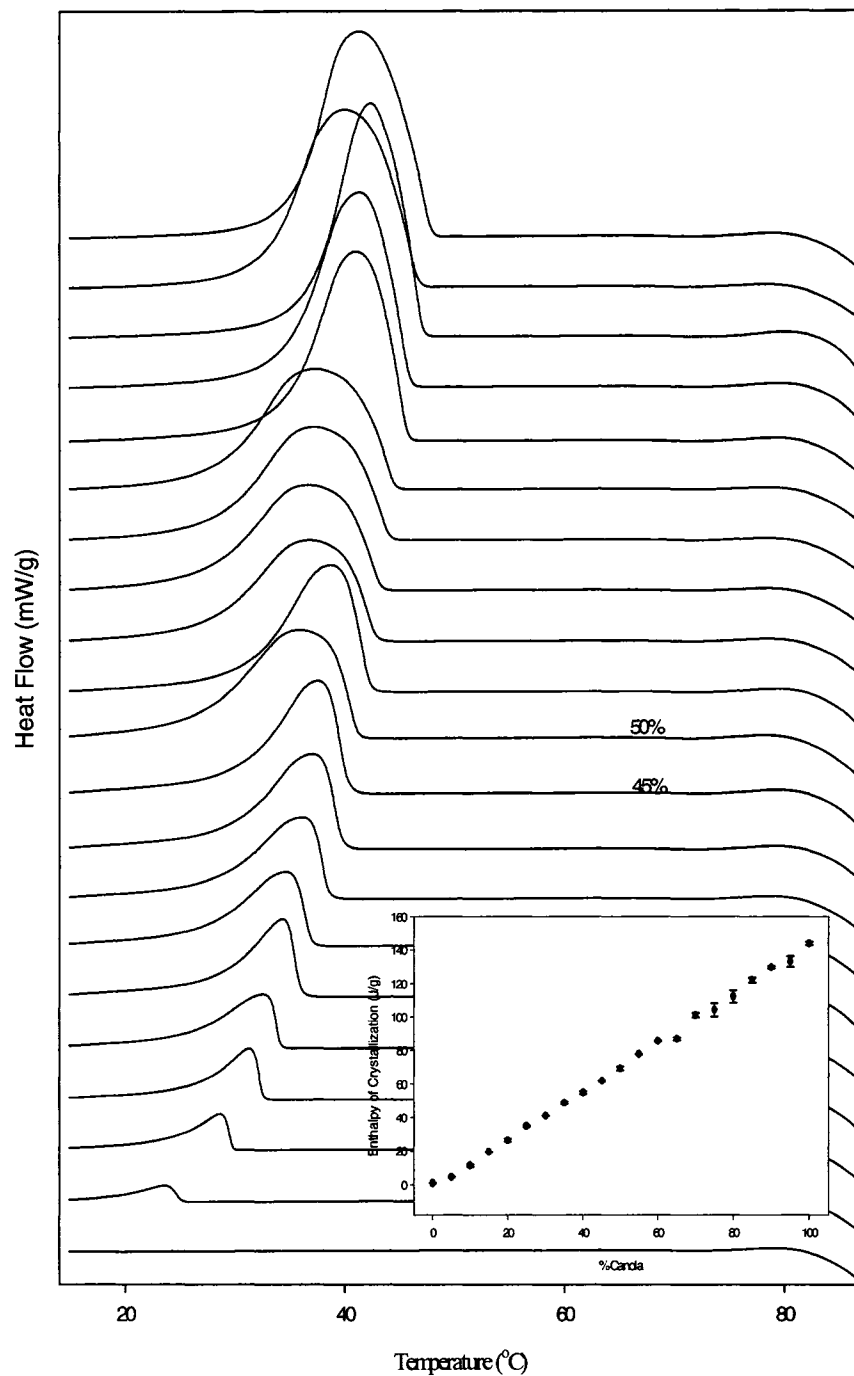


Figure A1.1: Crystallization heat flow versus temperature with inset enthalpy of crystallization versus composition curve. The 0% canola sample is the bottommost curve on the graph and the percent canola composition of the samples increases by 5% for each subsequent curve to the 100% canola sample at the top of the graph.

differences between the samples with respect to onset of crystallization, polymorphism, microstructure, and SFC are not attributable to the growth mode of the crystals. Adjacent curves in Figure A1.1 typically vary, in respect to full width half maximum (FWHM), by 1 °C or less. The one exception to this trend is for the 45 to 50% canola samples where a change of 4 °C occurs. Thus, the growth mode of the 50% sample is not similar to the growth mode of the 45% sample whereas this is not the case for all other neighboring samples.

Figure A1.2 shows the onset time of crystallization as it varies with the composition of the solution. The systematic error is ± 20 seconds due to the difficulties associated with obtaining the measurements at the 10 °C per minute cooling rate. Nevertheless, as the amount of canola in the melt increases, the time at which the induction of crystallization occurs also decreases with no significant deviations from the trend. This is expected, as one increases the amount of fully hydrogenated canola, which crystallizes at a higher temperature than soybean oil, the sample's onset time decreases.

The melting behavior for each sample, illustrated by the enthalpy of melt curve, is shown in Figure A1.3. Changes in the shape of the enthalpy curves are due to the variances in polymorphic structure assumed by the sample. There is a steady increase in the location of the melting peak maximum for the 5 to 65% canola solutions. One would expect these samples to be of similar polymorphic form. A new trend in peak maxima occurs for the 70 to 95% samples as the peaks become narrower with the maxima starting a new increasing trend beginning lower than the peak max of the 65% canola blend.

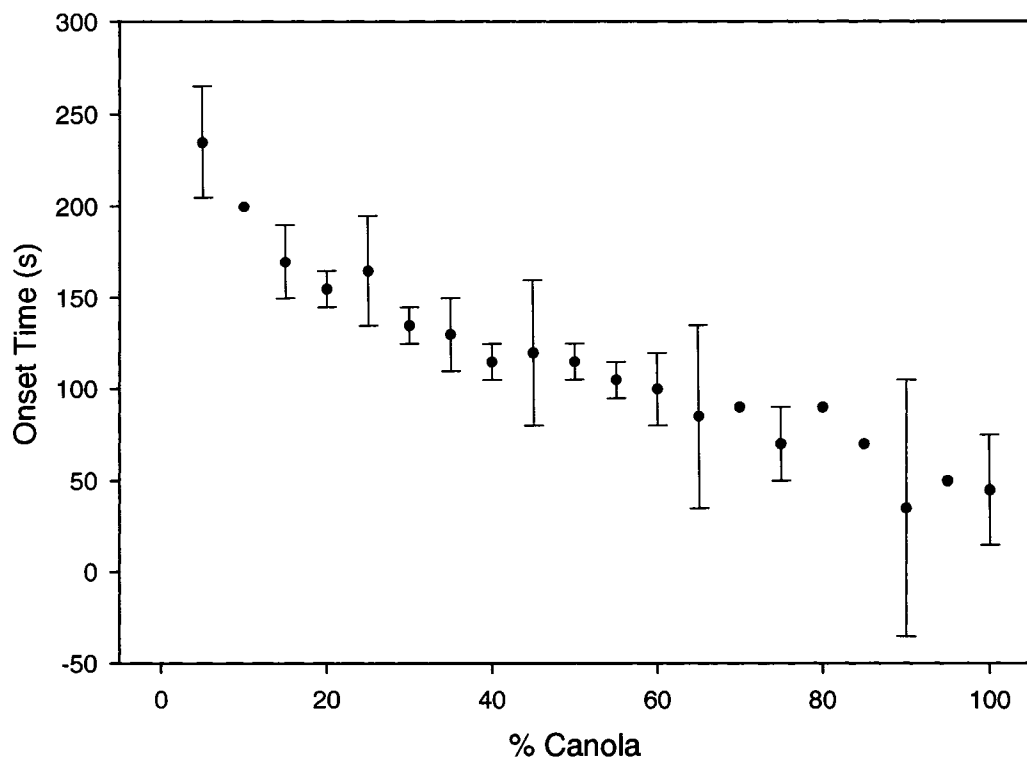


Figure A1.2: Crystallization onset time

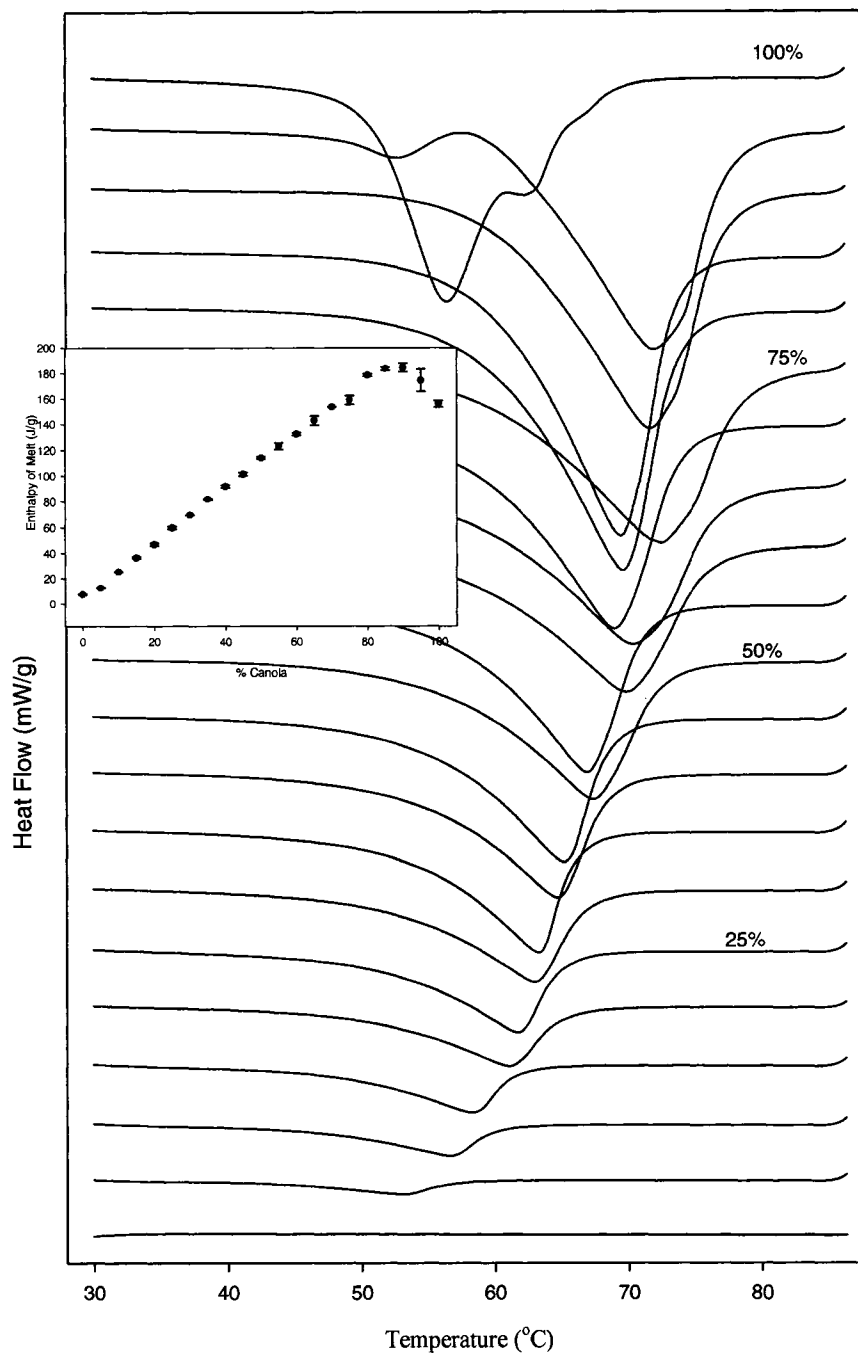


Figure A1.3: Melting heat flow versus temperature curves after 48 hours with inset enthalpy of melting versus composition curve. The 0% canola sample is the bottommost curve on the graph and the percent canola composition of the samples increases by 5% for each subsequent curve to the 100% canola sample at the top of the graph.

Clearly, for these samples, the polymorphic form is different than for the 5 to 65% samples. As well, the 95% canola blend has a unique type of melting behavior as the curve has a shoulder occurring at a lower temperature than the main peak. The melting behavior exhibited by the 100% canola sample is unique as the enthalpy curve is characterized by a shoulder peak at a higher temperature than the main peak, with the maximum value at a lower temperature (57 °C) than all but the 5 and 10% samples. Therefore, unique polymorphic forms are to be associated with the 95 and 100% canola samples.

Figure A1.4 shows an increasing hardness trend as the percent canola increases. The first three values, corresponding to the 5, 10 and 15% canola blends, are not zero but have very small values ($3.3 \times 10^{-5} \pm 4 \times 10^{-6}$ kgf/mm, $3.6 \times 10^{-5} \pm 2 \times 10^{-5}$ kgf/mm, $6.4 \times 10^{-5} \pm 2 \times 10^{-5}$ kgf/mm). The 0% canola sample was not tested for hardness as it was entirely soybean oil. Fluctuations, where the fat sample with a higher percentage of canola exhibited a smaller slope during the hardness measurement, occur in three areas of this graph; at the 50%, 65%, and 90% canola mixtures.

The deviation in Figure A1.4 at 50% canola is mirrored by inconsistencies in Figures A1.1 and A1.3. In Figure A1.1, one can see that the crystallization curve for the 45% solution has a steeper onset to its peak and a narrower peak than the 50% curve. Thus much of the crystallization and initial nucleation occurs simultaneously. This suggests good intersolubility between the hard canola and soybean oil, to form single

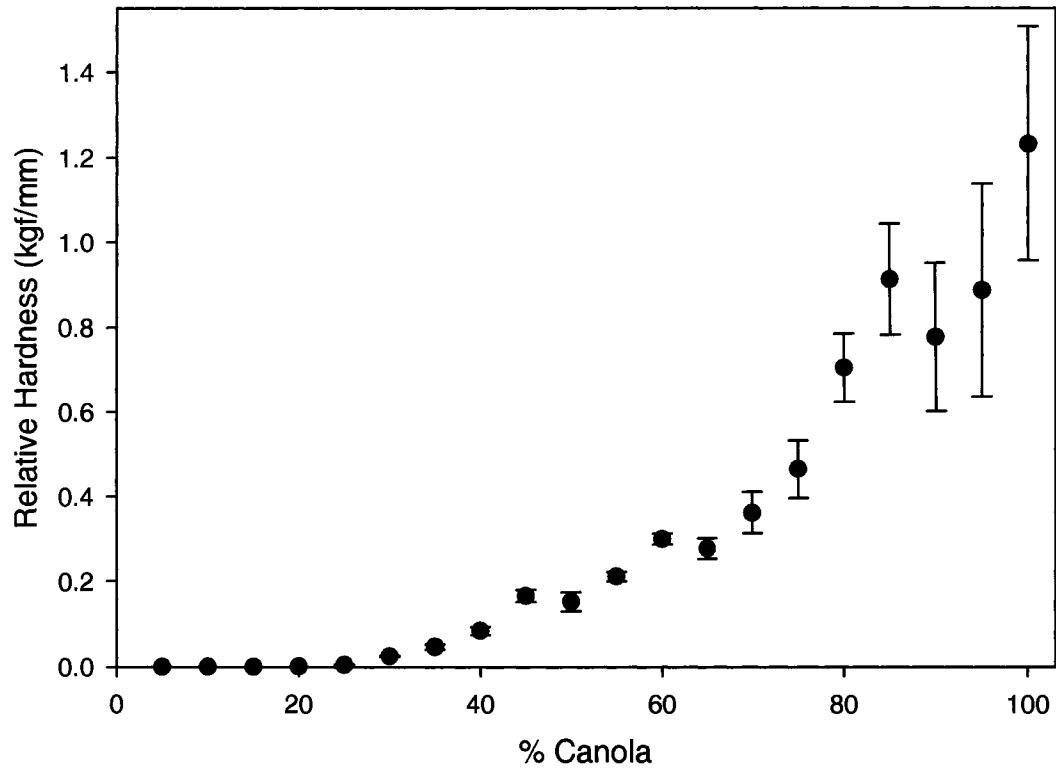


Figure A1.4: Variation of hardness with composition.

molecular compounds rather than a distribution of molecular compounds and therefore nuclei. As well, the FWHM of the crystallization curve for the 50% sample is much greater than that for the 45% canola blend (i.e. 9.35 °C compared to 6.23 °C). This would lead one to believe that the crystallization of the 45% sample occurs within a relatively short time period compared to the crystallization for the 50% canola sample. This relatively longer crystallization event would relate to a situation where nucleation occurs over a wider time span. Such a time span would allow a variety of nuclei related to the existence of a number of different molecular compounds due to the solution behavior to grow, thereby resulting in less crystal growth and more nucleation sites. Thus in the 50% sample, there are many small structures instead of the large ones found in the 45% sample (one can see this reflected in the microstructure, to be discussed later). Also, in Figure A1.3, there is a deviation in the trend of increase in location of melting peak max for 5-65 % blends at the 50% canola sample, indicating a change in melting behavior between the 45 and 50% blends (i.e. a polymorphic change).

Unlike the deviation in the hardness trend at 50% canola, the deviations in Figure A1.4 at the 65 and 90% canola blend are not due to the growth mode of the network. The curves in Figure A1.1 are quite similar (for the 60, 65, and 70% blends as well as the 85, 90, and 95% blends), suggesting the microstructure formed in these samples have been subjected to the same dynamics of heat and mass transfer. Thus the deviations in the hardness curve at 65 and 90% are not due to intersolubility effects alone. As well, the enthalpy of melt curves in Figure A1.3 are also similar for the 60, 65, and 70% blends as

well as the 85, 90, and 95% blends. Thus, deviations in Figure A1.4 at 65 and 90% are not due to growth mode selection or melting behavior of the samples.

The iso-solid line diagram constructed from the SFC of each of the fat samples is shown in Figure A1.5. The points sharing the same SFC value are connected using an iso-solid line. The iso-solid line at the very top of the figure is the zero SFC line. From the zero SFC line, the percent solid increases from left to right in 5% increments. It is evident that as the temperature and percentage of hydrogenated canola increases, the iso-solid lines converge to the right. The shape of each iso-solid line is similar to that of the neighboring lines with the slope of the iso-solid lines appearing to be similar. The iso-solid diagram also shows that a shortening made using fully-hydrogenated canola and soybean oil can have a 20% solid fat content at temperatures between 30 and 60 °C when the percentage hydrogenated canola is between 20 and 50%. It also shows that at temperatures above 55 °C, temperature variation must be carefully controlled as SFC varies greatly with temperature above this point. Figure A1.5 does not impart information as to the hardness of each sample as the deviations shown in Figure A1.4 are not seen here.

The phase changes caused by a change in the polymorphism between different fat blends can be measured with XRD. A change in the peak shape or position is indicative of a change in the polymorphism. Figure A1.6 shows the XRD spectra for all samples with 15% or more canola. Those samples with less than 15% were not measured due to difficulties in creating the requisite sample tubes. The lowest curve shown is the

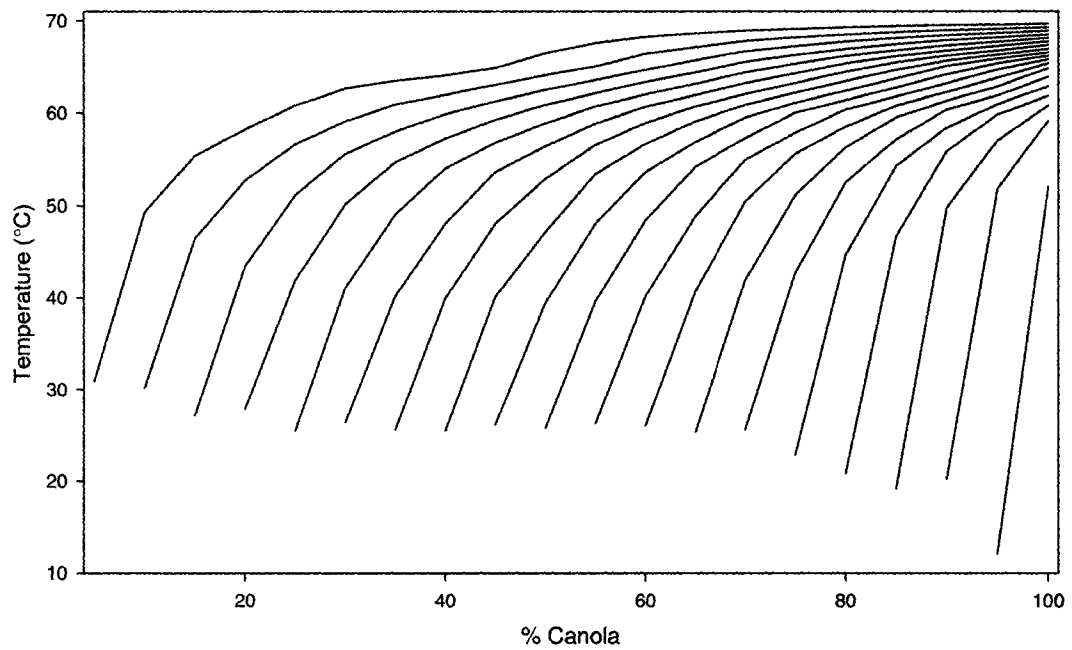


Figure A1.5: Iso-solid lines created using the interpolation method. Each curve connects points with a common SFC value. The leftmost curve is the 5% SFC line with the percent SFC increasing in 5% increments as one moves right on the graph.

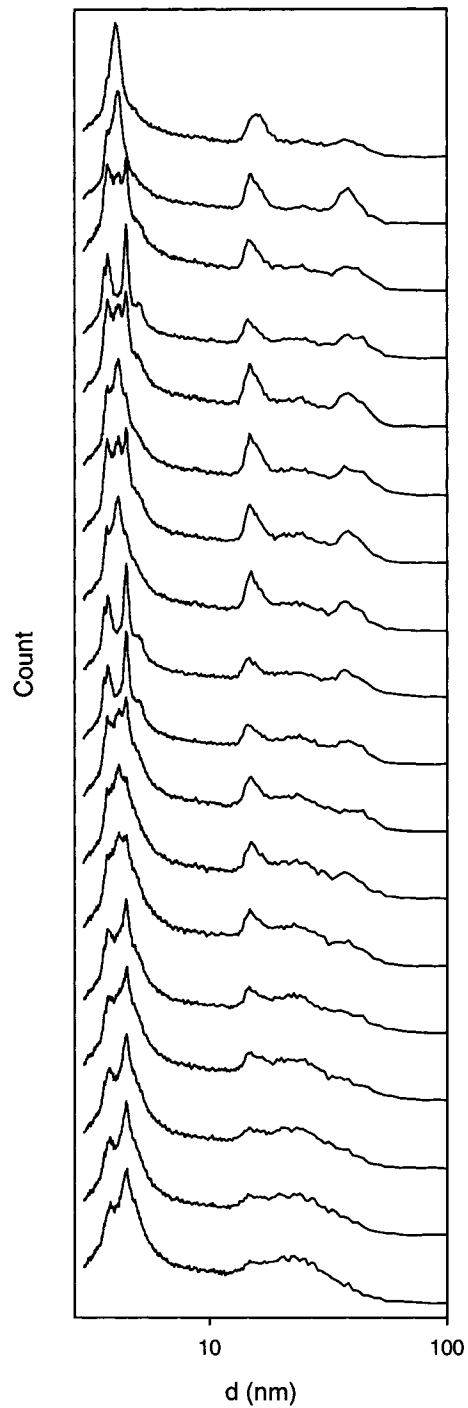


Figure A1.6: X-ray diffraction curves versus d . The bottommost curve is the 15% canola blend, and the percent canola increases by 5% for each curve above. The top curve is for the 100% canola sample.

spectrum for the 15% canola blend with subsequent lines representing samples with increasing canola content until the 100% canola blend spectra at the top of the figure. Two peak regions exist on each curve. The leftmost imparts information as to the polymorphic form of the crystals within the sample (the so-called short spacing), and the wider peaks on the right hand side of the curve which may be due to secondary reflections or the polytype of the fat. The peak shapes shown on the left side of the curves in Figure A1.6 can be divided into three categories. These categories are based solely on the positions and shapes of the peak as catalogued in Table A1.2. Within each category, different values of d are present as shown by Table A1.3 and these can be associated quantitatively with the possible polymorphic form, which have been defined for lipids. The alpha polymorphic form has a d value of 0.42 nanometers, the beta-prime d value is within the range of 0.42 to 0.43 nanometers and 0.37 to 0.40 nanometers, and the beta form has a d value of 0.46 nanometers [14].

The 100% canola peak is a well-defined single peak, and as one decreases the canola content to 95% a shoulder appears on the main peak. Further decreases of the canola in the sample leads to the appearance of 2 to 3 peaks on the left hand side of the XRD curve. For the lowest (15-35) percentages of canola, the peak shape assumed is a large well defined peak with a smaller shoulder peak on the left hand side. The right hand side peak on the curve is not well defined at lower concentrations of canola. At 40% canola a peak is defined and this becomes more apparent with increasing canola. At 65% canola, a second, smaller peak further right on the curve becomes clear, and at 95%

Table A1.2: Classification of XRD curves by shape

% Canola	Classification
100	A
95	A
90	B
85	C
80	B
75	AC
70	B
65	AC
60	C
55	C
50	B
45	AC
40	AC
35	C
30	C
25	C
20	C
15	C
10	n/a
5	n/a
0	n/a

Table A1.3: Average d value for each class of XRD curves

Class	Average d Values			
	A	0.406		1.541
B	0.373	0.446	1.473	3.891
C	0.379	0.443	1.621	
AC	0.374	0.438	1.469	3.740

canola these two peaks are of the same size distinction, with the rightmost peak disappearing in the spectra for the 100% canola sample.

A second peak on the right hand side of the XRD curves in Figure A1.6 for the 70 to 95% canola blends corresponds to the new trend in peak maxima in Figure A1.3 where the peaks become narrower with the maxima starting a new increasing trend beginning lower than the peak max of the 65% canola blend. Also in Figure A1.3, the 95% canola blend's unique melting curve is possibly due to a polymorphic change as seen by the presence of a distinct second peak on the right hand side of the curve in Figure A1.6. Again, the unique behavior of the 100% canola sample may be due to the polymorphism of the sample as the second peak on the right hand side of the curve in Figure A1.6 is not present.

The polymorphic data imparted by the XRD curves also assists one in explaining the deviations in Figure A1.4. From Figure A1.6 one can see the difference in polymorphic character with the curve for the 45% canola blend being of type $\frac{1}{2}$ A, $\frac{1}{2}$ C while the 50% canola sample being of type B. These changes in polymorphism also contribute to the variation in hardness, and support the difference in solution behavior proposed above. As well, the polymorphisms of the 60 and 65% samples differ as shown by the XRD curves. The curve for the 60% solution is of type C and that for the 65% canola blend is $\frac{1}{2}$ A, $\frac{1}{2}$ C. Thus, the hardness variations are due to the differences in the packing of molecules between the 60 and 65% canola samples. For the third deviation at

the 90% blend, the polymorphisms of the samples differ as shown by Figure A1.6. The curve for the 85% solution is of type C and that for the 90% canola blend is type B.

Figure A1.7 illustrates the microstructure of selected mixtures of fully hydrogenated canola oil and soybean oil. Except for minor deviations such as the placement of structures, the microstructures of the samples are alike with two exceptions. In the 50% canola blend, the structures appear smaller ($\approx 100 \mu\text{m}$) than that for the other solutions shown (average $\approx 500 \mu\text{m}$). In the 50% canola sample, the structures are not closely packed and have spaces between them ($\approx 10 \mu\text{m}$). The other samples exhibit the close packed arrangement as seen in the 45% canola sample. The 80 and 85% canola samples, though having the same crystal size as the 90 and 95% samples, are also more densely packed than those in the 90 and 95% samples as seen by the appearance of well-defined Maltese crosses. The distinct Maltese crosses indicate that these samples contain well-defined spherulites.

The deviation in increasing hardness from Figure A1.4 at the 50% canola solution is due to the microstructure assumed as well as polymorphism and intersolubility. In Figure A1.7, one can see that the sample with 50% canola is characterized by structures which are approximately $100\mu\text{m}$ in diameter with large ($\sim 10 \mu\text{m}$) spaces in between the structures. The other samples shown have large, closely packed structures approximately $500 \mu\text{m}$ in diameter. Note that these structures are clearly aggregates of micro-structural elements, which are themselves aggregates of crystals. Thus, one can expect that under

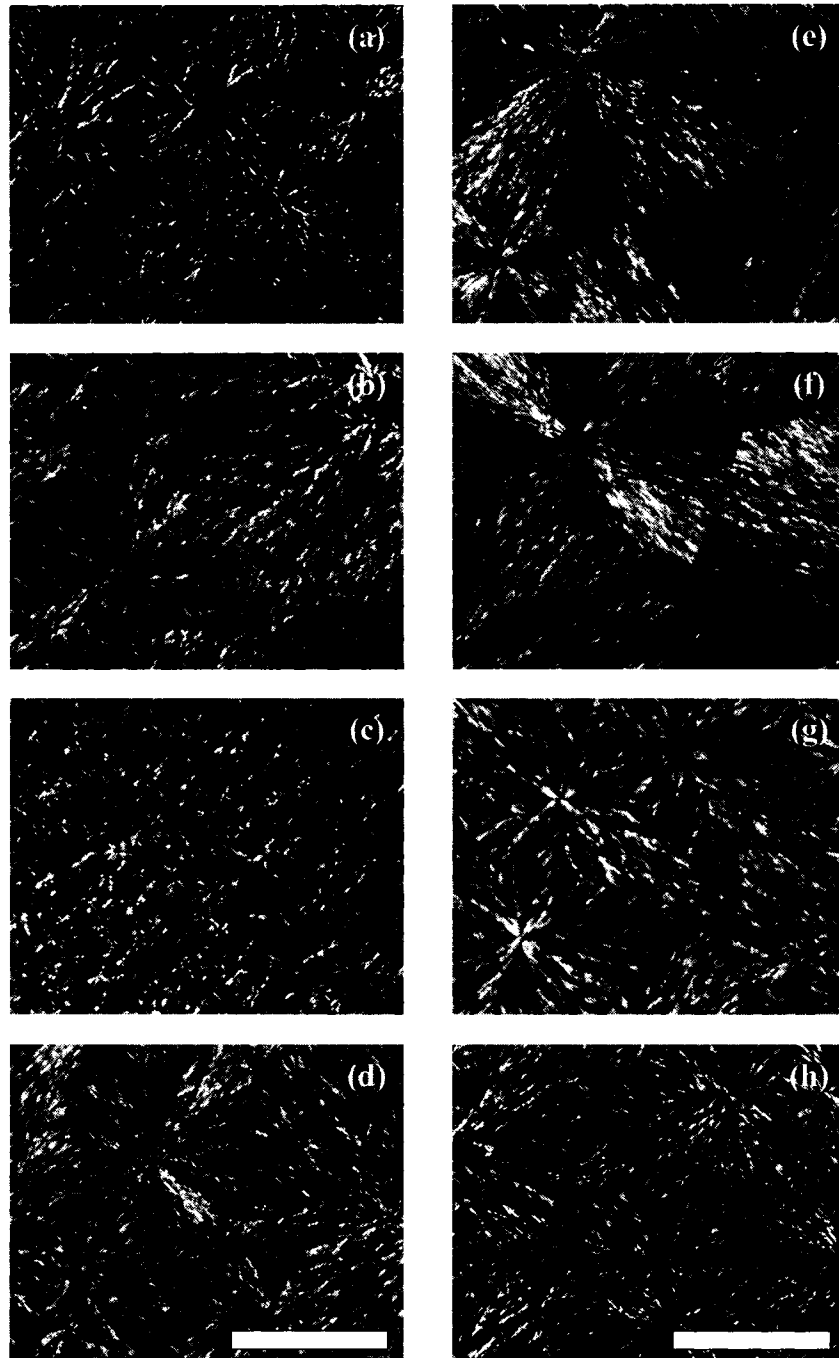


Figure A1.7: Composite diagram of the microstructure of selected samples after 48 hours. The given samples vary with respect to percent canola: (a) 40%, (b) 45%, (c) 50%, (d) 55%, (e) 80%, (f) 85%, (g) 90%, and (h) 95%. (bar = 500 μm)

pressure from an Instron cone the 50% sample will simply compress, with structures filling the spaces, whereas there is no room for similar compression in the 45% sample.

The deviation from the trend in the hardness curve at the 65% canola solution is not due to the microstructure assumed. All of the samples have a close-packed network of structures approximately 500 μm in diameter. Thus the variation in the hardness graph is not due to the microstructure of the samples.

The deviation from the trend in the hardness curve at the solution of 90% canola is partially due to changes in microstructure as well as polymorphism (as seen in Figure A1.6). The changes in microstructure can be seen in Figure A1.7 as the 85 and 90% blends have the same crystal size but the 85% canola sample is more densely packed and demonstrates greater spherulitic behavior as suggested by the well defined Maltese crosses indicating the presence of well defined spherulites.

Therefore, iso-solid lines, created with SFC data do not predict the final physical properties of a lipid network. The deviations in hardness found can be explained via the use of intersolubility, growth mode, polymorphic, and microstructure arguments.

A1.3 References

1. Moore, W., *States of Matter*, in *Basic Physical Chemistry*. 1983, Prentice-Hall Inc: Englewood Cliffs, New Jersey. p. 27.
2. Narine, S.S. and A.G. Marangoni, *Relating structure of fat crystal networks to mechanical properties: a review*. *Food Research International*, 1999. **32**(4): p. 227-248.
3. Narine, S.S. and A. Marangoni, *Factors Influencing the Texture of Plastic Fats*. *Inform*, 1999. **10**(6): p. 565-570.
4. Narine, S.S. and A.G. Marangoni, *Microscopic and rheological studies of fat crystal networks*. *Journal of Crystal Growth*, 1999. **199**: p. 1315-1319.
5. Norton, I., et al., *A calorimetric, NMR and X-ray diffraction study of the melting behavior of tripalmitin and tristearin and their mixing behavior with triolein*. *J.Am.Oil Chem.Soc.*, 1985. **62**: p. 1237-1244.
6. *Standard Methods for the Analysis of Oils, Fats, and Derivatives*, in *International Union of Pure and Applied Sciences*. 1979.
7. *Solid Content Determination in Fats by Low Resolution Nuclear Magnetic Resonance v. 2.150*, in *International Union of Pure and Applied Sciences*. 1987.
8. *Determination of Solid Fat Content by Pulsed NMR Method*, in *International Standard, Animal and Vegetable Fats and Oils*. 1991.

9. *AOCS Method Cd 16b-93*, in *Official and tentative methods of the American Oil Chemists' Society*, W.E. Link, Editor. 1998, AOCS Press: Champaign, IL.
10. Rossell, J., *Interactions of triglycerides and of fats containing them*. Chemistry and Industry, 1973: p. 832-835.
11. Timms, R., *Computer program to construct isosolid diagrams for fat blends*. Chem.Ind., 1979: p. 257-258.
12. Rousseau, D., et al., *Restructuring Butterfat Through Blending and Chemical Interesterification I. Melting Behaviour and Triacylglycerol Modifications*. Journal of American Oil Chemists Society, 1996. **73**(8): p. 963-970.
13. Narine, S.S. and K.L. Humphrey, *Extending the capability of pulsed NMR instruments to measure solid fat content as a function of both time and temperature*. J. Am. Oil Chem. Soc., 2004. **81**(1): p. 101-102.
14. Ghotra, B.S., S.D. Dyal, and S.S. Narine, *Lipid shortenings: a review*. Food Research International, 2002. **35**(10): p. 1015-1048.
15. Narine, S.S. and A. Marangoni, *Structure and Mechanical Properties of Fat Crystal Networks*, in *Physical Properties of Lipids*, A. Marangoni and S.S. Narine, Editors. 2002, Marcel Dekker Inc: New York. p. 63-83.

16. Wang, T., *Soybean Oil*, in *Vegetable Oils in Food Technology; Composition, Properties and Uses*, F.D. Gunstone, Editor. 2002, CRC Press LLC: Boca Raton, Florida. p. 21-22.

17. Neff, W.E., et al., *Oxidative Stability of Purified Canola Oil Triacylglycerols with Altered Fatty Acid Compositions as Affected by Triacylglycerol Composition and Structure*. *J. Am. Oil Chem. Soc.*, 1994. **71**(10): p. 1101-1109.

A2. Diminishing marginal utility of cooling rate increase on the crystallization behavior and physical properties of a lipid sample

A2.1 Introduction

Non isothermal crystallization studies of lipids are of significant interest, particularly for the food industry. The effect of processing conditions, such as cooling rate and degree of supercooling, on the structure and physical properties of crystallizing systems has been investigated by several researchers [1-6]. In this regard, the crystallization behavior of lipids, including cocoa butter and its alternatives, has been given particular attention [7-13]. It has been shown that the cooling rate (r) affects the structural order of a crystallized sample which in turn influences the final properties of the lipid network. Faster cooling rates during non-isothermal crystallization result in a higher degree of cooling than slow cooling rates at any point in time (t_1) during the cooling process, as shown in Figure A2.1. When a lipid sample is cooled quickly, the system crystallizes before the optimal spatial organization of the molecules is reached due to insufficient mass transfer rates. Conversely, during slower cooling rates, mass transfer rates are increased (due to lower viscosity and longer induction time prior to solidification) and the organization of the molecules occurs faster and to a greater extent

A version of this chapter has been accepted for publication.
Humphrey, K.L. and S.S. Narine, Diminishing marginal utility of cooling rate increase on the crystallization behavior and physical properties of a lipid sample. *Journal of the American Oil Chemists' Society*, 2007. 84: p. 709-716.

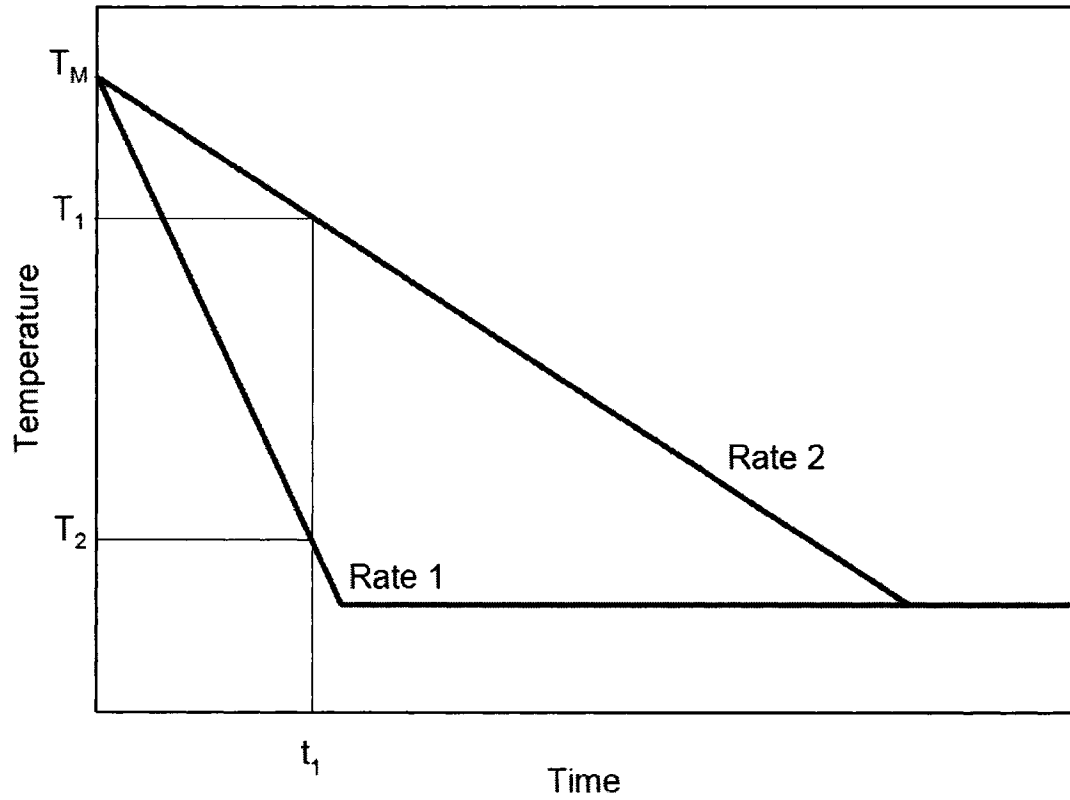


Figure A2.1: Effect of rate of cooling on the supercooling of a sample

[4, 6, 14, 15]. The rate of cooling may cause changes in the growth mode of the network, and can lead to polymorphic, microstructural, and solid fat content changes, and therefore changes in the final physical properties of the network [16, 17].

Cocoa butter alternatives (CBA) are of significant industrial importance. They are typically less expensive than cocoa butter and generally require much less careful tempering [9]. CBA can have a longer shelf life, be less afflicted by bloom, and tend to have a bland taste that can be easily masked during the production of confectionary products [9]. Although CBAs do not require the strict tempering regimes which cocoa butter demands, the processing conditions to which they are subjected are of importance to the confectionary industry, particularly from the perspective of influencing physical properties such as hardness.

This paper presents non-isothermal crystallization studies of a CBA, Temcote. It investigates the effect of the rate of cooling on the hardness, polymorphism, induction time, and enthalpies of crystallization and melt of a CBA, Temcote, by supercooling the sample at different rates varying from 0.1 °C/min to 20 °C/min. The range of cooling rates which produces notable changes to the crystallization process was particularly examined. The final physical properties of the sample were determined and discussed.

A2.2 Experimental Procedures

The lipid sample used in this study was Temcote, a CBA supplied by Bunge Oils (Bradley IL., USA). Unaltered Temcote, with a melting point of 34.7 ± 0.2 °C (when

crystallized at 10 °C/min and melted at 5 °C/min), was used for all measurements. The rates of cooling for the NMR and hardness measurements were determined using a soybean oil sample, which does not crystallize in the temperature range used. Sample cooling and heating rates are reported to a certainty of ± 0.1 °C/min. The static measurements were performed at a stage temperature of 15.0 ± 0.5 °C. The samples were stored in a cooling chamber at 15.0 ± 0.5 °C. All measurements were performed in triplicate ($n = 3$) and the mean values are reported with their subsequent standard deviations.

A2.2.1 Sample Preparation

The sample was heated to 90 °C and stirred with a mechanical stirrer for 2 minutes to ensure homogeneity and to destroy crystal memory and then transferred to the appropriate container (aluminum pans for DSC, brass compression mold for hardness and appropriate tubes for NMR and XRD) for analysis. The sample was equilibrated at 90 °C for 5 minutes and then cooled at a prescribed constant rate, ranging from 0.1 °C/min to 20 °C/min, down to a holding temperature of 15 °C.

A2.2.2 Relative Hardness Measurements

The molten fat was transferred into a brass compression mold to make sample disks of 2.4 ± 0.1 cm in diameter and 0.3 ± 0.1 cm thick. The brass mold containing the Temcote was then sealed and waterproofed. The Temcote samples were processed in the mold inside a water bath. The samples were cooled from 90 °C to 15 °C at 13 different

cooling rates (0.1, 0.5, 1, 2, 3, 4, 5, 6, 7, 8, 9, 10, and 20 °C/min). After thermal processing, the samples were stored for 24 hours at 15 °C, and subsequently removed from the mold prior to measurements.

The ‘Precision Penetrometer’ from Precision Scientific Company, Chicago, USA was used to measure the hardness. It was fitted with a stainless steel penetration cone of mass 45.0 ± 0.5 g and angle of 22.5°. The hardness is related to the distance into which the cone penetrates the sample over a 5 second time period. The displacement of the cone was read on the Vernier scale on the instrument in 1/10 mm.

A2.2.3 DSC Measurements, Thermal behavior

A “DSC 2920 Modulated DSC” by TA Instruments was used in the non-modulated DSC mode for thermal measurements. Liquid Temcote was pipetted in consistent amounts (10 to 15 mg each) into three aluminum DSC pans which were then hermetically sealed. An empty aluminum pan was used as a reference. The samples were first equilibrated at 90 °C for 5 minutes and then cooled at the prescribed rate (0.1, 0.5, 1, 2, 3, 4, 5, 6, 7, 8, 9, 10, 11, 12, 13, 14, 15, 16, 17, 18, 19, and 20 °C/min) down to -10 °C where they were equilibrated for 15 minutes to allow crystallization to complete. The sample was then heated to 90 °C at a constant rate of 5 °C/min to obtain the melting curve.

The data sampling and temperature control procedures were fully automated and controlled by the “TA Instrument Control” software program. The data was analyzed

using the “TA Universal Analysis” software and a method developed by our group [18]. All curves were normalized to a uniform sample mass of 15 milligrams.

A2.2.4 XRD measurements, Polymorphism

“Bruker AXS X-ray diffractometer” equipped with a filtered Cu-K α radiation source ($\lambda = 0.1542$ nm) was used for XRD analysis. The procedure was automated and commanded by Bruker AXS’ “General Area Detector Diffraction System” (GADDS V 4.1.08) software. The XRD samples were prepared by filling glass capillary tubes with the molten sample. The tubes were fitted with the brass sample holder and then tempered at a prescribed rate (0.1, 1, ... to 20 °C/min) down to the final holding temperature of 15 °C in a “Linkam LTS 350” temperature controlled stage (Linkam Scientific Instruments, Tadworth, Surrey, United Kingdom) using its “Air Jet” cooling system (Kinetics-Thermal Systems, New York, USA). The sample was held isothermally in the Linkam for 30 minutes at this final temperature. The sample tube with brass holder was then quickly transferred for analysis to the XRD stage where the temperature was maintained at 15 °C \pm 0.5 °C by an air jet cooling system. The XRD frames, obtained after 450 seconds exposure to a monochromatic Cu-K α X-ray beam, were processed using GADDS software and the resulting spectra were analyzed using Bruker AXS’s “Topas V 2.1” software.

A2.2.5 NMR measurements, SFC determination

SFC data was acquired using the pulse magnetic resonance spectrometer “minispec mq SFC analyzer” (Bruker Instruments, Milton, Ontario, Canada), equipped with a temperature controlled measurement chamber. SFC sampling as a function of time and temperature was accomplished using a custom-designed cooling system previously described [19]. The data sampling procedure was fully automated, and the SFC was calculated and displayed by the “minispec v2.20 Rev.01/NT” software [20-23].

The NMR tubes were filled with molten fat to a height of 3.5 ± 0.1 cm. To achieve the prescribed cooling rate, the samples were first heated to 90 °C and held there for 5 minutes before being cooled from 90 to 67 °C outside of the NMR apparatus using external water baths and then transferred rapidly into the NMR chamber and cooled from 67 °C to 15 °C inside the NMR chamber. The sample was then held isothermally inside the NMR chamber for 24 hours at 15 °C. Twelve cooling rates (0.1, 0.5, 0.9, 1.6, 3.0, 3.5, 4.3, 5.2, 7.7, 10.2, 12.5, and 15.9 °C/min) were used. The SFC was measured at 10 second intervals starting the instant the sample was introduced into the NMR chamber. The plateau portion of the SFC curve was determined unambiguously by using the first and second derivatives of the SFC versus time curve. The starting point of the plateau was taken to be the initial point of the constant portion of the first derivative and the zero of the second derivative. The first derivative was considered constant if its value was within 3 times the peak to peak (ptp) noise of its average. A portion of the curve is considered constant if the SFC values over the interval were within 2 times the ptp noise level of the average SFC value of the interval. The value for a linear portion of the

second derivative of zero was used accordingly. The reported final SFC value is the average of the experimental plateau portion of the curve.

A2.3 Results and Discussion

Figure A2.2 shows the hardness of the samples measured by cone penetrometry as a function of r . As the rate of cooling increases, the penetration distance decreases smoothly and rapidly from 1.70 ± 0.08 mm for the sample cooled at 0.1 °C/min to plateau at about 1.01 ± 0.01 mm, a hardness value first achieved by the sample processed at 3.0 °C/min. This represents an increase in hardness of 68.3 % over a 30-time increase in cooling rate. Interestingly, there is a 50% increase in hardness as the cooling rate increases by a factor of six from 0.5 °C/min to 3.0 °C/min. Clearly, the range of cooling rates over which the hardness of this sample is significantly affected is very small. Therefore, the data indicates that cooling tunnels through which this lipid sample is processed should be carefully regulated, as small changes in rate can potentially cause large changes in hardness. Furthermore, the data indicates that for this particular sample, slow cooling rates are sufficient to produce maximum hardness. Deviations from the increasing hardness trend at 4, 5, and 10 °C/min cooling rates are not significant enough to warrant an alternate explanation as the general trend is within error bars. Additionally, given the error spread in the data, the hardness at these rates are for all practical purposes within the plateau region.

Figure A2.3 shows the crystallization curves for all rates versus time with the curve for the sample cooled at 0.1 °C/min being the bottom line each subsequent curve

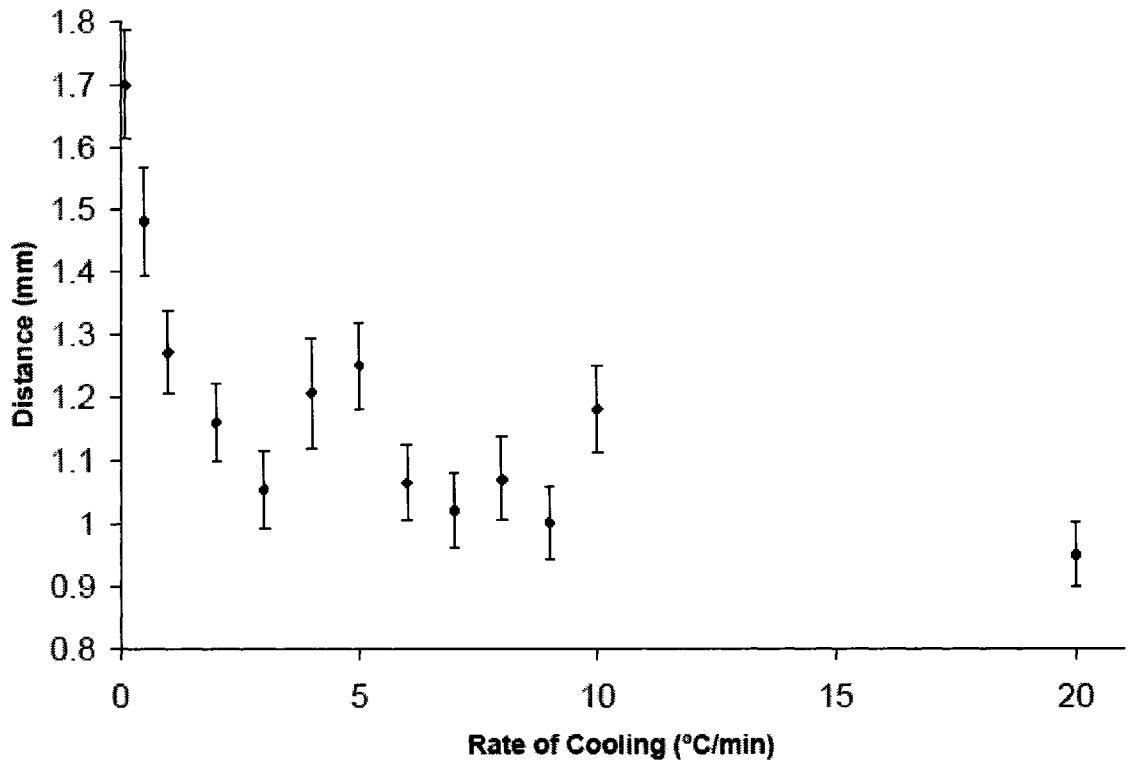


Figure A2.2: Hardness by cone penetrometry versus cooling rate

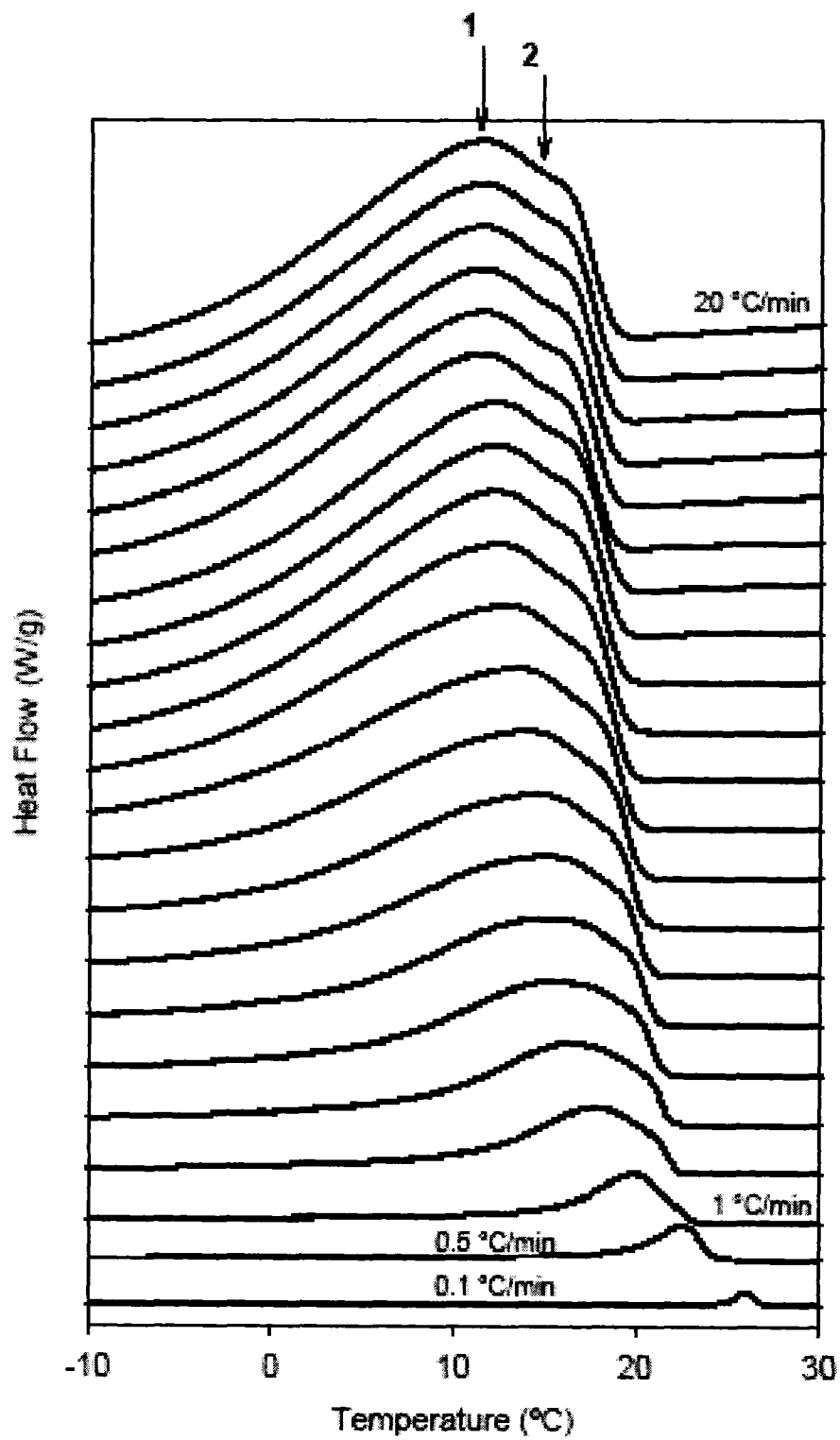


Figure A2.3: Stacked crystallization curves for samples processed at all cooling rates from 0.1 °C/min (bottom line) to 20 °C/min (uppermost line)

representing samples cooled at progressively faster rates of cooling with the 20 °C/min rate being the uppermost curve on the graph. The sample demonstrated relatively homogeneous crystallization behavior. The DSC crystallization curves (Figure A2.3) show a main broad peak (arrow 1) preceded by a shoulder (arrow 2) measurable for all cooling rates. As r is increased, the shoulder peak became increasingly more prominent suggesting the promotion of a growing discrimination in the crystallization of two fractions representative of differentiated molecular ensembles of the CBA. The onset of crystallization (T_o) and the start of crystallization (T_s) shown in Figure A2.4a, the maximum crystallization temperature (T_{max}) and the position of the inflection point of the shoulder shown in Figure A2.4b decrease almost linearly as the cooling rate increases from $r = 1$ °C/min to 12 °C/min and then plateau for higher cooling rates. The onset of crystallization was taken as the point of intercept of the tangent on the steepest slope of the peak to the baseline of the signal and the start of crystallization (T_s) was chosen as the point at which the heat flow signal first deviates from the baseline. It is interesting to note that the effective increase in supercooling due to increases in cooling rate has the effect of depressing the onset of crystallization. The most likely explanation for this is that the rate of increase of viscosity is high due to the faster rate of cooling, that mass transfer becomes a limiting factor in crystallization. This effect has been noted, if not explained, by others before [15].

With the final crystallization temperature not much removed from the melting temperature, if one compares low cooling rates to high cooling rates of the same lipid ensemble, regardless of the speed of the temperature decrease, at the point that the

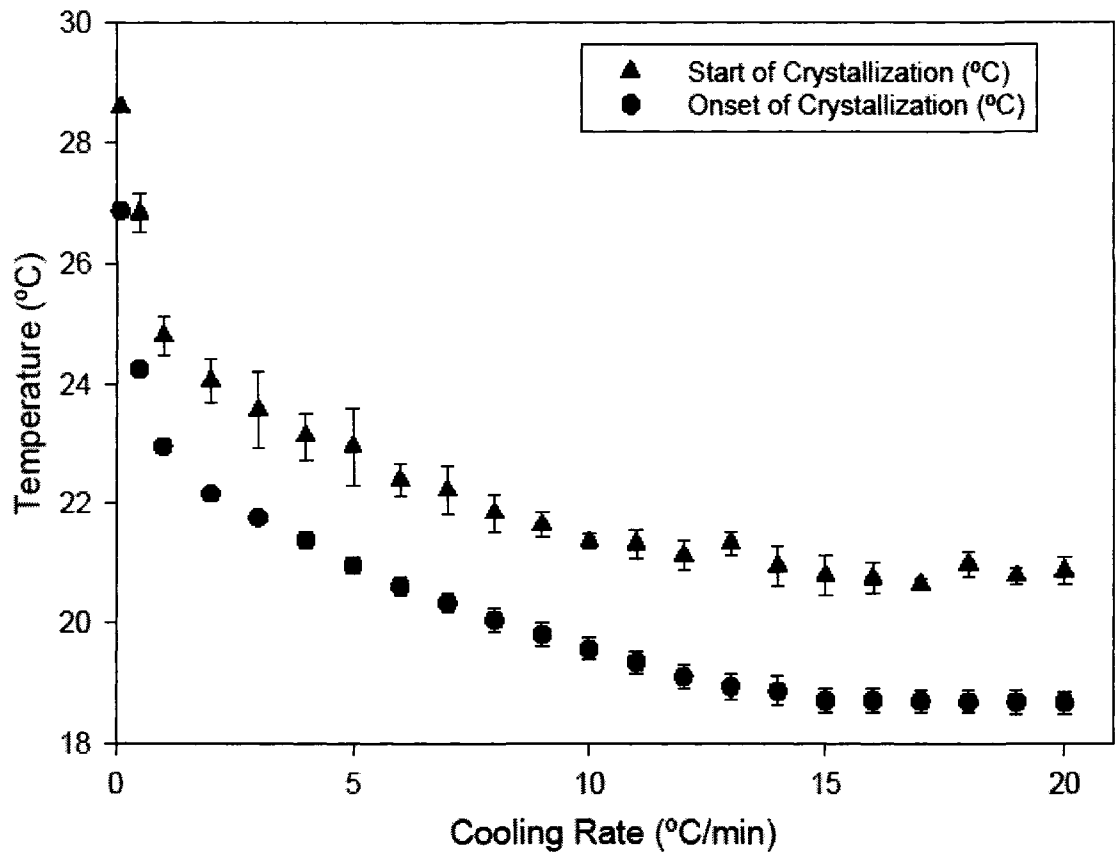


Figure A2.4a: Onset of crystallization and start of crystallization event versus cooling rate

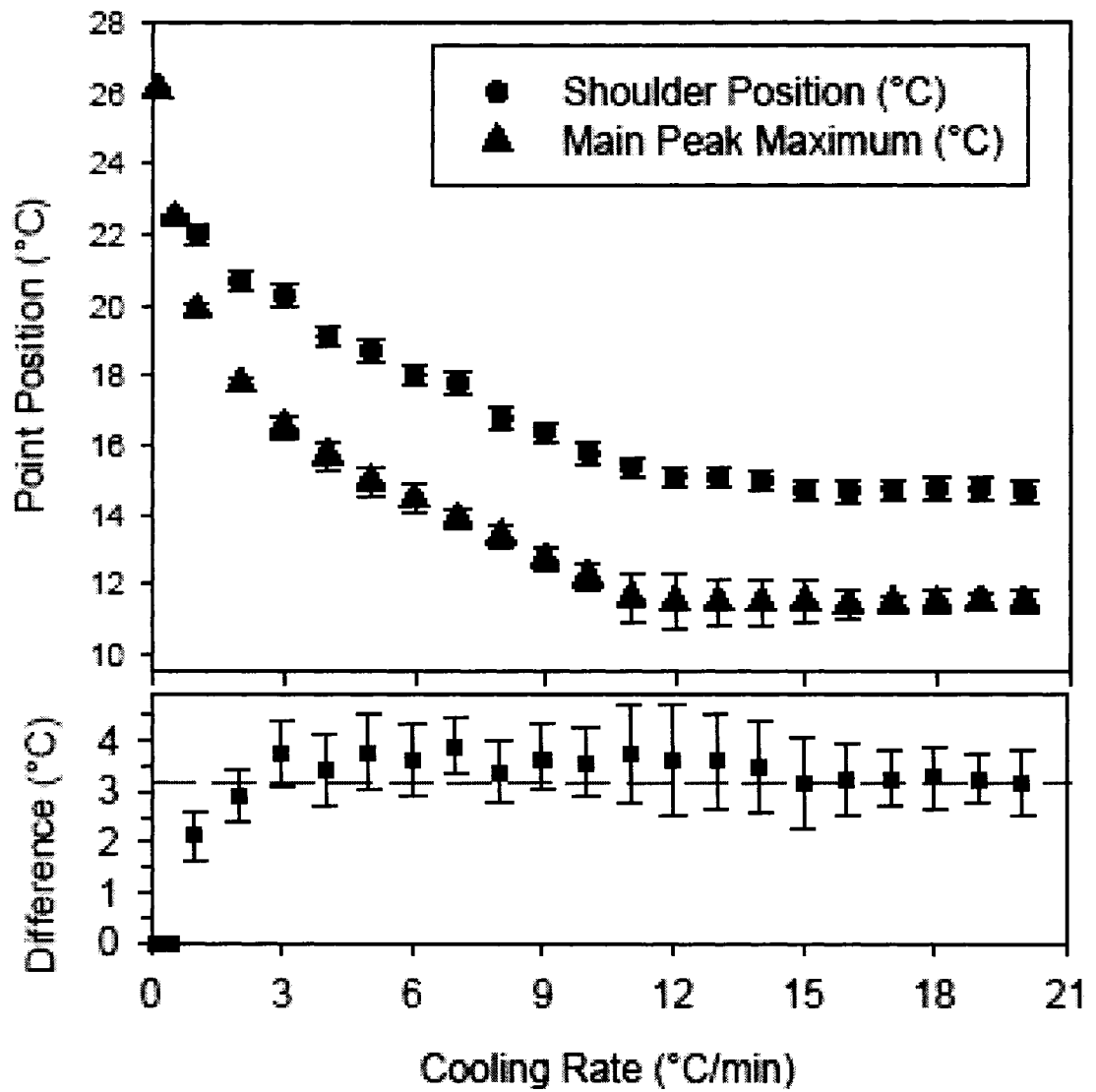


Figure A2.4b: Location of peak maximum and shoulder peak of the crystallization event versus cooling rate

crystallization temperature is achieved, the effective supercooling is relatively the same. Supercooling is dependent on the difference of $(T_M - T_C)$, where T_M is the melting temperature (or beginning of melt for a complex sample) and T_C is the crystallization temperature. Therefore, if $T_M - T_C$ is small, regardless of the speed at which this difference is achieved, the supercooling remains relatively unchanged. However, the rate of cooling in such circumstances does have a significant impact on the rate of viscosity increase. Liquid lipid samples demonstrate an exponential increase in viscosity as temperature is decreased as shown in Figure A2.5 for Temcote. Therefore, if the crystallization temperature is sufficiently high, as it was in this experiment with the onset of melt (16 ± 1 °C) being very close to the final crystallization temperature (15.0 ± 0.5 °C), one would have increased the viscosity (and therefore decreased the mass transfer of molecules in the melt) faster due to an increased cooling rate while providing a relatively small increase in thermodynamic driving force. Under such conditions it will take longer for mass transfer to occur prior to crystallization, resulting in a depression of the onset of crystallization. The extent to which the inception of crystallization, of molecular ensembles differentiated by radius of gyration and complexity of the molecule itself would be affected by such limitations to mass transfer, would provide the basis for the behavior demonstrated by the CBA sample in this experiment. Therefore, fractionation is possible by preferentially retarding the mass transfer of specific families of TAGs, thereby permitting some to crystallize earlier. Of course, it is expected that some limiting viscosity would be reached, at which point the differentiation and depression of onset of crystallization due to mass transfer limitations would no longer be relevant as demonstrated by the plateau region shown in Figure A2.4a. This is also in keeping with

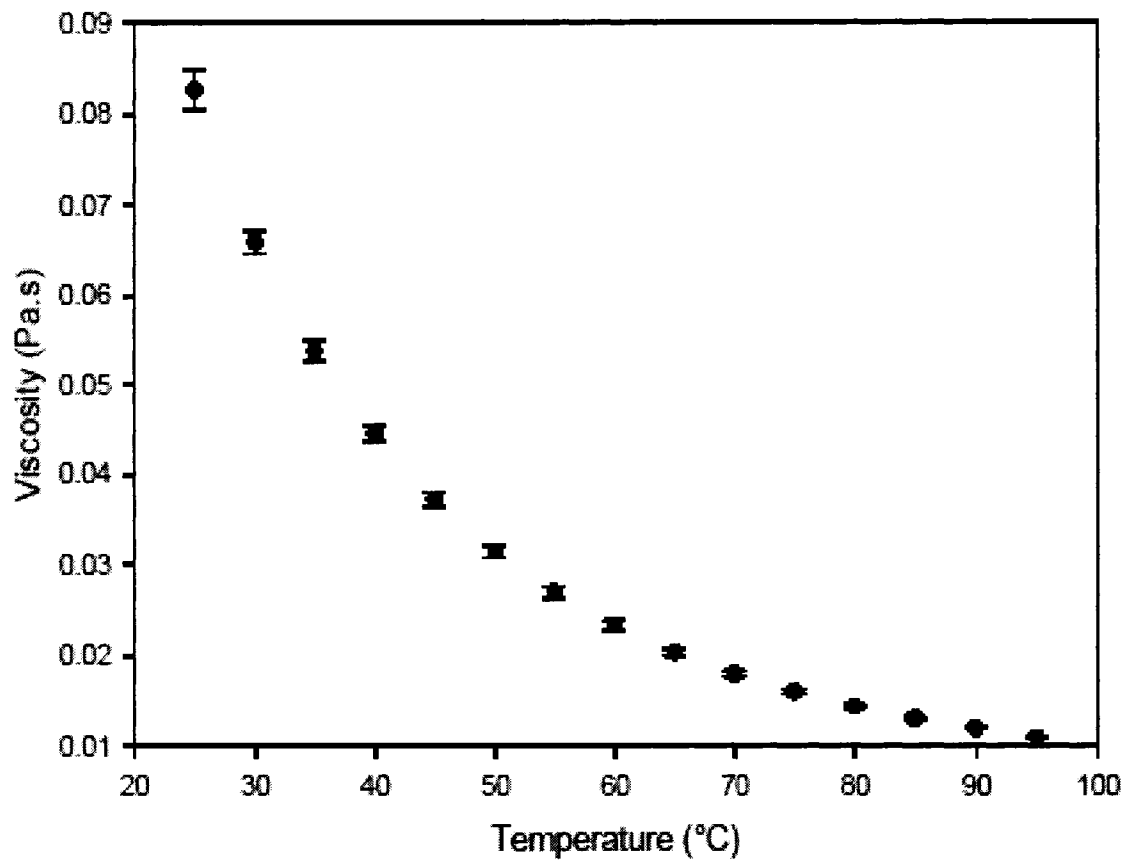


Figure A2.5: Viscosity of Temcote as a function of temperature

the exponential nature of the viscosity relationship with temperature (there is a plateau region). T_o decreases smoothly with increasing cooling rate from 22.9 ± 0.1 °C for $r = 1$ °C/min, and plateaus at 19.0 ± 0.3 °C for rates above 12 °C/min. T_s decreases similarly with an average difference in temperature ($T_s - T_o$) of 1.8 ± 0.1 °C. The temperature difference between the main peak and the shoulder is practically constant (3.5 ± 0.2 °C) for cooling rates higher than 5 °C/min indicating that the ensemble crystallizes homogeneously one before the other regardless of the magnitude of the cooling rate and that there is no thermal influence of one ensemble on the other. Therefore, at rates higher than 5 °C/min, the retardation effect of one fraction of molecules versus the other seems to be equally effective. The gap between the two events narrows when r is decreased below 5 °C/min. It would therefore seem that at these rates, the mass transfer limitations due to viscosity are less effective for one fraction versus the other. It is uncertain as yet how this behavior translates to the macro scale so that it affects hardness. It is worth noting that the hardness is also affected within the range where there is a discriminatory effect of the viscosity limitations to mass transfer of one fraction of molecules versus the other within the sample. Note also that the evolution of the crystallization event's main peak and shoulder heights mirror that of the respective positions. The heights increase in a linear fashion from $r = 1$ °C/min to 12 °C/min and then plateau for higher cooling rates.

Figure A2.6 shows the melting curves of the sample for all cooling rates. The lowermost line is the melting curve for the sample cooled at 20 °C/min, and subsequently higher curves represent the samples cooled at incrementally slower rates with the uppermost line representing the melting endotherm for the sample cooled at 0.1 °C/min.

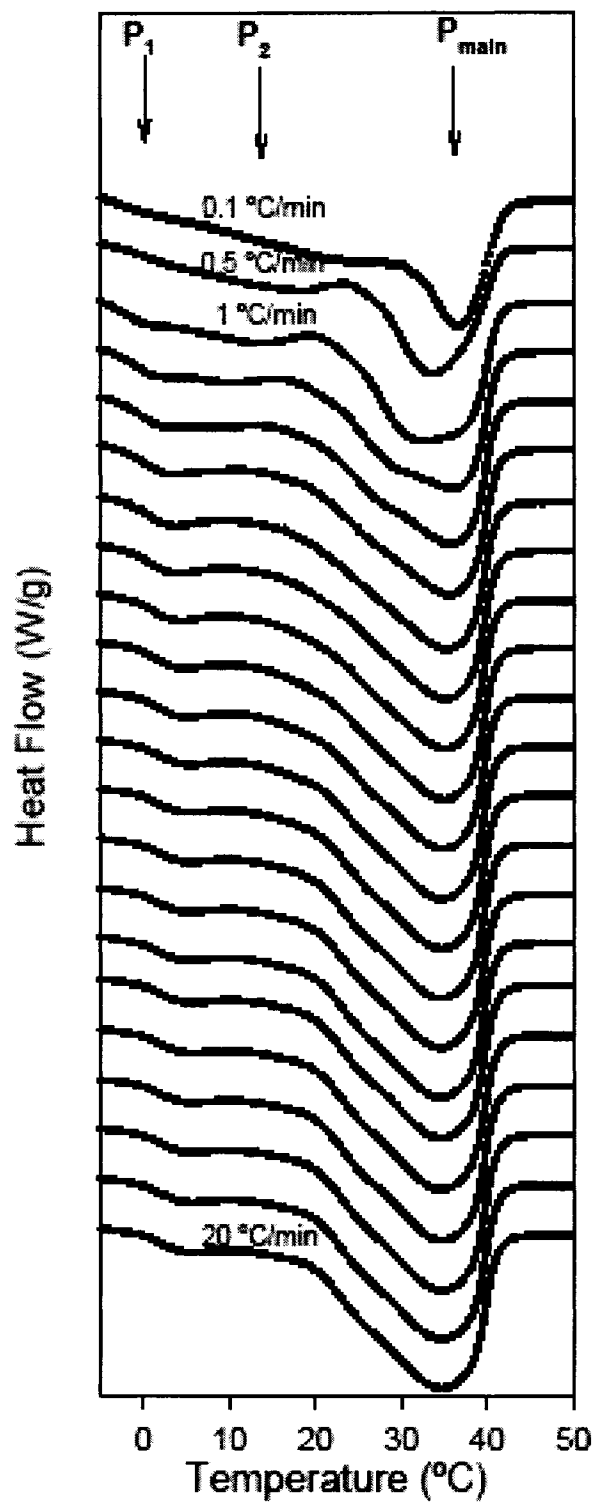


Figure A2.6: Stacked melting curves for samples processed at all cooling rates from 0.1 °C/min (uppermost line) to 20 °C/min (bottom line)

The overall time of melting as determined from the start to the end of the event is 10.4 ± 0.2 min for all rates. The melting curves display a small resolved peak (P_1) followed by a large main peak (P_{main}) made of overlapping events at the high end temperature. This complex melting behavior is commonly observed for lipid samples [24]. An extra intermediary minor peak (P_2) around $15\text{ }^\circ\text{C}$ is displayed in the curves obtained with the three first cooling rates ($r = 1, 2$ and $3\text{ }^\circ\text{C}/\text{min}$) and shows as a broad shoulder in the curves obtained with $r = 4$ and $5\text{ }^\circ\text{C}/\text{min}$. P_2 becomes incorporated in the main melting event as the main peak broadens. The appearance of such small peaks for samples cooled at slow rates of cooling is well known and is characteristic of the formation of compounds which would not have the time to grow otherwise. The disappearance of smaller peaks at higher rates of cooling is common and has been previously reported [25].

Due to the overlap of melting peaks, it is only possible to estimate the FWHM of the main melting endotherm by measuring the half width at half maximum starting from the end of the peak (and multiplying by 2). The main melting peak as described by its FWHM is narrow. As shown in Figure A2.7, FWHM increases smoothly with increasing r in an exponential-like manner from $6.5 \pm 0.1\text{ }^\circ\text{C}$ for the lowest r and plateaus at $10.1 \pm 0.1\text{ }^\circ\text{C}$. 95% of this value has been reached for $r = 11\text{ }^\circ\text{C}/\text{min}$. Note that the small variation, less than $2\text{ }^\circ\text{C}$ (for samples cooled at rates greater than $1\text{ }^\circ\text{C}/\text{min}$), would not be noticeable by the end consumer upon ingesting the fat product. Such a low FWHM with respect to temperature value combined with similar melting points is indicative of

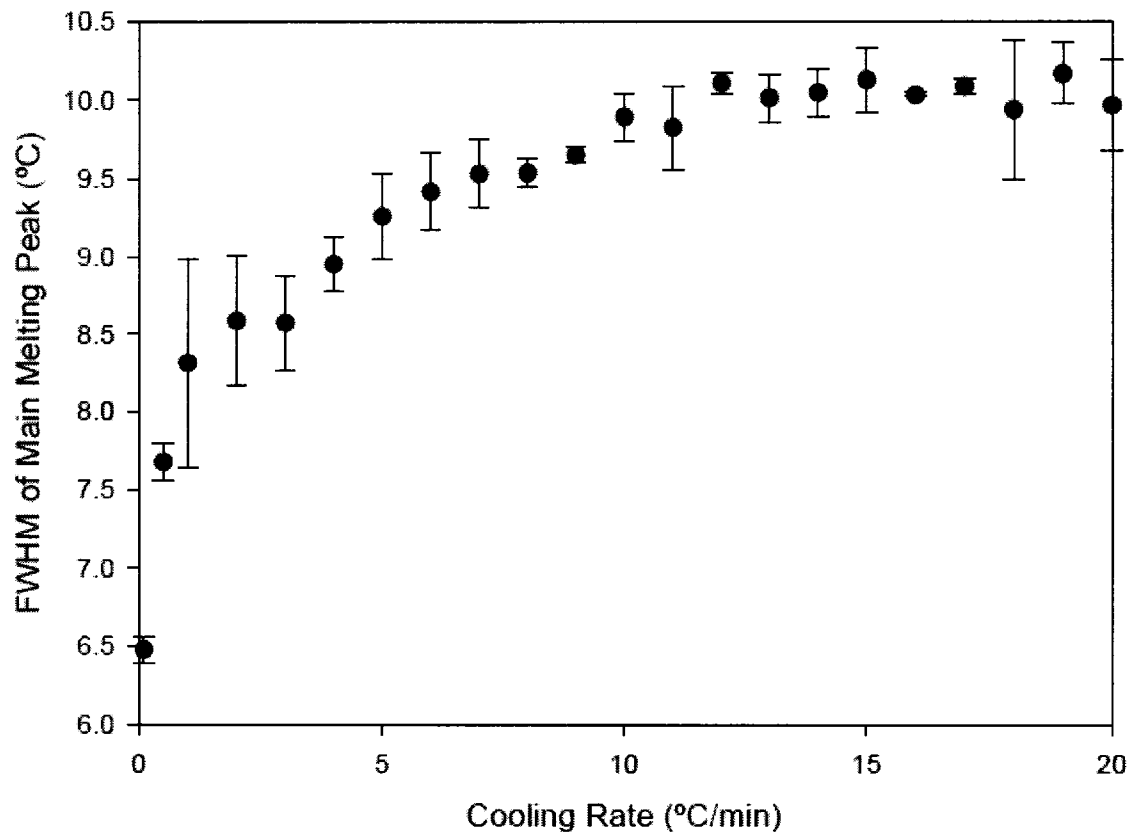


Figure A2.7: FWHM of the main melting peak versus cooling rate as a function of temperature

compounds melting catastrophically, leading to a mouthfeel independent of the rate of cooling.

The trend in FWHM of the main melting peak (as described above) matches the evolution of hardness. It is therefore reasonable to think that the larger number of compounds formed (indicated by a higher FWHM) greatly influence the evolution of hardness with softer samples having a lower FWHM and thus a greater similarity in the types of compounds formed. Thus crystallization at higher cooling rates (>5 °C/min) forms compounds which melt over a wider range of temperatures which lead to the formation of a harder final product. It is therefore possible to adjust the physical properties, such as melting and potentially hardness, and extend the range of cooling rates used beyond 4 °C/min by adjusting the composition of the CBA. The effect of changing the composition of a fat sample to alter its physical properties has been seen before [26-30]. Of course, such a possibility is dependent on the identification of the compounds responsible for the desired physical property.

Typically cocoa butter alternatives do not demonstrate polymorphic behavior. However, the polymorphism of the lipid sample versus cooling rates was investigated for completeness. The d -values (3.85 ± 0.01 μm and 4.23 ± 0.01 μm) obtained from XRD measurements were practically independent of r and are typical values indicative of the beta-prime polymorphic form. The resolution of our XRD system could not resolve for the different types of beta-prime polymorph and therefore the exact stable phases reached after the thermal treatment were not accessible. Time-resolved XRD analysis must be

used to solve for the polymorphic transitions occurring during melting and explain the occurrence of multiple melting peaks observed in the DSC thermogram [24]. However, because the principal polymorphic form of the sample desired for CBA based products is not affected, the cooling rate could be used to adjust parameters such as the onset time and melt temperature to achieve desired physical properties.

Figure A2.8a shows representative SFC versus time curves for cooling rates of 15.9, 1.6 and 0.1 °C/min. For the lower cooling rates, the crystallization event consists of at least two cascading events (as is evident for the 0.1 °C/min SFC curve and indicated by the arrow showing the prominent inflection region) suggesting the occurrence of secondary crystallization. Crystallization occurring over multiple steps in lipid materials has been frequently reported in the literature [13, 18, 31]. The onset time for crystallization, obtained via NMR (Figure A2.8b), decreases dramatically as r increases. One would expect longer onset time prior to crystallization due to the increased time for the required supercooling to occur prior to nucleation. However, samples may crystallize at higher temperatures when cooled at slower rates because the increased time at higher temperatures leads to the molecules within the melt having more internal energy allowing for the molecules to move about within the melt and achieve a desired conformation at a higher crystallization temperature. The variations of onset time of crystallization from DSC are similar.

The final SFC of the sample increases by 6% with increasing rate of cooling and plateaus at $65.5 \pm 0.4\%$ for a cooling rate of approximately 4 °C/min as shown in Figure

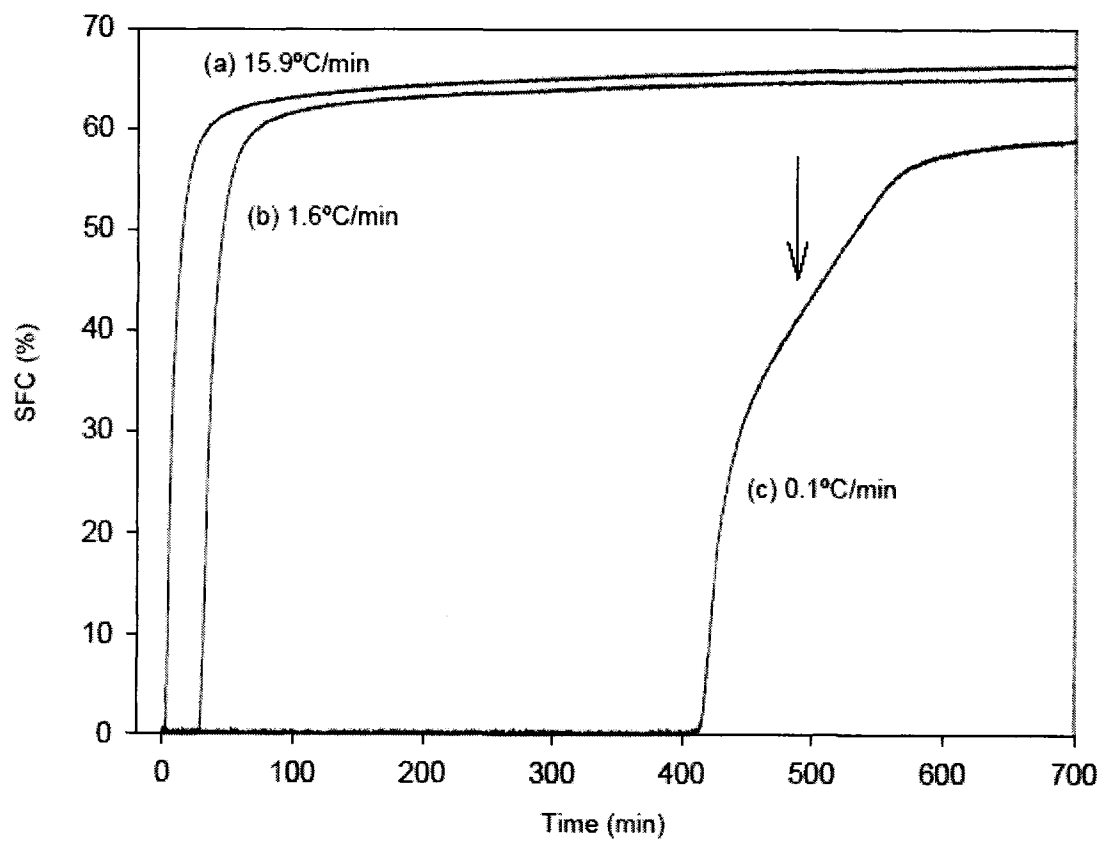


Figure A2.8a: SFC versus time. From left to right curves obtained with: 15.9 °C/min, 1.6 °C/min, and 0.1 °C/min cooling rate

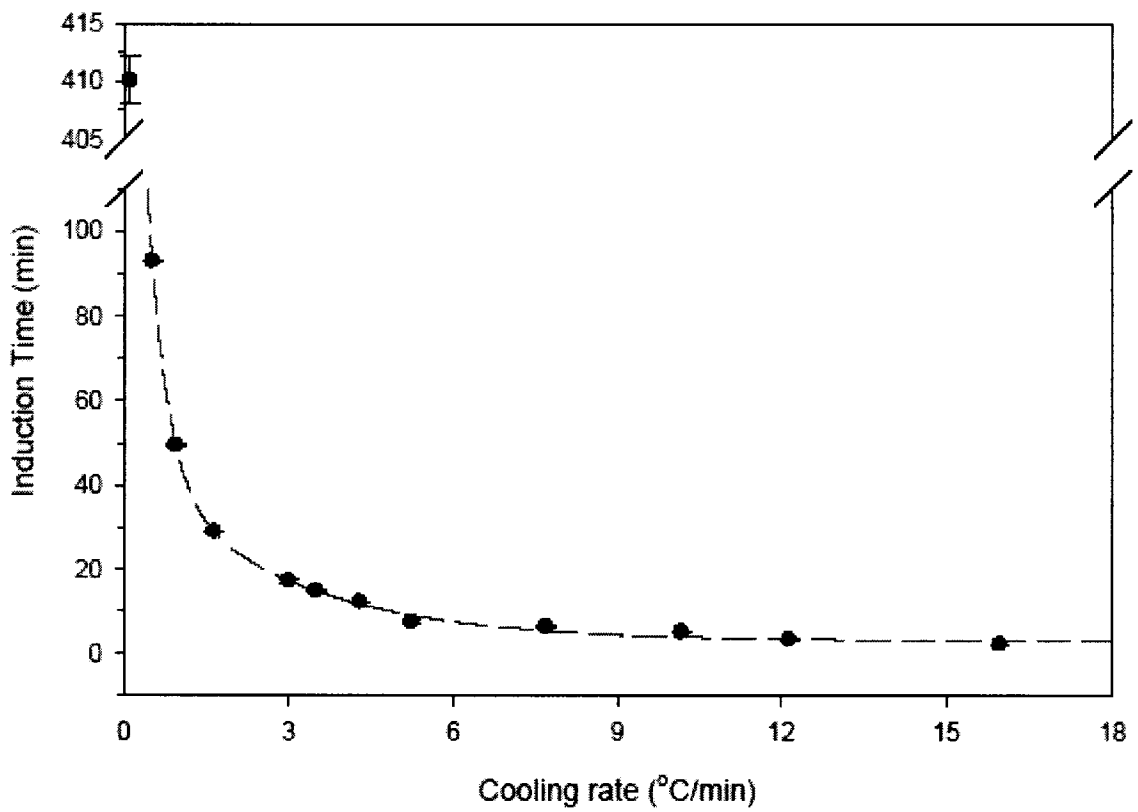


Figure A2.8b: Induction time versus cooling rate by NMR

A2.8c. 70% of the increase in final SFC occurred for samples cooled with 0.1 and 0.5 °C/min. This suggests that undercooling conditions were met for most of the components in the melt with cooling rates as small as 0.5 °C/min. It is interesting to notice that the 5 °C/min threshold is found again in the SFC characteristics and could further support the trends found in the hardness of the sample cooled at varying rates.

The cooling rate of a cocoa butter alternative can be altered to achieve the desired physical functionality without affecting the polymorphism. Variation of the cooling rate as a tool to modify physical functionality of the network was found to be effective only for cooling rates lower than 5 °C/min. The data demonstrates that the melting profile of the sample could be manipulated over a relatively narrow range of cooling rates. The thermal characteristics of the main CBA's components could be altered to some extent by varying the cooling rates lower than 12 °C/min. The components which are thought to be lower melting components of the CBA could be only affected by cooling rates lower than 5 °C/min. There is marginal utility to increasing the rate above these values, as there are limitations to the hardness and melting properties which one cocoa butter alternative can have.

Increasing the cooling rate could only be used to increase final SFC by approximately 6%. The variation of the main characteristics versus cooling rate determined by SFC is consistent with DSC data and account for hardness results. It is therefore suggested that the effect of cooling rate variation on modification of physical functionality of a lipid sample is effective over limited ranges of cooling rates,

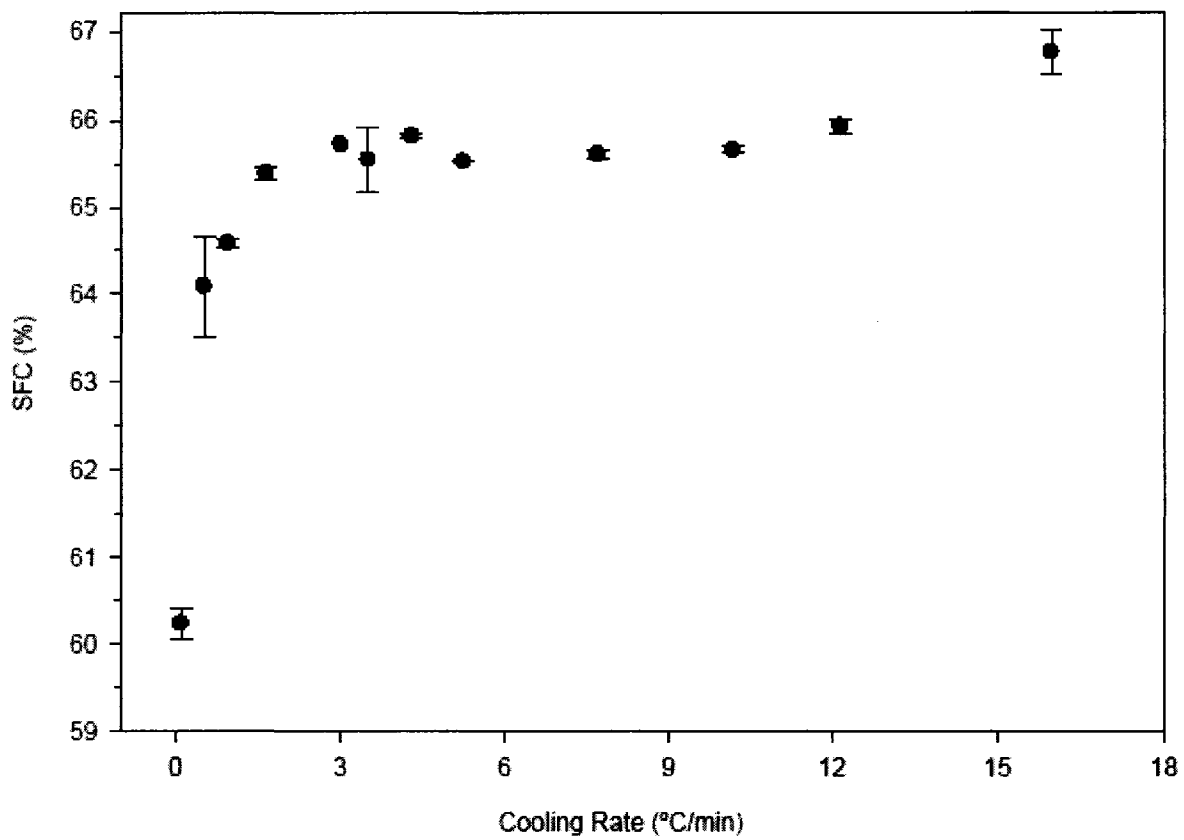


Figure A2.8c: Final SFC versus cooling rate by NMR

determined by the ability for the molecules to move within the melt at high temperatures prior to the crystallization event.

A2.4 References

1. Akazawa, T., et al., *Flux growth and physical properties of pyrochlore Pb₂Ru₂O_{6.5} single crystals*. Journal of Crystal Growth, 2004. **271**: p. 445-449.
2. Cashell, C., D. Corcoran, and B.K. Hodnett, *Control of Polymorphism and Crystal Size of L-glutamic Acid in the Absence of Additives*. Journal of Crystal Growth, 2004. **273**: p. 258-265.
3. Herrera, M., et al., *Isothermal Crystallization of Hydrogenated Sunflower Oil: 1. Nucleation*. J. Am. Oil Chem. Soc., 1998. **75**(10): p. 1273-1280.
4. Herrera, M., *Crystallization Behavior of Hydrogenated Sunflowerseed Oil: Kinetics and Polymorphism*. J. Am. Oil Chem. Soc., 1994. **71**(11): p. 1255-1260.
5. Herrera, M., et al., *Relationship Between Cooling Rate and Crystallization Behavior of Hydrogenated Sunflowerseed Oil*. J. Am. Oil Chem. Soc., 1992. **69**(9): p. 898-905.
6. Martini, S., M. Herrera, and R. Hartel, *Effect of Cooling Rate on Crystallization Behavior of Milk Fat Fraction/Sunflower Oil Blends*. J. Am. Oil Chem. Soc., 2002. **79**(11): p. 1055-1062.
7. Cebula, D.J. and K.W. Smith, *Differential Scanning Calorimetry of Confectionery Fats. Pure Triglycerides: Effects of Cooling and Heating Rate Variation*. J. Am. Oil Chem. Soc., 1991. **68**(8): p. 591-595.

8. Rousset, P. and M. Rappaz, *alpha-Melt-Mediated Crystallization of 1-Palmitoyl-2-Oleoyl-3-Stearoyl-sn-Glycerol*. J. Am. Oil Chem. Soc., 1997. **74**(6): p. 693-697.
9. Rousset, P. and M. Rappaz, *Crystallization Kinetics of the Pure Triacylglycerols Glycerol-1, 3-Dipalmitate-2-Oleate, Glycerol-1-Palmitate-2-Oleate-3-Stearate, and Glycerol-1, 3-Distearate-2-Oleate*. J. Am. Oil Chem. Soc., 1996. **73**(8): p. 1051-1057.
10. Kerti, K. *Thermal Analysis of Cocoa Butter and Cocoa Butter Alternatives Crystallization Using DSC Method*. in *In 2nd International Workshop on Control Applications in Postharvest and Processing Technology*. 1998. Budapest, Hungary.
11. Metin, S. and R.W. Hartel, *Crystallization Behavior of Blends of Cocoa Butter and Milk Fat or Milk Fat Fractions*. Journal of Thermal Analysis, 1996. **47**: p. 1527-1544.
12. Metin, S. and R. Hartel, *Thermal Analysis of Isothermal Crystallization Kinetics in Blends of Cocoa Butter with Milk Fat or Milk Fat Fractions*. J. Am. Oil Chem. Soc., 1998. **75**(11): p. 1617-1624.
13. Perez-Martinez, D., et al., *The Effect of Supercooling on Crystallization of Cocoa Butter-Vegetable Oil Blends*. J. Am. Oil Chem. Soc., 2005. **82**(7): p. 471-479.
14. Martini, S., M.L. Herrera, and R.W. Hartel, *Effect of Cooling Rate on Nucleation Behavior of Milk Fat - Sunflower Oil Blends*. J. Agric. Food Chem., 2001. **49**(7): p. 3223-3229.

15. Toro-Vazquez, J., et al., *Induction Time of Crystallization in Vegetable Oils, Comparative Measurements by Differential Scanning Calorimetry and Diffusive Light Scattering*. Journal of Food Science, 2002. **67**(3): p. 1057-1065.
16. Narine, S.S. and A.G. Marangoni, *Relating Structure of Fat Crystal Networks to Mechanical Properties: A Review*. . Food Res. Int. , 1999. **32**: p. 227-248.
17. Campos, R., S.S. Narine, and al, *Effect of Cooling Rate on the Structure and Mechanical Properties of Milk Fat and Lard*. . Food Res. Int., 2002. **35**: p. 971-981.
18. Bouzidi, L., et al., *Use of first and second derivatives to accurately determine key parameters of DSC thermographs in lipid crystallization studies*. Thermochemica Acta, 2005. **439**: p. 94-102.
19. Narine, S.S. and K.L. Humphrey, *Extending the capability of pulsed NMR instruments to measure solid fat content as a function of both time and temperature*. J. Am. Oil Chem. Soc., 2004. **81**(1): p. 101-102.
20. *Standard Methods for the Analysis of Oils, Fats, and Derivatives*, in *International Union of Pure and Applied Sciences*. 1979.
21. *Solid Content Determination in Fats by Low Resolution Nuclear Magnetic Resonance v. 2.150*, in *International Union of Pure and Applied Sciences*. 1987.
22. *Determination of Solid Fat Content by Pulsed NMR Method*, in *International Standard, Animal and Vegetable Fats and Oils*. 1991.

23. *AOCS Method Cd 16b-93*, in *Official and tentative methods of the American Oil Chemists' Society*, W.E. Link, Editor. 1998, AOCS Press: Champaign, IL.
24. Tan, C.P. and Y.B.C. Man, *Differential scanning calorimetric analysis of palm oil, palm oil based products and coconut oil: effects of scanning rate variation*. *Food Chemistry*, 2002. **76**(1): p. 89-102.
25. Herrera, M. and F. Marquez Rocha, *Effects of Sucrose Ester on the Kinetics of Polymorphic Transition in Hydrogenated Sunflower Oil*. *J. Am. Oil Chem. Soc.*, 1996. **73**(3): p. 321-326.
26. Humphrey, K.L., P.H.L. Moquin, and S.S. Narine, *Phase behavior of a binary lipid shortening system: From molecules to rheology*. *Journal of the American Oil Chemists Society*, 2003. **80**(12): p. 1175-1182.
27. Humphrey, K.L. and S.S. Narine, *A comparison of lipid shortening functionality as a function of molecular ensemble and shear: Crystallization and melting*. *Food Research International*, 2004. **37**(1): p. 11-27.
28. Narine, S.S. and K.L. Humphrey, *A comparison of lipid shortening functionality as a function of molecular ensemble and shear: microstructure, polymorphism, solid fat content and texture*. *Food Research International*, 2004. **37**(1): p. 28-38.
29. Marangoni, A. and R. Lencki, *Ternary phase behavior of milk fat fractions*. *J. Agric. Food Chem.*, 1998. **46**: p. 3879-3884.

30. Marangoni, A.G. and D. Rousseau, *The Influence of Chemical Interesterification on Physicochemical Properties of Complex Fat Systems - 1. Melting and Crystallization*. Journal of American Oil Chemists' Society, 1998. **75**(10): p. 1265-1271.

31. Christian, J.W., *Formal Theory of Transformation Kinetics*, in *The Theory of Transformations in Metals and Alloys*. 1975, Pergamon Press: Oxford. p. 525-548.

A3. Cream Icing Test (Method 17-73)

A3.1 Use for Shortenings

Emulsifier types, Vreamay

A3.2 Purpose

To evaluate the creaming property of emulsified shortenings by making a cream icing and measuring the final specific gravity of the icing.

A3.3 Apparatus

1 inch wide, 6 inch long metal spatula

Hobart mixer model C-100 with 10 quart bowl and flat beater

Mass balance with 1 gram graduations

Aluminum beaker 2.25 inches tall and 2.25 inches in diameter, 200 cc capacity

A3.4 Formula

All ingredients at 75 °F

XXX Sugar 1362.00 g

Test Shortening 397.25 g

Non-fat Milk Solids 85.10 g

Salt	7.08 g
Bourbon type Vanilla	7.08 g
Water	227.00 g

A3.5 Procedure

Weight all ingredients into bowl. Mix 30 seconds at first speed and scrape down bowl and beater. Cream at first speed for 15 minutes. Scrape down well at 3 minutes. Measure specific gravity at 15 minutes.

Report the specific gravity of the icing at 15 minutes and the cream icing score. The cream icing score is a combination of icing body and smoothness scores. The body score is determined as follows: With finished icing in mixing bowl, cut a 4 inch deep trench (almost to the bottom of the bowl) down the center with the metal spatula. Record the length of time before the bottom of the trench closes. Score assignments are as follows:

Seconds to closing	Points
0-5	0
6-15	1
16-30	2
31-60	3
>61	4

A4. Slump-Slide Test (Method 1-88)

A4.1 Purpose

An alternate method of measuring the structure of cream icing. Applicable to icings made from cream icing Test Method 17-73.

A4.2 Apparatus

Slump-slide box (shown in Figure 5.2)

8 inch metal spatula Rubber spatula Small paring knife

A4.3 Procedure

Place the base on a stable and solid table void of vibration. Level the base by adjusting the set screw legs. Make sure the slump-slide box is dry and at room temperature (70 °F to 76 °F). Icing temperature should be between 60 °F and 72 °F. While holding the box horizontal, fill the box completely full of prepared icing using a rubber spatula. With the metal spatula scrape the excess icing off so the box is level full. Scrape the excess icing from the bottom to the top of the box. Run small paring knife between the top of the box and the icing. Promptly stand the box on end and place the edge of the box even with the “0” line on the base. Let stand for 10 minutes and then read the scale on the base and back of the box.

A4.4 Report

Number of millimeters of slump (over onto the base) and compression (slide down the back of the slump-slide box).